The Chemical Speciation and Phase Distribution of Atmospheric Oxidized Mercury

Jim Avik Ghoshdastidar

Department of Chemistry
McGill University, Montréal

December 2018

A thesis submitted to McGill University in partial fulfillment of the requirements for the degree Doctor of Philosophy

Dedication

To my parents,

to my teachers

and to my students.

Acknowledgements

My sincere thanks to my supervisor, Professor Parisa A. Ariya, for her mentorship and support over the years, for giving me to opportunity to build my skills as a researcher and as an educator. Many thanks to my committee members, Professor Ian S. Butler and Professor Janine Mauzeroll for their thoughtful stewardship as I progressed through my degree.

I would like to acknowledge all of my group members, past and present, including Rodrigo Rangel-Alvarado, Uday Kurien, Dev Gangwar, Ryan Hall, Nermin Eltouny, Bryan Lee, Andrea Rocha, Dr. Daniel Deeds, Dr. Zhenzhong Hu, Dr. Yevgen Nazarenko, and the many undergraduate students we have had the privilege to work with including: Maxwell Morissette, Janani Ramamurthy, Simon Dib, Mayeesha Rahim, Arnold Downey, Connie Ye, Kuzi Murwira, Hannah Szeptycki and Emma Morris. Their friendship and support has been of immense value to me over these years.

Heartfelt thanks to Chantal Marotte, Rick Rossi, Weihua Wang and Jean-Philippe Guay and the faculty and staff of the Chemistry Department. Many thanks to all the students that I taught in Chem 110 and Chem 120 as a TA and later as an instructor and to all the residents, floor fellows and staff of New Residence Hall, McConnell Hall and Solin Hall where I have had both the privilege of working and living.

Finally, to my parents, Ashim and Sunanda, without whom none of this would be possible. I am ever in your debt.

Table of Contents

List of Tables

List of TOC Figures

List of Figures

Abstract

Mercury is a potent global neurotoxin that causes cognitive and neuromuscular damage. it is released through natural and anthropogenic processes, such as fossil fuel combustion, and travels far from its source of origin. A global concern, 130 countries have signed the 2013 UN Convention on Mercury, committing to reducing emissions.

Atmospheric mercury primarily exists as three bulk species of which gaseous elemental mercury (GEM) predominates. GEM travels far from its source of origin due to its long atmospheric residence time and deposits in marine and terrestrial environments following chemical transformation to the more water-soluble, bioavailable gaseous oxidized mercury (GOM) and after binding to particulates. In marine environments, oxidized forms of mercury may convert to the highly neurotoxic methylmercury organic species.

Conventional mercury analysis techniques cannot determine the chemical forms of mercury present in the atmosphere only whether mercury is present as GEM, GOM or particulate forms. It is also not clear that what is measured as gaseous mercury is entirely gaseous but may be comprised of nano-particulate mercury. Nano-particulate mercury would have significantly different chemical, biologic and human health implications, and would fundamentally change how we model the fate of mercury in the atmosphere, its transformations and risks to ecosystems.

In this work, we develop a technique to determine and measure the chemical speciation of atmospheric oxidized mercury using soft-ionization mass spectrometry, generate and characterize reproducible sources of oxidized mercury nanoparticles and assess the determine the gaseous and particulate contributions of mercury(II) bromide and mercury(II) chloride at pg/m^3 concentrations in Montreal urban air.

Abrégé

Le mercure est une neurotoxine globale puissante qui cause des détériorations cognitives et neuromusculaires. Elle est relâchée par des processus soit naturelles ou anthropique, tels que la combustion de carburants fossiles, et peut voyager loin de son lieu d'origine. Faisant l'objet d'une préoccupation globale, 130 nations se sont engagées à réduire son émission lors de la convention sur le mercure à l'ONU en 2013.

Le mercure atmosphérique existe principalement au sein de trois espèces dans lesquels prévale le mercure élémentaire gazeux (MEG). Grace à sa longue durée de vie dans l'atmosphère, le MEG peut se déplacer loin de son lieu d'origine et se dépose dans des environnements marins et terrestres en se transformant en mercure oxydé gazeux (MOG) qui est davantage hydrosoluble après un processus de liaison avec une particule. Dans les milieux marins, les formes oxydées du mercure peuvent se convertir en méthylmercure, une espèce organique extrêmement neurotoxique.

Les techniques d'analyse du mercure habituelles ne peuvent identifier les formes chimiques que prend le mercure présent dans l'atmosphère ; elles ne peuvent seulement identifier s'il est présent sous la forme de MEG, MOG ou particule. Nous ne sommes de plus pas certains que le mercure gazeux identifié soit en effet entièrement gazeux. Il pourrait être constitué de nanoparticules de mercure qui auraient de nettes différences concernant leur composition chimique et implication biologique et de santé, ce qui changerait fondamentalement la façon dont on modélise le comportement du mercure dans l'atmosphère ainsi que sa transformation et les risques que porte sa diffusion dans nos écosystèmes.

Dans cet article, nous développons une technique pour identifier et mesurer les espèces chimiques du mercure atmosphérique oxydé en utilisant la spectroscopie de masse à « ionisation douce », générons et caractérisons les sources reproductibles des nanoparticules de mercure oxydé et évaluons la contribution gazeuse ou particulaire du bromure de mercure(II) et chlorure de mercure(II) pour des concentrations de pg/m^3 dans l'air urbain de Montréal.

Manuscripts contributing to Thesis

Deeds, D.A., Ghoshdastidar, A.J., Raofie, F., Guerette, E.A, Tessier, A. and P.A. Ariya. 2015. **"Development of a Particle-Trap Preconcentration-Soft Ionization Mass Spectrometric Technique for the Quantification of Mercury Halides in Air."** Analytical Chemistry, 87 (10), 5109 – 5116. doi:10.1021/ac504545w – Contributing to Chapter 2

Ghoshdastidar, A.J., Hu, Z., Nazarenko, Y. and P.A. Ariya. 2018. **"Exposure to Nanoscale and Microscale Particulate Air Pollution prior to Mining Development near a Northern Indigenous Community in Quebec, Canada."** Environmental Science and Pollution Research, 25 (9), 8976-8988. doi:10.1007/s11356-018-1201-5 – Contributing to Chapter 5

Ghoshdastidar, A.J., Ramamurthy, J., Morrisette, M., and P.A. Ariya. 2019 **"Development of Methodology to Generate, Measure and Characterize the Chemical Composition of Oxidized Mercury Nanoparticles."** Analytical and Bioanalytical Chemistry. *Submitted [ABC-00761-2019]* – Contributing to Chapter 3

Ghoshdastidar, A.J. and P.A. Ariya. 2019. **"Is Gaseous Oxidized Mercury Solely Gaseous? – The Occurrence and Implications of Nanoparticulate Oxidized Mercury."** Scientific Reports. *Submitted [SREP-19-08088]* – Contributing to Chapter 4

<u>Manuscripts in Preparation</u>

Ghoshdastidar, A.J., and P.A. Ariya. 2019 **"Mercury on the Move – The Chemical Speciation and Phase Distribution of Atmospheric Mercury** Environmental Science: Processes and Impact. *Invited Review* – Contributing to Chapter 1

Chapter 1. The Chemical Speciation and Phase Distribution of Atmospheric Mercury

Environmental Science: Processes and Impact. *Invited Review*

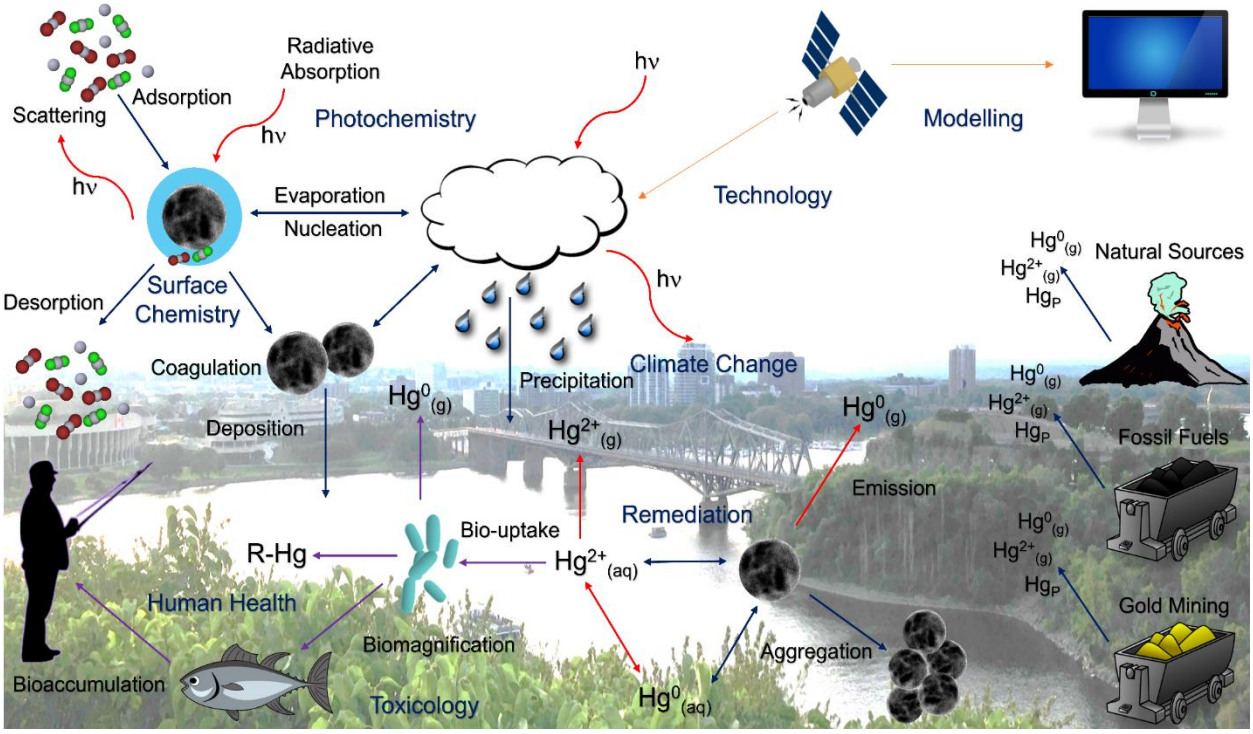

TOC Figure 1. The biogeochemistry of atmospheric mercury including emerging mercury nanoparticles

In this paper, we describe important milestones in the history and development of analytical techniques for the measurement of atmospheric mercury, the characterization of bulk mercury species and phases, and implications of phase and speciation to mercury biogeochemistry. Emerging chemical speciation of gaseous mercury species and particulate mercury are of particular interest for their impact on our understanding of the fate and transformation of mercury in the atmosphere.

Contribution by author: The introduction of this thesis is comprised of excerpts from a longer review invited for submission by Environmental Science: Processes and Impact. The review was written by A.G. under the supervision of P.A.A.

1.1. Introduction

1.1.1. Background

Mercury is a semi-volatile d^{10} transition heavy metal that is persistent, ubiquitous and heavily mobile in the environment [1-3]. Characterized by low melting (–39 °C) and boiling temperatures (357 °C) [4,5], mercury is the only metal, and only one of two elements to exist as a liquid at room temperature [4,6]. Mercury also possesses a significant vapour pressure (0.171 Pa at 20 °C) [7] and as the only non-noble atomic gas [4], it is emitted through natural or anthropogenic processes into the atmosphere, such as volcanic emissions, power generation or metallurgical processing.

From its source of emission, mercury can travel through the atmosphere contaminating remote and rural sites thousands of kilometres away. As a result of mixing, a long atmospheric residency time and cycles of emission, deposition and re-emission, global background levels of mercury are in the low ng/m^3 concentrations or mixing ratios in the part-per-quadrillion by volume (ppq_v) [8,9]. The majority (over 90%) of atmospheric mercury exists as the gaseous zero-valent element denoted as $Hg^0_{(g)}$ or gaseous elemental mercury (GEM) [10]. GEM serves as the primary means of transport to [11], dispersion in, and loading of ecosystems [12]. Elemental mercury can also undergo photochemical oxidation, with oxidants such as halogens, hydroxyl radicals (OH•) and ozone, to inorganic Hg(I) and Hg(II) species known as gaseous oxidized mercury (GOM) or reactive gaseous mercury (RGM). Both elemental and oxidized mercury species can also be present, or become bound to particles as particulate bound mercury denoted $Hg^P_{(s)}$ or PBM [13]. The conversion of GEM to GOM or adsorption to particulates provides a significant pathway for dry and wet deposition of atmospheric mercury (ng/L concentrations in rainwater) [14] to terrestrial and marine environments.

Like GEM, these bulk species of PBM and GOM can also be emitted directly from point sources; all have different chemical, physical and toxicological properties which impact their fate, transformation, mobility, bioavailability and human and ecological-related health risks [15-17]. In marine environments, highly toxic organomercury, is formed by methylating bacteria, where mercury readily bioaccumulates in organisms and biomagnifies in the food-chain (up to 10 million fold) [18] thereby posing a risk to public health. Consumption of

contaminated higher trophic-level, predatory fish serves as the primary and most significant exposure route for humans [19] as inhalation of ultra-trace concentrations of atmospheric mercury is seen to be insignificant [18]. In all of its forms, mercury poses a risk to human health in varying degrees depending on its speciation.

Human beings have utilized mercury throughout history including most significantly in metallurgical and medicinal applications [16]. Most crustal mercury is present in ores as cinnabar or mineralized mercury(II) sulphide and roasting cinnabar produces metallic mercury [6]. From antiquity, nearly 1 million tons of mercury was extracted from metallic mercury mining sites including Almadén, Spain, where nearly a third of all industrially produced mercury originates [6]; Idrija, Slovenia [20,21], Mt Amiata, Italy [5], Pachuca, Mexico [20], and Huancavelica, Peru [5]. Early uses of mercury include the production of vermilion dye, as a drug and preservative [5], by alchemists seeking to transform base metals into gold [5], in gold and silver extraction by colonial powers in the Americas, followed most recently by the chlor-alkali industry in the 20th century [6], where nearly 40% of globally produced mercury was used as late as 1996 [22]. Mercury has also found uses in skin-lightening cosmetics [23], thermometers [24], alkaline and Hg-zinc batteries [25], the electronics industry, medicine and vapour lamps, LCD flat monitors [26], pesticides, fungicides [27], and as a grain preservative [6,28].

With increasing anthropogenic production and usage of mercury, the accumulation of anthropogenic mercury in sediment, bog and ice cores begins to appear in the 19th century [8]. Following tragedies at Minamata and Iraq, increased scrutiny and concerns over the toxic properties of mercury, especially organic mercury forms, impacted mercury production in the 1960s when prices peaked at $16 USD/kg and but later cratered to $5 USD/kg [6]. Usage and deposition of mercury in Europe decreased significantly in the 1990s with the closures of chlor-alkali plants [8], as viable mercury alternatives in gold and silver production, the electronics industry, medicine and chlor-alkali further reduced mercury production, consumption and emission.

Table 1.1. Properties of elemental and atmospherically relevant species of gaseous oxidized mercury

Property	Elemental Mercury	Mercury(II) chloride	Mercury(II) bromide	Mercury(II) oxide	Methyl mercury(II) chloride	Dimethyl-mercury
Abbreviations	GEM, Hg0	$HgCl_2$	$HgBr_2$	HgO	MMC	DMM
Molecular Formula	Hg	$HgCl_2$	$HgBr_2$	HgO	CH_3HgCl	$CH_3Hg\ CH_3$
Molecular Weight (g/mol)	200.59 [29]	271.50 [29]	360.40 [29]	216.59 [29]	251.1 [30]	230.66 [29]
Melting Point (°C)	−38.8290 [29]	277 [29]	241 [29]	Decomposes at 500 [29]	Sublimates at 174 [31]	−43 [32]
Boiling Point (°C)	356.619 [29]	304 [29]	318 [29]	N/A	N/A	93 [29]
Normal State	Liquid	Solid	Solid	Solid	Solid	Liquid
Density (g/cm^3)	13.5336 [29]	5.6 [29]	6.05 [29]	11.14 [29]	4.06 [30]	3.1874 [20 °C] [30]
ΔH_{fus} (kJ/mol)	2.295 [29]	19.41[29]	17.9 [29]	NR	NR	NR
ΔH_{vap} (kJ/mol)	59.11 [29]	58.9 [29]	58.89 [29]	NR	NR	34.6 [33]
Aqueous Solubility @ 25 °C [mol/kg]	5.6×10^{-5} [30]	0.269 [34]	1.70×10^{-2} [34]	2.45×10^{-5} [34]	3.99×10^{-4} [21 °C] [30]	4.3×10^{-3} [21 °C] [30]
Vapor Pressure (kPa) @ 25 °C	2.613×10^{-4} [29]	8.99×10^{-6} [20 °C] [15]	2.12×10^{-5} [35]	9.20×10^{-15} [15]	1.76×10^{-4} [15]	8.30 [29]
Polarizability (10^{-24} cm^3)	5.08 [29]	11.6 [29]	14.5 [29]	2.88	NR	NR
Ionization energy (eV)	10.4375 [29]	11.380 [29]	10.560 [29]	NR	7.3 [36]	9.33 [37]
TLV (TWA) (mg/m^3)	0.025 [38]	0.025 [38]	0.025 [38]	0.025 [38]	0.01 [38]	0.01 [38]

N/A – not applicable; NR – Not recorded; TLV –Threshold limit value; TWA – Time-weighted average

1.1.2. Sources

The contribution of mercury into the atmosphere has been long thought to be comparable between natural and anthropogenic sources [39]; though in urban areas, anthropogenic sourced emissions can predominate. In metropolitan Mexico City, 81% and 93% of GEM and GOM measurements, respectively, were estimated to have originated from anthropogenic point sources [40]. For natural and anthropogenic emissions, GEM is nearly always the dominant form of emission and there is generally greater percentage contributions of GOM and PBM from anthropogenic sources [15,41]. Natural sources of mercury, or mobilization of mercury without human interference [11], include: volcanic eruptions and geothermal vents, release from forest fires, re-emission from deposited mercury from soils and routinely dissolved mercury supersaturated surface water (accounting for as high as 40% of global emission estimates) [21,42], and the weathering of

mercury-containing rocks [1,43-46]. Volcanic events [47], in particular, have been observed to raise local ambient mercury concentrations as high as 10^5 times [42], while other natural processes such as forest fires are associated with PBM elevation (nearly 15% of total mercury emissions) [48,49]. Significant re-emission of deposited mercury [40], accounts for as much as 400–1300 tonnes of atmospheric mercury per year [11].

Of the anthropogenic sources of mercury, fossil fuel combustion is the most prominent, with contributions estimated at 45% of total anthropogenic mercury emissions [50]. Anthropogenic emissions originate from a combination of point sources such as from power generation (including biofuel and biomass burning [40], and waste incineration) [1,44-46], industrial processes (steel, ferrous and non-ferrous metal production, lamp and LCD manufacturing, petroleum refineries, cement and chlor-alkali plants) [26,51], major transportation centres such as airports [44,49], and also non-point sources such as vehicular traffic and residential heating [49]. Agricultural biomass burning is particularly significant for the African continent and results in GEM enhancements in particular at the coastal marine boundary layer [52].

The distribution of bulk mercury species varies between and within emission sources. Zhang et al. found emissions from residential and industrial coal combustion in Shanghai consisted of 64.4% GEM, enriched GOM levels of 34.0%, and 1.6% PBM [43,45]. In the North America context, power generating facilities in Canada and the US were reported have a distribution of approximately 57%, 40% and 3% in 2005, and in 2016 of 73%, 24.5% and 2.5% for GEM, GOM and PBM in emissions, respectively [53]. While any fossil fuel combustion will release mercury, Freitas et al. observed sites close to coal-generation had significantly higher PBM concentrations to sites with equidistant oil-fired power generation plants [54]. When comparing contributions of anthropogenic sources in Beijing, Schleicher et al. found the greatest enrichment of mercury in residential-use coal (300 ng/g) in compared to automotive emissions (88 – 126 ng/g), and the wearing and production of concrete, mortar and cement construction materials (37 and 48 ng/g). In comparison, relatively pristine Gobi sand had a mercury concentration of 5 ng/g [55].

The remainder of anthropogenic mercury emissions includes small-scale or artisanal gold mining (18%) [46], landfill emissions from improper mercury-containing product disposal [18], and industrial processes such as metallurgy, cement, gold and mercury

production [39,55]. Of the emissions from gold and cement production, nearly half of all emissions arise from China [55,56] with Wang et al. estimating that China alone produces 218 tonnes of mercury [57,58]. At Almadén, Spain, despite decades of advancements in cinnabar roasting efficiency and pollution control, total gaseous mercury (TGM) emissions from the facility in the 20th century averaged a remarkable 600 ng/m^3 [6]. This is consistent with one of the first ever atmospheric mercury measurements of 600 ng/m^3 made by Neville near a mercury mine [42,59].

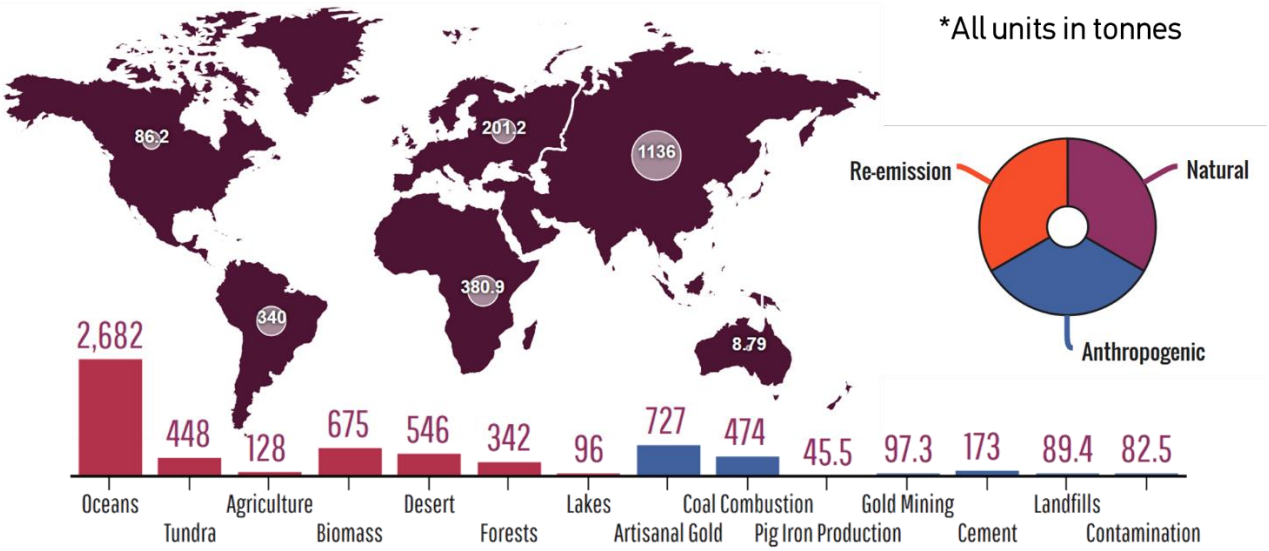

Figure 1.1. Worldwide atmospheric mercury emission and source estimates based on UNEP's Technical background report for the global mercury assessment 2013 [56].

Several national, state and local jurisdictions estimate facility point-source mercury emission data. In the United States, this is performed through a National Emissions Inventory which is released every three years [60]. Canada and Mexico each have the National Pollutant Release Inventory and the Pollutant Release and Transfer Register, respectively, with the latter restricted to industrial emission sources under Federal jurisdiction. [40] Despite growing emission data collecting, total anthropogenic outputs, and many of the estimates thus far provided, have presumed uncertainties of at least 30% [11].

The majority of mercury emissions, approximately half to two-thirds, arise from Asia [1,44,46,61,62] fueled by growing economic development and industrial productivity in China and India [3,63], with China alone accounting for a third of global emissions [55,56,64]. Despite the preponderance of Asian emissions, as a result of its significant capacity for transport and re-emission [51], GEM can be transported to remote and rural communities

thousands of kilometres from its source [3], while GOM and PBM dominate wet and dry mercury deposition (nearly 95%) thus restricting mobilisation to local and regional transport [41]. In areas where pollution controls are developing, urban concentrations of PBM can be as high as ten times higher than in remote areas [1], thus pollution controls have some of the greatest impacts on those jurisdictions where the controls are enacted. Still, Huang et al. 2017 observed an elevated pollution event in Florida with long-range transport of mercuric(II) bromide (GOM) originating in Asia and travelling from the stratosphere or free troposphere before mixing with local polluted air [65] suggesting that the impact of GOM emissions may be more global than initially anticipated.

Global anthropogenic emissions estimates have remained steady in the most recent decades with 2,200 tonnes of mercury released in 2000, reducing to 1,930 tonnes in 2005 [39], though 4,000 tonnes was predicted by the UNEP [26,66]. By 2007, direct anthropogenic emissions accounted for 2400 tonnes of mercury released [18]. In 1994, 6,000 tons of mercury was estimated to be in the troposphere, and almost 11,000 tons in freshwater and marine environments [26,67], with Europe contributing 700 tonnes a year [8]. Mercury accumulates in sediment, and despite flattening mercury concentrations and deposition, sediment concentrations in remote areas will change along decade and century timelines, however concentrations near local sources will experience more significant changes. [8] It is estimated that as much as 500,000 tonnes of anthropogenically released mercury is present in surface sediments and soils thus as global temperatures continue to rise, elevated emissions from soil evasion are expected [11].

1.1.3. Toxicity and Health Impacts

Major mercury poisonings have occurred in recent decades at Minamata Bay and Niigata in Japan, in Iraq, and in communities around the world including Pakistan, Guatemala, Yugoslavia and Canada [16]. As early as the 1920s, health problems were reported for 36% of miners at the Almadén mercury mine; chronic exposure to mercury vapour resulted in adverse neurological and renal effects known as hydragyrism disease [6]. At Minamata, mothers exposed to methylmercury through the consumption of fish during pregnancy bore children with significant neurological and muscular impairments [68,69]. The WHO has established a concentration limit for fish of 0.5 mg/kg, [8] and pregnant women are advised

to avoid eating higher trophic level fish such as pike, perch, tuna and among others to limit their intake [8]. Again, at the levels that mercury is generally present in the atmosphere, inhalation does not pose a health risk. [18,21]

The most significant exposure pathway for mercury occurs through human consumption of contaminated marine fish,[70] and to a lesser extent through inhalation. [71] Mercury binds to sulphur-containing groups of enzymes, amino acids and cellular membranes altering their function. [39] The result of methylmercury is neurodegenerative, [39] causing motor activity problems and renal, cardiovascular, reproductive and immune system issues. [72] For inhaled Hg particulates, the hazard is associated with the degree of penetration of these particles into the respiratory system [2] in conjunction with their chemical composition [62]: 4.7 μm for the nose and pharynx, 3.3 μm for the trachea and bronchi, 2.1 μm for the secondary bronchi and 1.1 μm for the bronchioles. Below 1.1 μm, particles can penetrate the pulmonary alveoli. [2]

1.1.4. Regulation

Several conventions, protocols and programs have been legislated, signed and ratified to curtail the release of anthropogenic mercury into the atmosphere across nations. In 1998, Canada, the US and 32 European nations signed the Protocol on Heavy Metals in the Convention for Long-Range Transboundary Air Pollution as part of the United Nations Economic Commission for Europe [73]. In 2001, the United Nations Environment Program established plans to govern and assess international industrial mercury usage with the aim to reduce emissions and ensure proper disposal and storage [6,62,66], followed by the Clean Air Mercury Rules for coal power plants aiming for 70% emission reductions by 2025 [18]. The EURLex 2005, from the European Commission, aimed at a mercury phase out and export ban [6] and the Mercury Policy Project from the United States established deadlines around mercury export bans [6], eventually leading to the Mercury and Air Toxics Standard in 2011 [62,74] which the Trump administration has since looked to weaken [75]. The Global Minamata Treaty was signed by 130 nations in 2013 and designed to protect human health and the environment [3]. As of May 2018, 128 countries have signed the treaty with 101 signatories ratifying.

Recommendations and regulations for atmospheric mercury vary across nations. The World Health Organization air quality guidelines for Total Gaseous Mercury (TGM) is 1,000 ng/m^3 [6]. Both the United States Environmental Protection Agency (USEPA) and the Ministry of Environmental Protection of China have a maximum allowable atmospheric mercury concentration of 300 ng/m^3 [61]. Individual regions, states and even municipalities may also have their own quality guidelines. Philadelphia, for examples, had an air quality guideline of 240 ng/m^3 for total mercury [76]. Beyond total mercury, regulations also have been enacted for bulk species concentrations. The European Union has mandated a 50 ng/m^3 annual average of elemental mercury in 24 hour samples taken of total particulate matter [54].

1.2. Chemical Speciation of Gaseous Mercury in the Atmosphere

Background concentration of total mercury in the atmosphere, away from significant point sources, are in the range of 1.1 – 1.7 ng/m^3 [11], with the majority of atmospheric mercury present as GEM [39] which is mixed well globally [77]. Total mercury concentrations have increased between two- and five-fold from pre-industrial levels and mercury deposition to terrestrial and aquatic environments has increased two to four-fold [11,39,67,78]. Total atmospheric mercury is split into gaseous and particulate forms, with gaseous mercury split into elemental and oxidized mercury compounds [10,42]. As a result of its ultra-trace presence, the quantitative determination of bulk mercury species such as PBM and GOM is challenging and the exact chemical speciation of those species even more so [16]. Early analytical techniques for atmospheric mercury are provided in Table 1.2. In recent decades, there may be a global decreases in background (or remote) atmospheric mercury levels [49,79], for both GEM and GOM concentrations [65], however despite this decreases, concentrations in soils and sediments continue to increase in some areas, for example the remote northern forests of Sweden [8]. These concentrations have decreased from the 6 – 8 ng/m^3 concentrations observed in the 1980s (Table 1.3), however most of these measurements occurred in urban sites often near mercury sources. [42] Slemr et al. proposed that global background levels have in fact remained stagnant from the time of first atmospheric mercury measurements [11,80].

Table 1.2. Early techniques for measuring atmospheric mercury

Reference	Analysis	Sample Collection	Sample Preparation	Separation	Analysis
Braman and Johnson 1974 [81]	Total Mercury	Gold-coated glass beads	Air drawn through speciation stack at 1.5 L/min passes through glass wool filter before a gold-coated glass trap.	Heated to 470 °C, GEM is transferred to the detector with helium carrier gas.	DC Discharge Emission Spectroscopy
	Gaseous Elemental Mercury	Silver coated glass beads	Air drawn through speciation stack at 1.5 L/min passes through 1) glass wool filter, 2) HCl treated Chromosorb W trap, 3) NaOH treated Chromosorb W trap, and a combined silvered glass followed by gold-coated glass bead trap.		
	Gaseous Hg(II) type compounds	HCl treated – Chromosorb-W		Heated to 250 °C for 12 minutes and transferred to a gold trap heated 470 °C with helium carrier gas.	
	Gaseous Methylmercury (II) type compounds	NaOH treated Chromosorb-W		Heated to 300 °C for 6 minutes and transferred to a gold trap heated 470 °C with helium carrier gas.	
	Gaseous Dimethylmercury	Gold-coated glass beads		Heated to 470 °C and transferred to the detector with helium carrier gas.	
	Particulate Bound Mercury	Quartz Type A Filters		Heated in a blanked pyrex tube at 550 °C and transferred to the detector with helium carrier gas.	
Dumarey et al. 1978, 1979 [82,83]	Total Gaseous Mercury	Gold-coated sand	Air is sampled between 2.5 – 3.5 L/min through a filter on to gold-coated sand absorption tubes.	Desorption at 0.1 L/min at 800 °C.	Mercury Analyzer System – Coleman MAS-50
	Particulate Mercury	Quartz Filter		Filter is heated to 800 °C and mercury-free air sweeps mercury through 800 °C heated silver wool, silica, alumina, room-temperature magnesium perchlorate to remove interferents before amalgamation to a gold-trap.	
Schroeder and Jackson 1985, 1987 [16,76]	Gaseous Elemental Mercury	Gold Wire	Ambient air is drawn through a quartz fibre filter and then through a four sorbent speciation train at 6 L/min for 10 to 60 minutes. Chromosorb-W (HCl) and Carbosieve B sorbent traps were held at 180 °C while the Gold Trap and Tenax GC sorbent trap was at ambient temperatures. Particulate mercury was collected for 24 hours.	Each collector tube is sequentially heated between 250 °C and 450 °C for 5 – 10 minutes and desorbed to a pyrolyzer. Elemental mercury from the decomposition of species is collected on a gold trap, concentrated and desorbed at 500 °C and measured using a spectrophotometer. Particulate mercury was decomposed to GEM and desorbed at 900 °C	AFS - Barringer
	Gaseous Mercuric Chloride	HCl treated – Chromosorb-W			
	Gaseous Methylmercuric Chloride	Tenax GC			
	Gaseous Dimethyl Mercury	Carbosieve B			
	Particulate Bound Mercury	Quartz Filter			
Brosset and Lord 1995 [84]	Methylmercury chloride	MilliQ Water	Ambient air was drawn through a quartz bubble with 200 mL of milliQ at sub L/min flow rates for 6 to 10 days. Methylmercury chloride was extracted using dichloromethane and concentrated in a small volume of milliQ by heating off the organic layer and collecting on a Carbotrap column	Analytes were introduced to a cryogenic GC column and separated, pyrolyzed to GEM at 700-800 °C.	CVAFS

1.2.1. Gaseous Elemental Mercury (GEM/Hg^0)

Gaseous elemental mercury (GEM) or zero-valent mercury (Hg^0) is the dominant form of mercury in air [39] mainly due to its volatility, inertness and low solubility [26]. As a consequence, elemental mercury has long atmospheric residence times, estimated to be months to a year [11,51,85,86] thereby allowing mercury to be transported to areas, with no anthropogenic point sources, such as rural and Arctic regions [87]. As it has the longest atmospheric residence time of the bulk mercury species, GEM is mainly responsible for the global distribution of mercury. Wet and dry deposition of elemental mercury does occur, especially quickly under certain conditions, such as in polar regions and around the marine boundary layer [11] where residence times can be hours or weeks, respectively [52].

Even in these areas, the loss of GEM is primarily due to conversion and subsequent deposition of GOM and PBM [88]. In aqueous environments, Hg^0 has limited solubility [26]; Henry's solubility ranges between 0.9 and 1.4 x 10^{-3} mol/m^3 Pa and the oceans act as a significant emission source into the atmosphere [89,90]. Terrestrial surface immobilization of GEM is limited due to re-emission or secondary emissions, thus the chemical lifetime of GEM may actually be much shorter but through the course of oxidation, deposition, reduction and emission processes, may appear longer.

1.2.2. Gaseous Oxidized Mercury (GOM)/Reactive Gaseous Mercury (RGM)

Gaseous oxidized mercury (GOM) is a bulk species of gaseous Hg^I and Hg^{II} compounds, which are more reactive, have higher deposition velocities, are more soluble with larger scavenging coefficients [9,15], are less volatile with shorter residence times (hours to days) [1,91], and ultimately present at lower concentrations than GEM. In aquatic environments, these species are more bioavailable than zero-valent mercury [10,92]. Often used interchangeably, reactive gaseous mercury (RGM) is operationally defined as water soluble, divalent inorganic species of mercury [93] that are semivolatile, gaseous and capable of being reduced by stannous chloride ($SnCl_2$) [39,73]. Gaseous oxidized mercury has long been suspected to be comprised of species such mercury(II) chloride [13,94-97], mercury(II) bromide [98], mercury(II) hydroxide [94], mercury(II) nitrate monohydrate [94], mercury(II) oxide [94,99], among others. Each of these species has different chemical and physical properties [10,15] and can be bound to or present in particulates as well

[11,13,100]. GOM is generated through photochemical oxidation of GEM, or emitted, directly or indirectly, from point sources, such as waste incineration and chloralkali plants [65,101]. Notably, GOM is the predominant emission from waste incineration [14], one of the rare occasions where GEM does not dominate. Organomercury species, such as methylmercury(II) halides are relatively similar in volatility as GOM [81], but are present at trace pg/m^3 concentrations [73]. Little organic mercury is expected to be transported in the atmosphere [11,13] though early mercury speciation studies (Table 1.3) show significant concentrations especially near wastewater treatment plants.

The combination of gaseous elemental mercury and gaseous oxidized mercury is known as total gaseous mercury (TGM) [62] which comprises nearly 99% of total atmospheric mercury [73].

1.2.3. Distribution of Atmospheric Mercury Speciation

Of the distribution of bulk atmospheric mercury species, the most substantial proportion is present as GEM with generally less than 10% comprised of GOM and PBM [1,3,15,102]. In recent decades, the proportion of GEM in measurements has often increased beyond 95% and above especially in remote and rural areas [26,51]. Even in metropolitan urban areas, such as a year-long study in Toronto, 99.2% of measured mercury species were present as GEM [17]. The measurement of atmospheric mercury and its bulk species helps to determine source influences, mobility and transport potential, and the long-term behavior and fate of these species [43]. The distribution of these bulk species is influenced by meteorological conditions[103], seasonal and diurnal influences, the atmospheric chemistry of the region as well local and regional sources [41,87].

The absolute concentrations of total atmospheric mercury and the three bulk mercury species are generally higher in urban areas. Comparing urban Detroit and rural Dexter in Michigan, concentrations of GEM, GOM and PBM were 1, 2 and 3-fold higher at Detroit, respectively [41]. These differences arise from reactive mercury (RM) enriched local industrial mercury sources, atmospheric formation enhanced by mercury oxidant concentrations, and RM-enriched plume transport [17,104]. These RM rich anthropogenic urban source emissions tend to produce more significant variation in these bulk species [41], and a lower proportion of GEM in urban settings is expected.

Table 1.3. Early measurements of atmospheric mercury species

Reference	Site	Time	GEM (ng/m^3)	GOM (pg/m^3)	PBM (pg/m^3)	Notes
Johnson and Braman 1974 [42]	Tampa, FL (USA)	3 August and 3 November 1973	4.5 [2, 7]	ND	1 [0, 2]	Urban Site
			11.0 ± 15.8 [2.4 – 49]	$HgCl_2$: 35 ± 81 [ND – 220] (× 10^3) MMC: 8 ± 10 [ND – 2.2] (× 10^3) DMM: 100 ± 350 [ND – 1000]	2.8 ± 4.8 [ND – 13] (× 10^3)	Industrial Sites
			2.9 ± 1.4 [ND – 4.4]	$HgCl_2$: 8.1 ± 8.9 [ND – 24] (× 10^3) MMC: 5.6 ± 7.6 [ND – 19] (× 10^3) DMM: ND	1.8 ± 2.5 [ND – 7] (× 10^3)	Suburban Sites
Dumarey et al. 1979 [82]	Ghent, East Flanders (Belgium)	> November 1978	1793 ± 553 [1448 – 2616]		NA	Mercury Laboratories
			103 ± 50 [54 – 158]			University Buildings
			789			Room – Mercury Spill
			7.16 ± 0.30			Outdoor Urban
Dumarey et al. 1980 [83]		> September 1979	1076 ± 849 [205 – 1903]		809,000 ± 626,000	Mercury Laboratories
			112 ± 24 [90 – 145]		25,000 ± 15,000	University Buildings
			14 ± 14		320 ± 110	Outdoor Urban
Brosset 1987 [105]	Unknown	April – June 1982	1245 ± 1183 [520 – 3010]	1618 ± 580 [800 – 2070] (× 10^6)	NA	Coal Combustion Smoke
	Ekeröd, Skåne (Sweden)	July – November 1983	2.65	190		Rural site
	Onsala, Halland (Sweden)		2.52	140		Rural site
	Vindeln, Västerbotten (Sweden)		2.13	90		Rural site
Schroeder and Jackson 1987 [76]	Toronto, ON (Canada)	October 20 – November 9 1981	7.5 [3 – 24]	$HgCl_2$: ND MMC: 1.3 [ND – 3] (× 10^3) DMM: 200 [ND – 1900]	70 ± 17 [60 – 90]	Rural Site
			8.2 [4 – 13]	$HgCl_2$: 300 [ND – 1900] MMC: 2.2 [ND – 6.2] (× 10^3) DMM: 400 [ND – 1300]	70 ± 26 [40 –100]	Urban Site
			12.4 [8 – 19]	$HgCl_2$: ND MMC: 1.9 [0.2 – 3.5] (× 10^3) DMM: 700 [ND – 1600]	45 ± 21[30 – 60]	Near Incineration and Waste Treatment
			90.9 [62 – 110]	$HgCl_2$: 1.4 [0.5 – 2.4] (× 10^3) MMC: 800 [ND – 2200] DMM: 1.6 [ND – 3.7] (× 10^3)	160	Mercury Battery Manufacturing Site
Brosset and Iverfeldt 1989 [106]	Onsala, Halland (Sweden)	November 1987	3.01 ± 0.62 [2.23 – 4.15]	37.5 ± 22.5 [10 – 70]	85 ± 137 [10 – 420]	

MMC –methylmercury chloride; DMM – dimethylmercury; ND – not detected

Sharp drops in GEM concentrations in measurements (to concentrations >0.1 ng/m^3) [11] known as atmospheric mercury depletion events (AMDE), occur due to photochemical oxidation processes and result in GOM and PBM measurement increases [103]. Mercury depletion events have been associated with reactive halogen species, especially bromine, and ozone, and were first observed by Schroeder et al. 1998, and later in the marine boundary layer with sea salt halogens [52,91], near the Dead Sea [107], free troposphere and stratosphere, and in particular in the Arctic [87]. During these events, bulk mercury species distributions at rural or remote sites favour higher mean concentrations of GOM and PBM fractions of 4.5% and 7% respectively, [87] and result in deposition of 100 – 150 tonnes of atmospheric mercury per year [11].

1.2.3.1. Correlation with other Pollutants

The correlation of bulk mercury species with co-contaminants may occur for a variety of reasons including co-emission from point sources, occurrence in the same air mass being sampled, or because of simultaneous photochemical production. Observed dips in GEM are often observed with high co-pollutants concentrations during or causing periods of enhanced heterogeneous-driven photochemistry [60]. Measuring co-pollutants also allows changes in atmospheric mercury concentrations to be linked to the transport of air masses.

Ozone (O_3) is a product of photochemical processes and is dependent on the intensity of solar radiation. Like GOM, it has a short residency time, on the order for a few weeks, and is indicative of local sources. While several studies report positive correlations between O_3 and GOM concentrations [19,108-110], others have not [1,43,77]. No statistically significant correlation between GOM and O_3 is often interpreted to suggest that other oxidants such as halogens may be responsible for the production of GOM or that local anthropogenic sources are largely responsible for changes in GOM [77]. Conversely, a correlation of GOM with O_3 that does not feature concurrent spikes implies a common anthropogenic emission origin rather than formation through atmospheric photochemical reactions [17]. GOM production related to enhanced photochemistry involving O_3-like oxidants will often be associated with positive correlations with O_3 and UV intensity accompanied by negative correlations with GEM [41,101].

A positive correlation of GEM with carbon monoxide (CO) is often indicative of co-emission from vehicular emissions [60,101]. GEM can also be related to CO because of a common origin in coal combustion and industrial processes like cement, iron, and steel production. Ratios between co-pollutants and mercury can be used to relate a plume to a potential source [111]. For example, the GEM/CO ratio (ng/m^3 per ppm_v) is much higher for zinc and lead smelting processes (120 –150 ng/m^3 per ppm_v) than for coal combustion (0.6 ng/m^3 per ppm_v) [43], while TGM/CO ratios are on average 11 ng/m^3 per ppm_v for industrial activity in the US and 14 ng/m^3 per ppm_v for biomass burning [111].

Carbon dioxide, NO_x and SO_x species are often related to emissions from coal-power fired power plants and industries that concurrently emit mercury [77]. Li et al. observed GEM spikes with increased concentrations of carbon dioxide (CO_2), nitric oxide (NO) and nitrogen dioxide (NO_2) species, and particulate matter 10 μm and less (PM_{10}) consistent with mercury-enriched air parcels which HYSPLIT back trajectories point to highly industrialized regions origins. In Shanghai, GEM was correlated with SO_2 and NO_x [43,101], and night-time GOM levels were better predicted by SO_2 than O_3 suggesting local coal-related emissions instead of photochemical production [41]. Finally, in the earliest of mercury measurements, Williston observed correlations of mercury with smog [42,112] and Brosset found co-occurrence of non-reactive mercury with high soot particle concentrations and identified significant concentrations in smoke from coal combustion [105].

During the polar sunrise, gaseous elemental mercury in the Arctic is photochemically oxidized to GOM and PBM through O_3 and halogen chemistry and snow surface deposition [87]. Distinguishing between photochemical and transport effects can be determined by examining the GOM change based on plume dilution during an air mass change; Ren et al. suggest both processes can occur on the same day [60]. Rutter et al. identified significant mercury-enriched plume episodes on average lasting a few hours. These spikes exhibited noticeable increases in reactive mercury (PBM and GOM) concentrations as few were concentrated enough in GEM to register a noticeable increase. The result was a greater plume proportion of GOM [40]. Photochemically produced GOM, conversely, can be identified through correlations with oxidants such as the bromine monoxide radical (BrO), the simultaneous presence of co-emitted O_3 and SO_2, and O_3 concentrations above 50 ppb_v [60]. In the case of air mass changes, GOM-co-pollutant correlations can be indicative of

sources. For example, a GOM correlation with CO can often differentiate between continental and marine sources given CO concentrations in marine air masses tend to be less than 100 ppb_v. Oxidation of GEM producing GOM is known to readily occur at the marine boundary layer [13] although marine GOM is often scavenged by sea salt aerosols and the ocean surface keeping GOM concentrations low [52,60].

1.2.3.2. Macro- and Micro-meteorological Influences

The concentration and distribution of atmospheric mercury species vary with wind direction, wind speed [17], temperature, and solar radiation. Near point sources, wind speed and wind direction heavily influence measured concentrations of mercury [26]. Wind direction correlations with GOM, for example, are indicative of source and transport-based enhancements especially when present with high co-pollutant SO_2 levels [60]. Wind direction is particularly important for Arctic AMDEs, with most events at Alert coinciding with winds originating from the Arctic Ocean [87]. Also, TGM across sites has a very strong anticorrelation with wind speed in areas where point-source emission dominated mercury dissipates [26]. With increased solar radiation, it is suspected that rural TGM concentrations were related to mercury evasion from soils at warmer temperatures while urban TGM concentrations were closely related to emission differences [51]. Similarly, Jen et al. found a strong correlation between TGM and temperature, and a moderate correlation with UV-B likely related to soil, water and particle-to-gas emissions, and enhanced photochemical reductions, respectively [26].

GEM spikes are often observed with shallow nocturnal boundary layers, low wind speeds, and higher local anthropogenic inputs [101]. Given equivalent emissions, a lower planetary boundary layer (PBL) would result in higher GEM concentrations, trapping mercury near the surface [101], and lower GEM concentrations throughout the day as solar irradiation increases the PBL height [104]. Higher boundary layers heights are also promoted by thermal mixing and higher wind speeds [101]. Related high-pressure conditions are also important for the enhanced photochemical oxidation of GEM to GOM [60].

The distribution of species is also influenced by sampling location and height as architectural features and structures can influence air flow patterns [17]. Sampling at heights ranging from 0.1 to 10 metres above ground, Johnson and Braman found lower

atmospheric mercury concentrations with increasing sampling heights with 4.9 ng/m^3 at 1 metre versus 2.7 ng/m^3 at 10 metres. This may be due to stable night-time vertical temperature and wind profiles which maintain an ground level emission-created mercury-height gradient [42]. Correlation of GEM with ground-emitted Radium can often support this finding [42].

1.2.4. Diurnal Influences

Johnson and Braman were among the first to study a diurnal influence on mercury measurements and found morning GEM dips when relative humidity was highest [60]. Conducting their research in urban Tampa in the early 1970s, they found higher concentrations of TGM, GEM and mercury(II) type compounds at night [42]. At sites where anthropogenic source emissions dominate TGM, diurnal patterns are often difficult to discern though spikes in night-time TGM may relate to lower night-time boundary layer [77]. At Almadén, a site of major mercury production in Ciudad Real Province, Spain, Tejero et al. estimated a factor of 2 increase in the nocturnal TGM concentration from diurnal mixing layer contaminant dilution and a nocturnal boundary layer height reduction [6].

Song et al. reported GEM, GOM and PBM were all highest in the early morning hours in Toronto, Canada after rising steadily throughout the evening suggesting nocturnal emission source mercury trapped in the stable night-time boundary layer outweighed photochemical GOM production [17]. Especially during the rainy season in Brazil, Fostier and Michelazzo observed the highest concentrations of TGM during the day from increased emissions, off-gassing from soils, and mixing differences from day to night [51]. In rural environments, nighttime GEM depletion is thought to have originally occurred by nitrate ($\bullet NO_3$) and OH$\bullet$ radicals but may in fact be caused by dew related scavenging and vegetation related deposition [104]. Duan et al. found little variation in GEM though it was slightly lower throughout the day. Night-time GEM concentrations were higher due to lower wind speeds and weaker vertical winds [43]. When correlated with a number of co-pollutants, GEM peaks at daytime were less likely due to photochemical oxidation [101] and instead from anthropogenic emissions.

Diel variation for GOM often shows enhancement in the afternoon from photochemistry with elevated O_3 or with co-emitted SO_2 [60,101]. No diurnal trends in GEM

was observed in a study in rural Germany, however, GOM concentrations increased during the day peaking in the early afternoon trending with solar irradiation induced local GOM-producing photochemical oxidation (offset by 2 hours). Marumoto et al., similarly, found daytime highs of GOM correlated with solar radiation across seasons likely due to GEM oxidation [111], as did Liu et al. at their rural Michigan site with concentrations rising from morning with increased solar radiation, O_3 concentrations, and boundary layer mixing heights. Indicative of photochemical transformation, weak but significant positive O_3 correlations with GOM were observed and negative correlations with GEM [41]. Lower concentrations of GOM at night are often associated to lower solar radiation (and thus lack of production) and its removal by high nocturnal relative humidity levels and lower temperatures which favour gas-particle partitioning [43]. At marine boundary sites, GOM diurnal cycles mirrored solar radiation except at low radiation, high RH (>90%) conditions where photochemistry is inhibited and gas-to-particle transformations are enhanced by aqueous phase aerosol coverage. [52]

1.2.4.1. Seasonal Influences

Atmospheric mercury and its bulk species will also undergo seasonal variations depending on location. Over a 10-year study of mercury at Alert, Nunavut, Steffen et al. observed GOM increases from March to July, peaking in May, from photochemical oxidation induced atmospheric mercury depletion events [13,43,103]. Though these events cease when temperatures rise above 0 °C, GOM levels remain high into July. As expected these increased concentrations coincide with drops in GEM concentrations [87]. In non-Arctic environments, increased springtime GOM concentrations may more closely related to snowmelt evasion [19]. At Fukuoka, Japan, GOM concentrations are highest in the Spring with lower GOM summer values resulting from humidity-enhanced scavenging [111]. GOM concentrations can also peak during other times of year. For example, during Michigan summers, Liu et al. observed higher GOM levels which they also related to enhanced photochemistry at higher temperatures involving oxidants like O_3 [41].

Table 1.4. Important milestones towards conventional atmospheric bulk speciation – GOM, GEM and PBM

Reference	Analysis	Sample Collection	Sample Preparation	Separation	Analysis
Stratton et al. 2001 [94]	Reactive Gaseous Mercury	HCl Absorbing Solution	Sampling at 15 – 20 L/min for 1 – 2 hours using a refluxing mist chamber with a fine mist of 20 mL of HCl/NaCl absorbing solution. A Teflon membrane retains the Hg(II)-enriched absorbing solution.	The absorbing solution and rinse solution for the chamber are withdrawn and reduced with stannous(II) chloride ($SnCl_2$) and measured as GEM.	CVAFS – Brooks Rand
Sheu and Mason 2001 [14]	Gaseous Oxidized Mercury	Cation Exchange Membranes	Sampling at 3 – 5 L/min over 6 and 24 hours through a five-stage filter pack with Teflon and cation exchange membranes.	Reduction by $SnCl_2$.	CVAFS
	Particulate Bound Mercury	Teflon Filters		Filters oxidized in BrCl for 30 minutes followed by pre-reduction using hydroxylamine hydrochloride and reduction by $SnCl_2$.	
Dommergue et al. 2002 [77]	Total Gaseous Mercury	Gold Trap	Sampling at 1 L/min for 15 minutes through 0.5 µm Teflon filter with amalgamation to gold trap.	Double amalgamation and thermal desorption.	CVAFS – Gardis 1A+
Sakata and Marumoto 2001 [113]	Particulate Bound Mercury	Quartz Filters	Sampling at 1200 L/min for 24 hours.	Thermal desorption to AAS.	CVAAS – Nippon AM-2
	Total Gaseous Mercury	Gold Trap	Sampling at 0.5 LPM for 55 minutes through Teflon filter with amalgamation to gold trap.	Thermal desorption to AAS.	
Landis et al. 2002 [93]	Gaseous Elemental Mercury	Gold Trap	Sampling at 1.5 L/min for 5 minute intervals.	Thermal desorption of amalgamated mercury to detector.	CVAFS – Tekran 2537
	Gaseous Oxidized Mercury	KCl Denuder	Sampling at 10 L/min through a 2.5 µm cut-point impactor maintained at 50 °C followed by a Teflon Filter Pack or quartz thermal filter tube for 1-2 hours.	Pyrolyzer heated to 800 °C to decompose mercury compounds to GEM. Filter heated to 800 °C to measure PBM followed by thermal desorption at 500 °C of the denuder in a clamshell furnace to decompose GOM to GEM.	CVAFS – Tekran 1130
	Particulate Bound Mercury	Quartz Filters			CVAFS – Tekran 1135
Freitas et al. 2005 [54]	Particulate Bound Mercury	Polycarbonate Filters	Sampling at 15 – 17 L/min for 10 min every 2h for 1 week using a Gent-type, stacked-filter unit sampler with PM10 and PM2.5 fractions.	Filters placed in polyethylene or Al foil containers were subjected to thermal neutral irradiation for 7 hours with Hg determined based on gamma emissions 4 weeks later.	INAA
Lynam et al. 2005 [109]	Particulate Bound Mercury	Quartz Filter	Sampling at 10 LPM through a 2.5 µm Teflon-coated cyclone, to denuded and undenuded filters where KCl and/or KI denuders were heated to 50 °C. Sampling times ranged for 10, 14 and 24 hours.	Filters heated to 700 °C and swept by argon carrier gas to an ICP-MS.	ICP-MS
Xiu et al. 2005[114]	Particulate Bound Mercury	Glass Fiber and Quartz Fiber Filter	Sampling at 600 L/min for 24 hours through four size fractionator with 18 µm, 8 µm, 3.7 µm and 1.6 µm cut-offs.	Filters are digested in $KMnSO_4/H_2SO_4$ solution at 95 °C under reflux and then Hg^{2+} is reduced by $SnCl_2$ to GEM.	CVAAS
	Inert Particulate Phase Mercury			The difference between TPM and the sum of VPM and RPM	
	Reactive Particulate Phase Mercury			VPM Filters are sonicated for 30 minutes to release RPM.	
	Volatile Particulate Phase Mercury			Filters extracted with 0.33 M HCl and solution bubbled with 600 L/min of N_2. Vapour collected in $KMnSO_4/H_2SO_4$ and analyzed as above.	

1.2.5. The Oxidation, Reduction and Methylation of Mercury

The chemical and physical transformation of GEM, GOM and PBM have important implications for the fate of atmospheric mercury and has previously been described by Subir et al. [115,116] GEM can be oxidized to GOM [13,117] through photo- and surface-enhanced oxidations with oxidants such as: O_3 [103,118], OH• [103], hydroperoxyl radicals (HO_2•) [103], hydrogen peroxide (H_2O_2) and the OH• radicals it produces [14], hypochlorous acid/hypochlorite ion ($HOCl/OCl^-$) [14], nitrogen pentoxide (N_2O_5) [103], nitrogen dioxide radicals (•NO_2) [103], nitrate (NO_3) [14], chlorine (Cl_2), [103,119] and bromine (Br_2) [103,119,120]. Still the oxidation of elemental mercury to oxidized species in the atmosphere, and the species formed, remain poorly understood [13]. These photo-oxidation processes are major drivers of diel GEM and GOM patterns especially in rural and Arctic environments [104,121].

Springtime mercury oxidation chemistry is often associated with high concentrations of hydrogen peroxide which can be produced by HO_2• radicals, formaldehyde, carbonyl, nitrous oxide and nitrous acid photolysis [43]. Siegneur et al. suggested the resulting species of the oxidation of GEM with hydrogen peroxide was mercury hydroxide ($Hg(OH)_2$) [13]. Oxidized mercury species Additional oxidants, OH• and O_3 can be produced on haze days from fine particulate and other pollutants.

Mercury depletion events during the Arctic spring that involve oxidation by bromine species produce mercury(II) bromide and HgBrOH [13,98]. In polar regions, at the marine boundary layer and the upper atmosphere, the oxidation of mercury by halogens is actually favoured at lower temperatures [11,91]. The rates of these reactions differs greatly between halogens and are much slower oxidations by atomic halogens [109].

Mercury oxide (HgO) can arise from the oxidation of elemental mercury with O_3 on heterogeneous surfaces [39,122], NO_3 [13,123], and is readily observed on fine, micron-sized particles [39]. Doubt exists as to whether the gaseous species can occur or whether it only exists on particulates; a proposed HgO_3 intermediate decomposes to particles [124] or forms $Hg(OH)_2$ with water [13,125].

GOM can also be photo-reduced to GEM on surfaces such as dust [39,126], by O_3 on quartz surfaces [13,127], in power plant flumes [11], and by sulfur species in the atmosphere

such as SO_2 and in aqueous systems by sulfite ion (SO_3^{2-}) [43,122] and hydroperoxyl ions [14]. Oxidized mercury is also capable of being reduced by iron in aqueous systems [43,128,129].

Mercury methylation occurs in soils, on sediment, in lake and wetland anoxic zones [18], and within sulfur reducing and methylating microorganisms. From water to plankton, methyl mercury concentrations increase one hundred thousand times alone [18]. In 100 ppb mercury(II) chloride artificially contaminated soils, Johnson and Braman found releases of methylmercury(II) and dimethyl mercury compounds [42]. Demethylation can also occur in soils and sediments releasing GEM [42,130]. Dimethylmercury is transformed by free chlorine atoms, OH• limiting its lifetime [16,131] and undergoes disproportionation with $HgCl_2$ to form methylmercurychloride [42]. In the 1970s, Braman and Johnson measured significant concentrations of methylmercury (40% of total mercury) and mercury(II) type compounds [42] and in the early 1980s, Schroeder and Jackson measured a substantial amount of gaseous organic mercury as mono-methylmercury chloride (14%) near a municipal wastewater plant [16]. Dimethylmercury emissions can also evade the ocean surface [11,132]. Aside from work by Brossard and Lord, few atmospheric organic mercury measurements have been taken since as they are thought to only comprise of low pg/m^3 concentrations [11].

1.2.6. Consequences of Atmospheric Mercury Speciation

The chemical speciation of atmospheric mercury determines its dry and wet deposition velocities, solubility, bioavailability and toxicity [13], mobility [16], and ultimately, the atmospheric residence time of the species [103]. Wet deposition, or precipitation-driven atmospheric mercury removal processes [53], and dry deposition rates are expected to be similar; dry deposition is harder to measure [133] and wet deposition processes account for 2 – 5% of the year [11]. Total mercury deposition rates are estimated to have increased as much as 20 times from pre-industrial backgrounds to 25 $\mu g/m^2 \cdot$year [88]. Ocean systems receive 90% of their mercury influx through atmospheric deposition processes [14,67], but can also serve as major mercury emission source through evasion [52]. Dry deposition velocities for GOM generally range between 1 – 5 cm/s [93] and differ based on surface type

with GOM measured as 0.4 cm/s on grass, 7.6 cm/s for wetland canopy [134] and 1 cm/s on snowpack. As high as 40% of deposited mercury is re-emitted depending on the surface [11].

Liu et al. observed little GOM variation in rural Dexter suggesting that the lifetime of GOM species from long range transport from urban anthropogenic sources is limited due to deposition and gas-particle conversion [41], to as little as a few days [18]. Elevated or variations in GOM concentrations in rural areas then is likely due to local photochemical production, locally emitted sources or particle-to-gas conversations from less readily deposited particulate mercury [41].

Dry deposition can be directly measured but is often modelled based on GOM data captured by KCl denuders. The deposition velocities of GOM are the highest of the bulk mercury species [87] but will differ based on chemical speciation. For example, the dry deposition velocity of HgO is estimated to be twice that of $HgCl_2$ [99]. Varying scaling factors used in modelling, for potential GOM compounds, will produce marked differences in dry deposition velocities and comparisons between actual and modelled data can help surmise potential compounds that are being collected by the denuders. These determinations are complicated when more than one GOM compound, with different chemical and physical properties, are co-collected. As a result, correlations between measured and modeled dry deposition values are difficult to attain [65], with uncertainties in total deposition fluxes ranging from ± 30–50% [11].

Though the concentrations of GEM are much higher than GOM and PBM, dry deposited GEM is not expected to remain deposited and is re-emitted even on snow in Arctic environments [87,135]. The deposition velocity of GEM to vegetation is dependent on stomatal exchange and corresponds roughly to 0.01–0.05 cm/s [133,136]. Nearly 95% of deposited mercury is expected to be GOM or PBM. Deposited GOM on snow is also subject to re-emission or photoreduction and re-emission as GEM. Butler et al. report that nearly half of all deposited mercury is reemitted within 24 hours as GEM [101]. Still, mercury concentrations in snow tend to follow seasonal trends of GOM and increase when GOM predominates over Arctic PBM suggesting that the dry deposition of GOM predominates over PBM wet deposition by snow [87].

Wet deposition is determined by measuring mercury concentrations in rain or snow and the rate of precipitation [53]. While the solubility of GOM species will vary, it is estimated

that the major contributors to mercury in rain is GOM, emitted as such or in-cloud oxidized GEM. GOM is soluble in cloud droplet water and thus readily scavenged [11,26]. While Stratton et al. and others have typically seen decreased concentrations of GOM following precipitation events [94], wet deposition is not necessarily or solely correlated to precipitation [137] but also to atmospheric convection during storms and down mixing from the free troposphere [65,138]. Henry's solubility is often used to predict wet deposition velocities [15]and are species dependent. $HgCl_{2(g)}$ has a Henry's solubility between 6.3 x 10^2 and 4.2 x 10^4 mol/Pa·m^3 [70,89].

The pH, chlorinity and organic content of surface waters all have an impact on the bioavailability of mercury and the degree to which mercury is absorbed into microorganisms where methylation is possible. Methylmercury is the predominant form of mercury found in fish and accumulates in the body's tissue. At equilibrium, methylmercury will be present 1,000,000 times more in water than air and has a Henry's solubility of 15 to 26 mol/m^3 Pa [84,90]. Hence, despite forming very little of total atmospheric mercury, methylmercury consists of between 0.5 – 2.5% of mercury in precipitation [11]. Despite major decreases in the mercury emitted in the 1990s in Europe, mercury in fish in Sweden only decreased by 20% and exceeded health limits of (0.5 mg/kg) in half of Sweden's lakes. Concentrations of methylmercury remain five times higher than the end of the 19th century [8]. In the Clean Water Act, the USEPA recommends fish tissue have less than 0.3 mg/kg of methylmercury content [18].

Soils and sediment act as sinks for mercury where the element sequestered due to complexation with organic compounds thereby accumulating. Here, microbial processes are impacted (at 0.2 – 0.3 mg/kg concentrations in soils), flora and fauna ingest the contaminant, and mercury leaches into ground and surface water if the complexes formed are soluble in runoff [8].

1.2.7. Techniques of Measuring Atmospheric Gaseous Mercury Speciation

Elemental mercury and particulate mercury were the first bulk species of atmospheric mercury measured [81]. Early studies of mercury involved trapping multiple mercury species in either potassium permanganate solutions on solid sorbents such as activated carbon, or thin films noble metals [82]. Later, mercury was speciated into three main bulk

species: gaseous elemental mercury (GEM), gaseous oxidized mercury (GOM) or reactive gaseous mercury (RGM) and particulate bound mercury (PBM).

1.2.7.1. Gaseous Elemental Mercury

Gaseous Elemental Mercury (GEM) is conventionally measured through amalgamation to gold traps, thermal desorption followed by detection using cold vapour absorption (CVAAS) or fluorescence spectroscopy (CVAFS) at a wavelength of 253.7 nm. This wavelength corresponds to the $^1S_0$ to $^3P_1$ transition consistent only with GEM, and no other mercury species. Thermal decomposition to GEM from other GOM species, or chemical digestion of PBM releasing GEM, allows for GOM, PBM and total mercury measurements [81]. For CVAFS, a plume of elemental mercury absorbs 253.7 nm light and phosphoresces with a detector perpendicular to the incoming beam [16]. CVAAS, conversely, measures the difference in intensity between the incident and transmitted 253.7 nm light through the plume. Instruments are calibrated using temperature-controlled permeation sources of elemental mercury or through direct injection of a known quantity of saturated mercury vapour. The absolute analytical detection limit using these methods can be low as 0.5 pg when combined with double gold trap amalgamation pre-concentration [139]. Method detection limits of CVAFS methods using the routinely used Tekran 2537A is on the order of tens to hundreds of pg/m^3 with a manufacturer analytical detection limit of 0.75 pg [87]. These detection limits are many times lower than background GEM concentrations, irrespective of site [41], thus allowing for high temporal resolution as short as 5 minutes [52,139]. The range of linearity for CVAFS, and for other techniques for measuring GEM like dc discharge emission is 10^3 [16,81], and the reproducibility for a CVAFS, like the Tekran 2537A, is approximately 20% [52].

In determining possible sorbents for pre-concentration, Braman and Johnson initially set out to test silver wool, silver-coated glass beads, activated charcoal and gold-coated glass beads. Silver wool failed to desorb mercury completely and suffered from hardening with use. Activated charcoal, similarly, suffered from incomplete desorption and interferent collection. [82] Both thinly coated silver and gold glass beads readily captured and desorbed mercury with heating, though gaseous organic mercury was not captured on silver [82]. Silver would also been oxidized by hydrogen sulfide and SO_2 slightly reducing its response

Table 1.5. Selected studies of atmospheric mercury involving major advancements or notable new site locations in conventional mercury speciation measurements

Reference	Site	Time	GEM (ng/m^3)	GOM (pg/m^3)	PBM (pg/m^3)	Notes
Munthe et al. 2001 [73]	Tuscany, (Italy)	June 1998	NA	22 [3 – 41]	56 [13 – 314]	
			1.98 [12.8 – 3.38]			
			NA	18 ± 5 [10 – 23]	NA	Tubular Denuder
				20 ± 12 [4 – 35]		Annular Denuder
				17 ± 11 [3 – 32]		Mist Chamber
				39 ± 2 [37 – 41]		Annular Denuder Rinse
Sheu and Mason 2001 [14]	Solomons, MD (USA)	July 1998, October 1999	1.89 ± 0.94	40 ± 50	20 ± 50 [ND – 147]	Filter Pack Method
			1.83 ± 0.43 [1.03 – 2.50]			Filter Pack Method
Stratton et al. 2001 [94]	Oak Ridge, TN (USA)	March 1995	NA	123, 106	NA	Research Watershed
				361, 458	NA	Laboratory Rooftop
	Richmond, IN (USA)	September – October 1995	NA	102 ± 29	NA	0.05 M NaCl, Sept.
				94 ± 16	NA	0.25 HCl, Sept.
				141 ± 44	NA	0.25 NaCl/0.01 M HCl, Sept
				80 ± 14	NA	0.25 NaCl/0.01 M HCl, Oct
Dommergue et al. 2002 [77]	Grenoble, ARA (France)	November 1999, January, April, July 2000	3.4 ± 3.6 [0.1 – 37.1]		NA	Near Chlor-alkali plant
Feng et al. 2004 [140]	Toronto, ON (Canada)	November 2001	2.5 ± 0.5		24.8 ± 1.4 [23.2 – 25.9]	PM10
Lynam and Keeler 2005 [109]	Detroit, MI (USA)	July 2001, 2002	No Data	No Data	[1 – 31], [4 – 20]	KCl denuded filters
					NA , [2 – 13]	KI denuder filters
					[3 – 39], [4 – 28]	KI/KCl denuded filters
					[2 – 18], [4 – 17]	Undenuded filters
Wang et al. 2006 [58]	Beijing (China)	Monthly 2003; Seasonally 2004	No Data	No Data	680 ± 620 [130 – 2400]	Suburban site
					1180 ± 820 [180 – 3510]	Urban site
Fostier and Michelazzo 2006 [51]	Campinas, São Paulo State (Brazil)	December 2002 & May 2003	7.7 ± 7/1 [0.8 – 37.8]		465 ± 252 [104 – 778]	Residential Site
		January & May 2003	6.3 ± 3.9 [0.3 – 15.4]		332 ± 351 [24 – 1231]	Industrial Site
Choi et al. 2008 [19]	Huntington, NY (USA)	June 2006 – May 2007	1.4 ± 0.4 [0.5 – 2.5]	1.8 ± 2.2 [ND – 45.4]	3.2 ± 3.7 [ND – 54.0]	
Li et al. 2008 [101]	Femman, Göteborg, (Sweden)	January – March 2005	1.96 ± 0.38 [1.35 – 6.42]	2.53 ± 4.09 [0.34 – 32.84]	12.50 ± 5.88 [3.89 – 20.26]	Industrial Site
	Rörvik, (Sweden)		1.63 ± 0.19 [1.37 – 19.7]		No Data	Rural Site
Rutter et al 2008 [133]	Milwaukee, WI (USA)	April 2004 and May 2005	No Data	[3 – 55]	[3 – 90]	< 2.5 μm
Rutter et al. 2009 [40]	Mexico City, USA	March 2006	7.2 ± 4.8	62 ± 64	187 ± 300	< 2.5 μm
Song et al. 2009 [17]	Toronto, ON (Canada)	December 2003 – November 2004	4.5 ± 3.1 [0.5 – 44.1]	14.2 ± 13.2 [<4 – 284]	21.5 ± 16.4 [<4 – 252]	< 2.5 μm
					46.9	Total Filterable Mercury
Xiu et al. 2009 [88]	Shanghai, China	July 2004 – April 2006	NA	NA	560 ± 220 [7 – 1450]	Urban Site
					330 ± 90 [200 – 470]	Suburban Site

while gold is relatively inert for most atmospheric species [82,106]. The synthesis methods for both metallic-coated glass beads described by Braman and Johnson produced 90% coverage and 13.8% silver (w/w), and between 50 – 70% coverage and 20% gold (w/w), respectively. Dumarey et al. were able to achieve nearly complete coverage (80 – 100%) with higher mass contents of silver (35% w/w) and comparable mass content of gold (15 – 20% w/w) on sand. Breakthrough of mercury occurs only beyond loadings of 1 – 3 μg of mercury per gram of gold [82].

Assembled as tubes filled with sorbent, GEM amalgamated to the first 1.0 cm of the gold sorbent [81]. Before desorption, these traps were sealed with Parafilm to limit mercury loss and dust contamination [42]. Blanking and desorption occurred at 500 °C and upon desorption, elemental mercury was ionized with Helium plasma and detected using highly sensitive and selective dc discharge emission detection at the 253.65 nm Hg emission line [42,81]. Below 450 °C, mercury is incompletely desorbed [82]. Two (gold) sorbent traps are placed in sequence to reduce interferents and a low flow rate of 0.1 L/min produced the highest and sharpest signals. Desorption occurred using a gas-stop technique where heating/desorption occurs with no carrier gas flow before a pulse of carrier gas sweeps the mercury plume to the detector [82]. Carrier gases for CVAAS, CVAFS and dc discharge emission detection include Helium [81] and Argon. Gases are generally scrubbed of mercury and particles using a gold trap and particulate filter, respectively before transferring sample to the detector. Initial absolute mass detection limits were on the order of 100 pg [82] but have since been reduced to 5 pg and below, with calibrations performed using a temperature controlled saturated mercury vapour sources [42].

Weigelt identified four significant errors in GEM detection: the efficiency of the gold cartridges, sample volume errors, calibration and detector signal drift [139]. Organics and other contaminants de-activate the gold cartridge and require frequent replacement as do the mercury lamps used in detection. Accuracy in sampling flow rates is essential to ensure precise sampling volumes as is precise temperature control as even a few degrees can impact the amount of saturated mercury vapour present in a calibration standard.

1.2.7.2. Total Atmospheric Mercury

Determining total atmospheric mercury (TAM) has typically involves amalgamation to gold and either thermal desorption/decomposition or pyrolysis. Both methods involve conversion to GEM for subsequent measurement. Johnson and Braman used gold coated glass beads to trap TAM which operationally was defined as the sum of gaseous elemental, mercury(II) type, dimethyl mercury, and methylmercury(II) type compounds that were capable of amalgamating to gold [42]. Through thermal desorption and decomposition to GEM, the sum of these species can be measured by dc discharge emission, CVAFS or CVAAS. As the method involved amalgamation, PBM would have likely been missed unless the entire particle was trapped in the sorbent.

Schroeder and Jackson, conversely, built a pyrolysis tube to measure TAM by placing crushed quartz chips (10 – 20 mesh size) situated between two quartz wool plugs within a quartz tube. All mercury species were thermally decomposed to GEM by heating to high temperatures. To achieve 100% pyrolysis efficiency, dimethyl mercury, methylmercuric chloride and mercuric chloride species required temperatures of at least 500 °C, 700 °C and 900 °C, respectively [16]. To blank pyrolysis tubes, Schwartzendruber et al. heated the tube and quartz chips for 15 hours at 550 °C [133].

1.2.7.3. Total Gaseous Mercury

Total gaseous mercury (TGM) is operationally defined as volatile and semivolatile elemental mercury and inorganic mercury species that have passed through 0.45 μm filter or quartz wool plugs and either amalgamated or adsorb on gold, silver or other metals [73,106]. Total gaseous mercury can be measured using the same instruments as GEM and have analytical detection limits, interferents, calibration procedures and maintenance.

The Tekran 2537A measures TGM by drawing air through a polytetrafluoroethylene (PTFE) filter at 1.5 L/min for 10 minutes on to a gold cartridge, before thermal desorption and decomposition and measurement as GEM. The system employs two gold cartridges which alternate between sampling and analysis. The detection limit is 0.15 ng/m^3 [73]. TGM measurements using a Gardis CVAAS similarly, involves drawing sample through a PTFE membrane for 10 minutes at 1 L/min with ambient air acting a carrier gas. A detection limit of 0.1 ng/m^3 is achieved [73]. Both methods are semi-continuous and automated. TGM can

also be measured using manual gold traps where air is drawn through gold wire-quartz glass trap at 0.5 – 2 L/min and subsequently analyzed using CVAFS [73]. In all cases, the detection limit well below typical background levels of gaseous mercury present in the atmosphere [111].

Weigelt et al. using EN 15853 method for TGM achieved a method detection limit (MDL) of 33 pg/m^3 for a 15 L sample volume [139]. Low MDLs (concentrations at which there is 99% confidence that the measured concentration is distinguishable from blanks) were ensured through regular maintenance including gold cartridge replacement, lamp adjustments and filter replacement. QA/QC tests include a zero blank, linear span checks, and the variability between identical instrumental units was found to be 12 – 12.5% for TGM from 0.1 ng/m^3 and 4 ng/m^3 concentrations [139]. Like GEM, the linearity for TGM curves are greater than 0.99, with no calibration point deviating more than 10% from the curve [26].

1.2.7.4. Organomercury and Hg(II) Type Compounds – Sorbent Tubes

There are a number of techniques that have been developed for measuring gaseous oxidized mercury including: refluxing mist chambers, ion-exchange membranes, KCl-coated tubular/annular denuders [93], thermal desorption analysis, sorbent preconcentration and desorption, and mass spectrometry.

Johnson and Braman developed a speciation sorbent stack method of measuring GEM, Hg^{II} type and methylmercury(II) type, and dimethylmercury compounds through selective sorption to, and sequential desorption from, a series of sorbents packed in quartz tubing. Hg^{II} type compounds, with chloride, bromide, nitrate and acetate counters ions, were selected for their volatility and as a proxy for atmospheric inorganic mercury species [81]. The speciation stacks sorbents were chosen for their selectivity for each bulk species. Sorbent tubes were connected with PTFE Teflon, sealed airtight, blanked and were used to for sample ambient air at 0.75 – 2 L/min flow rates for 10 minutes to 2 hours, depending on ambient concentrations. Johnson and Braman explored the short term variability of mercury concentrations and found no significant difference between long-term sampling (70 minutes) and the average from shorter–term samples (10 minutes) [42]. The sorbent tubes were sealed with parafilm and sampled within 24 hours through thermal

decomposition/desorption and measurement as GEM by dc discharge [81]. The MDL for the method was 130 pg/m^3 and 70 pg/m^3 for Hg(II) type and dimethylmercury, respectively [42].

The method of speciation sorbent stacks relies on species-selective trapping. Dimethylmercury did not absorb on copper or silver sorbent but did amalgamate to gold. Hg^{II} species were retained on HCl-vapour treated Chromosorb-W as a proposed hexachloromercurate complex [81]. Methylmercury(II) species absorbed on silver but slowly off-gassed at ambient temperatures. The species were believed to form methylmercury(II) chloride on the HCl-vapour Chromosorb-W sorbent, and were absorbed quantitatively and selectively to NaOH treated Chromosorb-W as methylmercury(II) hydroxide [81]. Braman and Johnson remarked that while ethylmercury(II) chloride would be retained on the Chromosorb-W (NaOH) sorbent, the less volatile phenylmercury(II) chloride was retained and contaminated the Hg^{II} type HCl treated Chromosorb-W trap. Both dimethylmercury and methylmercury(II) chloride were demethylated and Hg^{II} species decomposed to GEM upon heating of the sorption tubes. In terms of interferents, hydrogen sulfide, SO_2 and water vapour were not seen to interfere with the measurements nor were there reactions between any of the target species [81].

Brosset classified mercury compounds in four classes based on their Henry solubility: vapor phase Hg^0 (Hg^{Ia}), organic mercury in the form Org-Hg-Org (Hg^{Ib}), inorganic mercury (Hg^{IIa}) in the form Inorg-Hg-Inorg, and organic mercury with inorganic counter ions (Hg^{IIb}) as Org-Hg-Inorg. Hg^{IIa} species differed from the Hg^{IIb} in that only the former is reduced by $SnCl_2$ but both species were reducible with sodium borohydride. Through careful experimentation, Hg^{IIa} was later believed to be formed by oxidation occurring during sampling while Hg^{IIb} was anthropogenically emitted especially from coal-fired plants [105].

Like Johnson and Braman, Brosset and Iverfeldt used sorbents to capture a variety of mercury species. Iverfeldt's gold trap consisted of quartz and gold grain layers whereas Ferm-Brosset gold traps involved coating gold on quartz pellets. Hg^{II} was trapped on Porapack-Q polymer in addition to water bubblers. Species were either bubbled or desorbed to gold traps before measurement by double amalgamation atomic-emission spectroscopy [106]. The reproducibility of the gold traps were higher than 98% with a near-complete retention of 98% for 0.36 m^3 samples. At large surface volumes, gold traps were deactivated

by interferent surface coverage (thought to be ammonium salt or ammonia complexes) but were restored by heating above 200 °C or washing. Porapack traps suffered from slow desorption, and bubblers were influenced by species in ambient air, like hydrogen peroxide and O_3, which impacted the solution pH and either oxidized Hg^0 or reduced Hg^{2+}.

Using a favourable Henry's solubility, Brosset and Lord bubbled ambient air through milliQ water trapping methylmercury chloride and extracting it with dichloromethane. To this organic layer, a small quantity of milliQ water was added before boiling off the organic layer. Sodium tetraethyl borate transformed the species into volatile methylethyl mercury which when subsequently extracted to a Carbotrap column. The Carbotrap column was heated to 250 °C to transfer the species to cryogenic GC column which separated the volatile mercury species. Eventually, the species were pyrolyzed at 900 °C and measured using CVAFS as GEM [84]. The method, unfortunately, suffered from long sampling times of weeks and was biased by blanks [84].

1.2.7.5. Gaseous Oxidized Mercury – Refluxing Mist Chamber

Mist chambers involve passing GOM-containing air through a nebulizer produced, water-soluble gas scrubbing/absorbing mist of dilute HCl that extracts GOM species into the liquid phase [14,94]. Flow rates of 10 – 20 L/min allow for short sampling times ranging from a half hour to two hours [14]. The absorbing solution, consisting of micron droplets, is retained by a hydrophobic Teflon membrane thus refluxing the scrubbing solution [94]. At the conclusion of sampling, a small volume of HCl is used to rinse the chamber collecting the 10% of total GOM lost to chamber walls. Samples are usually processed within hours of collection with $SnCl_2$ used to reduce the Hg(II) species to GEM which is subsequently measured by CVAFS [73]. With mist chambers, MDLs as low as 5 – 10 pg/m^3 are possible with inter-comparison chamber agreement within 20% [14,94].

Trace-metal grade reagents are used to reduce blanks and sodium chloride, used to enhance scrubbing solutions efficiency, is baked at 500 °C to remove mercury [94]. Mist chambers are washed with 1% bromine(I) monochloride (BrCl) solution and similarly baked at 500 °C [94]. Stratton et al. observed infiltration of the Teflon membrane with GOM resulting in memory effect contamination which was only able to be cleaned by frequent rinsing with HCl [94]. Across multiple samples, back-up mist chambers were found to have

similar GOM concentrations with no correlation with GOM concentrations in the sampling mist chambers [94]. Only at high GOM concentrations, above 500 pg/m^3, was collection efficiency in the sampling mist chamber impacted [94].

The scrubbing solution could reduce other water-soluble gases which GEM or GOM could react with however given the short sampling time; this oxidation was negligible [14]. As a precaution, the mist chambers were covered with aluminum foil to block sunlight [73]. Teflon packs could be used to remove particulates from the air stream [14], though Stratton et al. found no significant differences between filtered and unfiltered samples [94]. Between one and four nozzle nebulizer designs, Stratton et al. found no statistical difference in measurements though higher flow rates were possible with a four nozzle design [94]. GOM collection efficiency was dependent on the concentration of HCl peaking at 0.5 M where Hg^{II} was predominantly present as the non-volatile and stable $[HgCl_4]^{2-}$ complex instead of semivolatile mercury(II) chloride. Adsorption of GOM on the surface of the chamber was disrupted by pHs lower than 1.5 [94]. Soda-lime traps are placed downstream of the chamber and upstream from the pump to prevent corrosion [94].

Sheu and Mason found good agreement between HCl mist chambers and KCl-coated denuders though collection was 34% higher with mist chambers than membrane filter packs though no breakthrough was observed in the backup exchange membrane suggesting possible GEM oxidation in the reflux chamber [14].

1.2.7.6. Gaseous Oxidized Mercury – KCl-coated tubular denuders

Denuders have been used to separate reactive gases, such as ammonia, nitric acid and sulphur oxides, from polluted air and particulates [73]. Tubular denuders are 8 mm in diameter quartz tubes whose interiors are coated with KCl. Air is sampled at 1 L/min while the tube is heated to 45 °C to prevent water from condensing, the denuder is heated to 450 °C and drawn into a CVAFS using N_2 [73]. Tubular denuders are hampered by lower flow rates in comparison to annular denuders [73].

1.2.7.7. Gaseous Oxidized Mercury – KCl-coated annular denuders

The use of KCl-coated denuders with mercury was first explored by Larjava et al., Xiao et al., modified by Landis et al., and later commercialized by the Tekran Corporation [141].

Denuders are comprised of a 15 mm outer quartz tube with an 8 mm inner quartz annulus. KCl solution is drawn into the space between the inner annulus and outer tube to coat tubing with etched surfaces. Excess KCl solution is wiped from the inlet, dried in Hg-free air and heated to 500 °C to blank. Upstream from the denuder is a cyclone removing large micron-sized particles, generally 2.5 μm and larger [14]. Ambient air is drawn through the heated denuder between 5 L/min [73] to 10 L/min, and GOM species undergo an interaction with the KCl matrix [10]. Smaller particles travel unhindered due to laminar flow nor does GEM adsorb to the surface [10]. GOM is collected with a diffusion coefficient greater than 0.1 cm^2/s. Downstream from the denuder is often a particulate filter for measuring particulate bound mercury (PBM). After sampling, the denuder is heated to 500 °C for a half hour to an hour, resulting in the thermal decomposition of GOM species to GEM which is analyzed using atomic fluorescence [10]. GOM can also be measured by rinsing the denuder with ultrapure water, $SnCl_2$ reduction and measurement of GEM via CVAFS [73]. Field denuders are analyzed within 1–4 days and lab denuders within the day [10,133].

KCl denuders suffer from having a consistent calibration method as trapping efficiencies vary between the chemical compounds that comprise GOM. Instead, elemental mercury is used to calibrate the method following the thermal decomposition of GOM species. Absolute detection limits of 0.5 – 1 pg are readily possible [10,139], with MDL at sub pg/m^3 concentrations [139]. Denuder blanks can be hampered by incomplete episodes of desorption, memory effect from previous sampling runs and worsening trapping efficiencies with coating age requiring regular, if not weekly, replacement of the denuder coating [14,41]. Still, the response of the Tekran analyzer is linear over several magnitudes of order [139]. Manual denuders used by Liu et al. were found to have an MDL of 2.2 and 2.4 pg/m^3 for a rural and urban Michigan site respectively. Unlike GEM, a significant percentage (64% and 13%) of ambient rural and urban GOM measurements were below detection [41]. In comparing manual and automatic denuders, higher signal responses were found with the automated denuder systems [21].

Table 1.6. Recent advancements in atmospheric mercury chemical speciation techniques

Reference	Analysis	Sample Collection	Sample Preparation	Separation	Analysis
Huang et al. 2013 [141]	Gaseous Elemental Mercury	Gold Trap	Ambient air, scrubbed of particles, sampled at 1 L/min.	Thermal desorption of amalgamated mercury. See AMnet guidelines for standard operating and cleaning procedures	CVAFS – Tekran 2537
	Gaseous Oxidized Mercury	KCl Denuder	Ambient air, scrubbed of particles, sampled at 4 L/min for manual denuders for either 1 or 2 hours followed by 1 hour desorption time.	Thermal desorption from denuder followed by pyrolysis decomposition to GEM. See AMnet guidelines for standard operating and cleaning procedures	CVAFS – Tekran 1130
		Cation Exchange Membranes	Sampling at 1 L/min for 8 hours through two membranes in series.	Membranes were heated in a tube furnace whose temperature was ramped 2.2 °C/min from 60 °C to 185 °C. Desorbed mercury passed through a pyrolyzer to fully convert species to GEM, before passing through soda lime and Teflon particulate filter on route to the CVAFS. Residual mercury analyzed using EPA Method 1631E.	CVAFS – Tekran 2537
		Nylon Membranes			
Deeds et al. 2015 [142]	Mercury(II) Bromide Mercury(II) Chloride	Shredded PFA Teflon	Sampling at 1L/min through traps heated to 50 °C for 12 – 24 hours.	Analytes are heated in a modified APCI-MS inlet at 200 °C for 1.2 minutes before desorbing using 1 L/min SF_6:Isobutane carrier gas drawing analyte into the APCI ion source forming mercury(II) halide-fluoride adducts.	APCI-MS – Agilent 6130
Gustin et al. 2016 [143]	Gaseous Elemental Mercury	Gold Trap	See AMnet guidelines. Sampling at 7 LPM through 3.0 µm impactor, denuder and particulate filter following a 1 hour sampling and 1 hour desorption cycle.	See Landis et al. 2002.	CVAFS – Tekran 2537
	Gaseous Oxidized Mercury	KCl Denuder			CVAFS – Tekran 1130
	Particulate Bound Mercury	Quartz Filter			CVAFS – Tekran 1135
	Reactive Mercury - UNRRMAS	Cation Exchange Membranes	Six port sampling system with three sets of two cation exchange and three sets of two nylon membranes in series.	See Huang et al. 2013	CVAFS – Tekran 2537
		Nylon Membranes			
Jones et al. 2016 [13]	Mercury(II) Bromide Mercury(II) Chloride	Quartz wool Filters	Sampling at 30 L/min for 3 hr.	Filters placed in a deactivated fused silica coated stainless steel chamber with analytes desorbed between 80 – 160 °C with UHP Helium. A cryotrap focuser was set at 0 °C and analytes were desorbed at 240 °C into an 100% dimethyl polysiloxane GC column set to 140 – 220 °C.	GC-EI-MS – Shimadzu GC-2010 Plus & QP2010 Ultra MS
		Nylon membranes	Sampling at 1 L/min for 2 weeks. See Huang et al. 2013.		
Siudek et al. 2016 [49]	Particulate Bound Mercury (+ Retained Gaseous Species)	Quartz and Glass-Fiber Filters	Pre-combust fiters at 500 °C for 5 hours. Sampling at 30 L/min for 24 hr at an urban site and 1 week at a rural site. No preceding denuder.	Microwave acid digestion in 60% HNO_3 following EPA 1631E.	CVAFS –P.S. Analytical 10.025

Where calibration has been attempted using GOM proxies such as $HgBr_2$ and $HgCl_2$, permeation tubes are employed. Here, ultra-high purity GOM proxies are placed into a tube where semivolatile compounds permeate at a given rate at a given temperature. Lyman et al. found a stable permeation rate ± 8% [10]. According to Weigelt et al., with no commercially available reference materials, no long-term inter-comparability studies have been published [139]. Lynam et al. 2010 found that uncoated denuders collect $HgCl_2$ as efficiently as coated KCl denuders [10], however other GOM proxies may not be collected as efficiently with uncoated denuders. Breakthrough of ambient GOM concentration through denuders range between 2.1% and 6% [10]. Within the same lab, Ren et al. showed GOM inter-comparability between two collocated mercury speciation systems had slopes of 0.99 and 0.81 [60], while Soerensen et al. reported a 28% reproducibility of RGM measurements [52].

During sampling, denuders are maintained at 50 °C to prevent condensation of GOM in the inlet and hydrolysis of the KCl coating [62], or heated as high as 100 °C to minimize wall losses and sampling line contamination without GOM decomposition [10]. Wilcox and Blowers determined a theoretical thermal decomposition rate for mercuric chloride approximately 1×10^{-26} s^{-1}, negligible to impact GOM concentrations if mercury(II) chloride comprised a major component [10,97].

KCl denuders are hindered from interference from O_3 and humidity [10,65], and homogeneous and heterogeneous reactions on the coating surface which can produce GOM or PBM [49]. KCl denuders remove O_3 with decreasing efficiency with concentration, and when a denuder precedes a filter, PBM concentrations can be either higher or lower than undenuded samples depending on whether O_3 concentrations are above or below 80 ppb [109]. Laboratory studies of $HgCl_2$ and $HgBr_2$ loaded on coated and uncoated denuders that were subjected to O_3 concentrations between 6 ppb and 100 ppb for 30 minutes, would face Previous studies by Lynam and Keeler found that the KCl coating destroyed 95% of a 29 ppb sample of O_3 as it passed through the KCl coated denuder [109]. GOM losses between 29% and 55%, respectively. These losses were independent of water vapour concentrations, GOM load concentrations, and no significant dependence was found with O_3 concentration. For field denuders, losses on exposure of 30 ppb O_3 varied between 3 and 37% for three different field deployments which may be due to different GOM species or coating variations.

Table 1.7. Selected measurements of GEM, GOM and PBM in studies with concurrent qualitative or quantitative detection of GOM chemical species.

Reference	Site	Time	GEM (ng/m^3)	GOM (pg/m^3)	PBM (pg/m^3)	Notes
Gustin et al. 2016 [143]	Reno, NV (USA)	Winter 2013 – 2014	2.3 ± 0.5	27 ± 7	24.3 ± 13.2	Tekran
				76 ± 56		CEM (GOM only)
		Spring 2014	2.1 ± 0.4	22 ± 5	36.2 ± 9.6	Tekran
				59 ± 11		CEM (GOM only)
		Summer 2014	1.9 ± 0.3	18 ± 2	13.7 ± 4.8	Tekran
				106 ± 29		CEM (GOM only)
		Spring 2015	1.7 ± 0.2	14 ± 11	11.4 ± 3.9	Tekran
				38 ± 22		CEM (GOM only)
Huang et al. 2017 [65]	Pensacola, FL (USA)	Summer 2012	1.2 ± 0.1	0.6 ± 1.3	2.4 ±2.6	Tekran
		Fall 2012	1.2 ± 0.1	1.1 ± 2.8	3.6 ± 3.8	Tekran
		Winter 2012	1.3 ± 0.1	1.0 ± 2.2	7.3 ± 8.8	Tekran
		Spring 2013	1.2 ± 0.2	2.9 ± 6.8	5.9 ± 6.8	Tekran
				43 ± 110		Cation-exchange
				4 ± 10		Nylon Membranes
		Summer 2013	1.1 ± 0.1	0.5 ± 1.0	2.3 ± 2.0	Tekran
				24 ± 57		Cation-exchange
				0.4 ± 1.3		Nylon Membranes
		Fall 2013	1.0 ± 0.1	1.1 ± 2.1	2.9 ± 2.3	Tekran
				14 ± 18		Cation-exchange
				1.2 ± 1.1		Nylon Membranes
		Winter 2013	1.2 ± 0.3	1.3 ± 2.5	4.9 ± 5.3	Tekran
				17 ± 23		Cation-exchange
				0.6 ± 0.6		Nylon Membranes
		March 2014	1.2 ± 0.1	2.0 ± 3.6	4.0 ±3.4	Tekran
				24 ± 15		Cation-exchange
				0.6 ± 0.5		Nylon Membranes

In a final set of experiments, $HgCl_2$ collected was 21% lower in the presence of 50 ppb O_3 as compared to O_3-free air. Lack of GOM on additional downstream backup denuders suggest that GOM losses result in conversion to GEM thereby leaving TGM unchanged if not lost. Finally, when coupled to particulate mercury filters, larger amounts of particulate mercury collected downstream from KCl coated denuders than undenuded samples, though this contradicted other findings [49,109,144].

1.2.7.8. Gaseous Oxidized Mercury – Filter Packs and Ion Exchange Membranes

The filter pack method involves the collection of PBM on Teflon filters followed by GOM collection of cation-exchange membranes; a typical set-up would involve two Teflon filters in sequence followed by three cation-exchange membranes [14]. The initial Teflon and cation-exchange filters are used for quantification, the second set of filters for blanks and breakthrough, and the third cation-exchange filter to prevent diffusion from the pump [14]. Filter pack MDLs are typically in the low pg/m^3 range (7 pg/m^3) [14].

Ebinghaus et al. used ion-exchange membranes to trap gaseous oxidized mercury followed by acid extraction, and reduction to GEM for analysis using CVAFS. The technique quantitatively measures a variety of GOM compounds but not all. Lynam et al. used Polysulfone cation-exchange membranes and found that concentrations of GOM on ion exchange membranes can be an order of magnitude higher than KCl-denuder measurements [65]. Based on dry deposition modelled results and actual measurements, Huang et al. determined found the collection efficiency of $HgN_2O_6 \bullet H_2O$ on cation-exchange membranes was 12.6 times higher than on the KCl denuder [65]. While Huang et al. found the membranes could be stored for up to 3 weeks, [65] the method requires at minimum 24 hour sampling times, can suffer from PBM volatilization or GOM adsorption on some types of filters (i.e. quartz filters) can occur at low flow rates [14].

Nylon membranes used to trap GOM were found to be impacted by humidity, decreasing the efficiency of trapping for some species, and not quantitative for others [65]. Huang et al. transported samples in a thermally isolated cooler and stored their samples at -20 °C until analysis [65].

1.2.7.9. Gaseous Oxidized Mercury – Thermal Deposition Analysis

Offline thermal deposition analysis (TDA) involves the collection of PBM and GOM on uncoated and KCl-coated quartz fibre filters [133]. Filters are preconditioned and blanked by heating at 550 °C prior to use. Filter punch-outs are heated to 500 °C to thermally desorb KCl and decomposed GOM through a pyrolyzer at 900 °C in a quartz sample furnace. Rutter et al. found condensed KCl could cause losses of GEM; KCl melts at 771 °C and condenses at lower temperature downstream. There is good agreement between TDA GOM and Tekran KCl-denuder GOM measurements where a plot of TDA GOM vs. Tekran KCl-denuder GOM has a slope that is not statistically different from 1 [133].

1.2.8. Measurements of Atmospheric Mercury Speciation

Early measurements of total mercury concentrations averages between 5 – 10 ng/m^3 with high source-related variability [42]. In the past twenty years, atmospheric mercury measurements typically range between 1.5 and 1.7 ng/m^3 [11,39,40,145] with concentrations higher in the northern hemisphere than the southern hemisphere [146-148]. As a result of anthropogenic emissions, mercury is estimated to be 2 – 5 times higher than pre-industrial times [67], and deposition rates are 3 times higher [39,78]. Urban concentrations of mercury are typically higher than in rural areas due to anthropogenic sources at urban sites [17]. Measurements taken at marine boundary layer sites are often lower than continental sites, with an average of 1.5 ng/m^3 measured across 9 sites by an eight-month circum-global expedition [52]. GOM background concentrations range from 1 – 5 pg/m^3 in North America [41,103,109] both the measurements and percent of these species have decreased over decades [42], but are thought to be biased low because of O_3 and water vapour interference with KCl denuder measurements [13]. Song et al. identified some extreme GEM, GOM and PBM values that were all correlated with a similar anthropogenic emission origin [17].

Studies featuring measurements vary in length from proofs of concept of techniques to long-term monitoring programs. Long-term measurements provide information on the local and regional mercury sources and transport, local biogeochemistry and the impact of mercury controls and emission regulations [139].

Table 1.8. Recent advancements in particulate mercury chemical speciation techniques

Reference	Analysis	Sample Collection	Sample Preparation	Separation	Analysis
Xiu et al. 2009 [88]	Particulate Bound Mercury	Glass Fibre Filter	Air was sampled at 600 L/min four 24 hours through a four-stage fractionator: with an 18 µm inlet cutoff, and three stages with 8.0, 3.7, 1.6 µm cutoffs and a final filter.	Filters were digested in 10 mL of 5% $KMnSO_4$ and 5 mL 1:1 H_2SO_4 at 95 °C under reflux. Then Hg^{II} is reduced with $SnCl_2$ with NH_2OH•HCl to GEM.	CVAAS
	Exchangeable PM			Filters are digested in 15 mL 0.1 M $CaCl_2$ with sonication followed by analysis for PBM.	
	HCl-soluble PM			Filters are then digested in 20 mL 1 M HCl and 0.5 mL 1% $CuSO_4$ stabilizer, sonicated and analyzed for PBM.	
	Elemental PM			Filters are then digested in 10 mL 2 M HNO_2, sonicated and analyzed for PBM.	
	Residual PM			Filters are finally digested as per PBM analysis.	
Arruti et al. 2010 [149]	Particulate Bound Mercury	Glass Fibre Filters	High volume sampler operated at 500 L/min for 24 hours.	Microwave digestion using nitric acid – hydrogen peroxide acid mixture slowly heated to 185 °C.	ICP-MS
Zverina et al. 2014 [39]	Morphology and Elemental Analysis	Fibrous Filters	Sample was fixed to glass plate and coated with a layer of 20 nm thick gold.	None	SEM-EDX – JEOL JSM-6490 LV
	Total Mercury		Sample placed in nickel boat.	Combustion of solid sample through dry ashing.	CVAAS – Altec AMA-254
	Water extractable Mercury		Trapped dust samples are dried at ambient temperatures and screened through four-sieve size fractions. 100 mg samples are successively extracted using leaching solutions. See Coufalik et al. 2012.	Samples extracted with deionized water for 18 hours in a end-over-end shaker set to 300 min^{-1}, centrifuged then analyzed. Solid residue is rinsed and extracted in the next step.	
	Acid-released Mercury			Extraction with 0.5 M HCl.	
	Organic-bound Mercury			Extraction with 0.2 M KOH.	
	Elemental and complex bound mercury			Extraction with 50% (m/v) HNO_3. Elemental and complex bound fractions are separated through a 48hour desorption at 105 °C.	
	Residual mercury			Solid residue from previous extraction is dried for 48 hour at 45 °C and analyzed.	
Pyta et al. 2016 [2]	Particulate Bound Mercury	Quartz Filters	Sampling at 21.67 L/min through 13-stage impactor ($PM_{0.03}$ to PM_{40}).	Pyrolysis of PM samples at 700 °C, with interfering nitrogen oxides, sulfur oxides and halides removed through additives and catalytic oxidation at 850 °C. Mercury trapped on gold trap and thermally desorbed.	CVAAS – Nippon MA-2 Analyzer
Siudek et al. 2016 [49]	Particulate Bound Mercury (+ Retained Gaseous Species)	Quartz and Glass-Fiber Filters	Pre-combust fiters at 500 °C for 5 hours. Sampling at 30 L/min for 24 hr at an urban site and 1 week at a rural site. No preceding denuder.	Microwave acid digestion in 60% HNO_3 following EPA 1631E.	CVAFS –P.S. Analytical 10.025
Bełdowska et al. 2018 [71]	Particulate Bound Mercury	Glass Fibre Filters	Sampling at 23 L/min for 48–96 h until Hg^{Tot} > 2 ng.	Samples were burned in pure oxygen environments based on four, six or twenty-two temperature steps. (See Saniewska and Bełdowska 2017)	UV-AAS (Milestone DMA-80)
Kumari and Kulshrestha 2018 [9]	Particulate Bound Mercury	Quartz Filters – Whatman QM-A	Pre-treat filters by baking at 450 °C for 1 hour. Weigh filters after equilibrating in a desiccator for 24 hours. Sample at 910 – 1240 L/min for 24 hours.	Extraction from the filter using 5% nitric acid with sonication and passing through 0.22 mm nylon filter.	DPASV – Metrohm 797 VA Computrace

There are a number of regional, national and international monitoring programs that contribute to atmospheric mercury measurements. These can vary from local and state level programs such as the Michigan Atmospheric Mercury Monitoring Network [41], to national programs like the National Atmospheric Deposition Program (NADP) [41], and the Clean Air Status Monitoring Network [41]. In Europe, there is the European Monitoring and Evaluation Programme (EMEP). The European Commission DGXII operates the Mercury Over Europe (MOE) and Mediterranean Atmospheric Mercury Cycle System (MAMCS) programs [73], and the European Union air quality directive 2004/107/EC aims to establish elemental, particulate and GOM background measurements in addition to other contaminants every 100,000 km^2 to analyze site variation and identify long-term trends [139]. In Canada there is the Canadian Atmospheric Mercury Measurement Network, CAMNet and the Atmospheric Mercury Network AMNet in the US [53,139]. The Global Monitoring Plan for Atmospheric Mercury aims to standardize operating and quality control practices for mercury measurement studies around the world [139]. Wet deposition measurements, measuring atmospheric mercury removal through precipitation, is measured by the Mercury Deposition Network [133] in the US with methodologies available at the NADP [53]. In terms of emission records, the US has the EPA Toxics Release Inventory and Canada, the Canadian National Pollutant Release Inventory [53].

1.2.9. Analysis of Data

In analyzing mercury, co-contaminant and meteorological data, a number of statistical tests are used. Published by Spearman in 1904 and 1906, used in many fields, Spearman Coefficients used for bivariate correlation. [41,51,62] For data below the detection limit, a random number between 0 and detection limit is used [104]. The non-parametric Mann-Whitney U test is used to compare the difference between two sets of data [51], for example, comparing PBM concentrations at urban vs. suburban sites [58]. Similarly, the Wilcoxon and Kruskal-Wallis Tests are used to measure variation between more than two groups [41]. Kolmogorov-Smirnov test for normality and whether log transformation is required and multiple linear regressions assess multiple unrelated independent variables to exclude the "inter-influence of inter-correlated variables [104]."

The Hybrid Single Particle Lagrangian Integrated Trajectory (HYSPLIT) Model can be used to assess back trajectories of air parcels based on starting height and time [104]. The upper limit of boundary layer heights is often chosen as the starting heights [111]. In doing so, HYSPLIT can help to identify potential sources for contaminants in a given parcel of air. Individual air mass transport trajectories can be averaged to determine average trajectory clusters which can simplify the variance observed and determination regional air mass sources [41].

Potential Sources Contribution Function (PSCF) analysis can similarly identify potential sources, pathways, and factors which influence GEM, GOM and PBM behaviour [43], by determining the probability that the sampled air mass trajectory, in a high concentration event, passed through a geographic area or cell containing a potential source [19]. These probabilities and the resulting mercury concentrations are used in conjunction with known emission rates and Spearman coefficients, and spatial correlations are determined. Spatial correlation is used to determine variance due to data point distance [19].

1.3. Chemical Speciation of Mercury in the Atmosphere

1.3.1. Sorbent Profiles

In Braman and Johnson's speciation stack studies of elemental, mercury(II) and organomercury species, significant fractions of Hg^{II} type (25%) and monomethyl mercury (21%) were observed though measurements were highly variable and often site dependent. Organomercury species were initially targets of speciation studies (see Table 1.9) because of their volatility, presence in soil and aquatic environments, and their toxicity, however dimethylmercury was only found in trace amounts [42,81].

Schroeder and Johnson's mercury speciation train allowed for the separation of GEM, gaseous $HgCl_2$, gaseous monomethylmercury chloride, and gaseous dimethyl mercury through collection on a series of selective sorbent traps, sequential desorption and decomposition to elemental mercury. Chromosorb-W sorbent treated with HCl was highly selective and efficient for mercuric chloride. Silver and gold-coated glass beads were highly efficient traps but had no selectivity. Schroeder and Johnson optimized mercury collection and desorption by adjusting the sample flow rate, sorbent trap temperature, the physical dimensions of the traps, desorption time and desorption temperature. Sorbents were chosen

for their availability, lifetime, regeneration potential, thermal stability and adsorption and desorption consistency. Gaseous $HgCl_2$ concentrations were only detected in proximity to a battery manufacturing plant, and dimethyl- and monomethylmercury chloride were highest at sites near wastewater treatment plants [16].

1.3.2. Thermal Desorption Profiles

Using desorption profiles using a series of possible GOM compound standards from nylon membranes, Huang et al. were able to compare standard nylon-membrane desorption profiles for GOM proxies to experimental profiles. Standards include halogenated mercury compounds such as $HgBr_2$ and $HgCl_2$, nitrogen compounds such as $HgN_2O_6 \bullet H_2O$, $HgSO_4$, and HgO. Between March 2013 to January 2014, Huang et al. observed a variety of compounds [65] as shown in Table 1.9. Gustin et al. (2015) observed nitrogen and sulfur-based compounds in the marine boundary layer and highway sites, halogenated mercuric compounds ($HgCl_2$ and $HgBr_2$) from the free troposphere [150]. Huang et al. 2017 observed desorption profiles from the Pensacola Outlying Landing Field resembling an unknown organomercury species, halogenated mercury (either $HgBr_2$ or $HgCl_2$), $HgSO_4$, and HgO and nitrogen-based mercury species.

1.3.3. Gas Chromatography-Mass Spectrometry

Gas chromatography-mass spectrometry allows for stable, volatile mercury-containing gaseous species to be separated, ionized, chemically identified and quantified. Jones et al. developed a method for identifying and quantifying mercury(II) chloride and mercury(II) bromide involving sample collection on quartz wool-filled tubes and nylon membranes, thermal desorption to a cryo-focuser, and second desorption into a GC column and detection by ultra-sensitive electron impact mass spectrometry [13]. Sample collecting surfaces were hampered by interference by sorbent breakdown products, which either masked the desired signal or slowed the analyte desorption during cryotrap heating or high breakthrough. Still, with quartz wool-filled perfluoroalkoxy (PFA) tubes and nylon membranes allowed for identifiable peaks. Siltek deactivated fused silica-coated stainless steel heated to 160 °C was chosen for sampling lines after PFA, PEEK and stainless steel were lower and more Hg^0 was observed. A range of temperatures was tested to determine an optimal focusing and

desorbing temperature with higher desorption temperatures providing the largest peak area best peak shape. The flux from permeation tubes at 100 °C was evaluated by passing air through a pyrolyzer at 800 °C to detect GEM using a CVAFS with the $HgBr_2$ rate at 37 pg/s [13]. An absolute detection limit of 90 pg was determined for mercuric(II) bromide and spectra associated with Hg^+, $HgBr^+$ and $HgBr_2^+$ were observed. Neither mercuric(II) nitrate and mercuric(II) oxide from permeation sources showed molecular ion spectra though both spectra showed prominent Hg^+ peaks. An HgO^+ fragment was observed in from a direct probe injection of solid $Hg(NO_3)_2$ in addition to other breakdown products such as $HgNO_3^+$. Solid mercuric oxide direct probes did not show species beyond Hg^+. Ambient air sampled, with reactive mercury concentrations for 38 ± 9 pg/m^3, did not result in a positive detection for mercury halides [13].

1.3.4. Soft-Ionization – Mass Spectrometry

Mass spectrometry offers a unique opportunity to detect and quantify species of oxidized mercury if preconcentration is sufficient to exceed the absolute detection limit and if the species that are collected remain intact and unchanged through analysis and detection. Atmospheric chemical pressure ionization is a softer ionization process to electron impact, using a carrier gas to transfer charge to analyte indirectly as opposed to bombardment by an electron; as a result, there is less fragmentation, and molecular ions are often more readily preserved. Deeds et al. developed a method of preconcentration on micro- and nano-particle sorbent traps, thermal desorption in a modified APCI-MS inlet, softer ionization using carrier gas charge transfer and detection of the molecular ion or species which retains the identity of the analyte of interest [142]. While molecular ions were detected for compounds such as mercury(II) bromide and mercury(II) chloride, these signals were dominated by complexes formed with carrier gas fragments. In cases where these adducts preserved speciation, these replaced molecular ions as target analytes, other fragmentation and complexation products such as HgX_3^- ions or their complexes were targets for reduction. When a 10:90 isobutane:nitrogen blend was used as a carrier, prominent $[M+26]^-$ peaks were observed and similarly $[M+19]^-$ indicative of fluoride ion release from sulfur hexafluoride fragmentation when an SF_6 in isobutane blend was used. APCI source parameters, such as the corona current, capillary and fragmentation voltage, drying gas temperature and flow

rate, were optimized to increase the overall detection of desired analytes, minimize their fragmentation and limit fragmentation by-products. When both mercury(II) bromide and mercury(II) chloride were present in standards, a series of mixed halogen species such as HgBrCl were formed [142].

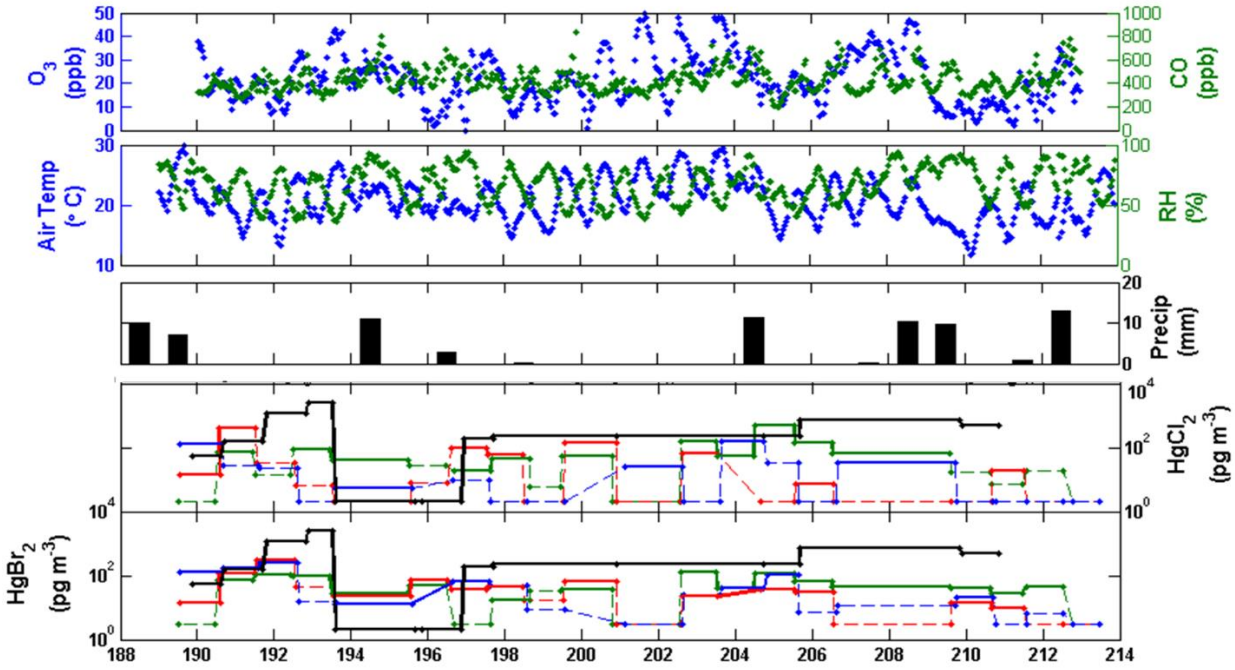

Figure 1.2. Soft Ionization Mass Spectrometry measurements of mercury(II) chloride and mercury(II) bromide in Montreal Urban Air.

HgX_2 concentrations in Montreal urban air during July 2014, collected onto Teflon traps A (green), B (red) and C (blue) and analysed by APCI-MS with SF_6:IB CI gas. GOM measurements by KCl-CV-AFS (black), precipitation, air temperature, relative humidity, O_3 and CO measurements are also plotted for comparison. Dashed sections of the HgX_2 time-series indicate no detection of HgX_2.

A variety of pre-concentration microparticle and nanoparticle-based sorbent traps were tested for their ability to quantitatively trap and thermally desorb mercury(II) halide species. These included: polysulfide-coated copper-doped iron nanoparticles, shredded PFA Teflon, magnetite, cobalt chloride, silver pellets, gold-coated quartz and glass wool. Mercury(II) halide standards were needed and evaluated for their mercury content using a KCl denuder; later the breakthrough on these sorbent traps and their thermal desorption was assessed using the KCl denuder – CVAFS technique.

Table 1.9. Chemical Speciation of Oxidized Mercury

Reference	Site	Time	Operational Bulk Species	Target Chemical Species	In GOM (pg/m^3)	In PBM (pg/m^3)
Schroeder and Jackson 1987 [76]	Toronto, ON (Canada)	Oct – Nov 1981	NA	$HgCl_2$	300 [ND – 1900]	NA
				Monomethylchloride	1650 [ND – 6200]	
				Dimethylmercury	600 [ND – 3700]	
Brosset and Lord 1995 [84]	Onsala, Halland County (Sweden)	March – September 1993	NA	Methylmercury	20 ± 25 [2 – 75]	
Deeds et al. 2015 [142]	Montréal, QC (Canada)	Aug, Oct 2013 and January 2014	NA	$HgBr_2$ – Urban Air	<4 – 100	NA
				$HgCl_2$ – Urban Air	<11 – 90	
				$HgBr_2$ – Pool Air	40 – 80	NA
				$HgCl_2$ – Pool Air	<11 – 29	
Gustin et al. 2016 [143]	Reno, NV (USA)	July – November 2014	Nitrogen and Sulfur-base Compounds	$HgN_2O_6•H_2O$, $HgSO_4$	Qualitative Detection	NA
	Peavine Peak, NV (USA)	June 2014	HgO	HgO	Qualitative Detection	
		June – October 2014	$HgCl_2/HgBr_2$	$HgCl_2/HgBr_2$	Qualitative Detection	
Jones et al. 2016 [13]	Reno, NV (USA)		NA	$HgBr_2$	ND (> 90 pg)	NA
				$HgCl_2$	ND (> 90 pg)	
Huang et al. 2017 [65]	Pensacola, FL (USA)	April 2, 2013	Unknown organomercury compound	NA	4.5 ± 8.5 (Tekran), 5.6 ± 0.1 (Nylon), 45.0 (ICE 450)	13.3
		April 9, 2013			1.4 ± 1.5 (Tekran), 34 ± 30 (1CE450)	5.6
		May 21, 2013			2.3 ± 3.7 (Tekran), 1.4 ± 0.9 (Nylon)	2.7
		May 7, 2013	Nitrogen-based mercury compound	NA	2.9 ± 3.4 (Tekran), 2.1 ± 0.1 (Nylon), 49.3 ± 29.0 (ICE450)	2.4
		May 21, 2013			2.3 ± 3.7 (Tekran), 1.4 ± 0.9 (Nylon)	2.7
		August 27, 2013			0.7 ± 1.0 (Tekran), 0.9 ± 0.1 (Nylon)	2.6
		March 19, 2013	NA	$HgBr_2$ and $HgCl_2$	3.8 ± 4.1 (Tekran) 6.7 ± 8.7 (Nylon), 23.3 ± 2.0 (ICE450)	6.2
		November 19, 2013			1.3 ± 1.9 (Tekran) 2.3 ± 0.2 (Nylon), 16.3 ± 23.0 (ICE450)	4.5
		September 24, 2013	NA	$HgSO_4$	0.3 ± 0.7 (Tekran) 1.1 ± 0.7 (Nylon), 20.0 ± 16.0 (ICE450)	1.7
		October 22, 2013	NA	HgO	3.4 ± 3.1 (Tekran), 2.2 ± 0.1 (Nylon)	2.3

Detection limits between 4 – 10 pg/m^3 were achieved for mercury(II) chloride and 11 – 28 pg/m^3 for mercury(II) bromide and required both a quantifier ion to be at least 3σ beyond the average blank for the quantifier ion and for at least three qualifier ions to be within 2 σ of the theoretical ratio [142].

A series of urban and indoor air samples were collected and assessed for mercury(II) chloride and mercury(II) bromide. During sampling, air was drawn in at 1 L/min for 12 hours while the sorbent traps were heated to 50 °C to prevent the condensation of water in the traps; after sampling, traps were capped with parafilm, and transported in plastic bags and analyzed the same day [142].

The technique suffered from co-desorption of mercury(II) chloride and mercury(II) bromide which resulted in the formation of a mercury mixed halide species, long sampling times preventing higher temporal resolution, and memory effect issues which required labour-intensive trap cleaning [142].

1.4. Phase Distribution of Mercury in the Atmosphere

1.4.1. Particulate Mercury

Particulate mercury, represented as Hg^P, PHg or PBM (for particulate-bound mercury), consists of Hg^0 and Hg(II) species [78] absorbed to solid particulates, dissolved in liquid, [2] or incorporated into the particle [73]. Particles themselves may consist of one or more phases and vary in their chemical composition, even within the same particle [109]. PBM can be directly emitted from natural and anthropogenic point sources or formed from the gas-to-particle partitioning of GEM or GOM [53], nucleation following GEM oxidation, or reactions of GEM or GOM on surfaces [151]. PBM has high solubility in water, high deposition velocities and scavenging coefficients [3,152]. Its atmospheric residency time lasts several hours to weeks [1,15,58,85,86] with lifetime decreasing with increasing size. [39,58,153,154] As a result, it is considered to make up only a few percent of atmospheric mercury (by mass) [2] and only significant to local and regional transport [14], though early studies found high variability in and occurrence of extreme PBM values [42].

In general, there are three modes for particle populations: the finer nucleation (≤ 50 nm) and accumulation modes (50 – 1000 nm) , and coarse particle modes (≥ 1 μm); each is operationally defined by the size of filters used for trapping [2]. Fine PBM are released

primarily by combustion processes [39], while coarse particle mercury enrichment is believed to occur through the adsorption of Hg^0 and Hg^{II} on particulate matter, in particular sea-salt aerosols [39,53,78]. Finer fractions of PBM travel further including remote areas [2] and consists of the majority of particulate bound mercury [41,154] thus resulting in regional-scale transport [51]. Background concentrations for PBM typically are below 100 pg/m^3 [154]. In rural or remote areas, PBM consists of approximately 1% of total atmospheric mercury [51], while in industrial areas, particulate mercury can comprise up to 20% of TAM.

1.4.1.1. Variation with Size Distribution

In Zabrze, Pyta et al. only found 3% of PBM (by mass) was present in coarse particles; 97% was inhalable (PM_{10}), 83% was respirable ($PM_{2.5}$), and 66% was submicron (PM_1). Only 6% of PBM was ultrafine by mass [2]. Wang et al. similarly observed the highest concentrations of mercury were found in submicron particulates accounting for ~45% of PBM varying between 25–30% to 65% of total PBM with no noticeable seasonal trend [58]. In general, 30% is the seen as the limit for the contribution of coarse PBM though this contribution may peak at 50% in coastal areas where there is high sea-salt aerosol GOM partitioning [53]. Mercury content decreases from fine to coarse particles; the latter has a higher enrichment of biological material [39].

1.4.1.2. Correlation with other Pollutants

PBM occurrence is influenced by local sources, atmospheric chemistry, and meteorological conditions [1]. In terms of sources, PBM correlation with co-pollutants can be indicative of co-emission. Coal combustion and traffic source co-emission of black carbon and PBM has readily been observed [55]. PBM is often strongly and positively correlated with sulfate (SO_2) from conventional coal fired power generation sources [1,3,151]. NO_3 and carbon monoxide (CO), similarly show a strong, positive correlation with PBM due to traffic co-emissions [1,3,88,151]. However, sulfate and nitrate aerosol can also arise from the oxidation of SO_2 and nitrogen oxides and mercury binding to secondary organic aerosols [3].

Higher enrichment of halogens, such as chlorine (Cl), bromine (Br) and iodine (I), in particulates, favour higher mercury particulate content. Typical mole ratios between Hg:Br

and Hg:I range between 0.009 and 0.016, and 0.040 and 0.001 for urban to island sites, respectively [151].

Furthermore, the origins of PBM can also be gleaned from correlations with metallic elements. Strong positive correlations with calcium and magnesium ion sources indicated crystal and crustal dust sources especially in rural environments [3,9]. Correlations with potassium often serve as a biomass burning marker, crustal contributions [9] and waste incineration [3], as is the biomarker Levoglucosan [40]. A significant positive correlation between mercury and manganese in Mahasar, India suggested a common origin from brick kilns [9]. Multivariate factor analysis (often used in geochemistry) can be used to group elements which then can be used to account for explained variances. Using factor analysis, Schleicher et al. found a significant correlation between PBM to a "coal combustion factor" during the daytime and to "anthropogenic emission factor" comprising of elements such as Mg, Al, K, Sc, Ti, V, Fe, Sr and Ba from coal combustion and traffic sources [55].

Correlations between PBM and total suspended particle (TSP) concentrations suggest gaseous Hg may have adsorbed on to particulates that arrived in the same air mass and the degree of mercury enrichment in particulate matter can provide clues to the source of ambient PBM [3], with higher enrichments suggesting anthropogenic origins. Early measurements of particulate mercury by Braman and Johnson show a correlation between condensation nuclei concentrations and PBM [42], as did Weigelt et al. in rural Germany, where PBM showed a similar seasonal trend to $PM_{2.5}$ with increasing heating-related winter emission and boundary length height [139]. In the Arctic, Steffen et al. observed a greater proportion of PBM associated with particles with higher surface areas and volumes of particles either due to the transport of particulates from mercury-rich regions or the adsorption of GOM to these surfaces [87].

1.4.1.3. Meteorological Influences

Precipitation impacts the rate of PBM scavenging and is a far more effective means of removal than dry deposition [3,15]. Particle concentrations tend to plummet following precipitation events [3], and there is often a strong negative correlation between PBM and humidity [60]. High humidity in Arctic environments, where ADMEs are often observed, serve as important marker for PBM decreases [87,151].

Positive correlations with wind speed suggest greater transport contributions from remote sources while negative correlations with wind speed suggest local emissions or stagnant accumulation [9]. Due to high deposition velocities, particulate mercury is mostly found in the troposphere in the vicinity of emission sources [11,49]. Siudek et al. found increased PBM concentrations from local sources, especially higher coarse mercury concentrations, in periods of less turbulent wind conditions [26]. Strong advective winds increased the remote source contribution, [49] but also result in the diffusion, dilution and dispersion of particulate mercury [9]. Windrose diagrams can help determine how wind direction and thereby how sources influence Hg species concentrations [17,40]. For example, at Ryerson University, the highest observed PBM mercury concentrations were associated with winds from the southwest, the location of a major commercial area [17].

In general, positive PBM correlation with temperature is seen to be indicative of photochemical PBM formation while negative correlations consistent with gas-to-particle deposition [88]. At Alert, Steffen et al. found PBM increased from February peaking in April coinciding with high Arctic haze aerosol transport and sea salt particle concentrations. At lower temperatures, GOM partitioning to particles is favoured [151]. Decreases in May and the summer months coincide with higher temperatures resulting in higher GOM values [87]. In the Kathmandu Valley, both the concentration of PBM and the enrichment of mercury increased with temperature [3] while little variation was observed at the rural Jeziory site in Poland with sources varying variation between vegetation and industrial emissions [49]. In Toronto, Song et al. measured the highest concentrations for GEM, GOM and PBM in June as did Jen et al. who found PBM levels four times higher in Summer [26].

1.4.1.4. Diurnal and Weekly Variation

Urban areas will have more variation in their diurnal cycles and in general, higher concentrations of all three bulk atmospheric species [101], due to coal-fired energy production, industry and waste incineration [40]. In Beijing, Schleicher et al. found greater concentrations of particulate mercury in weekday vs. weekday samples and all but the site in the inner city showed higher concentrations during the day than at night. Higher nighttime concentrations of PBM may arise from residential fuel combustion at small domestic and street restaurants/heaters. Conversely, in Shanghai, PBM was at its lowest during the day

[43], and Song et al. found reported PBM in Toronto, was highest in the early morning hours rising steadily throughout the evening suggesting nocturnal emission sources outweighing photochemical sources [17].

1.4.2. Gas-Particle Transformations

Gas-particle partitioning of mercury is influenced by temperature, humidity, aerosol-enriched air masses and wind speed [87]. Where PBM is negatively correlated with temperature, gas-to-particle transformation dominates whereas a positive correlation implies enhanced PBM from photochemical transformation [9]. During the winter months at temperatures below 5 °C, there is generally an anticorrelation with PBM due to the absorption of GEM/GOM on PBM. Steffen et al. found the partitioning of GOM to PGM predominates at low temperatures and enhanced PBM levels were related to this partitioning as opposed to mercury enhanced-PBM transport which happened to coincide to these lower temperatures [87]. Poissant et al. found a correlation between solar radiation, wind speed and transformation from Hg^0 to PBM through photochemical oxidation to GOM followed by gas-to-particle transformation [1,103].

GOM readily adsorbs to aerosols [13,155,156] especially at high RH [1], with dry NaCl [157], ice crystals [87,157], sodium nitrate and potassium chloride [70]. During Arctic atmospheric mercury depletion events in March and April, GOM adsorbs to sulfate and carbonaceous particles transported from Europe and North America, known as Arctic haze [87]. Conversely, ammonium sulfate and organic aerosols can act as a source of GOM [70], and as ammonium sulfate aerosols tend to be present as fine particles, mercury in this mode is reduced [88]. Hg-enriched aerosol may be a significant global mercury flux to oceans due to sea-salt aerosol [70].

1.4.3. Consequences of Atmospheric Mercury Phase Distribution

PBM plays an important role in the dry and wet deposition of atmospheric mercury to terrestrial and aquatic environments where it can be transformed into methylmercury by sulfur-reducing bacteria in sediment and the water column [3,158]. The bioavailability of mercury in aquatic systems from suspended particulate matter depends on its speciation and thus speciation has an important link to toxicity [140].

Table 1.10. Mercury Content of Fractionated Particulate-Bound Mercury

Reference	Site	Time	Size Fraction	Mercury Content (PBM/Size Fraction) [ng/g]	Chemical Composition
Freitas et al. 2005 [54]	Carregado, Greater Lisboa (Portugal)	March 1995 - 1996	PM_{10}	3500	Elemental
	Monchique (Portugal)	November 1994 – July 1995	$PM_{2.5}$	11000	
			PM_{10}	9000	
	Sines (Portugal)	July 1994 – 1995	$PM_{2.5}$	91000	
			PM_{10}	59000	
Xiu et al. 2005 [114]	Shanghai (China)	March 2002 – September 2003	PM1.6	3720 ± 620 [2700 – 4240]	Elemental
			PM8	1900 ± 1040 [1020 – 3390]	Elemental
			TSP	1700 ± 800 [1030 – 2850]	Elemental
Xiu et al. 2009 [88]	Shanghai (China)	July 2004 – April 2006	$PM_{1.6}$	2740 ± 910	Elemental
			$PM_{1.6\text{-}3.7}$	3000 ± 1020	
			$PM_{3.7\text{-}8}$	1480 ± 440	
			$PM_{8\text{-}18}$	900 ± 300	
			$PM_{>18}$	760 ± 300	
			TPM	1780 ± 460	
Arruti et al. 2010 [149]	Santander, Cantabria (Spain)	2008	$PM_{2.5}$	56000 ± 175000 [800 – 133200]	Elemental
			PM_{10}	77000 ± 64000 [18000 – 261000]	
Zverina et al. 2014 [39]	Prague (Czech Republic)	2009 – 2011	< 25 μm	820 (± 1.8%)	Elemental
			< 63 μm	760 (± 0.4%)	
			63 – 119 μm	650 (± 7.2%)	
			119 – 507 μm	500 (± 3.8%)	
Schleicher et al. 2015 [55]	Beijing (China)	2006	$PM_{2.5}$ (day)	2270	Elemental
			$PM_{2.5}$ (night)	2900	
Duan et al. 2017 [43]	Shanghai (China)	2014	$PM_{2.5}$ - Summer	3960	Elemental
			$PM_{2.5}$ - Autumn	1280	
			$PM_{2.5}$ - Winter	3870	
Cheng et al. 2017 [151]	Shanghai Xuhui (China)	September 2014 – August 2015	$PM_{2.5}$	2080 ± 2450	Exchangeable
				3090 ± 2600	HCl-soluble
	Shengsi, (China)			7690 ± 11390	Exchangeable
				5470 ± 8550	HCl-soluble
Guo et al. 2017 [3]	Kathmandu Valley (Nepal)	2013 – 2014	Total	2590 (± 2070)	Elemental
Kumari and Kulshrestha 2018 [9]	Mahasar, Haryana (India)	2014 – 2015	PM_{10}– Winter	5270 ± 2300 [2790 – 12300]	Elemental

PBM has large dry deposition velocities [3,152]. Dry deposition velocity depends on meteorological parameters such as wind speed, relative humidity and ambient temperature [3,159]. On average, the dry deposition of particles is only slightly larger than GEM [11]. The rate of dry deposition increases with particulate size though large coarse particulates correspond to more than 90% of dry deposition fluxes [2,3,58]. Conversely, finer particulate mercury can travel further polluting remote areas [2]. Deposition fluxes can be estimated from concentrations of size-fractioned particles and the deposition velocities for those sized particles which can be calculated using transport models such as the global MOCAGE model [58]. Unlike GEM and GOM, which have remission pathways, PBM is largely expected remain on surfaces such as the snow pack [87]. That the concentration of mercury on snow is largely based on contributions from atmospheric transport is observed in that surface snow concentrations (top 1 cm layer) are higher than ground samples and that mercury concentrations in snow follow the season variation patterns of GOM [87].

Similarly, wet deposition velocities are related to particle size [26] with coarse particulate mercury more easily removed [160]. Wet deposition fluxes fall along a gradient with deposition highest by major emission sources, local and regional for example deposition in southern Sweden averaged 5 – 10 $\mu g/m^2 \cdot$year and was double that of northern Sweden [8].

1.4.4. Techniques of Measuring Atmospheric Particulate Mercury Speciation

Particulate mercury is generally present at low pg/m^3 concentrations [109], and generally involves the trapping of mercury-containing particulates on filters, release of mercury through digestion or pyrolysis and analysis using spectrometric CVAAS, CVAFS or ICP-MS methods [73,83].

1.4.4.1. Particulate Mercury Filters

PBM is generally measured using particulate traps and filter packs that are operationally defined by the pore size of the filter used [49,141] as shown in Table 1.8. Filters are a simple, compact, store-able, robust and economical method of capturing particulate mercury [109], but are impacted by positive (sorption/reaction of mercury to trapped mercury) and negative artifacts (mercury volatilization from trapped particles) that are often influenced

by sampling time [49,58]. Flow rates and sampling times for trapping particulate can vary (from 1 L/min to as high as 1240 L/min) [9,58] and are often determined by the absolute detection limit of the instrument and anticipated ambient concentration. With concentrations in the low pg/m^3 range, it is not uncommon to have long sampling times and still find undetectable concentrations of particulate mercury. Liu et al. found 21% and 8% of their PBM measurements at rural and urban Michigan sites were below detection [41].

Glass fibre is often used as medium for trapping particles for its strength and thermal stability, cost-effectiveness and low blanks [58,83,161]. To lower blank concentrations, quartz filters are often pre-combusted to remove mercury and organics at high temperatures (500 °C and higher) [49,58,81], Teflon filters are acid pre-cleaned with nitric and sulphuric acid solution at 80 °C [73]. Filter assemblies are similarly rinsed in detergent, 0.5% trace metal grade nitric grade, deionized water and acetone [133]. Liu et replaced filter assemblies every 3 months [41].

In typical sampling trains, PBM is collected alongside GOM and GEM with KCl-coated denuders attached upstream to remove GOM [109]. Without an upstream KCl-coated denuder, Lynam and Keeler suggested the potential for positive artifacts resulting from adsorbing GOM species on particulate filters [58,109], however Rutter et al. 2008 did not observe a positive artifact and in another study, PBM was higher (with a preceding denuder up to 33 pg/m^3) with high O_3 concentrations [109]. Gold coated denuders have also been suggested for removing GEM. However, the potential gold flake release from the sampling surface and contaminating particulate filters has largely nixed this idea [58,161].

PBM filters samples are transported from the field in sampling coolers, kept at temperatures 0 °C and lower, and are stored in freezers at -20 °C to prevent mercury volatilization [133]. Preservation and storage of filters may vary from being wrapped with aluminum foil and being placed in polyethylene bags [9], to acid-cleaned petri dishes [109]. Handling of PBM filters should be conducted in class-100 cleanrooms where particulate counts are $<100/ft^3$ reduce background PBM level [41], and mercury-free such as by using gold-impregnated cheesecloth over the air intake to remove mercury [133].

For analysis, particulate mercury can be measured through pyrolysis, thermal desorption and combustion to GEM or through digestion, conversion to Hg^{2+} species, and subsequent reduction to GEM. Both methods involve detection particulate mercury as GEM

using CVAFS, CVAAS [58] or ICP-MS [109]. Digestion benefits from fewer organic pyrolysis interferents but suffers from longer analysis times and ultra-trace purity reagents thus digestion is preferable for membrane and organic fiber filters and pyrolysis suitable for quartz fibre filters [83].

Mercury from particulates is extracted by immersing the filter or part of the filter in acids such as nitric [9] often in combination with sonication or microwave digestion from an hour to longer [9,73]. Kumari and Kulshrestha determined an extraction efficiency between 97 to 99% when using 5% nitric acid with an hour of sonication and 4.6% RSD across three replicates [9]. Arruti et al. used microwave digestion with a nitric acid/hydrogen peroxide mixture at 185 °C which was diluted for ICP-MS analysis [149]. Digests from a particulate filter can be oxidized using BrCl and subsequently reduced with $SnCl_2$ forming Hg^0 which is purged with an inert gas and analyzed via CVAFS/CVAAS [73]. In cases where mass differences are used to calculate parameters such as PM_{10} for mercury enrichment measurements, filters are often equilibrated in desiccators before and after sampling [9].

1.4.4.2. Particulate Mercury – Thermal Deposition Analysis

Offline thermal deposition analysis (TDA) involves the collection of particulate mercury (PBM) on uncoated and KCl-coated quartz fibre filters [133]. Particulate filter punch-outs are heated to 900 °C. San Joaquin soil and urban dust were used to simulate atmospheric aerosols; recoveries were 93% and 100% respectively. Human hair and lobster was used to simulate complex organic matter were 103% and 89% recoveries. Loaded $HgCl_2$ ranged between 200 pg and 4 ng. Punchouts had a repeatability of 11% for the uncoated quartz fibre filters, and 17% for the KCl coated quartz fibre filters.

1.4.4.3. Particulate Mercury – Sequential Particulate Extraction

Zverina et al. used size fraction sieves to measure mercury among four-micron sized fractions [39]. Sequential extraction resolves particulate mercury into a series of groups [162]: water extractable mercury, acid-released mercury, organic-bound mercury, elemental and mercury-bound complexes, mercury sulphide and residual mercury; each category is operationally defined depending on the solubility of compounds undergo leaching conditions [140]. The extraction process involved loading filters into 10 mL glass centrifuge

tubes with leaching solution onto an end-over-end shaker for 18 h at 300 min^{-1}. 200 uL aliquots of the solution were introduced to the analyzer.

Xiu et al. similarly used sequential particulate extraction to quantify operationally defined groups of particulate mercury: exchangeable PM, HCl-soluble PM, elemental-soluble PM and residual PM [88]. Exchangeable PBM was mainly believed to be $HgCl_2$, some HgO and $HgSO_4$, while HCl-soluble PM consisted of the remaining HgO. Elemental mercury PM was GEM which was nearly quantitatively oxidized by nitric acid in addition to Hg_2Cl_2 and organic-bound mercury [88].

1.4.4.4. Particulate Mercury – Thermal Desorption Analysis

Thermal desorption involves heating solid sample at progressively higher temperatures thereby desorbing mercury in different fractions. Steps in temperature can range; Bełdowska et al. utilized a four, six and 22 step fractionation to characterize mercury content by fraction [71]. Under a four-step fractionation, nearly 90% of mercury was bound to labile forms across seasons. Under a six-step fractionation, 37% of PBM was associated with Hg^0 and mercury halides, and mercury sulphide consisted of roughly 20%. Under a 22 step fractionation, 21 – 55% of mercury was released between 100 – 150 °C related to Hg^0 and poorly adsorbed surface species of mercury while another 34 – 73% was related to adsorbed species of likely halogenated mercury species released between 175 – 225 °C [71].

Particulate chemical speciation is difficult due to the picogram quantities of mercury present in particulate matter, and handling, transfer and sample preparation losses and contamination [140]. Feng et al. used 6 mm, 10 μm pore sized quartz fibre, filter free of mercury through heating at 500 °C in an argon environment, to trap particulates at 3.4 – 4.5 L/min flow rates for approximately 94 hours. The filter disk was housed in a quartz trap mini-device, sealed with parafilm and triple bagged. The mini-device was connected to an ICP-MS and a source of particulate scrubbed argon carrier gas and placed in a tube furnace capable of temperatures up to 800 °C at a 50 °C/min temperature ramp. The ICP-MS detector was set to monitor the most abundant mercury isotope, ^{202}Hg with an absolute sub-picogram detection limit. A thermogram, measuring mercury signal over the heating cycle, is produced with overlapping signals deconvoluted using PeakFit software.

Mercury species can be identified within a sample through comparison to standards in matrices that are similar to atmospheric particulates [140]. Feng et al. prepared mercury-enriched atmospheric particulates by heating coal fly ash to remove mercury at 550 °C for 4 hours and allowing the fly ash to equilibrate with a sealed saturated mercury vapour environment or mechanically mixing in mercury species before diluting with mercury-free fly ash. Species are identified by the appearance temperature where the Hg signal exceeds background; these temperatures are dependent on the matrix and experimental conditions.

1.4.5. Chemical Compound Speciation of Atmospheric Particulate Mercury

The chemical speciation of mercury is essential in determining its fate in the environment as speciation impacts chemical and biological behaviour such as bioavailability, solubility and toxicity [88]. Possible species of mercury include: Hg^0 adsorbed to the surface, oxidized mercury species such as mercury halides, mercuric oxide and mercuric sulphide [83,140]. Mercury sulphide is only found associated with particulate matter. It enriches coarser particulates [39], and is found in crustal rocks and ore [140]. HgO likely only present as particulates because of decomposition of intermediate HgO_3 on particulates or reaction with water to form $Hg(OH)_2$ [13,124,163].

A number of chemical species have been indirectly observed in particulate matter. Feng et al. identified mercury(II) oxide, elemental and mercury(II) chloride in particulate samples using thermal desorption. Cheng et al. found HCl-soluble particulate mercury (mainly HgO, $HgSO_4$) consisted of 45% of PBM at urban Shanghai and had higher concentrations than that at the Shengsi island site though the mercury enrichment of HCl-soluble PBM (5470 ng/g) and elemental-soluble PBM (7690 ng/g) was almost double that of Shanghai (3090 ng/g, 2600 ng/g respectively) [151]. Within Shanghai, HCl-soluble PBM dominated sampling in a suburban area heavy traffic while residual particulate mercury dominated at a downtown site [88]. The occurrence of the HCl-soluble PBM was promoted by higher temperature and increased solar radiation [88].

Table 1.11. Chemical Species Measurements in Particulate Bound Mercury

Reference	Site	Time	Operational Bulk Species	Target Chemical Species	In PBM (pg/m³)
Brosset and Lord 1995 [84]	Onsala, Halland County (Sweden)	March – September 1993	NA	Methylmercury	20 ± 25 [2 – 75] [GOM +PBM]
Feng et al 2004 [140]	Toronto, ON (Canada)	November 2001	NA	Hg^0	6.8 ± 2.6 (27%)
				$HgCl_2$	5.8 ± 1.3 (23%)
				HgS	2.3 ± 0.5 (9%)
				HgO	9.8 ± 2.4 (40%)
Xiu et al. 2005 [114]	Shanghai (China)	March 2002 – September 2003	Inert PM	$HgSO_4$, HgS, HgO, organic mercury	37% [64% for $PM_{1.6}$]
			Reactive PM	Adsorbed or Soluble Hg(II) – $HgCl_2$	28% [21% for $PM_{1.6}$]
			Volatile PM	Hg^0, slightly soluble Hg(II)	35% [15% for $PM_{1.6}$]
Xiu et al. 2009 [88]	Shanghai (China)	July 2004 – April 2006	HCl-soluble PM	HgO, $HgSO_4$, $HgCl_2$	107 ± 19
			Elemental PM	Hg^0	118 ± 53
			Residual PM	HgS, HgSe, organic-bound mercury	206 ± 156
Zverina et al. 2014 [39]	Prague, CZ	2009 – 2011	Water extractable & Acid-released mercury	HgO, $HgSO_4$, $HgCl_2$	(ND – 5%)
			Organic-bound mercury	NA	(19% – 40%)
			Elemental & Mercury-bound complexes	NA	(44 – 73%)
			Residual mercury	Hg encapsulated in Si, HgS	(2% - 25%)
Cheng et al. 2017 [151]	Shanghai Xuhui (China)	September 2014 – August 2015	Elemental-soluble	Hg^0	150 ± 100 [NR]
			HCl-soluble	$HgCl_2$, HgO_2, and $HgBr_2$	270 ± 120 [80 –880]
			Residual	HgS, HgSe, organic-bound mercury	190 ± 120 [NR]
	Shengsi, (China)		Elemental-soluble	Hg^0	90 ± 70 [NR]
			HCl-soluble	$HgCl_2$, HgO_2, and $HgBr_2$	100 ± 50 [30 –200]
			Residual	HgS, HgSe, organic-bound mercury	230 ± 180 [NR]
Bełdowska et al. 2018 [71]	Gdynia, Pomeranian Voivodeship, (Poland)	January 2016 – 2017	Labile Hg	HgI_2, $HgBr_2$, $HgCl_2$, $Hg(ClO_4)_2 \bullet xH_2O$, $Hg(CN)_2$, $(CH_3COO)_2Hg$, $Hg(NO_3)_2 \bullet H_2O$, CH_3Hg, humic acids	(90%)
			Stabile Hg	HgS	(<10%)
			Labile-2 Hg	$HgSO_4$, HgO (red), HgF_2	(<2%)
			Mineral Matrix Hg	NA	Negligible
			Aerosolized Hg	Adsorbed Hg^0 and GOM	10 ± 7 (37%)
			Adsorbed Hg	HgI_2, $HgBr_2$, $HgCl_2$	8 ± 5 (33%)
			Absorbed Hg	$Hg(NO_3)_2 \bullet H_2O$, CH_3Hg, humic substances	4 ± 2 (20%)
			NA	HgS	2 ± 2 (9%)
			Adsorbed-2 Hg	$HgSO_4$, HgO (red), HgF_2	(<1%)
			Residual Hg	NA	(Negligible)

Elemental-soluble particulate mercury was favoured in the winter in Shanghai due to enhanced condensation and physisorption at lower temperatures [88] and surprisingly in summer in Shengsi possibly due to increased ocean evasion [151]. It was predominantly found on particles larger than 1.6 μm [88]. Xiu et al. only observed exchangeable mercury in the summer and surmised that this may consist mostly of physisorbed $HgCl_2$ [88].

In dust from the Czech Republic, less than 5% of mercury was water-soluble or acid-released species such as mercury oxide, mercury sulphate and mercury chloride [39]. Mercury-bound to humic organic matter was a dominant fraction in dust and coarse material (40%) while elemental mercury and complexed-bound mercury dominated (44% – 73%) in finer fractions.

1.5. Rationale and Objectives

Though the majority of mercury in the atmosphere exists as GEM, gaseous oxidized and particulate mercury play essential roles in the transformation and fate of mercury in ecosystems. Until very recently, the speciation has been limited to the operationally defined bulk species of gaseous oxidized mercury and particulate mercury. The result is discrepancies in measured and modelled concentrations of GOM because of measurement uncertainties in the chemical species that comprise GOM and lack of validated calibrated methods for those species. [53] The primary objective of our work is to make the first direct determination of two long-suspected chemical forms of gaseous oxidized mercury: mercury(II) chloride and mercury(II) bromide in an urban environment and achieve accurate quantitation of these species at part-per-quadrillion concentrations. What has been developed is a sorbent preconcentration, thermal desorption, soft ionization, mass spectrometric method for detecting and quantifying halogen-based oxidized mercury species. Measurements of the bulk species of gaseous oxidized and particulate mercury are influenced by operational methodology; gaseous oxidized mercury by KCl-coated annular denuders and particulate mercury by pore-selective filters. Two works are presented where the methodology is assessed for contamination of one measured by another, that is to say how much of what we currently measure as gaseous oxidized mercury could be nanoparticulate mercury in nature and another where the distribution of mercury(II) chloride and mercury(II) bromide in the gaseous and particulate phase is assessed.

1.6. Thesis Overview and Principal Findings

This thesis is presented in six chapters beginning with the Introduction in Chapter 1, built from an invited review to Environmental Science: Processes and Impact.

Chapter 2, entitled "Development of a particle-trap preconcentration-soft ionization mass spectrometric technique for the quantification of mercury halides in air," as published in Analytical Chemistry, explores the development of a speciation technique for oxidized mercury compounds in liquid and gaseous phases and the eventual determination of mercury(II) chloride and mercury(II) bromide in urban air. Detection limits between 4 and 11 pg/m^3 are achieved for mercury(II) bromide and mercury(II) chloride in ambient air with sporadic detection in urban and indoor air.

In Chapter 3, "The Generation of Mercury Halide Nanoparticles, Capture by KCl denuder and Quartz Filters, and Characterization using Mercury Mass Spectrometry," nanoparticulate oxidized mercury methods are developed and the products characterized using instrumentation and techniques novel for the mercury sciences. These nanoparticles are stable under tropospheric conditions as well as in aqueous environments and show capture rates by KCl denuder as high as 95% for nanoparticles ~11.5 nm across species, and filter penetration rates for nanoparticles ranging from 10^{-5} to 65%.

"The Existence of Mercury Nanoparticles," or Chapter 4, explores the evidence for nanoparticulate oxidized mercury using mercury mass spectrometry and electron microscopy techniques. Particulate mercury is assessed to comprise as much as 50% of oxidized mercury in winter with the first image of an ambient mercury nanoparticle 10 nm in diameter detected.

Chapter 5 titled "Exposure to Nanoscale and Microscale Particulate Air Pollution prior to Mining Development near a Northern Indigenous Community in Québec, Canada" is an application of scanning mobility and optical particle sizing techniques to measure indoor and outdoor air quality in the Cree Nation of Waswanipi and at a near mining development site. The highest nanoparticulate concentrations are observed within the home as high as 10^4/cm^3 with concentrations of a variety of particulate metals including mercury measured (45 pg/m^3) near the mining site.

Finally, Chapter 6 concludes with major findings and future directions for study.

Chapter 2. Development of a Particle-Trap Preconcentration-Soft Ionization Mass Spectrometric Technique for the Quantification of Mercury Halides in Air

As adapted from Analytical Chemistry 2015, 87, 5109-5116

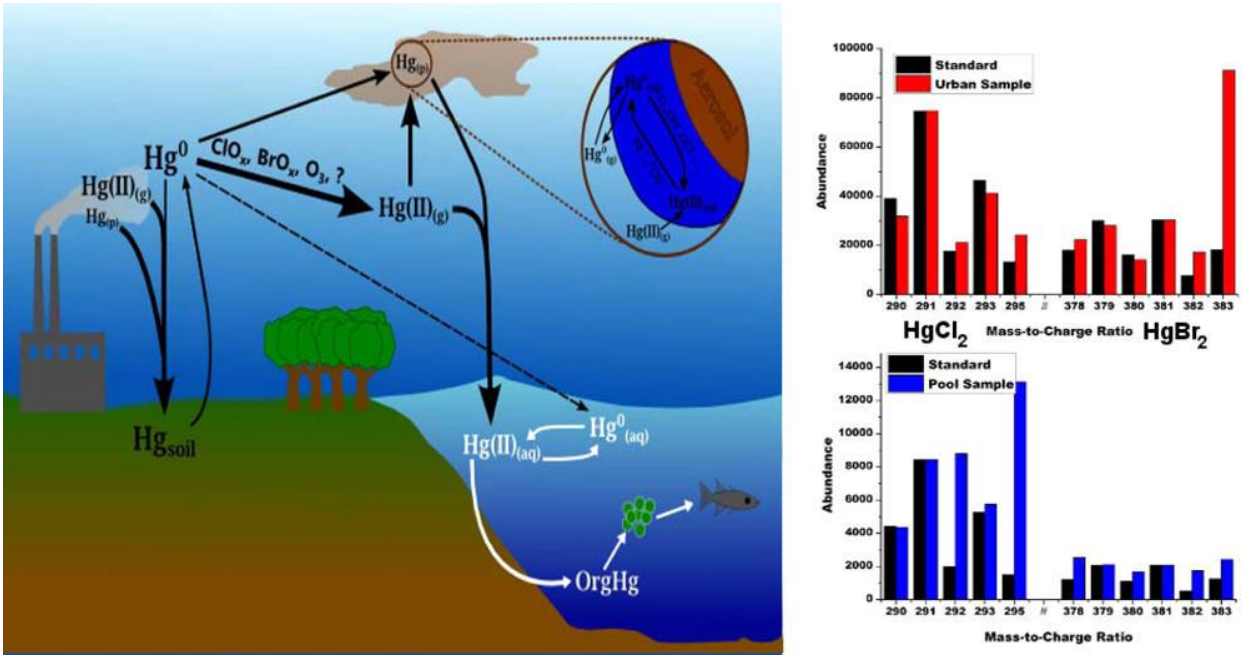

TOC Figure 2. The fate of atmospheric mercury and the first detection of $HgCl_2$ and $HgBr_2$ in urban air
*[Originally published in Analytical Chemistry as TOC Figure]

In this paper, we develop a technique for qualifying and measuring chemical species long suspected to comprise the bulk atmospheric mercury species "gaseous oxidized mercury," using mass spectrometry and pre-concentration using nano- and microparticle sorbent traps.

Contribution by author: My contribution to this paper was the optimization of the APCI-MS technique using PFA-sorbent traps in addition to polysulfide traps including, characterization of the trapping and desorption efficiencies of a variety of sorbent traps, assessing sampling breakthrough and retention, and the analysis of mercury(II) chloride and mercury(II) bromide in air. I also assisted in the preparation of the manuscript including preparing figures and additional experiments requested by reviewers during the peer-review process.

Abstract

Measurement of oxidized mercury, Hg(II), in the atmosphere poses a significant analytical challenge as Hg(II) is present at ultra-trace concentrations (picograms per cubic meter air). Current technologies are sufficiently sensitive to measure the total Hg present as Hg(II) but cannot determine the chemical speciation of Hg(II). We detail here the development of a soft ionization mass spectrometric technique coupled with preconcentration onto nano- or microparticle-based traps prior to analysis for the measurement of mercury halides in air. The current methodology has comparable detection limits (4–11 pg m^{-3}) to previously developed techniques for the measurement of total inorganic mercury in air while allowing for the identification of HgX_2 in collected samples. Both mercury chloride and mercury bromide have been sporadically detected in Montreal urban and indoor air using atmospheric pressure chemical ionization-mass spectrometry (APCI-MS). We discuss limitations and advantages of the current technique and discuss potential avenues for future research including quantitative trace measurements of a larger range of mercury compounds.

2.1. Introduction

Mercury, a toxic heavy metal that bioaccumulates up aquatic food chains [164], is elevated above preindustrial levels in the environment due primarily to emissions associated with precious metals mining and coal-fired power plant production [165,166]. The oxidation state (0 vs II) and phase of anthropogenic mercury (gaseous vs particle-bound) largely determines its removal rate from the atmosphere [15,167], with $Hg(0)_{(g)}$ being relatively insoluble and inert compared to $Hg(II)_{(g)}$ or particle-bound Hg [15,167]. Understanding the chemical makeup of anthropogenic mercury emissions and subsequent chemical transformations after release is a crucial step toward assessing the balance between mercury deposition to nearby soils and waterways [15,156,167] and transport to remote, pristine environments (e.g., the Arctic) [168].

Current atmospheric mercury measurements are mainly limited to the study of bulk mercury reservoirs: specifically, mercury is measured as gaseous elemental mercury (GEM, Hg^0), as Hg^0 derived from the chemical reduction or pyrolysis of gaseous oxidized mercury (GOM, or reactive gaseous mercury, RGM) or as Hg^0 derived from the pyrolysis of particulate-

bound mercury (PBM or $Hg_{(P)}$) collected onto filters. The GOM and $Hg_{(P)}$ reservoirs are user-defined, in that no standardized analytical method has been accepted by the community. Methods for the measurement of GOM are presented in Table 2.1. [35,93,94,127,128,141,169]

Table 2.1. Summary of Gaseous Oxidized Mercury Measurement Techniques

Reference	Sample Collection	Analyte Recovery	Detector	Form of Hg(II) Measured	Sampling Time	Max. GOM Measured[a]	Detection limit
					(h)	(pg m^{-3})	
Tong et al., 1999	None	None	PFFS	$HgBr_2$	0.003	8×10^{11}	1.5×10^{8}
Stratton et al., 2001	HCl/NaCl Mist Chamber	Chemical Reduction	CV-AFS	Total GOM	1	3000	4
Landis et al., 2002	KCl Denuder	Pyrolysis	CV-AFS	Total GOM	1 – 12	1500	0.5 – 6
Olson et al., 2002	MnO_2 Sorbent	Solvent Trapping + Injection	GC-MS	$HgNO_3$; $HgCl_2$	1	NR	NR
Lyman et al., 2010	Cation Exchange Membrane	Chemical Reduction	CV-AFS	Total GOM	336	60	2 – 7
Lyman and Jaffe, 2012	None	Pyrolysis	CV-AFS	GOM+ $Hg_{(P)}$[b]	0.04	1100	70
Huang et al., 2013	Nylon Membrane	Thermal Desorption + Pyrolysis	CV-AFS	HgO; $HgCl_2$; $HgBr_2$[c]	8	50	NR
Huang et al., 2013	Cation Exchange Membrane	Chemical Reduction	CV-AFS	Total GOM	8	3000	3
This Study	Particle-based Sorbent Trap	Thermal Desorption	APCI-MS	$HgCl_2$; $HgBr_2$	24	480	4;7

*[Originally published in Analytical Chemistry as Supplementary Table S1]

PFFS – Laser Photofragment Fluorescence Spectroscopy; CV-AFS – Cold Vapor Atomic Fluorescence Spectroscopy; APCI-MS – Atmospheric Pressure Chemical Ionization Mass Spectrometry; GC-MS – Gas Chromatography Mass Spectrometry

a – Reported values not necessarily upper limits for techniques

b – Inferred from total mercury and elemental mercury measurements

c – Identified from thermal desorption curves

Inter-comparison of mercury speciation methods, including equivalent instrumentation, has shown large differences in measured mercury speciation, [150] attributed to incomplete mercury capture and to wall losses or heterogeneous reactions in the sampling manifold. In addition, KCl denuder-cold vapor atomic fluorescence spectroscopy (CV-AFS), a technique often used to measure GOM, may preferentially collect

certain types of Hg(II) [141] and is susceptible to passivation by atmospheric oxidants and humidity at atmospherically relevant concentrations [10,170].

Thermal decomposition to Hg^0 allows for sensitive detection of total GOM or $Hg_{(P)}$ but destroys their chemical identity. These measurements provide insight into the transfer of mercury between the atmosphere, waters, snow, and soils (e.g., refs [156], [168], [107,171,172]) but may not necessarily inform one about rates of deposition to, reemission from, and methylation in aquatic environments [164]. The direct chemical speciation of mercury in the atmosphere would close crucial gaps in the geochemistry of mercury, providing better ability to assess the impact of mercury emissions on the environment.

Gas chromatography–mass spectrometry has been used to directly identify mercuric nitrate and mercury chloride in simulated flue gases, but the concentrations involved (μg Hg m^{-3}) are significantly higher than the atmospheric GOM background [169]. Recent method development has begun to address the chemical speciation of mercury through thermal decomposition profiles of captured Hg [150], but profiles produced are complicated by co-desorption of contaminants.

Mercury halides (HgX_2, X = Cl, Br, I) are thought to be one of the principal forms of oxidized mercury in the atmosphere [15,167]. In particular, $HgBr_2$ is implicated in atmospheric mercury depletion events observed at the poles [168] and midlatitudes [150]. As of yet, mercury halides have not been directly observed in the atmosphere; their presence in air is instead inferred from correlations of GOM with atmospheric oxidants such as BrO and Br [150]. Other potential forms of Hg(II) are HgO, $HgSO_4$, $Hg(NO_2)_2$, and $Hg(OH)_2$ [116,173,174].

We report here an analytical methodology for the detection of mercury halides at atmospherically relevant concentrations (10^{-12} g Hg m^{-3} air) by nano- or micro-particle trapping coupled with atmospheric pressure chemical ionization-mass spectrometry (APCI-MS). We also present initial measurements of mercury halides in urban and indoor air. The limitations and potential future applications of the technique will be discussed.

2.2. Method Development

This section details the tests taken to address the analytical challenge posed by the trace quantities of oxidized mercury present in the atmosphere. We discuss APCI optimization through selection of a CI gas for facile HgX_2 identification (APCI Source Parameter Optimization.) while minimizing side products and the selection of APCI ionization parameters to improve ion production and transmission into the MS. We then discuss development of particle-based sorbent traps (Sorbent Trap Packing.) for HgX_2 collection from ambient air (HgX2 Breakthrough and Retention.). We end by detailing initial tests of the complete APCI-MS system in urban and indoor air (Air Analyses, McGill University, Montreal Quebec, Canada.).

2.2.1. Source Modification and CI Gas Selection.

Gas phase HgX_2 species were detected using an Agilent 6130 single quadrupole MS with APCI ion source installed. APCI-MS was chosen over electron ionization MS (EI-MS) as EI-MS fragments HgX_2 into Hg^+ and X^- ions (Figure 2.1a) that are indistinguishable from those produced by elemental mercury or halogenated species in air extracts. EI-MS can produce small amounts of molecular ion for Hg(II) detection [169] but only at high concentrations applicable to extreme atmospheric conditions (e.g., power plant flue gas).

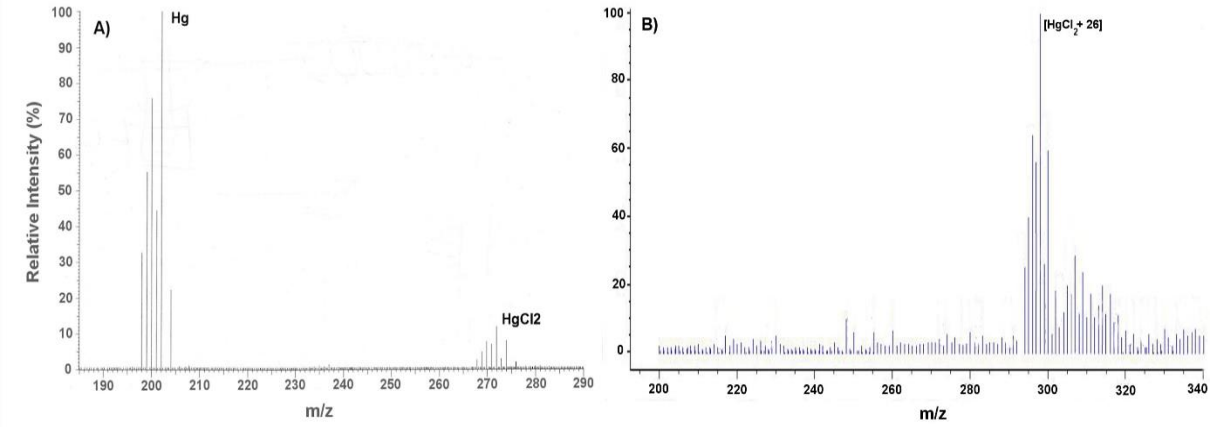

Figure 2.1. A comparison of EI-MS analysis of ~1 µmol $HgCl_{2(s)}$(a) and APCI-MS analysis of ~1 pmol $HgCl_{2(g)}$ using 10% isobutane in nitrogen as a CI gas (b).

The EI-MS spectrum shows significant fragmentation (i.e. loss of chemical identity), while the APCI-MS preserves the mercury halide as an ion complex with an isobutane fragment (m/z=26) that is readily interpretable as originating from $HgCl_2$. *[Originally published in Analytical Chemistry as Supplementary Figure S1]

In contrast, APCI is a "soft" ionization producing mainly molecular ions with less fragmentation than EI-MS due to indirect ionization via a solvent and due to minimal wall-

losses and ion thermalization at the ambient pressures of the inlet (Figure 2.1b). The APCI inlet of the Agilent 6130 nebulizes aqueous samples for gas-phase analysis; we removed the inlet nebulizer and widened the inlet to accommodate a 6 mm gas-line or sorbent trap (Figure 2.3 Left). A programmable oven heats the inlet, such that wall losses of analytes are minimized or desorption of analytes can be performed.

Moving from aqueous- to gas-phase APCI analysis required the replacement of the solvent with a reagent gas. Ionization via charge transfer from nitrogen resulted in high residual energy on ionized HgX_2, causing extensive ion fragmentation (Figure 2.2a,b). A variety of CI reagent gases were tested for retention of incoming mercury species (Table 2.2). In almost all tests, the CI gas was supplied by placing a 3 L dual side-arm glass flask containing 1 atm of reagent gas in-line between a UHP nitrogen tank (at 80 psig, flowing at 1 L min^{-1}) and a 6 L dual side-arm glass flask containing HgX_2 powder (~10 g) under a nitrogen headspace. Nitrogen gas from the tank mixed sequentially with CI gas and HgX_2-rich gas in the 3 and 6 L flasks, respectively, prior to entering the APCI ion source. One-hour tests showed no signal decrease from HgX_2 standards, indicating a constant flux of mercury halide over this time period.

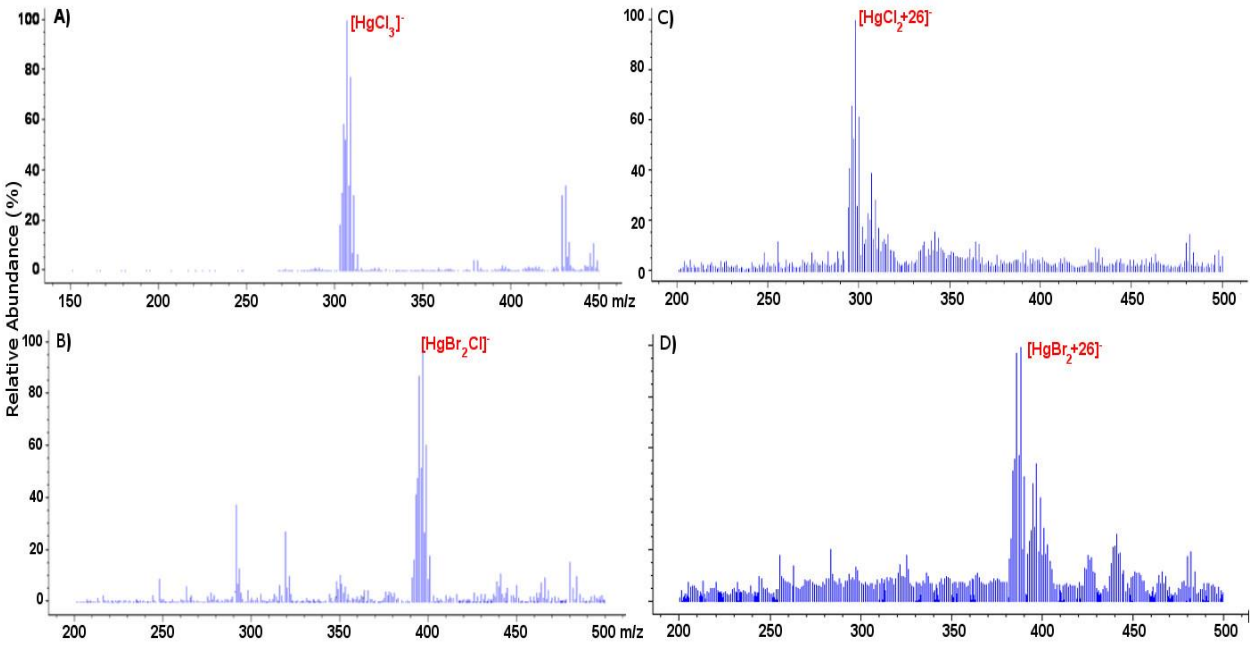

Figure 2.2. APCI scans of $HgCl_2$ and $HgBr_2$ packed standards with nitrogen (a,b) and 10% isobutane in nitrogen (c,d) as CI gas.

HgX_2 is fragmented by nitrogen, forming mixed halide ion complexes, while isobutane transforms mercury halides primarily into an ion complex with a fragment from isobutane (m/z=26). $HgBr_2$ forms $[HgBr_2Cl]^-$ with residual Cl^- from previous $HgCl_2$ runs. *[Originally published in Analytical Chemistry as Supplementary Figure S3]

Moving from aqueous- to gas-phase APCI analysis required the replacement of the solvent with a reagent gas. Ionization via charge transfer from nitrogen resulted in high residual energy on ionized HgX_2, causing extensive ion fragmentation (Figure 2.2a,b). A variety of CI reagent gases were tested for retention of incoming mercury species (Table 2.2). In almost all tests, the CI gas was supplied by placing a 3 L dual side-arm glass flask containing 1 atm of reagent gas in-line between a UHP nitrogen tank (at 80 psig, flowing at 1 L min^{-1}) and a 6 L dual side-arm glass flask containing HgX_2 powder (~10 g) under a nitrogen headspace. Nitrogen gas from the tank mixed sequentially with CI gas and HgX_2-rich gas in the 3 and 6 L flasks, respectively, prior to entering the APCI ion source. One-hour tests showed no signal decrease from HgX_2 standards, indicating a constant flux of mercury halide over this time period.

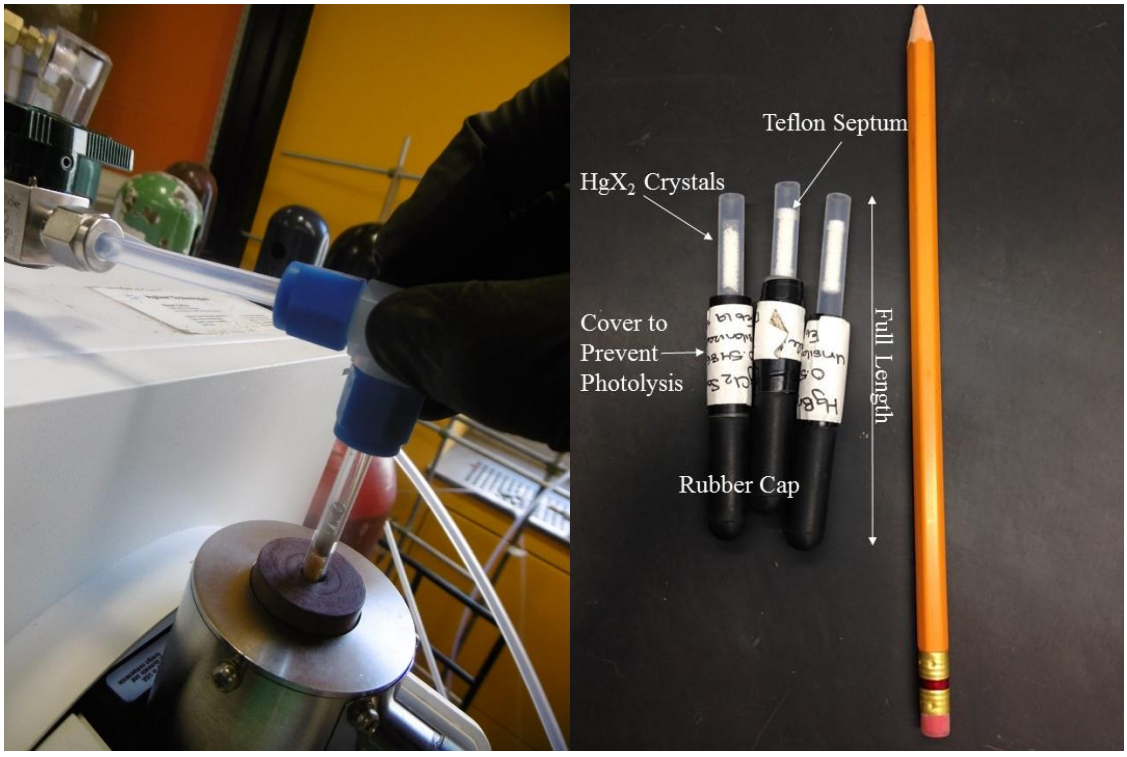

Figure 2.3. (Left) Photograph showing sorbent trap being inserted into modified APCI inlet while connected to the CI gas line with no gas flow. (Right) Photograph of mercury halide packed standards, with no. 2 pencil as size reference.

The standard consists of a roughly 10 cm length of 6.3 mm ID PFA tubing containing approximately 5 g of mercury chloride, mercury bromide, or a 50:50 $HgCl_2$:$HgBr_2$ blend, held in place by either glass wool or Teflon septa. The section of tubing containing HgX_2 is covered to prevent potential photolysis, and the standard is capped by rubber caps, when not in use. *[Originally published in Analytical Chemistry as Supplementary Figures S2 and S4]

Continuous scan-mode monitoring of masses in negative-ion mode ($175 \leq m/z \leq 550$) allowed for detection of ions formed from incoming HgX_2 as the reagent gas was diluted with the nitrogen pushing gas. Qualitative results of CI gas tests are presented in Table 1. Several aqueous phase analyses are presented as well, including one for mercuric oxide. Aqueous mercuric oxide (at pH = 7) was detected as $[Hg(OH)_2]^+$ using positive-mode APCI. Early tests on CI gases were performed using a Waters Micromass Quattro tandem quadrupole LC-MS at the Center for Biological Applications of Mass Spectrometry (CBAMS) at Concordia University. The Quattro LC-MS inlet line for aqueous analytes was replaced by 6.3 mm PTFE tubing for direct connection to HgX_2 standards.

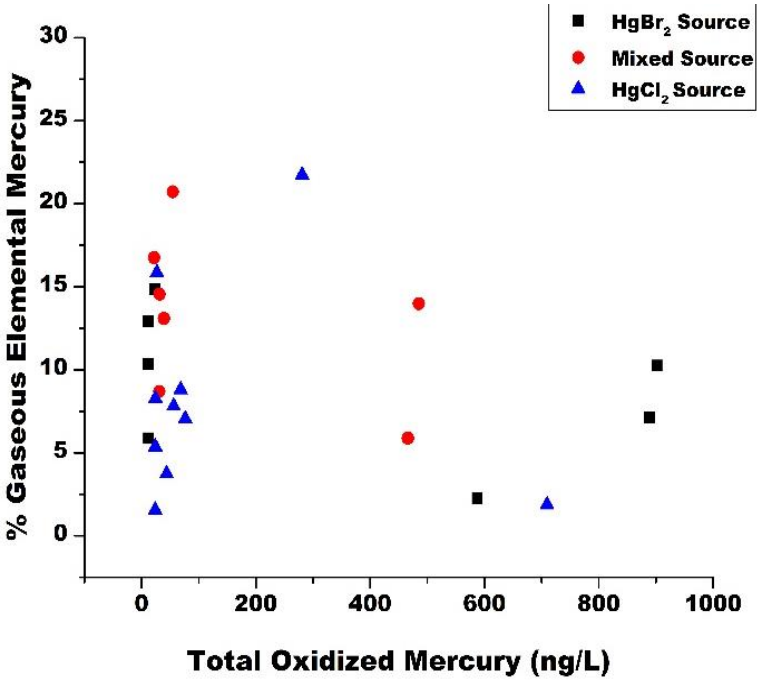

Figure 2.4. Denuder breakthrough for single and mixed HgX_2 standards at varying Hg(II) concentrations.

*[Originally published in Analytical Chemistry as Supplementary Figure S5]

Tests for the CI blend of isobutane (MEGS, >99.5% purity) and sulfur hexafluoride (MEGS, >99.95% purity) replaced the 3 L flask and nitrogen tank with pressurized tanks whose outflow were controlled via flowmeters to a total flow of 1 L min^{-1} (at 10 psig). The standard used for these tests consisted of 5-mesh HgX_2 pellets or powder packed into a 6 mm ID PFA tubing with dichlorodimethylsilane (DCDMS)-coated glass wool or Teflon septa (Figure 2.3 Right). We transitioned from the flask standard to packed standards as they were more compact, portable, and easier to manipulate in the laboratory. Packed standards were

calibrated by repeat measurement of emitted HgX_2 by KCl denuder coupled with CV/AFS. The KCl denuder was found to collect 90 ± 6% (n = 26) of incoming Hg(II) from standards based on CV/AFS analysis during sampling of standards vs during denuder heating at 500 °C (Figure 2.4). HgX_2 packed standards emitted Hg concentrations of 50 ± 20 ng Hg L^{-1}.

Mercury halides preferentially undergo complexation with other constituents in the ion source (Table 2.2). Many of the ions observed can be attributed to atmospheric contaminants, such as $(H_2O)_n^-$ (m/z = n × 18) or O^- (m/z = 16). Masses of m/z =19, 35, and 80 correspond to the halides F^-, Cl^-, and Br^-. The APCI source for the Agilent single quadrupole MS was freer of contaminants than the Waters tandem quadrupole MS: the Agilent MS produced only $[HgCl_3]^-$ with 100% N_2 (Figure 2.2a). The presence of HgX_3^- ions suggests that fragmentation occurred, although it was mainly limited to when the reagent gas recombination energy (equivalent in magnitude to its ionization potential) was greater than the analyte's ionization energy. In this case, the residual energy left after charge transfer resulted in ion fragmentation.

Of the CI gases studied, we initially selected isobutane (IB) as it produced simple spectra consisting of an ion complex ($[M+ 26]^-$) of the analyte and an isobutane fragment (m/z = 26, speculated to be C_2H_2) and small peaks corresponding to the molecular ion and to trihalide ions (e.g., $[HgCl_3]^-$, $[HgBr_2Cl]^-$). Isobutane and UHP nitrogen were blended in proportions of 0–100% IB/N_2 using flowmeters (total flow of 1 L min^{-1} at 10 psig) connected by a PFA tee to a single HgX_2 packed standard connected directly to the APCI inlet. A blend of 10:90 IB/N_2 was selected as a compromise between high sensitivity detection of both $HgCl_2$ and $HgBr_2$ and economizing reagent gases (Figure 2.5). We note that direct chemical identification of Hg(II) via $[M]^-$ was possible using 100% IB as a CI gas, but the relative yield of $[M]^-$ in selected ion monitoring (SIM) mode (e.g., 1.2 × 10^4 cts) was an order of magnitude less than the yield of $[M + 26]^-$ for the same standard with a 10:90 IB/N_2 CI gas (e.g., 2.2 × 10^5 cts in SIM mode).

Table 2.2 HgX_2 Ions from Aqueous or Gas Samples with Varying CI Reagents

[a]Boldface type indicates the principal ions observed in a spectrum. Unless specified, analyses were performed using the Waters Micromass Quattro tandem quadrupole LC-MS. [b]Analysis using the Agilent 6130 single quadrupole LC-MS. [c]Estimated from HgX_2 saturation vapor pressures at room temperature, CI gas flow rate, and scan duration. [d]Analysis using packed HgX_2 tubing standards rather than a saturated 3L flask.

Target Species (M)	Phase	Reagent gas/solvent	Ionization potential (IP) or CI reagent (eV)	Estimated analyte abundance per scan (mol, ±20%)[c]	Hg-containing ions detected
$HgCl_2$ (IP = 11.380 eV)	Aqueous	Distilled water	12.59	2×10^{-9}	**$[M + 36]^-$**
		Acetonitrile[b]	12.20		**$[M + 36]^-$**
		Ethanol[b]	10.47	1×10^{-9}	**M^-, $[M + 26]^-$**
		Isopropanol[b]	10.12	2×10^{-9}	**$[M + 36]^-$**
	Gas	N_2	15.58	5×10^{-10}	M^-, $[M + 16]^-$, **$[M + 35]^-$**, $[M + 44]^-$, $[M + 80]^-$
		N_2[b]			**$[M + 35]^-$**
		$C_2H_2F_4/N_2$[b]	12.64		M^-, $[M + 19]^-$, **$[M + 35]^-$**, $[M + 80]^-$,
		Isobutane/N_2[d]	10.68		M^-, **$[M + 26]^-$**, $[M + 35]^-$,
		SF_6/isobutane	16		M^-, **$[M + 19]^-$**, $[M + 35]^-$,
$HgBr_2$ (IP = 10.560 eV)	Aqueous	Ethanol	10.47	5×10^{-11}	M^-, **$[M + 26]^-$**,
	Gas	He	24.59	5×10^{-10}	**None**
		Ar	15.76		**M^-, $[M + 35]^-$, $[M + 46]^-$,** $[M + 80]^-$,
		N_2	15.58		**M^-,** $[M + 16]^-$, **$[M + 35]^-$**, $[M + 80]^-$,
		H_2	15.4		**$[M + 46]^-$**
		Acetylene/N_2	11.41		**M^-, $[M + 26]^-$, $[M + 35]^-$,** $[M + 80]^-$,
		Isobutane/N_2[b]	10.68		M^-, **$[M + 26]^-$**
		Acetone/N_2	9.703		M^-, **$[M + 26]^-$,** $[M + 42]^-$,
		SF_6/Isobutane	16		M^-, **$[M + 19]^-$**
		NO_2/N_2	9.60		**$[M + 18]^-$** , $[M + 28]^-$, $[M + 62]^-$
		Benzene/N_2	9.25		M^-, **$[M + 26]^-$,** $[M + 35]^-$,
HgO	Aqueous	Distilled water	12.59	2×10^{-10}	**$[Hg(OH)_2]^+$**

*[Originally published in Analytical Chemistry as Main Text Table 1]

To test for analyte loss to in-source reactions, we introduced both $HgCl_2$ and $HgBr_2$ into the APCI ion source from a 50:50 (by mass) $HgCl_2$/ $HgBr_2$ standard consisting of 5-mesh HgX_2 particles in a 6 mm ID PFA tube packed between Teflon septa. The mixed standard source was placed upstream of a shredded Teflon sorbent trap (discussed below in Sorbent Trap Desorption: Timing and Temperature. and Sorbent Trap Packing.), blanked at 200 °C in the APCI inlet, and connected to a field pump. HgX_2 was collected onto the trap for 1 min at 1 L min^{-1} prior to desorption into the APCI source at 200 °C with a 10:90 IB/N_2 CI gas flowing through the trap at 1 L min^{-1}. $HgCl_2$ and $HgBr_2$ sequentially desorb from the trap into the APCI source (Figure 2.6). The major ion observed during APCI-MS analysis of the mixed halide was m/z = 343, corresponding to $[HgBrCl + 26]^-$. HgBrCl was detected only after both HgX_2 compounds are present in the APCI inlet suggesting that HgBrCl was an artifact of ion reactions rather than being a desorbed analyte. Currently, HgBrCl cannot be considered a legitimate environmental signal if detected in air extracts.

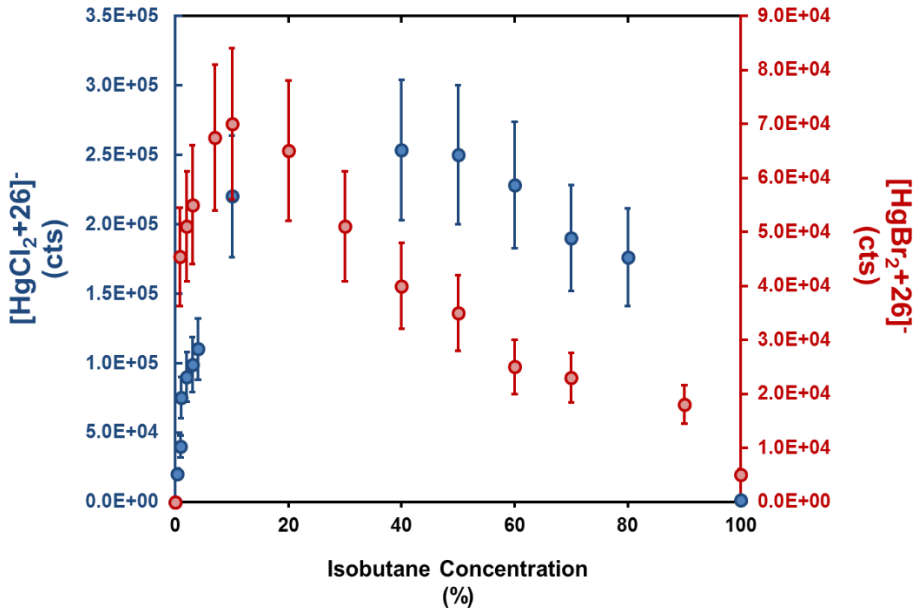

Figure 2.5 Principal ion signal ($[M+26]^-$, cts) for APCI-MS analyses of $HgCl_2$- and $HgBr_2$-saturated gas streams with varying concentrations of isobutane in nitrogen.

The yield of $[M+26]^-$ increases with increasing isobutane concentrations up to 10-40% isobutane, due to a shift from direct ionization of HgX_2 (and fragmentation) by nitrogen to indirect ionization through isobutane. Increasing isobutane concentrations further reduces $[M+26]^-$ yields, highlighting the role nitrogen plays in producing isobutane ion fragments (M=26, presumably $C_2H_2^-$) for complexation with HgX_2. *[Originally published in Analytical Chemistry as Supplementary Figure S6]

In an attempt to limit ion reactions in the APCI inlet, we analyzed the $HgCl_2/HgBr_2$ standard using a sulfur hexafluoride/IB blend as a CI gas. Sulfur hexafluoride (SF_6), a strong electron acceptor [175], decomposed into $SF_5^+ + F^-$ in the APCI ion source (Figure 2.6 Right). Fluoride ion complexed with HgX_2 to produce m/z = 291 ($[HgCl_2F]$; 40% relative abundance), m/z = 336 ($[HgBrClF]^-$; 100% relative abundance), and m/z = 381 ($[HgBr_2F]^-$; 80% relative abundance). Although the SF_6/IB CI gas does not prevent insource ion reactions, it provides a complementary analysis yielding alternate ions that may aid in positive identification of HgX_2 where contaminants are present at m/z of $[M + 26]^-$. Target ion abundances in scan-mode spectra with CI by IB/N_2 and SF_6/IB were comparable, with principal ion abundances on the order of $(2–3) \times 10^4$ cts. The yields of $[M + F]^-$ for blends of 0.5:99.5 to 99.5:0.5 SF_6/IB were relatively constant suggesting that HgX_2 supplies a limited ion complex formation rather than F^- production. To conserve SF_6, a 0.5% SF_6 in IB blend was used for all subsequent SF_6/IB tests.

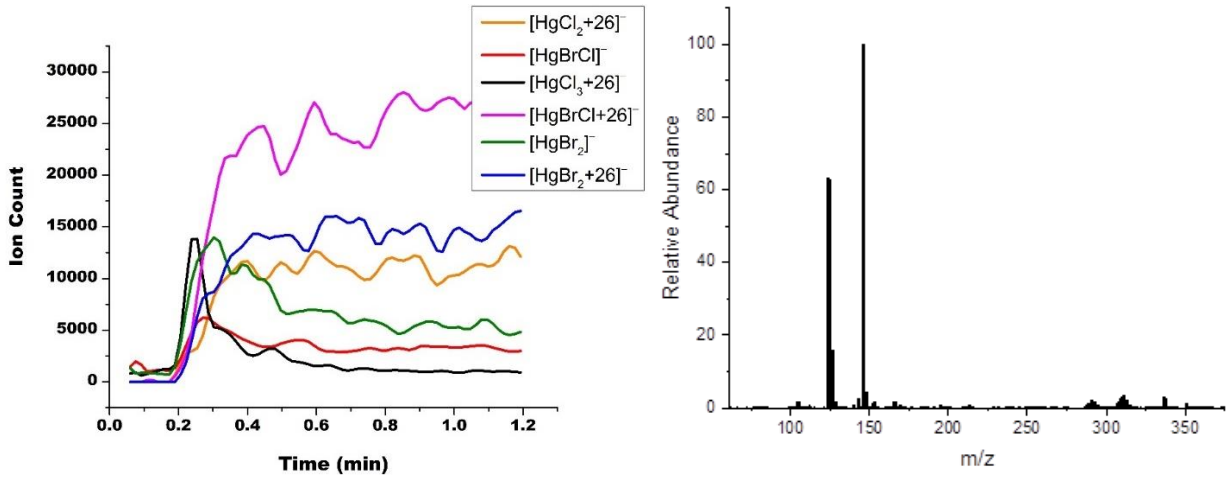

Figure 2.6 (Left) Time evolution of the APCI signal for $HgCl_2$ and $HgBr_2$ ions formed using a 10% isobutane in nitrogen CI gas. HgX_2 was collected for 1 min onto a shredded Teflon trap prior to desorption into the APCI inlet at 200ºC. (Right) Scan mode (m/z 50 – 400) of 0.5% sulfur hexafluoride in isobutane.

The formation of $[HgBrCl]^-$ (red line) and $[HgBrCl+26]^-$ (pink line) occurs after both $HgCl_2$ (as $[HgCl_3+26]^-$, black line) and $[HgBr_2]^-$ (green line) ions are present in the APCI inlet. Principal ions formed (probable ion in brackets) are m/z = 147 ($[SF_6H]^-$), 124 ($[SF_4O]^-$) and 127 ($[SF_5]^-$). *[Originally published in Analytical Chemistry as Supplementary Figures S7 and S8]

2.2.2. Sorbent Trap Desorption: Timing and Temperature.

Direct insertion of HgX_2 standards into the APCI inlet led to persistent blanks (Figure 2.2) and signal degradation over time. To introduce controlled, smaller quantities of analyte, we collected HgX_2 onto homemade sorbent traps consisting of 6 mm ID glass tubing packed with

copper-doped iron nanoparticles silanized with bis[3-(triethoxysilyl)propoyl] tetrasulfide [176]electrostatically held on 5 µm glass beads or with shredded PFA tubing, held in place with glass wool and stainless-steel wire (Figure 2.7 left). Standards were connected with PFA connectors upstream of a sorbent trap attached to a field pump, with flow controlled to 1 L min^{-1} by an acrylic flowmeter downstream of the trap (Figure 2.7 right).

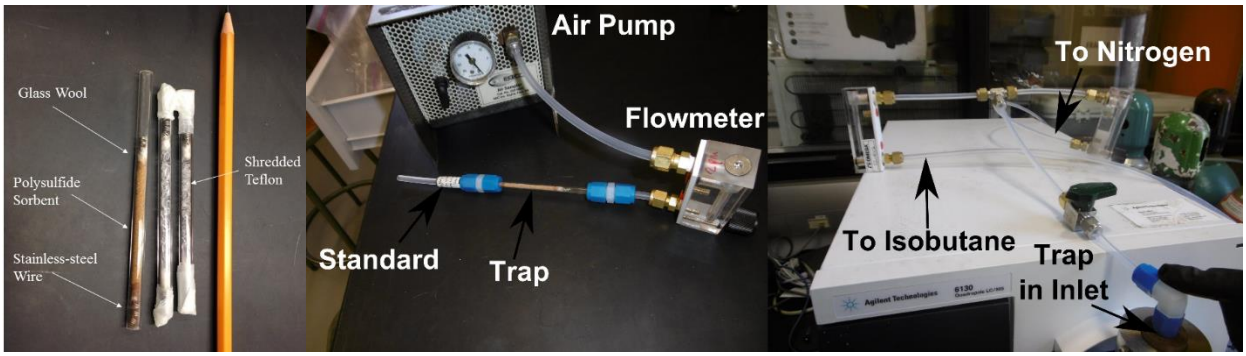

Figure 2.7 (Left) Photograph of polysulfide and teflon sorbent traps used in this study. (Middle) Photographs showing HgX_2 collection and desorption into APCI inlet (Right).

Sorbent is held in place with glass wool and stainless-steel wire and capped with paraffin film when stored. The nitrogen gas line could be reconnected to a sulfur hexafluoride tank when necessary. *[Originally published in Analytical Chemistry as Supplementary Figures S9 and S10]

After pumping, a sorbent trap was immediately connected to a gas line teed to CI gases via a blanked PFA elbow and inserted into the APCI inlet. Initial tests indicated an optimal desorption temperature of 200 °C, with CI gas flow starting at 0.2 min after insertion (Figure 2.8). A decreased signal at 225 °C may result from thermal decomposition of HgX_2 [177]. A desorption of 1.2 min was sufficient to release captured analyte into the APCI inlet. Unless stated otherwise, the following tests involve HgX_2 collection over 1 min followed by desorption into the APCI inlet as described in this section.

2.2.3. APCI Source Parameter Optimization.

Ion production in the APCI source is controlled through manipulation of three main parameters: the current through the corona discharge pin, the voltage applied across the capillary between the APCI source and MS, and the voltage excess applied to the fragmentor, a charged section between the capillary and MS that accelerates ions for controlled fragmentation. These parameters control coronal intensity, in-source fragmentation, and ion complexation (corona current), as well as ion transmission to the MS (capillary and fragmentor voltage). APCI analyses of $HgCl_2$ and/or $HgBr_2$ collected on polysulfide traps for

1 min at 1 L min^{-1} (Sorbent Trap Desorption: Timing and Temperature.) using the IB/N_2 CI gas were taken at corona currents of 10, 20, 30, and 40 µA. For each step in corona current, triplicate measurements using capillary voltages of 500, 1500, 3000, and 4000 V were taken. For each capillary voltage, the fragmentor voltage was set to 20, 40, and 60 V above the capillary voltage. Inlet and drying gas temperatures were set to 200 °C with a drying gas flow rate of 3 L min^{-1}. HgX_2 was detected in SIM mode for m/z of 294–301 ($HgCl_2$) and 382–391 ($HgBr_2$), with the principal signal for the compounds taken as the height of m/z = 298 and 388, respectively.

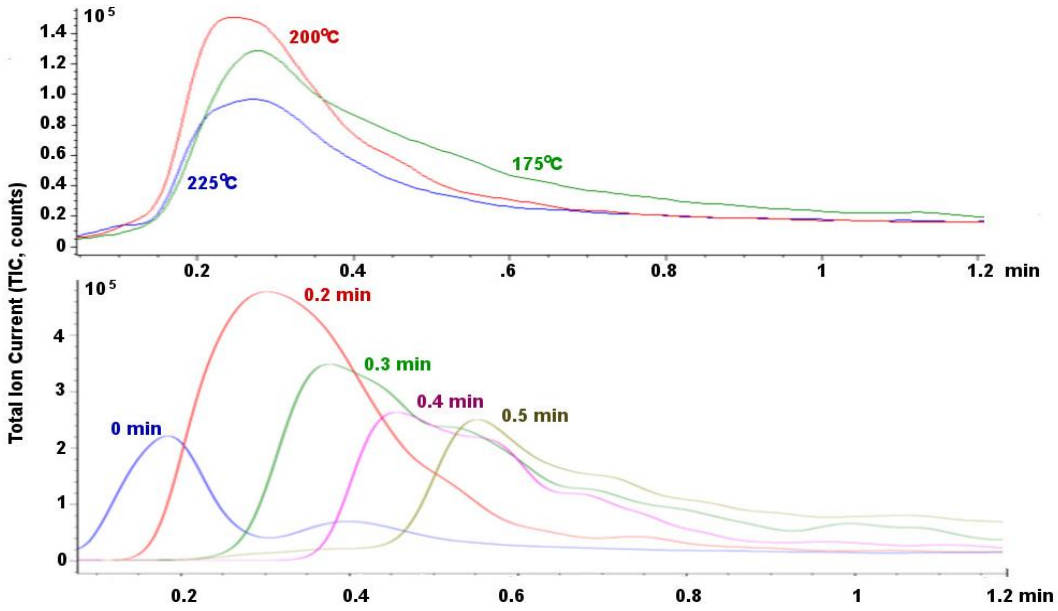

Figure 2.8 Total Ion Current (TIC) for IB:N_2 APCI detection of $HgCl_2$ desorbed from a polysulfide trap exposed to a packed $HgCl_2$ standard over 1 minute at 1 L min^{-1}.

Each TIC signal represents the desorption curve of one $HgCl_2$ collection. The upper plot shows TIC signal for varying inlet temperatures. The lower plot shows TIC as a function of delay between trap insertion and start of CI gas flow (i.e. length of heating period). Heating traps at 200ºC for a period of 0.2 min (12 sec) before CI gas flow produced the most well-defined desorption peak. *[Originally published in Analytical Chemistry as Supplementary Figure S11]

$HgCl_2$ and $HgBr_2$ ion production and transmission using SF_6/IB were also tested for 1 min extracts of air passing through the mixed HgX_2 standard onto a shredded Teflon trap, at capillary voltages of 500, 750, 1500, 2500, and 4000 V (30 µA corona current) and at corona currents of 1, 5, 10, 20, 30, and 40 µA (750 V capillary voltage). Drying gas and inlet temperatures were set to 200 °C with a drying gas flow rate of 5 L min^{-1}, and the fragmentor excess voltage was set to 60 V. A series of tests at fragmentor voltages of 20, 40, 60, 80, 100,

120, and 140 V was also performed with similar inlet temperature/flow conditions and a corona current of 30 μA and capillary voltage of 750 V. HgX_2 was detected in SIM mode for m/z of 290–295 ($HgCl_2$) and 378–383 ($HgBr_2$), with the principal signal for the compounds taken as the height of m/z = 291 and 381, respectively.

2.2.4. Sorbent Trap Packing.

In addition to polysulfide and shredded Teflon traps, we also tested the performance of magnetite, silver pellet, cobalt chloride, and glass wool traps for collection of HgX_2. Construction of these traps was as described in Sorbent Trap Desorption: Timing and Temperature. A full-Teflon trap consisting of shredded Teflon packed into a 6 mm PFA tube was also tested. HgX_2 was collected from air pumped through the $HgCl_2$ particle or mixed mercury halide standard for typically 1 min at 1 L min^{-1}, followed by desorption into the APCI source at 150–200 °C. APCI source parameters were set to the optimums described below in APCI Parameter Optimization. using the SF_6/IB CI blend. HgX_2 was detected in SIM mode for m/z of 290–295 ($HgCl_2$) and 378–383 ($HgBr_2$), with the principal signal for the compounds taken as the height of m/z = 291 and 381, respectively. Results can be found in Table 2.3.

2.2.5. HgX_2 Breakthrough and Retention.

Initial HgX_2 breakthrough testing involved two polysulfide traps connected in series with a $HgCl_2$ source, flowing air through the standard onto the traps at 1 L min^{-1} for varying exposure times (5 s –14 min). After exposure, traps were removed and inserted into the APCI inlet for IB/N_2 analysis. The order of traps was noted; the proportion of total HgX_2 collected on each trap gave a measure of trap breakthrough. The order of traps was changed between runs to prevent possible order bias on the results. A total of 17 runs was collected.

For Teflon traps, we compared the Hg mass collected on a KCl denuder from direct exposure to a mixed HgX_2 standard to the mass of Hg collected with a shredded Teflon trap connected in-line between the denuder and the same HgX_2 standard under identical conditions. Flow through the standard to the denuder was 1 L min^{-1} for 10 s. After sampling, the denuder was placed in-line with the CV/AFS and heated to 500 °C to decompose trapped Hg(II) for CV/AFS analysis. Meanwhile, the Teflon trap, if used, was capped with paraffin film

until analysis. After the denuder analysis, the Teflon trap was placed back in-line with the denuder (at room temperature), wrapped in heating tape, connected to a UHP nitrogen source, and heated to 200 °C for 1 min under a N_2 flow of 1 L min^{-1} to transfer collected HgX_2 onto the denuder. The denuder was then reconnected to the CV/AFS for heating and Hg analysis.

Table 2.3 A Comparison of HgX_2 Trapping and Recovery with Differing Trap Composition

Trap Composition	HgX_2 Standard Used	Exposure Time (sec)	Desorption Temperature (˚C)	Peak Height m/z=291 (cts)	Peak Height m/z=381 (cts)
Shredded Teflon	$HgCl_2$	5	150	2.6×10^3	—
				3.3×10^3	—
				1.5×10^3	—
	8:1 $HgCl_2$:$HgBr_2$	60	200	9.4×10^3	6.6×10^3
Polysulfide S4	$HgCl_2$	5	150	~~4×10^2~~	—
		10		~~4×10^2~~	—
		60	200	1.4×10^4	—
				2.0×10^4	—
	8:1 $HgCl_2$:$HgBr_2$			4.9×10^3	3.6×10^3
Magnetite	$HgCl_2$		50	not detected	—
Silver			150	~~5×10^2~~	—
			200	5.8×10^3	—
				6.0×10^3	—
				5.2×10^3	—
			325	1.6×10^3	—
	8:1 $HgCl_2$:$HgBr_2$		200	1.5×10^4	1.1×10^4
				7.6×10^3	4.8×10^3
All Teflon[a]	$HgCl_2$		150	1.2×10^3	—
CoCl			200	1.6×10^3	—
	8:1 $HgCl_2$:$HgBr_2$			8.8×10^3	7.1×10^3
Glass Wool	$HgCl_2$			~~9×10^2~~	—

*[Originally published in Analytical Chemistry as Supplementary Table S2.]
Strike through – Non-identification of HgX_2 due to contaminants; Value given is an upper limit to target ion peak height. [a] – Shredded Teflon trap capped with Teflon frits in a 6.3 mm PFA tube

The elevated concentrations emitted by our standards (μg Hg m^{-3}) preclude testing of long-term retention of Hg(II) on our sorbent traps. To assess HgX_2 retention, we began by collecting HgX_2 onto the Teflon trap as described above. The HgX_2 -containing trap was then connected to the UHP N_2 line and left under a flow of 1 L min^{-1} N_2 for 24 h. At the end of 24 h, the trap was connected back in-line with the KCl denuder, wrapped in heating tape, and

heated to 200 °C for 1 min under a N_2 flow of 1 L min^{-1} to transfer retained HgX_2 onto the denuder for decomposition to Hg^0 and CV/AFS analysis.

2.2.6. Air Analyses, McGill University, Montreal Quebec, Canada.

Air samples were collected during Fall 2013 and Winter 2014 from the roof of Burnside Hall (~60 m height) on the McGill campus for same-day analysis by APCI-MS (SF_6/IB method). Typically, two of the traps were a polysufide and a shred Teflon trap, with a third trap for alternate trap compositions. Air sampling for all traps was 1 day in length (4 PM to 4 PM).

Traps were blanked in the APCI inlet at 200 °C before being plumbed via PFA connectors and tubing to rotometers connected in parallel to a field pump. Trap inlets were exposed directly to the air. Traps were wrapped in heating tape at 50 °C to inhibit water condensation. At the end of sampling, traps were removed from the manifold, sealed with paraffin film, placed in new plastic bags, and transported into the laboratory for analysis. Time between the end of sampling and analysis was typically 15–30 min. Traps were analyzed as described in Sorbent Trap Desorption: Timing and Temperature.

To test whether $HgCl_2$ may be produced by chlorine emitted by swimming pools, we installed the air sampling equipment on the deck of the Memorial Pool at McGill University from January to March 2014. Samples were collected for 12 h overnight (10 PM to 10 AM). Sampling setup and analysis was identical to the setup installed on Burnside Hall.

2.3. Results and Discussion

2.3.1. APCI Parameter Optimization.

Figure 2.9 displays HgX_2 ion complex production at varying capillary voltage and corona current for IB/N_2 or SF_6/IB CI gases. Broad patterns are evident, and optimal conditions for APCI analysis of HgX_2 are discussed below.

The response of the APCI-MS to $HgCl_2$ generally decreased with increasing capillary voltage (Figure 2.9a,c). The $HgBr_2$ signal was relatively constant with increasing capillary voltage for the single standard but decreased for the mixed standard (Figure 2.9b,c). The discrepancy may arise from comparison of the more variable flux coming off fine powder single-compound standards versus the large-particle mixed HgX_2 standard. The relative

decrease in $[HgX_2 + 19]^-$ with increasing capillary voltage was similar for both $HgBr_2$ and $HgCl_2$ using either CI gas. Capillary voltages in the range of 750–1500 V are optimal for APCI analysis of HgX_2.

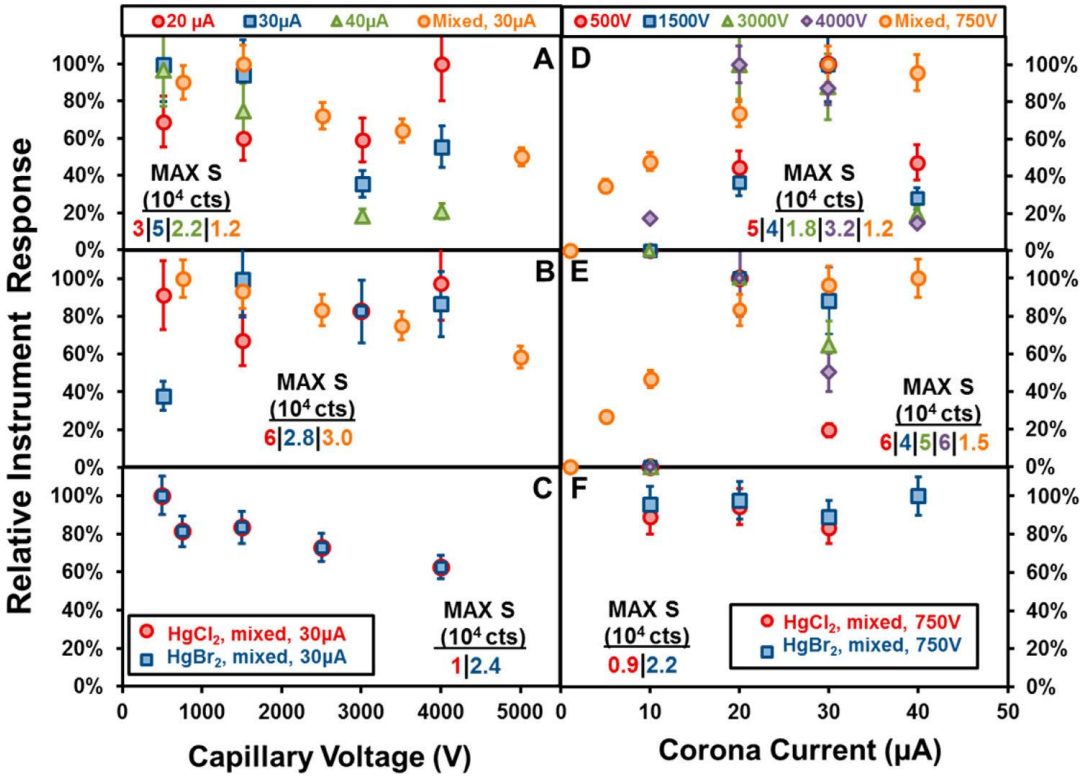

Figure 2.9 Comparison of the APCI-MS response with varying capillary voltage (left-hand side plots) or corona current (right-hand side plots) for $[HgCl_2 + 26]^-$ (A, D) and $[HgBr_2 + 26]^-$ (B, E) using a 10:90 IB/N_2 CI gas blend and for both compounds (as $[M + 19]^-$) using a SF_6/IB CI blend (C, F).

Most tests used single HgX2 standards with the exception of those marked "mixed" which used the 50:50 $HgCl_2$/HgBr2 mixed standard (described in Source Modification and CI Gas Selection). Values are relative responses (% of maximum signal) segregated by corona current (in µA, for capillary voltage tests) or by capillary voltage (corona current tests) and are the mean of 3–6 measurements, with standard deviations of around ±30%. *[Originally published in Analytical Chemistry as Main Text Figure 2]

In this study, corona current optimization balances CI gas fragmentation with ion complex preservation. The effect of these competing phenomena is illustrated in the peak HgX_2 signal for corona currents of 20–30 µA (Figure 2.9d–f). When using 10:90 IB/N_2 as a CI gas, lower corona currents (<20 µA) resulted in little to no $[M + 26]^-$ formation, presumably due to limited isobutane fragmentation. At high corona current, the $[M + 26]^-$ yield either decreased or remained constant, suggesting that analyte was lost to fragmentation and/or complexation with an ionized contaminant. For APCI using SF_6/IB, the yield of $[M + 19]^-$ was

relatively constant with varying corona current. At a capillary voltage of 750–1500 V, the optimal corona current for APCI analysis of HgX_2 is 30 µA.

The fate of HgX_2 with nonoptimal corona currents varied depending on which HgX_2 standard was used; scans ($200 \le m/z \le 500$) of single HgX_2 standards with the IB/N_2 CI blend showed the predominant complex formed at low and high corona current was $[HgX_3]^-$. $HgBr_2$ from the single standard runs was converted into $[HgBr_2Cl]^-$, not $[HgBr_3]^-$, in the ion source, suggesting that chloride contamination was not solely from analyte fragmentation. The sorbent traps used for single $HgBr_2$ tests contained DCDMS-coated glass wool packing; it is probable that at inlet temperatures of 200 °C chlorine containing gases were emitted from the glass wool into the source. Tests using the mixed HgX_2 standard involved direct introduction of an analyte-rich gas stream without preconcentration. Scans of the mixed HgX_2 standard predominantly showed $[M + 32]^-$ at corona currents <20 µA and $[M + 16]^-$, $[M + 17]^-$, and $[M + 32]^-$ at a corona current of 40 µA, consistent with complexation with atomic oxygen (O^-, m/z =16), hydroxide (OH^-, m/z = 17), and molecular oxygen (O_2^-, m/z = 32) formed from molecular oxygen and water in the ion source.

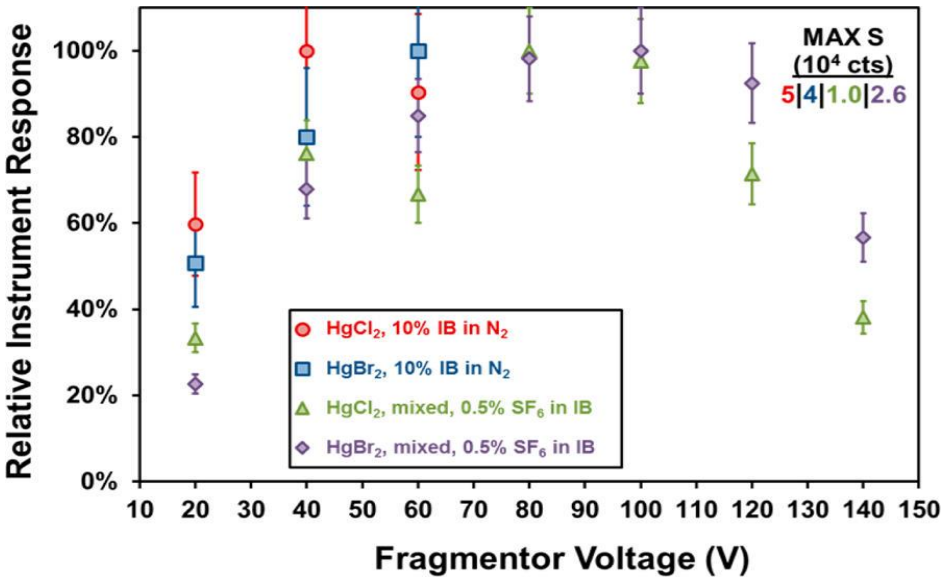

Figure 2.10. Comparison of the APCI-MS response with varying fragmentor voltage for $HgCl_2$ and $HgBr_2$ using either a IB/N_2 or SF_6/IB CI blend. IB/N_2 tests used single HgX_2 standards while SF_6/IB runs used the 50:50 $HgCl_2$/ $HgBr_2$ mixed standard.

As described in Source Modification and CI Gas Selection, values are relative responses (% of maximum signal) and are the mean of 3 measurements, with standard deviations of around ±10–30%. *[Originally published in Analytical Chemistry as Main Text Figures 3]

Figure 2.10 shows the APCI response to HgX_2 for varying fragmentor voltage. Initial tests using the IB/N_2 CI blend at voltages of 20–60 V suggested that ion transmission was relatively constant for voltages >20 V. Later, tests using SF_6/IB at voltages of 20–140 V indicate the highest ion transmission between 80 and 100 V. We therefore selected a fragmentor voltage of 80 V as optimal for HgX_2 measurement.

Figure 2.11 plots the APCI response to HgX_2 with varying drying gas temperature and flow rate. In routine APCI-MS, the drying gas evaporates solvent, facilitating charge transfer to the solute, and acts as a screening gas to prevent neutral molecule transmission into the MS. Additionally, the drying gas temperature must be sufficiently elevated to prevent HgX_2 adsorption to the capillary inlet. These conditions were met by increasing drying gas flow rate and temperature to 5 L min^{-1} at 200 °C. Increasing the flow rate past 5 L min^{-1} might decrease instrument sensitivity to HgX_2, due to increased N_2 concentrations in-source or to lower HgX_2 residence times in the APCI inlet.

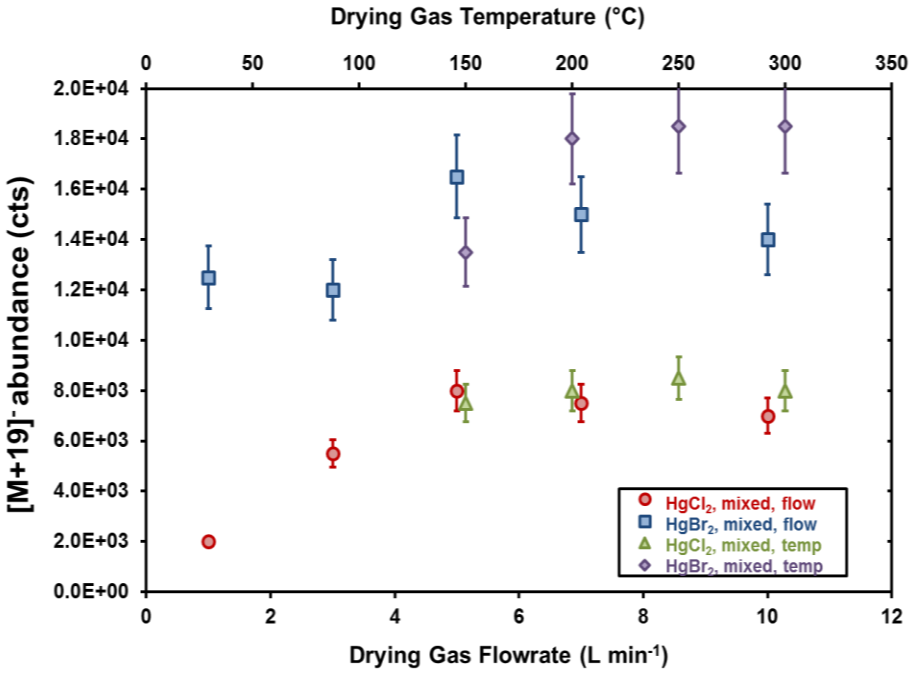

Figure 2.11 The APCI-MS response to $HgCl_2$ and $HgBr_2$ from the mixed HgX_2 standard with varying drying gas flow rate and temperature for $HgCl_2$ and $HgBr_2$ using the 0.5% SF_6 in IB blend CI gas.

Values are the mean of 3 measurements, with standard deviations of ± 20%. Drying gas temperature for flow tests was 200ºC, and drying gas flow rate for temperature tests was 5 L min^{-1}. *[Originally published in Analytical Chemistry as Supplementary Figure S12.]

2.3.2. HgX_2 Breakthrough and Retention.

For exposure times of ≤7.5 min, $HgCl_2$ was observed only on the first trap in retention tests for polysulfide traps. At exposure times of 10–14 min, 4–25% of total $HgCl_2$ was collected on the second trap in the series (average of 15 ± 9%, n = 4).

The results of HgX_2 breakthrough and retention tests for Teflon traps can be found in Figure 2.12. Average HgX_2 breakthrough through Teflon traps was 28 ± 15% (n = 3). The population mean of HgX_2 collected on a Teflon trap desorbed immediately after loading into the KCl denuder versus after a 24 h pumping of N_2 through the trap at 1 L min^{-1} was not significantly different (n= 3, p = 0.21).

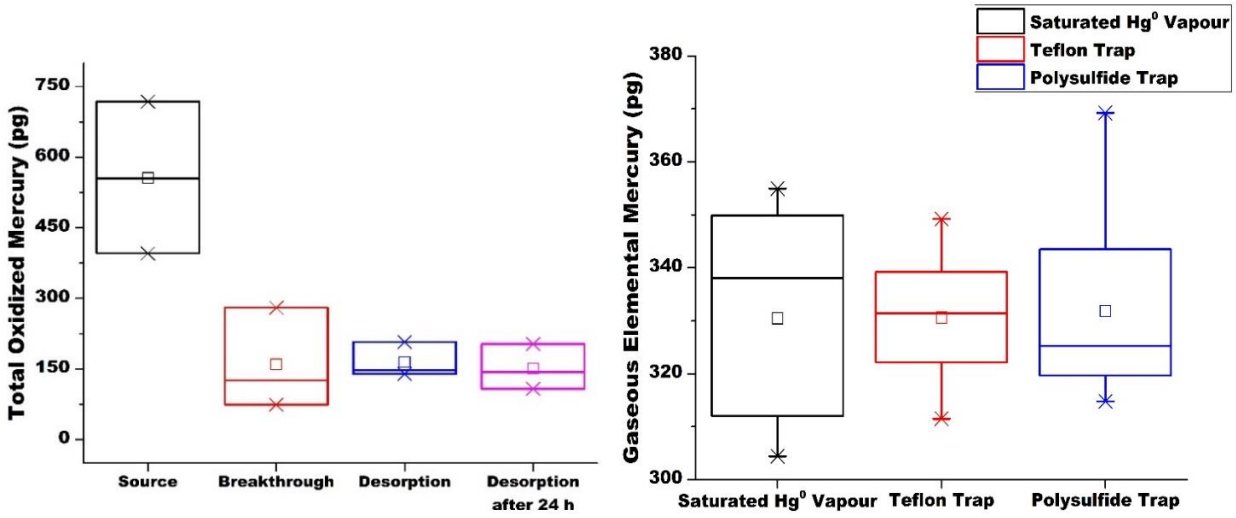

Figure 2.12 (Left) Total Oxidized Mercury (TOM) generated from a mixed $HgCl_2$/$HgBr_2$ source ("Source") and TOM passing through a Teflon Trap to a KCl denuder downstream ("Breakthrough"). (Right) Collection of Hg^0 vapor on Teflon and Polysulfide (PS) Trap.

TOM that was collected on the Teflon trap was desorbed at 200 °C for 1 minute into a KCl denuder ("Desorption"). Finally, TOM was measured from a desorption of $HgCl_2$ and $HgBr_2$ loaded onto a Teflon Trap after 24 hours of N_2 flow at 1L min^{-1} through the trap ("Desorption after 24h"). At the 0.05 level, the population mean of Hg^0 vapour (from TOM thermal decomposition) not trapped on a Teflon Trap ("Breakthrough") is significantly lower (n=3, p=0.0044) than the TOM generated by the source (n=3). The average amount of breakthrough is 28±15%. At the 0.05 level, the population mean of Hg^0 vapour (from TOM thermal decomposition) from desorption immediately after loading versus desorption allowing 24 h pumping of N_2 through the trap at 1 L min^{-1} was not significantly different (n=3, p=0.21). At the 0.05 level, the population mean of Hg^0 vapour injected through a Teflon Trap (n=7, p = 0.988) or the PS Trap (n=7, p=0.894) are NOT significantly different from the mean of a direct injection (n=7). *[Originally published in Analytical Chemistry as Supplementary Figures S12 and S17.]

2.3.3. Calibration, Detection Limit Estimation, and Uncertainty.

Figure 2.13 shows representative calibration curves for APCI analysis of HgX_2 standards using either polysulfide preconcentration and the IB/N_2 CI gas ("PS:IB") or Teflon preconcentration and the SF_6/IB CI gas ("PFA/SF_6"). Instrument responses presented in

Figure 2.13, are the peak height of target masses for $HgCl_2$ and $HgBr_2$. The absolute mass of HgX_2 collected on a sorbent trap was estimated from the collection time, and the HgX_2 emission rate from the standard (pg HgX_2 min^{-1}) was estimated from a concentration of 50 ± 20 ng Hg L^{-1} and a flow rate of 1 L min^{-1}. Masses were increased by 28% for Teflon traps and were not adjusted for polysulfide traps, as exposure times were <10 min (HgX2 Breakthrough and Retention.).

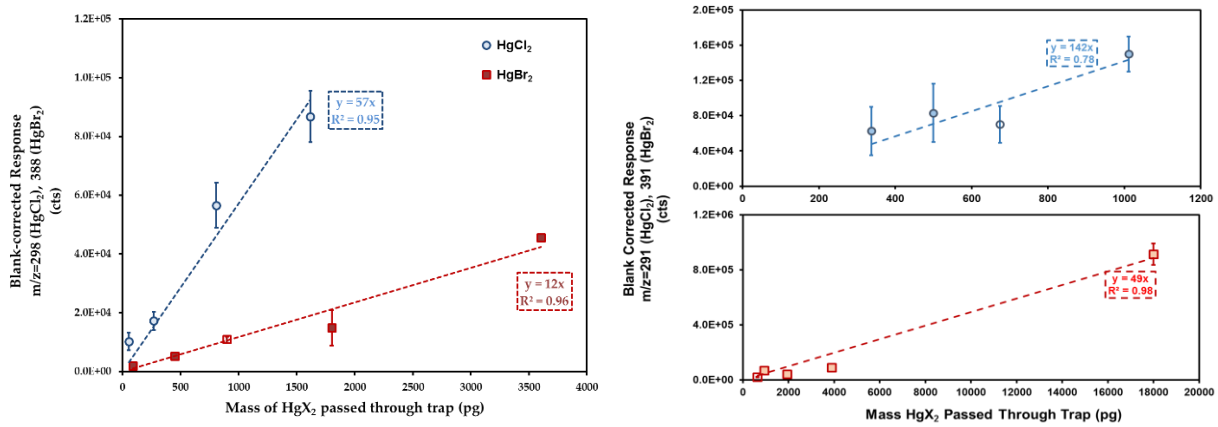

Figure 2.13 A multi-point calibration of APCI-MS analysis of $HgCl_2$ (blue circles) and $HgBr_2$ (red squares) using the PS:IB (left-hand figure) and PFA:SF_6 techniques (right-hand figures).

Each point represents the mean 3 measurements (empty symbols 2 measurements), with whiskers indicating 1 standard deviation from the mean. *[Originally in Analytical Chemistry as Supplementary Figure S14.]

Practical equipment constraints prevented trapping of less than 40 ± 10 pg $HgCl_2$ and 50 ± 10 pg $HgBr_2$. To estimate detection limits, we extrapolated from the range covered by calibration curves down to 3σ of the background noise. Detection limits are estimated to be 14 pg $HgCl_2$ and 40 pg $HgBr_2$ for the PS/IB method and 6 pg $HgCl_2$ and 17 pg $HgBr_2$ for the PFA/SF_6 method. Quantities between detection limits and the lowest quantities directly measured are semiquantitative but mainly cover the range below the limit of quantitation. For a sampling period of 1 day at 1 L min^{-1}, the detection limits presented correspond to concentration-based detection limits of 10 pg $HgCl_2$ m^{-3} and 28 pg $HgBr_2$ m^{-3} by PS/IB and 4 pg $HgCl_2$ m^{-3} and 11 pg $HgBr_2$ m^{-3} by PFA/SF_6. The sensitivity of the PFA/SF_6 technique was 1.4 × 10^2 cts pg^{-1} $HgCl_2$ and 5 × 10^1 counts pg^{-1} $HgBr_2$, higher than sensitivities using PS/IB (6 × 10^1 cts pg^{-1} $HgCl_2$ and 12 cts pg^{-1} $HgBr_2$). The sensitivity of either technique may be lower than that estimated from single HgX_2 standards due to ion reactions in the APCI

source. Concentrations determined using these calibration curves should be considered lower limits to atmospheric HgX_2 concentrations during sampling.

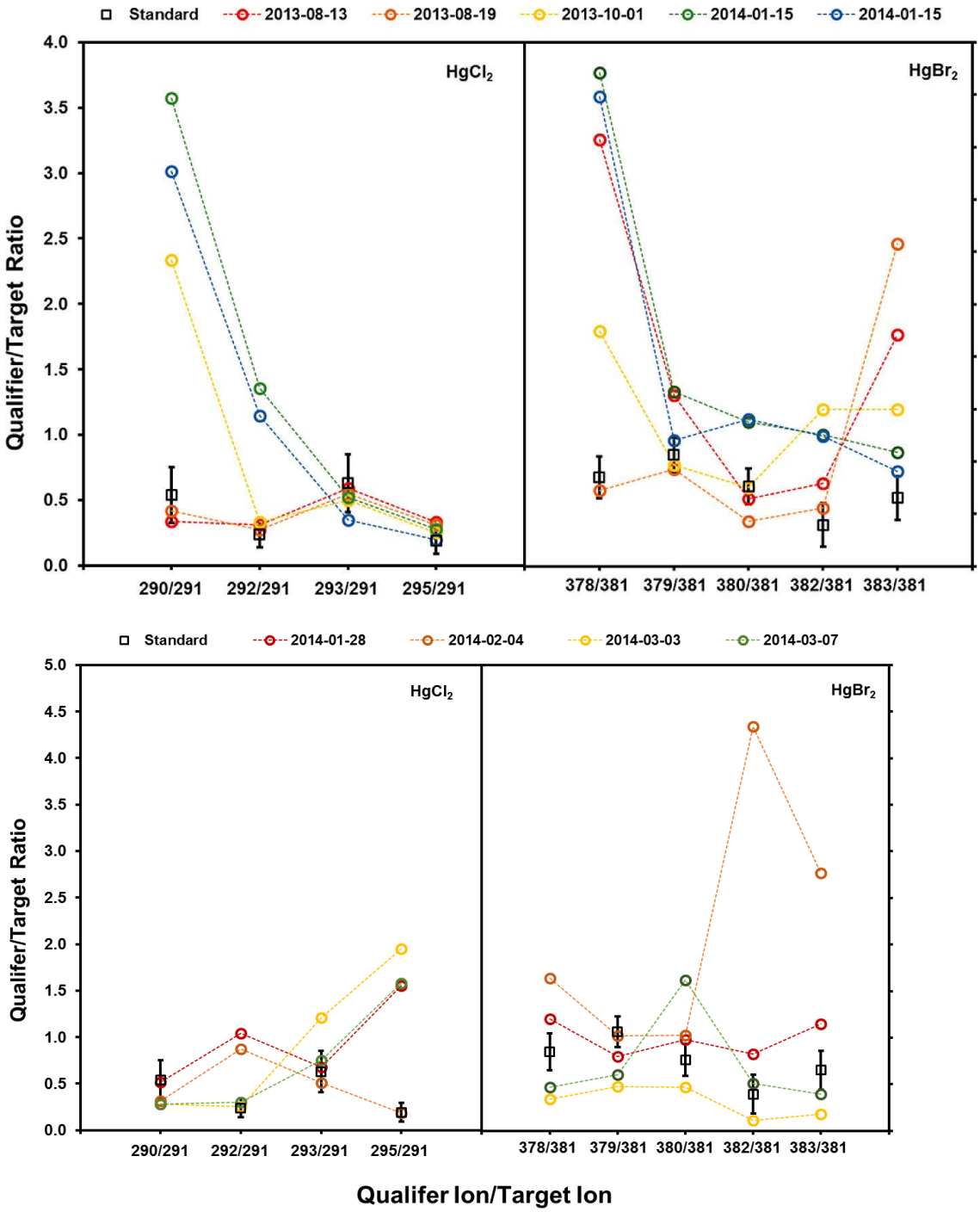

Figure 2.14 Qualifier/target (Q/T) ion ratios for SIM mode analyses of $HgCl_2$ and $HgBr_2$ in Montreal urban air from August 2013 to January 2014 and pool air from January to March 2014.

HgX_2 standard Q/T ratios are shown in black with whiskers equal to 2 times their standard deviation. Sample Q/T ratios falling within the range indicated by whiskers indicate a positive match with standard Q/T ratios. . *[Originally published in Analytical Chemistry Main Text Figure 3 and Supplementary Figure S15.]

The results presented in Figure 2.9 and Figure 2.10 suggest that the reproducibility of HgX_2 preconcentration and APCI analysis is ±30%. Estimates of HgX_2 concentration (pg m^{-3}) include uncertainty from calibration (±40%) and volume sampled (±10%, based on flowmeter variability). Propagating relative errors gives an uncertainty of measurement of ±50%.

2.3.4. Air Measurements.

Table 2.4 Urban/indoor air measurements in Montreal, Canada 2013-2014

Year	Start Date	Stop Date	Trap	$HgCl_2$	$HgBr_2$
				pg m^{-3}	
Burnside Hall, McGill University Campus, Montreal Canada (urban, ~50 m above ground level)					
2013	224.67	225.67	PS	5×10^1	<11
			Tef A	1×10^2	$<6 \times 10^1$ *
			GB	7×10^1	19
	228.67	231.67	Tef A	8×10^1	9×10^1
			TL	<17*	12
			Tef B + PS	<29*	<24*
	242.67	245.67	TL	<12*	<11
			Tef B + PS	<6*	<11
	273.67	274.67	Tef A	4×10^1	3×10^1
			TL	$<4 \times 10^1$ *	<24 *
			T	29	9×10^1
2014	14.67	15.67	PS	<4	<11
			Tef A	7	<11
			Tef B	<6 *	<11
Memorial Pool, McGill University Campus, Montreal Canada (indoor)					
2014	27.92	28.42	PS	$<6 \times 10^1$ *	<19 *
			Tef A	8×10^1	$<6 \times 10^1$ *
			CoCl	$<2 \times 10^2$ *	<11
	34.92	35.42	PS	27	<26 *
			Tef A	5×10^1	29
	64.92	65.42	PS	16	5×10^1
			Tef A	8×10^1	$<1.4 \times 10^2$ *
	65.92	66.42	PS	<4	<11
			Tef A	4×10^1	$<1.2 \times 10^2$ *

PS – Polysulfide-coated copper/iron nanoparticles, GB – glass beads, Tef – shredded Teflon, TL – shredded Teflon in GC liner, T – shredded Teflon in Teflon tubing (all Teflon), CoCl – cobalt chloride crystals, Tef + PS – Teflon trap with PS precolumn. * - Contaminants present based on qualifier-target ion ratios. Concentration is an upper limit to possible HgX_2 concentration. *[Originally published in Analytical Chemistry as Supplementary Table S4]

APCI analyses of urban and pool air extracts collected on Teflon traps can be found in Figure 2.14 and Figure 2.15. Target ions were m/z = 291 ($HgCl_2$) and m/z = 381 ($HgBr_2$). Qualifier ions for $HgCl_2$ were m/z = 290, 292, 293, and 295 and for $HgBr_2$ were m/z = 378, 379, 380, 382, and 383. Positive identification of HgX_2 was made by comparing sample and

standard qualifier–target (Q/T) ion ratios (i.e., the ratio of a qualifier ion signal to the target ion signal).

Comparison was considered "excellent" if all sample Q/T ratios were within 2σ of standard Q/T ratios, "good" if 3 Q/T ratios matched, "acceptable" if 2 Q/T ratios were consistent, and "poor" if <2 Q/T ratios matched standard ratios. Representative SIM mode APCI analyses (PFA/SF_6 method) for samples collected at Memorial Pool and Burnside Hall, including trap blanks, are shown in Figure 2.15. Trap blanks are significantly smaller than air measurements indicating that compounds detected are not analyte carryover.

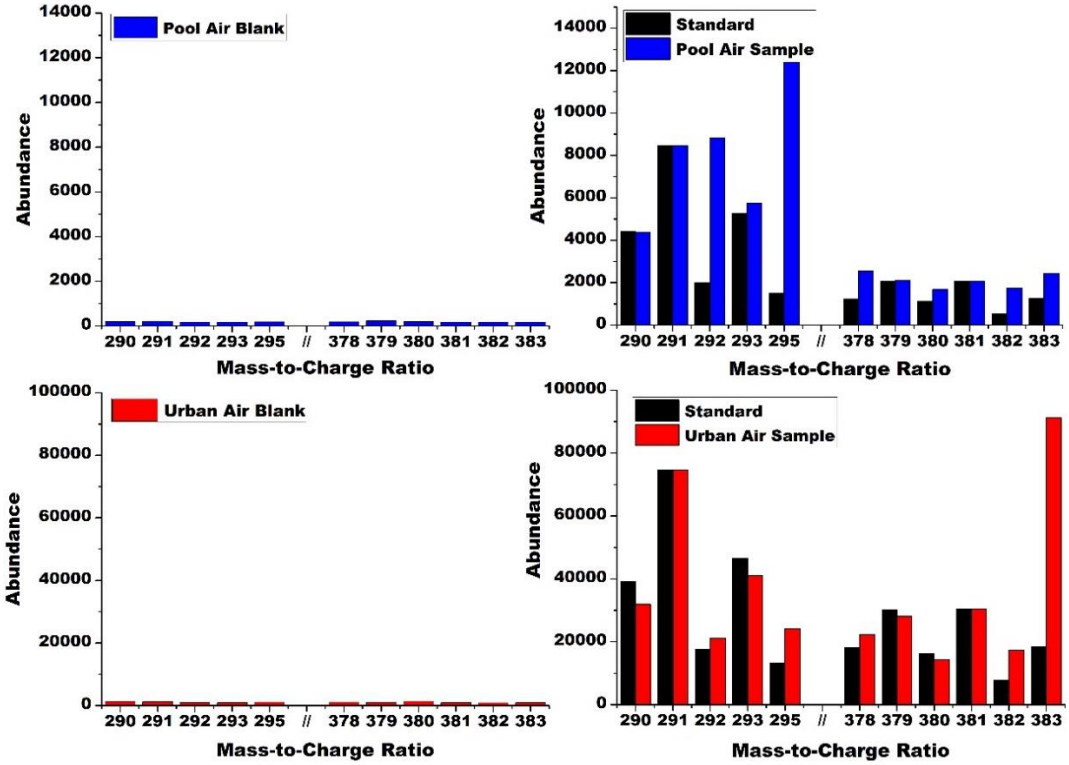

Figure 2.15 Representative SIM-mode mass spectra for indoor pool air and urban air runs in Montreal, Quebec. Trap blanks (left-hand plots) are negligible compared to air measurements.

A SIM-mode spectrum for a 50:50 $HgCl_2$:$HgBr_2$ source is presented for comparison. *[Originally published in Analytical Chemistry as Supplementary Figure S16]

$HgCl_2$ detection was excellent in August 2013, good in October 2013, and acceptable in January 2014. $HgBr_2$ detection was acceptable during August and October 2013 and possibly during January 2014, but identification was complicated by highly variable Q/T ratios. $HgCl_2$ detection in pool air was good throughout the sampling campaign, with $HgBr_2$

only detected at an "acceptable" level once during the period. Hg^0 injections through polysulfide and Teflon traps are statistically indistinguishable from direct Hg^0 injections to the CV/AFS (Figure 2.12 Right) suggesting that HgX_2 observed does not result from collection of Hg^0 followed by heterogeneous oxidation to Hg(II).

HgX_2 concentrations for analytes collected onto shredded Teflon traps ranged from <4 to 1×10^2 pg $HgCl_2$ m^{-3} and <11 to 9×10^1 pg $HgBr_2$ m^{-3} in Montreal urban air and (4–8) × 101 pg $HgCl_2$ m^{-3} and <11 to 29 pg $HgBr_2$ m^{-3} in pool air. A fault in the APCI inlet oven lead to incomplete desorption during pool sample analyses, and presented concentrations are lower limits.

2.4. Conclusions and Future Research

In this study, we provide the first chemical identification of atmospheric $Hg(II)_{(g)}$ using a novel nano/microparticle extraction-APCI-MS technique. Both $HgCl_2$ and $HgBr_2$ were detected in air extracts. Being trap-based, the technique is portable and shows promise as a valuable tool for studying mercury cycling in the environment. The technique could be extended to other forms of Hg(II) that may be present in the atmosphere, such as HgO or HgI2. Although in passing, we have shown that aqueous Hg(II) APCI analysis is feasible. Aqueous analysis using a softer ionization technique (electrospray ionization) may be a valuable avenue of research for a wider range of oxidized mercury in different environmental and nonenvironmental matrices. Optimized APCI-MS analysis of HgX_2 occurs at a corona current of 30 μA, capillary voltage of 750−1500 V, fragmentor voltage of 80 V, and a drying gas temperature and flow rate of 200 °C and 5 L min^{-1}.

The main weakness of this technique is the frequent presence of co-adsorbed contaminants and decreased sensitivity to HgX_2 from unwanted ion reactions in the APCI source. It would be advantageous to develop gas chromatographic separation of collected air samples, although GC separation may be limited by loss of Hg(II) to the column.11 The current sampling time of 24 h is long and needs to be reduced to bring the temporal resolution of Hg(II) measurements into parity with the much faster GEM and $Hg_{(P)}$ techniques typically used. We foresee that in near future various combination of mass

spectrometry techniques (e.g., MS/MS or MS/MS/MS or high-resolution units), will further improve identification and quantification of a wider range of mercury species at trace levels.

2.5. Acknowledgments

We thank H. Khan and Y. Eid for their aid in method development. We also thank P. Carpenter and D. Jacques for allowing us access to the Memorial Pool and Burnside roof for sampling. Funding for this study came from the Natural Science and Engineering Research Funding of Canada, Canadian Foundation for Innovation, Idea-to-Innovation, and Environment Canada. We thank Drs. A. Dastoor and C. Banic for their support. This manuscript benefited significantly from the input of three anonymous reviewers.

Chapter 3. Development of Methodology to Generate, Measure and Characterize the Chemical Composition of Oxidized Mercury Nanoparticles

Adapted from a submission to Analytical and Bioanalytical Chemistry [ABC-00761-2019]

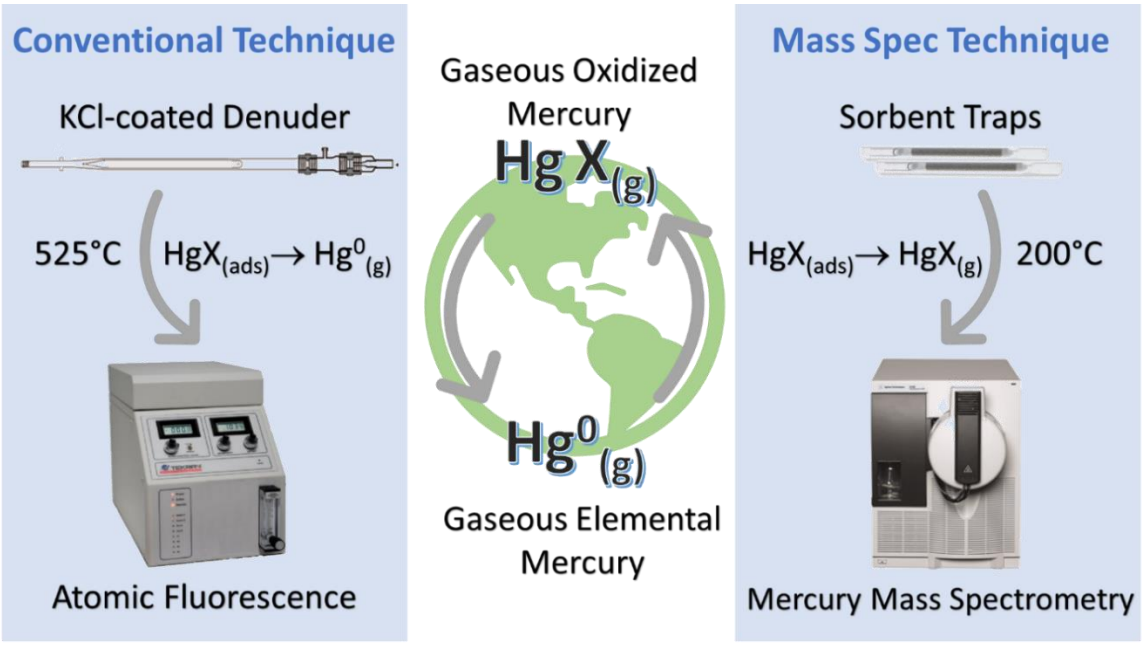

TOC Figure 3. A comparison between the conventional method for studying gaseous oxidized mercury and the novel mercury mass spectrometry method of measuring gaseous and particulate oxidized mercury.

In this chapter, two methods are used to generate oxidized mercury nanoparticles. Lack of standards in the mercury sciences, especially for oxidized mercury, has been a long-term issue. These nanoparticulate mercury aerosols are characterized using scanning mobility and optical particle sizing, electron microscopy and their stability is assessed in tropospheric and aqueous settings. The capture of nanoparticles is assessed by KCl denuder and by particulate filters, and by micro- and nano-particulate sorbents traps used in mercury mass spectrometry.

Contribution by author: In this work, I developed the experimental design, the method for vapour-phase condensation and aqueous nebulization using techniques used in literature for other metal and aerosol systems, performed the data analysis, and either conducted the experiments independently or in conjunction with undergraduate students under my mentorship.

Abstract

Oxidized mercury (OM) is an important global atmospheric contaminant that is present either as a gaseous species (GOM) or bound to particulates (PBM). While it makes up a fraction of atmospheric mercury, OM is regarded as more water-soluble, bioavailable, and a key intermediate in processes that lead to organic mercury transformation. Using vapour phase condensation and aqueous nebulization we generate particulate oxidized for three species: mercury(II) chloride, mercury(II) bromide, and mercury(II) oxide and characterize these aerosols using scanning mobility and optical sizing, electron microscopy and the novel mercury mass spectrometry technique.

The conventional methods for measuring gaseous and particulate oxidized mercury are KCl-coated annular denuders and filters, respectively. Placed downstream from the KCl-denuder during sampling, these mostly quartz fibre and Teflon filters are acid digested and dissolved particulate mercury species are reduced to elemental mercury and measured as GEM. Two concerns arise from this arrangement of sampling modules, what portion of particulate mercury contaminates KCl denuder-based GOM measurements and what portion of these particulates penetrate filters impacting particulate-bound mercury measurements?

Using generated oxidized mercury aerosols, we assess the degree to which they are captured by the KCl-coated annular quartz denuders and particulate filters and conclude a significant portion of nanoparticulate and sub-micron particulate mercury was trapped on the KCl-coated annular denuder and measured as gaseous oxidized mercury.

3.1. Introduction

Atmospheric mercury is characterized by three bulk, operationally defined species: gaseous elemental mercury (GEM), gaseous oxidized mercury (GOM) and particulate-bound mercury (PBM) [70]. GEM is the predominant species in the atmosphere and is measured using pre-concentration on gold traps, thermal desorption followed by cold-vapour atomic fluorescence spectroscopy (CVAFS), cold vapour atomic absorbance spectroscopy (CVAAS) or inductively coupled plasma mass spectrometry (ICP-MS). It is by far the most abundant mercury species in the atmosphere with concentrations in the low ng/m^3 range in urban areas [178,179].

Gaseous oxidized mercury (GOM), generally regarded as Hg^{2+} species, has been detected in both tropospheric and stratospheric air with in pg/m^3 concentrations. GOM is measured by trapping to KCl-coated annular denuders, followed by thermal decomposition and measurement as GEM. Until recently the chemical identity of gaseous oxidized mercury was largely unknown though mercury mass spectrometry has confirmed the detection of mercury(II) bromide and mercury(II) chloride in urban air. These compounds are more reactive and more water-soluble than Hg^0, which allows them to be easily be absorbed by rain droplets, deposited to terrestrial and aquatic environments and scavenged from the atmosphere.

Developed in the 1990s as a technique for measuring oxidized mercury species, KCl-coated denuders involve the conversion of oxidized mercury species to a $HgCl_4^{2-}$ species incorporated into the potassium chloride coating. At 600 °C, these species are decomposed producing gaseous Hg^0 which is measured using cold-vapour atomic fluorescence spectroscopy (CVAFS). In addition to differences in the efficiencies by which gaseous oxidized mercury species being trapped, KCl-coated denuders are affected by O_3 and humidity measurements [141]. Placing a KCl denuder upstream of PBM filters reduces a significant positive artifact caused by GOM adsorbed to the filter [93]. Despite this, KCl denuders continue to be used as they allow for simpler analytical procedures and high-time resolution measurements to be made.

The conventional methodologies of studying atmospheric mercury described are limited to determining whether mercury is elemental, inorganic or particulate in nature but fail to give the actual chemical species present. Gaseous oxidized mercury has long been suspected to be mercuric (Hg^{2+}) species such as HgO [122], $HgCl_2$ [119], $HgBr_2$ [180], $Hg(OH)_2$ [180], $HgSO_4$, $Hg(NO_2)_2$ [181], or cross-halogen species [182]. Evidence for stable Hg^{+1} has also been found such as HgBr from the oxidation of Hg^0 with BrO radicals [183]. $HgCl_2$ and $HgBr_2$ were however indirectly identified in field samples via thermo-desorption profiles for nylon exchange membranes [141] and more recently in Montreal urban air, directly by nano/micro phase adsorption interface coupled to atmospheric pressure chemical ionization mass spectrometry [142]. Nano and micro-particle interface atmospheric pressure chemical ionization mass spectrometry (APCI-MS) involves trapping

of gaseous reactive mercury onto solid phase sorbent traps, thermal desorption in the inlet of a modified APCI and detection using mass spectrometry.

Particulate-bound mercury is trapped on to quartz filters which are acid digested using nitric acid, aqua regia, or BrCl. The dissolved oxidized mercury species are then reduced using stannous (II) chloride to dissolved elemental mercury which is purged from solution and measured by CVAFS. Particulate bound mercury is suspected to be mostly mercury(II) oxide, mercury(II) halides, elemental mercury, mercury(II) chloride and mercury sulfide [2,140]. Both GOM and PBM have lower residency times in the atmosphere largely due to higher wet and dry deposition and also are more bioavailable to organic-mercury transforming bacteria in aqueous environments. The conversion of GEM to GOM and interaction of GEM to PBM is of prime importance to understanding the fate of mercury in our environment as both processes serve as important sinks [184]. Though particulate mercury concentrations are ultra-trace, PM_{10} is inhalable, $PM_{2.5}$ is respirable, and $PM_{1.0}$ can penetrate the pulmonary alveoli [2]. Understanding the contribution of particulate mercury is vital to understanding the ultimate risk of these species to human and ecological health. As with KCl denuders for measuring GOM, filters for measuring PBM can be influenced by artifacts. Gas-particle and particle-particle interactions on filters will increase over time and for the later increase with polydisperse particle populations [185]. Pyta and Rogula-Kozlowska (2016) found that mercury content decreases with particle diameter from 100 nanometers to 40 microns with maximum mercury content occurring between 400 and 650 nanometers [2].

In this study, we use two methods for forming oxidized mercury aerosols: vapour phase condensation and aqueous nebulization and characterize these aerosols using particle sizers, electron microscopy and mass spectrometry. We also determine the trapping efficiency of denuders for three aerosolized oxidized mercury species: mercury(II) bromide, mercury(II) chloride, and mercury(II) oxide. Mercury(II) chloride and mercury(II) bromide have already been detected in Montreal's urban air and the low vapor pressure of mercury(II) oxide supports condensation even at part per trillion concentrations [184]. Various dry conditions (<35% relative humidity) were used as the highest tropospheric reactive mercury (GOM + HgP) concentrations occur under those conditions [186]. Flow rates through the denuder were varied from 1.7 L/min to 10 L/min. In terms of particulates, laminar flow is said to

prevent small particles from impacting on the coating surface and cyclones and impactors large particles upstream of the denuder [70]. The degree of penetration of mercury nanoparticles through various filters was also assessed.

3.2. Materials and Methods

Nanosized and ultrafine oxidized mercury particles were formed from two methods: vapour phase condensation (3.2.1) and the nebulization of aqueous oxidized mercury species (3.2.4).

3.2.1. Formation of Mercury Halide Aerosols – Vapour Phase Condensation

Anhydrous 10-mesh granules of 99.9999% purity mercury(II) bromide and mercury(II) chloride was obtained from Sigma Aldrich and ~0.5 g of mercury(II) halide granules were packed between two Teflon® frits in ¼ inch I.D. x $^{3}/_{64}$ inch O.D. PFA Teflon® (Solon, OH). Sources were heated with heating tape connected to a temperature controller. A Big Hydrocarbon Trap Big Hydrocarbon Trap from Agilent Technologies (Mississauga, ON) and PVDF filters from Parker Balston (Haverhill, MA) were used to scrub high purity nitrogen produced by a Peak Scientific NM32LA Nitrogen Generator (Billerica, MA) of hydrocarbons and particles, respectively. An Omega low-flow inline heater was used to heat the nitrogen carrier gas to the desired temperature. Sources were equilibrated for 10 minutes at the desired source temperature before carrier gas of the equivalent temperature was used to introduced to the source.

3.2.2. Aerosol Characterization Process – High Resolution Scanning Transmission Electron Microscopy (HR-STEM)

Synthetic mercury aerosols were collected by the direct placement of TEM grids downstream from mercury halide sources purged with high purity N_2, through the use of an ESPnano 100 electrostatic precipitator (Spokane, WA) and in a microcosm experiment where TEM grids were placed 10 cm away from a watch glass holding 10-mesh mercury(II) bromide and mercury (II) chloride beads. The microcosm system was subjected to 0.51 m/s flow rates of laboratory air, visible light exposure at pressure of ~ 740 Torr at 23 ± 2 °C for one week to mimic tropospheric conditions. 200 mesh Formvar/carbon coated copper TEM grids and 400 mesh Formvar coated copper TEM grids were obtained from Electron Microscope

Sciences (Hatfield, PA) and SPI Supplies (West Chester, PA), respectively. Samples were analyzed using FEI Tecnai G^2 F20 kV Cryo-STEM with EDAX Octane T Ultra W/Apollo XLT_2 SDD and TEAM EDS Analysis System (Hillsboro, OR).

3.2.3. Aerosol Characterization Process – Aqueous Suspensions

Particle concentrations and size distributions for synthetic mercury (II) chloride and mercury (II) bromide particles suspended in aqueous media, with hydrodynamic radii of 30 nm – 2000 nm were obtained using a Nanosight NS500 from Malvern Instruments (Ann Arbor, MI). Sources were equilibrated to a given temperature for 10 minutes before a carrier gas flow rate of 0.25 LPM was initiated allowing flow to bubble into 500 µL of 0.1 µm filtered milliQ water. The results obtained were for the average concentration of ten replicates. Results obtained are for the average concentration of ten replicates. Nanoparticle tracking analysis (NTA) involves tracking the motion tracking of individual particles from scattered laser light and using Stokes-Einstein to determine a hydrodynamic radius.

3.2.4. Formation of Mercury Halide Aerosols – Aqueous Nebulization and Drying

30.1 mg of 99.999% trace metals basis mercury(II) chloride obtained from Sigma-Aldrich (St. Louis, MO) was dissolved with nanopure water into a 50.00 mL Pyrex No. 5460 volumetric flask. Similarly, 30.8 mg of 99.998% trace metals basis mercury(II) bromide and 31.3 mg of 99.0% ACS reagent mercury(II) oxide red obtained from Sigma-Aldrich (St. Louis, MO) to create 0.06% (w/v) solutions. Solutions were sonicated at 50 °C to promote dissolution. The aerosol formation process was adapted for the mercury sciences from [187] and depicted in Figure 3.1. 0.06% (w/v) aqueous oxidized mercury solutions were loaded into 10 ml Luer Lock tip sterile polypropylene syringes from Terumo Corporation (Laguna, Phillipines) and dispensed using a GenieTouch™ infusion dual syringe pump from Kent Scientific Corporation (Torrington, CT) at 10 µL/min. Solution enters a C-Flow 700d PFA Nebulizer from the Savillex Corporation (Minnetonka, MN) through platinum-cured, low-volatile grade, silicone tubing. Compressed air obtained from Praxair Canada (Mississauga, ON) scrubbed of particles using a Whatman HEPA-Cap 150 (Little Chalfont, Buckinghamshire, UK) was introduced to the nebulizer at 20 psi to create a consistent stream of aerosol.

3.2.5. Aerosol Drying Process – Aerosol Nebulization and Drying

The aerosol stream entered a three-port in-house built mixing chamber where laboratory air was introduced through a HEPA filter to compensate for the flow rates required for the experiments. Following dilution, aerosol entered a cylindrical polycarbonate silica gel-based double diffusion dryer where water from the aerosol is removed. The relative humidity of the aerosol stream leaving the diffusion dryers was measured using an iCelsius Sentinel Next Temperature and Relative Humidity sensor from Aginova Inc. (Mason, OH).

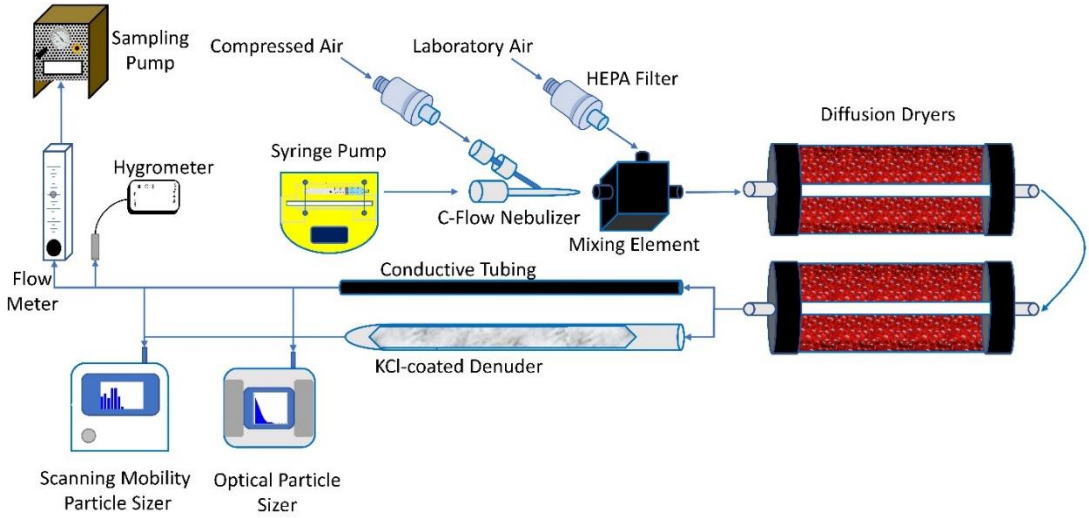

Figure 3.1. Experimental Set-up for Oxidized Mercury Aerosol Generation by Aqueous Nebulization and Drying, KCl denuder experiments and measurement by SMPS and OPS

*[Originally submitted to Analytical and Bioanalytical Chemistry as Main Text Figure 1]

3.2.6. KCl Denuder

The quartz annular denuder was rinsed and soaked with distilled water before cleaning with 10% reagent grade nitric acid, nanopure water and reagent grade methanol before being dried in a mercury-free laminar fume hood. 14.5 g of potassium chloride was dissolved in 100 mL of water and drawn by vacuum into a vertically positioned quartz annular denuder clamped in place to a ring stand. The solution was drawn up to the active denuder surface and slowly allowed to drain and repeated two times. Reagent grade (68-70%) nitric acid and reagent grade methanol (98.8%) for cleaning the quartz annular denuder was obtained from ACP Chemical Inc. (Montreal, QC) and crystalline ACS grade potassium chloride (99.0 – 100.5%) for coating the denuder was obtained from Fisher Scientific Company (Ottawa, ON). The inlet of the denuder was wiped dry before the entire denuder was dried with mercury-

free air produced using a Model 1100 zero air generator from Tekran Inc. (Toronto, ON.) The KCl-denuder was thermally conditioned in a Thermolyne Sybron F-21125 tube furnace oven from ThemoFisher Scientific (Waltham, MA) at 525 °C for 1 hour.

3.2.7. Denuder Uptake Experiments

The dry aerosol entered either a KCl-coated denuder or conductive tubing of equivalent length from TSI Incorporated (Shoreview, MN) before being drawn into a particle sizing instruments. A NanoScan Scanning Mobility Particle Sizer (SMPS) Model 3910 from TSI Inc. was used to determine the aerosol particle size distributions from particles ranging in size from 10 nm to 420 nm across 12 bins with 1 scan/minute measurement rate and a sampling rate of 1 L/min. An Optical Particle Sizer (OPS) Model 3310 from TSI Inc. was used to determine the aerosol particle size distributions for particles ranging in size from 300 nm to 10 μm across 16 bins with 1 scan per 10 minute measurement rate and a sampling rate of 0.7 L/min. A series of 10 1-minute runs for the SMPS or 1 10-minute run for the OPS would be considered a "batch," with 7 batches uptake experiments conducted under control and experimental conditions with batch order pre-determined at random. Three flow rates were assessed for the uptake experiments including: 1.7 L/min (from the combined sampling flow rates of the SMPS and OPS), 5 L/min and 10 L/min (achieved from the combining sampling flow rates of SMPS, OPS and a Vac-u-Go Air Sampler from SKC Incorporated (Eighty Four, PA). Humidity was varied by removing diffusion dryers from the set-up.

3.2.8. Particle Trap Preconcentration – Mercury Mass Spectrometry (Hg-MS)

Synthetic mercury(II) bromide and mercury(II) chloride aerosols were collected on particle traps consisting of a variety of sorbents including: gold fibre, glass beads, silver granules, PFA Teflon and polysulfide-coated copper-doped iron nanoparticles. Traps were housed in either ¼ inch O.D. glass or PFA Teflon tubing which sorbent held in place using silanized glass wool or PFA Teflon frits. Exposure times for the traps to mercury(II) halide aerosol generation flows varied from 5 seconds to 1 minute. Traps were placed in a modified atmospheric pressure chemical ionization inlet, heated for 1.2 minutes at 200 °C and desorbed using a 1L/min 1% SF_6 in Isobutane carrier gas. The Agilent 6140 single quadrupole mass spectrometer was optimized to the following set-points: corona current at

30 µA, capillary voltage to 750 V, N_2 drying gas flow rate and temperature at 5 L/min and heated to 200 °C, and fragmentor voltage to 90 V. Mercury (II) bromide, mercury (II) chloride and mercury (II) bromochloride were detected as fluoride complexes at m/z 287 – 295, 331 – 341, and 388 – 396, respectively. Other mixed mercury(II) halides were also identified such as $HgBr_2Cl$ and $HgCl_2Br$.

3.2.9. Aerosol Analysis

Average aerosol concentrations and standard deviations were determined for each bin size and compared between the conductive tubing control and KCl-coated denuder for the denuder uptake experiments. Analysis of variance (ANOVA) was performed using a 95% confidence interval over 70 samples. OriginPro 2016 software from OriginLab Corporation (Northampton, MA) was used for all statistical analyses.

3.3. Results and Discussion

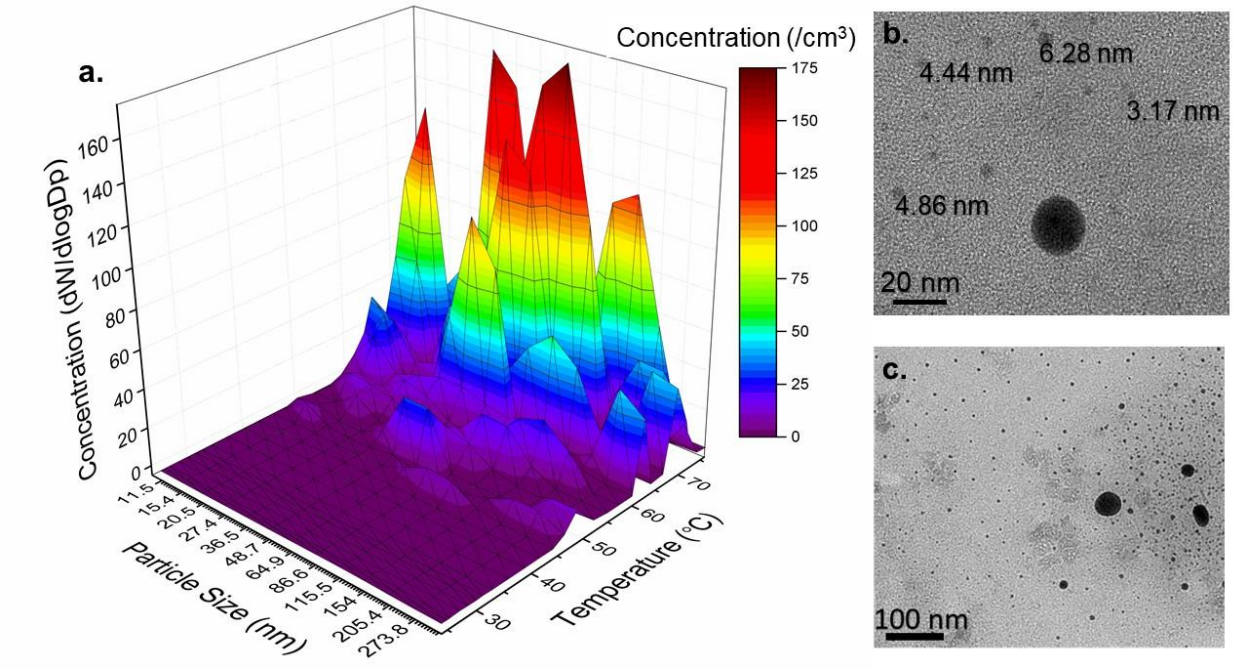

Figure 3.2 a) Particle size distribution surface for nanometer-sized mercury formed from a mixed 1:1 (by wt.) $HgCl_2$ and $HgBr_2$ source and b,c) High resolution transmission electron microscopy image of mercury aerosols from the mixed source.

The majority of particles detected by SMPS ranged between 50 and 175 nm in size. HR-TEM can identify mercury aerosols which are smaller than the 10 nm diameter limit of the SMPS. The majority of the particles were between 3 nm and 100 nm in size. *[Originally submitted to Analytical and Bioanalytical Chemistry as Main Text Figure 2]

3.3.1. Particle Formation from Oxidized Mercury sources via Vapour Condensation

Higher concentrations of particles were detected by SMPS and OPS with increasing source temperature and vapour concentration. (Figure 3.2) Significant fluxes of mercury aerosols consistently arise when the sources were heated to 50 °C. As the vapour pressure of mercury (II) bromide and mercury (II) chloride increases with temperature, concentrations of these species in the gas stream induce solidification reactions at lower downstream temperatures producing these mercury aerosols. Exclusion of mercury uptake onto existing particles was achieved through HEPA filtration of the carrier gas upstream of the source. Appearance of aerosols at lower temperatures were detected by the SMPS and OPS but may have been limited by deposition onto surface lining. Deposition of these aerosols on the tubing downstream from the heated sources suggests possible perfluoroalkoxy Teflon surface catalyzed reactions and deposition induced by declining temperature gradient [188].

3.3.2. Electron Microscopy Imaging of Nanoparticulate Oxidized Mercury via HR-STEM

Synthetic mercury aerosols were collected using an electrostatic precipitator with TEM grids placed in line with the outflow from mercury vapour flow sources heated from 25 to 50 °C. The EDS of selected particles confirm the presence of both chlorine and bromine, providing evidence for mixed-halide nanoparticle formation suggesting that these particles did not dislodge from the solid mercury(II) halide granules making up the sources themselves. Predominately spherical particles were observed with many smaller than (<10 nm) what was capable of being detected by either the SMPS or through NTA (Figure 3.2b,c). While only a laboratory result, the existence of small nanoparticles below 10 nm has not yet been observed in nature and would have important implications on the fate of mercury. Wet and dry deposition velocities of particulate-bound mercury decrease with particle size [26] allowing for greater transport distances. With decreased particle size, there is a surface to volume ratio enhancement where surface chemistry predominates [115]. The mechanisms for GOM and PBM deposition are different. As the diameter of particles decreases, they behave more like gases such as depositing through Brownian motion transport instead of gravitational settling [189]. The surface chemical and optical properties of nanoparticles also

differ from larger particles and gaseous compounds which has significance in radiative scattering, cloud condensation and ultimately in climate change [190].

3.3.3. Chemical speciation of mercury aerosols by Particle Trap Preconcentration Hg-MS

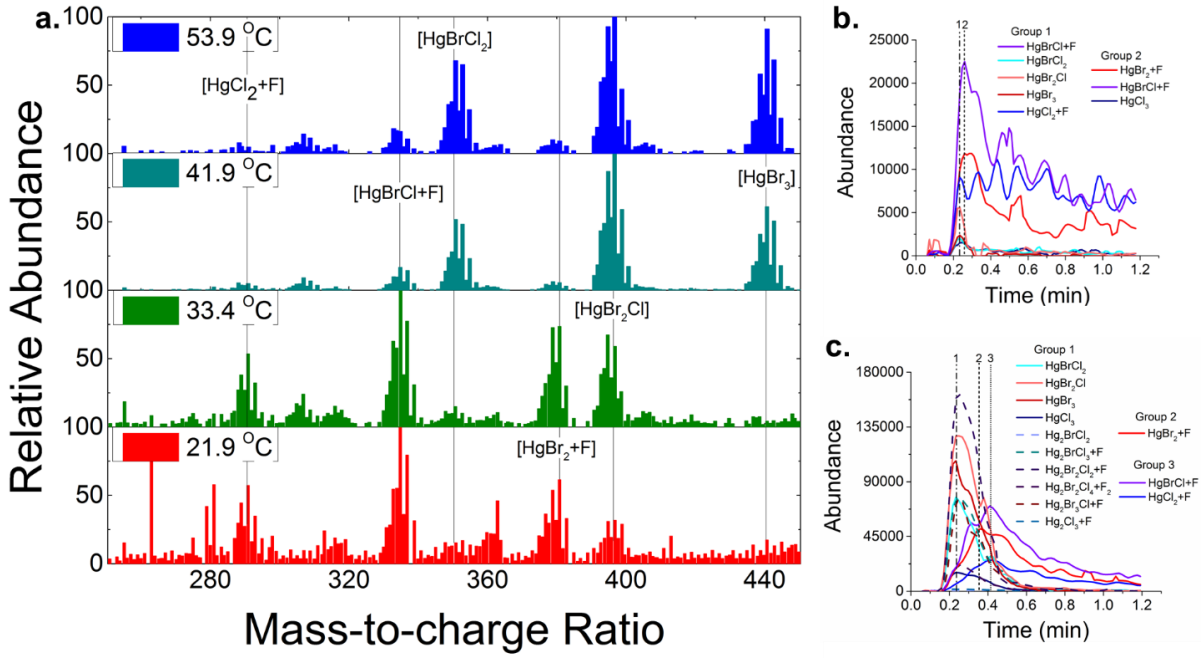

Figure 3.3. Mixed halogen species evolutions curves from sources heated to a) 20 °C and b) 50 °C.

Species evolution curves for species produced by mixed 1:1 (by wt.) $HgCl_2$ and $HgBr_2$ at 20 °C at 50 °C and trapped on PFA Teflon® traps following 1 minute of 1 LPM UHP nitrogen flow. *[Originally submitted to Analytical and Bioanalytical Chemistry as Main Text Figure 3]

A wide range of mercury-halogen species were observed when using the newly developed Hg-MS to characterize synthetic mercury aerosols as shown in Figure 3.3. These species included mixed halogen species and species containing multiple mercury atoms. Total ion counts increased with mercury source temperature consistent with the increased vapour pressure of GOM species and greater formation of aerosols with temperature-gradient based condensation. The formation of higher molecular weight species, including dimeric species, was readily observed for all sources and even at ambient temperatures though they are favoured with increasing source temperature. Their presence may be indicative of fragmentation from mercury aerosols and not source ion reactions as they peak earlier in species evolution curves suggesting a combination of aerosol decomposition and ion source complex formation.

3.3.4. Particle Stability and Microcosm Study

To examine potential transformation pathways of these particles, a borosilicate microcosm was operated to mimic tropospheric conditions in which 10-mesh mercury halide beads were exposed to airflow for one week. Mercury aerosols were detected on charged TEM grids placed in the system as shown in Figure 3.4 showing the stability (size and crystallinity) of these particles in air. These particles remain as condensed matter and are not immediately transformed to the gaseous phase, which is an important feature of their potential role in the atmospheric processes such as lifetime, and deposition rates. These particles also withstood the vacuum conditions present in the HR-STEM. A lack of mercury-containing tropospheric aerosol may then be attributable to deposition-based loses rather than gas-particle exchange losses [191].

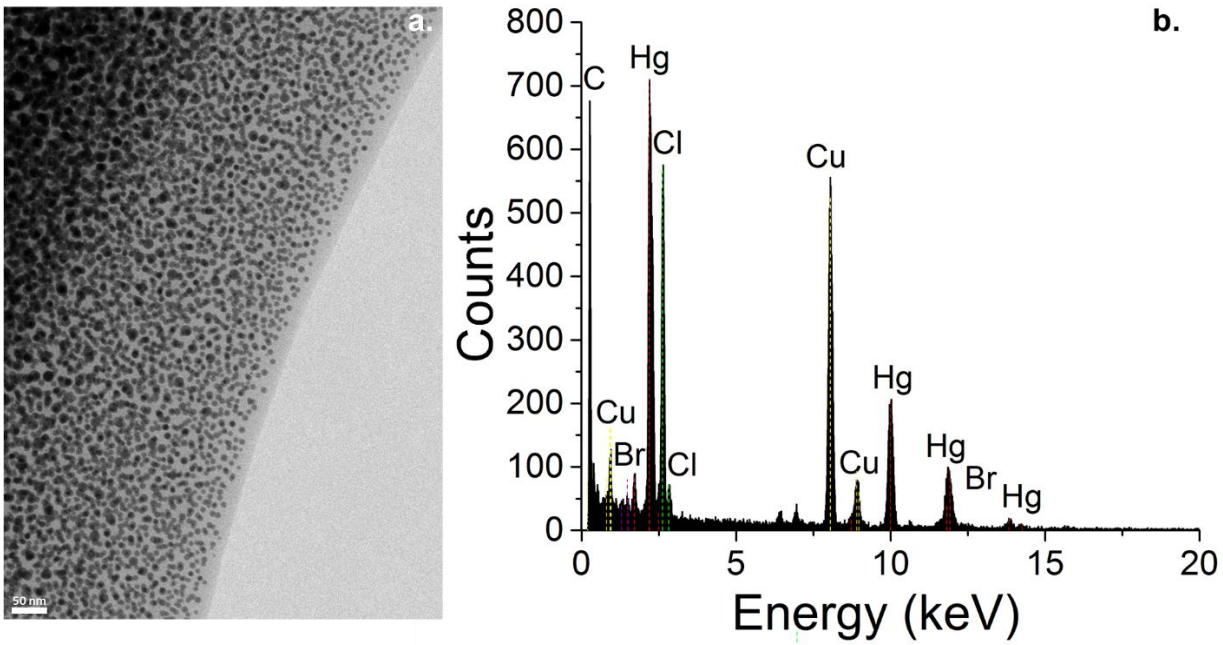

Figure 3.4. a) High-resolution transmission electron microscopy of mercury aerosols and b) Elemental analysis from Energy-dispersive X-ray spectra of mercury nanoparticle.

Image of mercury aerosols trapped on to a charged HR-TEM 400-mesh copper Formvar grid when exposed to mercury (II) bromide and mercury (II) chloride 10-mesh beads for a week under tropospheric conditions. The presence of mercury, chloride and bromine are found in a single mercury ultrafine particle suggesting that the particle is not a result of particles detaching from the beads and confirmation that mixed-halogen species can form. *[Originally submitted to Analytical and Bioanalytical Chemistry as Main Text Figure 4]

3.3.5. Mercury particles in aqueous samples

To examine the fate of atmospheric mercury nanoparticles, synthetic mercury nanoparticles were suspended in aqueous media. Though mercury(II) bromide and mercury(II) chloride are slightly soluble in water (0.017 mol/kg and 0.27 mol/kg, respectively) [192], nano-sized mercury particles were observed largely intact using NTA analysis (Figure 3.5a). Particle sizes, based on hydrodynamic radius, ranged from 20 nm to 350 nm, with the majority of particles between 75 and 250 nm, across a range of source compositions. Particles suspended from tubing deposits, appearing downstream of the heated mercury source, showed slightly larger modes with fewer particles below 100 nm (Figure 3.5b). Nanoparticles are known to form aggregates in aquatic environments based on concentration, pH, ionic strength and surface functionalization [190] and photoreactions of divalent mercury with thiogylic acid and dissolved organic matter has been observed to produce crystalline and nanoscale HgS particles, respectively [190,193,194].

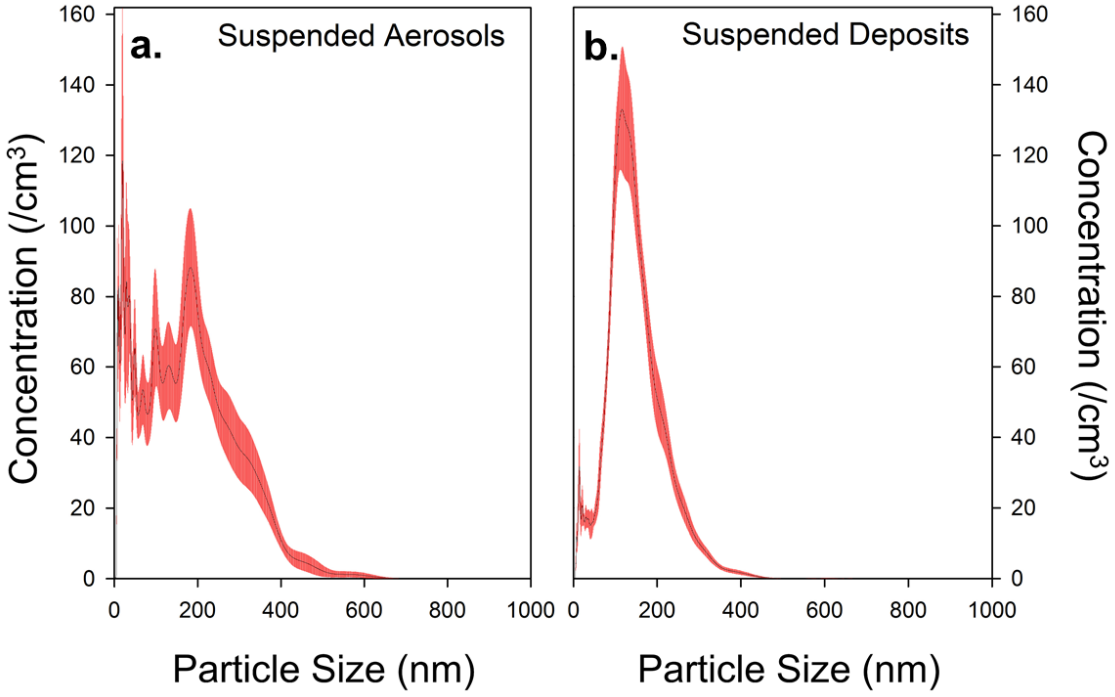

Suspension Source	Mean (n=10)	Mode (n=10)	Concentration (n=10)
c. $HgCl_2$ – 50 °C	144 nm ± 3.7 nm	134 nm ± 5.1 nm	1.52 x 10^8 /mL
$HgCl_2$ – Deposits	134 nm ± 3.1 nm	112 nm ± 5.6 nm	1.68 x 10^8 /mL
$HgBr_2$ – 50 °C	182 nm ± 11.8 nm	89 nm ± 18.1 nm	1.95 x 10^8 /mL
$HgBr_2$ – Deposits	176 nm ± 9.2 nm	143 nm ± 5.2 nm	0.58 x 10^8 /mL
Mixed – 50 °C	160 nm ± 18.9 nm	50 ± 17.3 nm	2.13 x 10^8 /mL
Mixed – Deposits	149 nm ± 3.4 nm	123 ± 5.3 nm	1.68 x 10^8 /mL

Figure 3.5. Particle size distribution for a) mercury aerosols and b) deposits suspended in aqueous media.

The modes of particle sizes ranged between 80 nm and 200 nm from a mixed 1:1 (by wt.) $HgCl_2$ and $HgBr_2$ source immersed directly into milliQ water and for suspension mercury deposits heated to 50 °C with UHP nitrogen carrier gas flow of 0.25 L/min. Shown is the average of ten replicates with standard errors shown in red. *[Originally submitted to Analytical and Bioanalytical Chemistry as Main Text Figure 5]

The formation of these particles under different carrier gas flow conditions may have influenced the resulting particle size distribution; aggregation and/or dissolution of particles in aqueous media may have also occurred. These latter processes are vital to the bioavailability of GOM species as they affect the surface area accessible for heterogeneous and biochemical reactions [190]. The distinct size distribution of suspended aerosols/deposits allows for the study of the chemistry of these aerosols in aqueous environments as surface functionalization with dissolved organics, and inorganic ions would change the breadth and maxima of the distributions [195]. This is particularly of importance, as functionalization will affect solubility, the degree of oxidized mercury ions release, and the potential to enter mercury-methylating microorganisms [190].

3.3.6. Particle Formation from Oxidized Mercury solutions via Aqueous Nebulization

More particles were generated with aqueous nebulization than vapour phase condensation as concentration of oxidized mercury in the nebulization solutions were orders of magnitude higher than the concentrated of vapour generated by the heated sources. Heating and sonication helped to promote dissolution of large particles. The concentration of nano- and nano-sized particles generated are shown in Table 3.1. The solubilities of oxidized mercury varies across chemical speciation; mercury(II) halides are sparingly soluble, mercury(II) oxide is somewhat soluble and mercury(II) nitrate is soluble [34]. Despite solubilities differing by orders of magnitude, the particle concentrations are similar across particle sizes with the highest concentrations of particles below 50 nm. Two separate mercury(II) oxide solutions produced comparable results showing the consistency of the aerosolization method**.** The concentrations of mercury(II) nitrate aerosols are significantly higher; despite a high solubility, in dilute solutions a basic insoluble mercury nitrate $Hg(OH)(NO_3)$ salt may form. By increasing the draw of a downstream sampling pump, particle fluxes for $HgCl_2$ solutions were found to decrease with flow rate, by a factor of 10. The impact of humidity under relatively dry conditions was insignificant as shown in Table 3.1.

Table 3.1. Nebulization Source Particle Concentrations at 1.7 LPM for Oxidized Mercury Species

Mean particulate concentrations [dw/dlogDp] for 12 nanoparticle and nano-sized particle bin sizes (nm) represented by bin midpoints for the transmission of nano-sized and nanoparticulate mercury produced through aqueous nebulization aerosol generation. (n=70) Strike-through measurements indicate no significant difference (p >0.05) from zero in a one-tailed t-test. *[Originally submitted to Analytical and Bioanalytical Chemistry as Main Text Table 1]

Nebulization Source Particle Concentration at 5 LPM for Oxidized Mercury Species													
	11.5	**15.4**	**20.5**	**27.4**	**36.5**	**48.7**	**64.9**	**86.6**	**115.5**	**154**	**205.4**	**273.8**	**365.5**
$HgCl_2$	468 ± 20%	530 ± 18%	356 ± 23%	573 ± 19%	567 ± 19%	356 ± 20%	146 ± 33%	84 ± 48%	86 ± 58%	65 ± 63%	21 ± 87%	2.8 ± 297%	1.5 ± 369%
$HgBr_2$	430 ± 36%	827 ± 21%	892 ± 16%	980 ± 18%	690 ± 26%	256 ± 47%	22 ± 181%	11 ± 186%	78 ± 60%	94 ± 47%	38 ± 57%	1 ± 339%	~~0.24 ± 490%~~
HgO	494 ± 28%	552 ± 25%	285 ± 40%	395 ± 50%	471 ± 36%	449 ± 27%	393 ± 28%	340 ± 26%	238 ± 35%	97 ± 61%	~~6.7 ± 302%~~	~~1.1 ± 535%~~	~~1.4 ± 484%~~
HgO 10 LPM	508 ± 16%	542 ± 15%	273 ± 27%	466 ± 24%	595 ± 16%	539 ± 15%	379 ± 22%	229 ± 25%	108 ± 68%	34 ± 133%	5.1 ± 317%	7.3 ± 227%	12 ± 165%
$Hg(NO_3)_2$ 1.7 LPM	9500 ± 64%	10847 ± 55%	6036 ± 77%	7580 ± 64%	6420 ± 58%	2810 ± 63%	294 ± 187%	88 ± 249%	330 ± 182%	692 ± 97%	422 ± 101%	28 ± 279%	~~5 ± 752%~~
Nebulization Source Particle Concentrations for $HgCl_2$ across Flowrates													
	11.5	**15.4**	**20.5**	**27.4**	**36.5**	**48.7**	**64.9**	**86.6**	**115.5**	**154**	**205.4**	**273.8**	**365.5**
1 LPM	3174 ± 77%	3845 ± 75%	2193 ± 80%	3109 ± 65%	3086 ± 61%	1993 ± 63%	751 ± 89%	297 ± 107%	221 ± 130%	223 ± 135%	122 ± 167%	31 ± 244%	24 ± 300%
1.7 LPM	850 ± 22%	1012 ± 21%	646 ± 24%	1056 ± 20%	1091 ± 19%	709 ± 19%	252 ± 25%	47 ± 33%	29 ± 137%	26 ± 124%	12 ± 150%	8 ± 189%	6 ± 229%
5 LPM	468 ± 20%	530 ± 18%	356 ± 23%	573 ± 19%	567 ± 19%	356 ± 20%	146 ± 33%	84 ± 48%	86 ± 58%	65 ± 63%	21 ± 87%	2.8 ± 297%	1.5 ± 369%
10 LPM	332 ± 23%	421 ± 20%	309 ± 22%	453 ± 17%	444 ± 16%	291 ± 19%	134 ± 33%	73 ± 43%	59 ± 67%	38 ± 75%	9 ± 135%	3 ± 256%	3 ± 231%
Nebulization Source Particle Concentrations for $HgBr_2$ across Humidity													
	11.5	**15.4**	**20.5**	**27.4**	**36.5**	**48.7**	**64.9**	**86.6**	**115.5**	**154**	**205.4**	**273.8**	**365.5**
10% RH	430 ± 36%	827 ± 21%	892 ± 16%	980 ± 18%	690 ± 26%	256 ± 47%	22 ± 181%	11 ± 186%	78 ± 60%	94 ± 47%	38 ± 57%	1 ± 339%	~~0.24 ± 490%~~
25% RH	503 ± 28%	1244 ± 21%	1276 ± 19%	1149 ± 15%	688 ± 14%	191 ± 29%	5.1 ± 334%	9.0 ± 178%	92 ± 50%	107 ± 41%	40 ± 54%	1.4 ± 440%	~~0.53 ± 616%~~
37% RH	223 ± 26%	542 ± 19%	524 ± 19%	490 ± 17%	340 ± 16%	171 ± 24%	83 ± 24%	83 ± 48%	91 ± 48%	58 ± 53%	9.0 ± 137%	0.85 ± 412%	0.48 ± 443%

3.3.7. Particle Capture by KCl denuder for Oxidized Mercury Nanoparticles

In comparing particle concentrations through the denuder and through an equivalent length of conductive tubing, we see increasing particulate trapping on denuders with smaller diameter particles (Table 3.2). As seen in Table 3.1, the particle counts for the largest nano-sized particles were often very low and not significant. In some cases, the particle counts for those highest nano-sized particles were often higher than produced by nebulization. This may be caused either by particles dislodging from the KCl denuder coating or due to

coagulation of smaller particles. At higher flow rates, the trapping was larger nanoparticles was less effective; however, we find greater transport at 1 LPM flow rates. A possible explanation is the flow was directed entirely to the SMPS instead of being teed-off to the OPS, or the OPS and the sampling pump. With higher humidity, the transportation of particles through the denuder is higher across all sizes.

Table 3.2. Nanoparticle Capture on the KCl Denuder for Oxidized Mercury Species (%)

Percent capture of nano-sized and nanoparticulate mercury across 12 particle bin sizes (nm), represented by bin midpoints, from a comparison between average particulate transmission through conductive tubing vs through a KCl denuder (n=70) Strike-through measurements indicate no significant difference (ANOVA, p>0.05) between the particulate transmission through conductive tubing and KCl denuder. Measures in red indicate higher particulate counts through the KCl denuder than through conductive tubing. *[Originally submitted to Analytical and Bioanalytical Chemistry as Main Text Table 2]

Nebulization Source Denuder Particle Capture at 5 LPM for Oxidized Mercury Species													
	11.5	**15.4**	**20.5**	**27.4**	**36.5**	**48.7**	**64.9**	**86.6**	**115.5**	**154**	**205.4**	**273.8**	**365.5**
$HgCl_2$	93.0	87.1	72.4	67.6	60.4	38.1	35.0	106	42.7	19.0	78.0	~~38.9~~	~~12.2~~
$HgBr_2$	95.4	81.9	69.6	66.6	65.1	60.4	~~27.7~~	69.5	78.1	73.1	~~61.2~~	305	~~1000~~
HgO	96.9	61.4	250	302	161	~~2.3~~	94.1	94.2	72.4	71.3	1640	634	~~54.2~~
HgO 10 LPM	95.7	96.3	95.1	88.4	84.6	81.5	79.6	81.7	85.5	87.4	73.1	~~38.1~~	61.6
$Hg(NO_3)_2$ 1.7 LPM	95.7	92.2	88.4	91.4	93.1	94.0	93.6	95.8	93.8	94.4	93.4	68.8	~~34.8~~
Nebulization Source Denuder Particle Capture for $HgCl_2$ across Flowrates													
	11.5	**15.4**	**20.5**	**27.4**	**36.5**	**48.7**	**64.9**	**86.6**	**115.5**	**154**	**205.4**	**273.8**	**365.5**
1 LPM	89.7	76.1	49.4	50.8	50.6	42.2	~~23.5~~	~~30.8~~	~~70.7~~	~~83.2~~	82.2	~~13.3~~	~~58.8~~
1.7 LPM	95.9	93.6	88.9	89.0	88.9	87.5	83.3	76.4	81.3	86.5	84.6	~~39.9~~	~~20.9~~
5 LPM	93.0	87.1	72.4	67.6	60.4	38.1	35.0	106	42.7	19.0	78.0	~~38.9~~	~~12.2~~
10 LPM	90.3	87.0	78.4	72.2	60.5	48.6	50.1	50.1	64.1	70.4	47.3	~~64.7~~	~~58.9~~
Nebulization Source Denuder Particle Concentrations for $HgBr_2$ across Humidity													
	11.5	**15.4**	**20.5**	**27.4**	**36.5**	**48.7**	**64.9**	**86.6**	**115.5**	**154**	**205.4**	**273.8**	**365.5**
10% RH	95.4	81.9	69.6	66.6	65.1	60.4	~~27.7~~	69.5	78.1	73.1	~~61.2~~	305	~~1000~~
25% RH	94.7	83.3	75.4	72.6	70.5	60.2	186	~~28.8~~	71.9	75.3	72.7	~~44.1~~	~~137~~
37% RH	89.5	83.3	80.2	77.8	73.3	59.0	28.3	30.8	47.4	57.7	55.8	~~68.3~~	~~170~~

3.3.8. Particulate Penetration through Membrane and Syringe Filters

Assessing a variety of filter types, the penetration of mercury nanoparticles through these filters was assessed. Table 3.3 summarizes these results. Overall, quartz and Teflon filters which are routinely used in the mercury field provide the best capture of particulate mercury with filters (~10^{-3} % for 10 nm nanoparticles) with larger pore sizes such as the QMA and Qualitative filters (~10^{-1} - 10^{1} % for 10 nm nanoparticles) allowing significant amounts of

particulates, including nanoparticles, to pass. It is expected that particles larger than the pore sizes of the filter would readily be captured and ultrafine particles, even those, many times smaller than the pore size will also have high deposition rates [189]. We expect the trapping curve, with respect to particle size, to be quadratic in nature. Larger nano-sized particles will have the highest rates of break-though.

Table 3.3. Nanoparticle Capture on the KCl Denuder for Membrane and Syringe Filters

The percent transmission of nano-sized and nanoparticulate mercury across 12 particle bin sizes (nm), represented by bin midpoints, through membrane and syringe filters. (n=70) *[Originally submitted to Analytical and Bioanalytical Chemistry as Main Text Table 3]

Particle Capture Across Membrane Filters in Filter Holders													
	11.5	**15.4**	**20.5**	**27.4**	**36.5**	**48.7**	**64.9**	**86.6**	**115.5**	**154**	**205.4**	**273.8**	**365.5**
FG Filter – HgO	5.7×10^{0}	4.5×10^{0}	5.3×10^{0}	5.7×10^{0}	5.0×10^{0}	3.4×10^{0}	1.8×10^{0}	1.3×10^{0}	2.3×10^{0}	4.3×10^{0}	1.6×10^{1}	2.1×10^{2}	8.4×10^{1}
Quartz – $HgBr_2$	7.4×10^{-3}	6.1×10^{-3}	7.6×10^{-3}	2.4×10^{-3}	1.9×10^{-3}	5.7×10^{-3}	1.6×10^{-2}	1.3×10^{-1}	3.2×10^{-1}	3.0×10^{-1}	3.0×10^{-1}	3.2×10^{-1}	1.8×10^{-1}
Quartz – $HgCl_2$	2.3×10^{-2}	9.8×10^{-3}	1.9×10^{-2}	1.0×10^{-3}	2.6×10^{-3}	2.1×10^{-3}	1.6×10^{-2}	2.1×10^{-2}	3.4×10^{-3}	1.2×10^{-2}	4.8×10^{-2}	3.1×10^{-2}	3.9×10^{-2}
Quartz – HgO	3.9×10^{-2}	1.5×10^{-2}	1.9×10^{-2}	3.0×10^{-2}	2.3×10^{-2}	3.7×10^{-2}	5.5×10^{-2}	1.4×10^{-1}	2.6×10^{-1}	3.8×10^{-1}	5.3×10^{-1}	9.8×10^{-1}	6.9×10^{-1}
Solsep – $HgBr_2$	8.7×10^{-1}	1.0×10^{0}	2.3×10^{0}	2.4×10^{0}	2.4×10^{0}	2.6×10^{0}	3.6×10^{0}	5.5×10^{0}	1.0×10^{1}	1.1×10^{1}	1.4×10^{1}	2.8×10^{1}	2.3×10^{1}
Solsep – $HgCl_2$	1.3×10^{1}	7.5×10^{0}	5.8×10^{0}	5.6×10^{0}	5.5×10^{0}	5.4×10^{0}	5.0×10^{0}	5.0×10^{0}	1.1×10^{1}	2.3×10^{1}	5.3×10^{1}	2.9×10^{1}	1.6×10^{1}
QMA – $HgBr_2$	3.6×10^{-1}	1.4×10^{-1}	1.1×10^{-1}	2.8×10^{-1}	3.4×10^{-1}	3.7×10^{-1}	4.2×10^{-1}	7.6×10^{-1}	3.0×10^{0}	8.2×10^{0}	1.3×10^{1}	1.4×10^{1}	8.8×10^{0}
Qualitative – $HgBr_2$	3.2×10^{0}	4.4×10^{0}	7.6×10^{0}	1.1×10^{1}	1.3×10^{1}	1.6×10^{1}	2.4×10^{1}	5.0×10^{1}	6.5×10^{1}	3.7×10^{1}	1.9×10^{1}	4.9×10^{1}	5.8×10^{1}
Particle Capture Across In-Line Syringe Filters in Filter Holders													
	11.5	**15.4**	**20.5**	**27.4**	**36.5**	**48.7**	**64.9**	**86.6**	**115.5**	**154**	**205.4**	**273.8**	**365.5**
PES – $HgBr_2$	4.9×10^{-1}	1.4×10^{-1}	2.7×10^{-4}	2.8×10^{-2}	7.2×10^{-2}	1.6×10^{-2}	2.6×10^{-2}	NA	3.1×10^{-1}	1.2×10^{0}	2.3×10^{0}	5.2×10^{-1}	5.7×10^{-1}
PTFE – $HgBr_2$	8.3×10^{-3}	2.4×10^{-2}	1.5×10^{-2}	3.4×10^{-4}	1.9×10^{-3}	7.6×10^{-3}	2.0×10^{-2}	4.9×10^{-3}	4.6×10^{-3}	1.4×10^{-2}	4.7×10^{-2}	4.7×10^{-1}	4.4×10^{-1}
Used PTFE – $HgBr_2$	4.6×10^{-3}	1.1×10^{-2}	6.1×10^{-3}	1.3×10^{-2}	1.1×10^{-2}	2.8×10^{-2}	7.9×10^{-2}	3.0×10^{-1}	4.7×10^{-1}	4.3×10^{-1}	2.6×10^{-1}	6.7×10^{-1}	1.5×10^{0}
PTFE – $HgCl_2$	4.0×10^{-5}	2.2×10^{-5}	5.7×10^{-6}	1.1×10^{-5}	1.5×10^{-5}	3.6×10^{-6}	8.1×10^{-6}	NA	5.5×10^{-5}	9.1×10^{-5}	4.9×10^{-5}	2.1×10^{-4}	3.6×10^{-4}
PTFE – HgO	4.7×10^{-2}	1.5×10^{-2}	1.7×10^{-2}	3.9×10^{-2}	4.1×10^{-2}	2.5×10^{-2}	2.3×10^{-2}	6.3×10^{-2}	1.3×10^{-1}	5.3×10^{-1}	3.5×10^{1}	1.8×10^{2}	8.7×10^{0}

3.3.9. Particle Capture and Speciation

As part of the emerging mercury mass spectrometry technique, the capacity for trapping oxidized mercury nanoparticles and nano-sized particles on to nano and micro-particle

sorbent traps used in the technique in provided in Table 3.4. Nanoparticles are readily captured on these traps with efficiencies as high as 98% for the smallest nanoparticles. There is a definite size effect as particle capture efficiency decreases with size. For larger nano-sized particles, we see that the PFA sorbent trap may provide surfaces for smaller nanoparticles to coagulate to form larger particles. The particulate counts for these larger-sized nano-sized particles tend to be orders of magnitude lower with high variability and thus some results are not statistically significant.

Table 3.4. Nanoparticle Capture on the two PFA Sorbent Mercury Mass Spectrometry Traps

Mean particulate concentrations [dw/dlogDp] for 12 nanoparticle and nano-sized particle bin sizes (nm) represented by bin midpoints for transmission of nano-sized and nanoparticulate mercury produced through aqueous nebulization aerosol generation. (n=70) Strike-through measurements indicate no significant difference ($p > 0.05$) from zero in a one-tailed t-test. Percent capture of nano-sized and nanoparticulate mercury across 12 particle bin sizes from a comparison between average particulate transmission through conductive tubing vs through a PFA Teflon sorbent trap. (n=70) Strike-through measurements indicate no significant difference (ANOVA, $p>0.05$) between the particulate transmission through conductive tubing vs through a PFA Teflon sorbent trap. Measures in red indicate higher particulate counts through the PFA Teflon sorbent trap than through conductive tubing. *[Originally submitted to Analytical and Bioanalytical Chemistry as Main Text Table 4]

Nebulization Source Particle Concentration at 1 LPM for Oxidized Mercury Species													
	11.5	**15.4**	**20.5**	**27.4**	**36.5**	**48.7**	**64.9**	**86.6**	**115.5**	**154**	**205.4**	**273.8**	**365.5**
$HgBr_2$ – Trap 1	901 ± 30%	1016 ± 25%	553 ± 24%	825 ± 22%	882 ± 20%	632 ± 20%	317 ± 27%	154 ± 32%	85 ± 58%	37 ± 101%	3.7 ± 257%	~~0.8 ± 696%~~	1.2 ± 382%
$HgBr_2$ – Trap 2	556 ± 31%	715 ± 22%	434 ± 29%	589 ± 27%	614 ± 24%	453 ± 22%	249 ± 24%	132 ± 36%	73 ± 66%	31 ± 89%	4.7 ± 236%	1.1 ± 372%	1.5 ± 291%
$HgCl_2$ – Trap 1	4506 ± 31%	5561 ± 21%	3256 ± 14%	4891 ± 14%	5568 ± 16%	4478 ± 20%	2645 ± 27%	1292 ± 39%	457 ± 68%	52 ± 207%	~~2.4 ± 756%~~	0	6.1 ± 398%
$HgCl_2$ – Trap 2	3595 ± 36%	4638 ± 24%	2949 ± 14%	4244 ± 13%	4543 ± 14%	3403 ± 15%	1816 ± 18%	810 ± 20%	299 ± 54%	64 ± 131%	~~0.6 ± 680%~~	~~0.7 ± 579%~~	5.1 ± 381%
HgO – Trap 1	407 ± 64%	688 ± 39%	504 ± 25%	568 ± 26%	588 ± 26%	541 ± 25%	472 ± 26%	401 ± 30%	275 ± 42%	109 ± 64%	3.4 ± 258%	~~0.2 ± 894%~~	1.5 ± 411%
HgO – Trap 2	18 823 ± 35%	23044 ± 37%	12147 ± 42%	12308 ± 44%	9365 ± 46%	3486 ± 39%	84 ± 503%	7 ± 688%	854 ± 52%	1314 ± 41%	595 ± 40%	0	0.39 ± 894%
Nanoparticle Capture on PFA Sorbent Traps (%)													
	11.5	**15.4**	**20.5**	**27.4**	**36.5**	**48.7**	**64.9**	**86.6**	**115.5**	**154**	**205.4**	**273.8**	**365.5**
$HgBr_2$ – Trap 1	97.3	94.6	88.3	85.5	82.7	75.4	63.4	62.8	64.5	67.3	–11.4	~~–1462~~	~~–897~~
$HgBr_2$ – Trap 2	97.9	93.0	81.0	79.2	79.7	78.3	74.0	68.8	67.1	66.4	~~48.1~~	~~–92.5~~	~~–52.6~~
$HgCl_2$ – Trap 1	98.3	97.1	93.5	92.0	91.7	91.2	90.4	90.4	92.1	88.7	~~79.0~~	~~NA~~	~~–5.9~~
$HgCl_2$ – Trap 2	98.3	96.9	93.1	91.5	91.4	91.2	90.9	90.8	89.7	82.6	~~–427~~	~~–397~~	~~15.2~~
HgO – Trap 1	95.2	92.9	88.4	86.3	86.1	86.3	87.0	87.7	87.7	85.5	~~0.6~~	~~–844~~	~~–2.4~~
HgO – Trap 2	94.5	91.8	88.6	90.1	91.6	92.4	~~83.3~~	~~61.7~~	93.1	92.9	92.4	~~NA~~	~~128~~

3.4. Conclusions

In conclusion, aqueous nebulization and vapour-phase condensation methods were developed to produce steady and reproducible distributions of mercury nanoparticles and nano-sized particles. These nanoparticles have been characterized using scanning mobility and optical particle sizing, microscopy and nanotracking analysis, and shown to be stable under tropospheric and aqueous conditions. Using mercury mass spectrometry, the chemical species present in these nanoparticles was assessed. Under the high temperatures of the ion source, these particles desorb mercury(II) halides which are readily measured. We also show the formation of mixed halide nanoparticles using both HR-STEM and mercury mass spectrometry. Finally, the interference of KCl denuder measurements of GOM is confirmed across a range of experimental conditions as high as 95% for the smallest nanoparticles (10 nm) and the efficiency of particulate filters and nano- and micro-particulate sorbent filters for capturing nanoparticulate mercury is also observed.

3.5. Acknowledgements

The authors acknowledge the financial support provided by the Natural Sciences and Engineering Research Council of Canada (NSERC), the Canadian Foundation for Innovation (CFI), Le Fonds de recherche du Québec – Nature et technologies (FRQNT), Environment and Climate Change Canada, McGill University and the Walter C. Sumner Foundation. Additionally, the authors thank David Liu and Dr. Hojatollah Vali of the Facility for Electron Microscopy Research also acknowledge Dr. Janusz Rak and Laura Montermini at the Montreal Children's Hospital for use of the Nanosight NS500.

Chapter 4. The Existence of Airborne Mercury Nanoparticles

Adapted from a submission to Scientific Reports [SREP-19-08088]

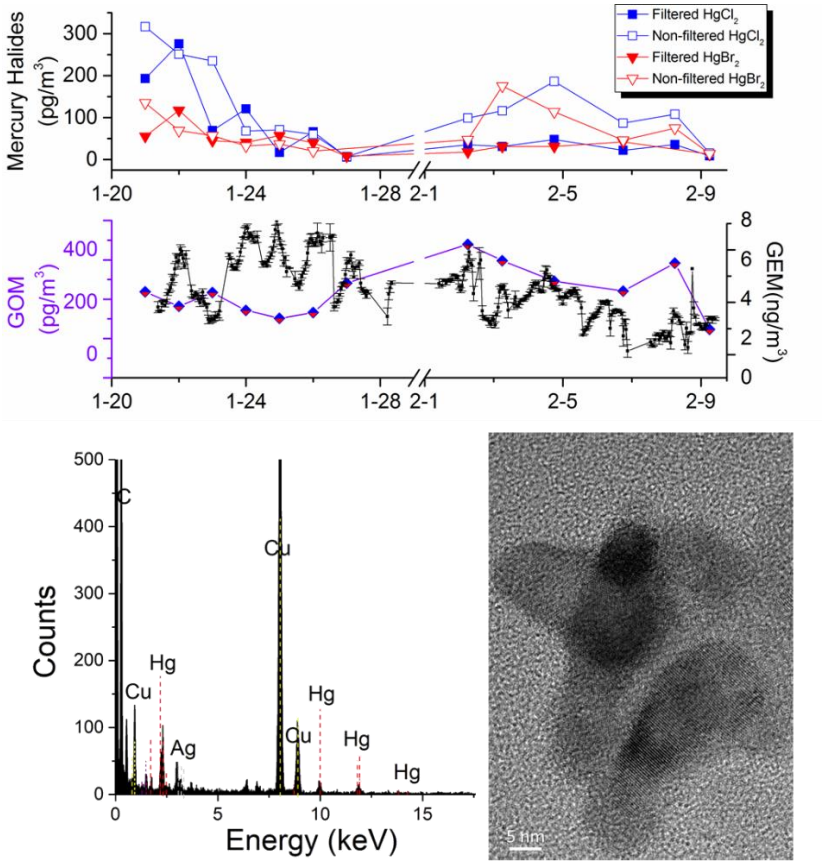

TOC Figure 4. Evidence for the existence of mercury and mercury(II) halide containing nanoparticles.

In this paper, evidence is provided for the contribution of mercury particulates that contaminate gaseous oxidized mercury measurements using mercury mass spectrometry techniques. PFA sorbent traps have been shown to readily capture mercury-containing nanoparticles and membrane and syringe filters show to exclude particles. By placing filters on sorbent traps, measurements of oxidized mercury, with and without particulates are provided with an estimate of the proportion of mercury(II) halides bound to particulates.

Contribution by author: The experimental design, method evaluation, data analysis, and drafting of the manuscript were conducted by me. Experiments were conducted, either by me or in conjunction with an undergraduate student who I mentored.

Abstract

Mercury is an important global toxic contaminant of concern that causes cognitive and neuromuscular damage in humans that can travel in the air, in water or be adsorbed to soils, snow, ice and sediment. While atmospheric mercury exists primarily in the gaseous elemental form (GEM), gaseous oxidized Hg^{2+} mercury (GOM) and particulate-bound mercury (Hg^{P}) play an essential role in the fate of mercury, its introduction to aquatic and terrestrial environments, and bioaccumulation and biomagnification in biotic systems. Herein, we show the occurrence of mercury nanoparticles in air. When present as or absorbed to nanoparticles, two GOM proxies, mercury(II)chloride and mercury(II) bromide can contribute to erroneous GOM measurements. Upwards of 95% of nanoparticulate mercury halides can be trapped onto KCl denuders, the conventional technique for measuring GOM worldwide. Following an urban air field campaign near a mercury point source, we provide evidence for mercury nanoparticles, smaller than 100 nm, using a suite of optical and mobility particle sizing analyzers, aerosol collection impactors, and high resolution scanning/transmission electron microscopy (HR-STEM). We estimate airborne mercury aerosols may consist of a maximum 50% of oxidized mercury measured in wintertime Montréal urban air using the novel mercury mass spectrometry (Hg-MS). These emerging mercury nanoparticles will influence important atmospheric and aquatic biogeochemical mercury processes and global mercury cycling.

4.1. Introduction

Mercury has no known beneficial function in the body and can cross both the blood-brain and placental barriers, with known adverse health effects [196-198]. It is introduced into the environment through natural and anthropogenic processes, with GEM spending upwards of a year in the atmosphere travelling far from its source of origin [15,64]. Through chemical conversion to the more water-soluble, bioavailable GOM, it is deposited to terrestrial and aquatic environments. Aquatic microorganisms convert GOM to the incredibly toxic, fat-soluble and bio-accumulative, organic methylmercury species whose concentrations can increase up to a million-fold in higher order fish [15].

Anthropogenic point sources also emit GOM, typically in higher proportions than what is generally found in the atmosphere, as GEM typically comprises 90% of total

atmospheric mercury and greater [115]. Concerns over the adverse effects of mercury and anthropogenic contributions to its release have prompted over 125 countries to sign the United Nations Environmental Programme's 2013 Minamata Convention on Mercury.

4.1.1. The Measurement of Atmospheric Mercury Species

The restriction to bulk mercury speciation arises from the difficulty in measuring mercury species present at ultra-trace concentrations. GEM is measured through a double-gold trap amalgamation pre-concentration, thermal desorption, and detection using CVAFS. With absolute detection limits in the low pg, elemental and total mercury are rarely if ever undetected even in the most remote locations. It is the only bulk species that is chemically speciated as both GOM and Hg^P require conversion to GEM before measuring. GOM is conventionally collected using KCl denuders [93], where oxidized species such as $HgCl_2$ are complexed as anions ($[HgCl_3]^-$ and $[HgCl_4]^{2-}$) and incorporated within the KCl matrix [199]. The denuder is heated above 500 °C resulting in the thermal decomposition of these stable complexes to GEM which is subsequently measured by double-amalgamation gold-trap preconcentration CVAFS. As a result of this conversion to GEM, any information on chemical speciation is lost.

Hg^P is collected on membrane, fibrous or quartz filters, with pore sizes ranging between 200 nm and 10 μm in size, as determined by the investigator [200]. The filters are acid-digested or pyrolyzed with trapped mercury species reduced to GEM which is measured by CVAFS. Nanoparticulate mercury, which we concern ourselves within this study, may be present as elemental or oxidized mercury, absorbed or adsorbed to chemically heterogeneous nanoparticles, or incorporated within the bulk of the particle. These particles may either be trapped and measured as Hg^P, or a fraction may be deposited through diffusion or electrostatic losses, on the denuder or sampling train surfaces.

4.1.2. Airborne Mercury Nanoparticles and its Transformation Pathways

The transformations between gaseous and particulate mercury aerosols have a significant impact on the fate of mercury in the atmosphere, its residence time and its eventual deposition to terrestrial and aquatic environments. Aerosols provide a surface for GEM, GOM and other gaseous atoms and molecules to adsorb, collide and react [115,201]. Nanoparticles

undergo coagulation processes and act as ice and cloud condensation nuclei promoting dry and wet deposition to marine and terrestrial environments [191,202]. GOM has already been shown to adsorb onto KCl and NaCl aerosols, thereby affecting mercury deposition rates [203]. Conversely, the release of gaseous mercury(II) chloride from inorganic and adipic acid aerosols to the gaseous phase has also been observed [204], as well as GOM release from fine fraction (<2.5 μm) Hg_p. [93].

Nano-sized mercury-containing particles, which have higher surface-to-volume ratios, would exhibit more significant release of bioavailable oxidized mercury in atmospheric and aquatic environments depending on the species adsorbed/absorbed to the surface of the particle. Though present in ultra-trace concentrations in air, nano-sized materials are respirable, deposited deep in the lungs, penetrable through tissue [205], and transportable through the bloodstream where they can be taken up by the placenta [206]. These physical and chemical transformation processes have far-reaching implications on remediation, human health, climate and biogeochemical modelling.

4.1.3. The Measurement of Nanosized Mercury Particles

No single technique can completely characterize both the physical and chemical properties of nano-sized particles. By using a variety of complementary techniques, many novel to the mercury sciences, the limitations of each are countered by the suite. We examine the propensity of the denuder technique for capturing nanoparticulate mercury to determine the potential for contaminated GOM measurements, using laboratory synthesized mercury aerosols produced at GOM concentrations relevant to stack conditions [207,208]. Using PFA-based sorbent traps and sampling with and without particle-removing filters, mercury-based particulates in wintertime urban air, focusing on GOM proxies, mercury(II) bromide and mercury(II) chloride are quantified. Tracking atmospheric co-pollutants and meteorological measurements, how these species influence both the chemical speciation and phase distribution of oxidized mercury is examined. Scanning mobility particle sizers (SMPS), optical particle sizers (OPS), nanoparticle tracking analysis (NTA), high-resolution transmission electron microscopy with energy-dispersive X-ray spectroscopy (HR-TEM-EDS) and our recently developed mercury mass spectrometry (Hg-MS) [142] are employed.

4.2. Experimental

4.2.1. Synthetic Mercury Aerosol Sources

Anhydrous mercury (II) bromide and mercury (II) chloride, 10 mesh beads, of 99.999% purity were obtained from Sigma Aldrich Canada Co. (Oakville, ON) and used to construct mercury halide sources in ¼ inch I.D. x $^{3}/_{64}$ inch O.D. Swagelok PFA Teflon (Solon, OH) tubing held in place by PTFE frits. Concentrations from the sources for total oxidized mercury and total particulates are provided in Table 4.2. Mercury halide aerosols were formed in the laboratory through two methods: vapour flow condensation and by nebulization of aqueous mercury(II) halides [209]. Particulate formation was confirmed using SMPS for sources constructed with mercury(II) chloride and mercury(II) bromide with a mixture of compositions (Table 4.1) [141]. The majority of particles formed across source compositions range in size from 50 and 175 nm for vapour flow condensation method, and under 65 nm for nebulization (Figure 4.1). The emission rates (in the hundreds of ng/min) from these vapour flow sources were comparable to others used in laboratory studies to simulate industrial stack GOM concentrations [221], but orders of magnitude higher than would be observed in nature [222].

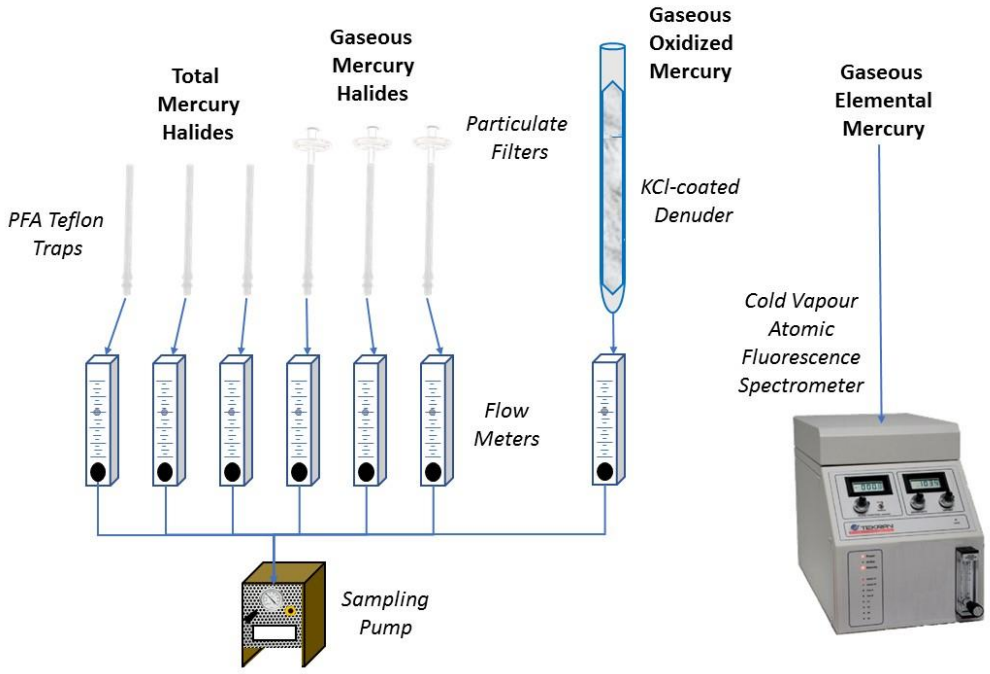

Figure 4.1. Experimental Setup with concurrent KCl denuder, total and gaseous mercury halide measurements. Gaseous elemental mercury was measured by CVAFS.

*[Originally submitted to Scientific Reports as Supplementary Figure 4]

High purity nitrogen, used as a carrier gas, was produced using a Peak Scientific NM32LA Nitrogen Generation (Billerica, MA) and was scrubbed of hydrocarbons using Big Hydrocarbon Trap from Agilent Technologies (Mississauga, ON) and particles using high chemical resistance – low flow PVDF filters from Parker Balston (Haverhill, MA). Humidity in the carrier gas line was verified to below 1% using an Aginova iCelsius wireless hygrometer (Mason, OH) and particle-free carrier gas was confirmed before each experiment using a TSI CPC 3007 condensation counter (Shoreview, MN). The carrier gas was heated using an Omega low-flow inline heater, and flow rates maintained using Omega acrylic rotometers (Laval QC).

4.2.2. Particle number density and distribution of synthetic mercury aerosols

Complementary techniques were used to determine the aerodynamic particle number density and size distribution of synthetic mercury aerosols from 10 nm to 10 µm. The size distributions of synthetic aerosols from 10 nm to 300 nm (in 13 bins) were obtained, over 1 minute scans, using a differential mobility-based Nanoscan SMPS Nanoparticle Sizer 3910 from TSI Incorporated (Shoreview, MN), and of aerosols from 300 nm to 10 µm (in 16 bins), using an Optical Particle Sizer (OPS) 3330. Conductive tubing was used to prevent electrostatic particle losses in the connections between the sources and the instruments. The inlet conditioner on the SMPS removes large particles from the aerosol stream and multiple charges applied to the particle can result in lower accuracy at larger sizes. Flow rates through the sources were maintained at 1 L/min, and temperature monitored using an Extech Instruments HD200 Differential Thermometer Datalogger (Nashua, NH).

4.2.3. Atmospheric Pressure Chemical Ionization-Mercury Mass Spectrometry (Hg-MS)

Mercury(II) bromide and mercury(II) chloride were measured using an Agilent 6140 single quadrupole mass spectrometer with an atmospheric pressure chemical ionization source. [142] Samples were collected on in-house made PFA-Teflon traps, heated at 200 °C for 1.2 minutes and desorbed into the APCI source inlet, which had been modified for aerosol and gaseous analysis, using a 1% sulphur hexafluoride in isobutane mixture carrier gas. In the ion source, sulphur hexafluoride decomposes to form SF_5^+ and F^- resulting in charge transfer

to the target mercury halides through negatively charged fluoride adduct formation ($[M+19]^-$ corresponding to m/z = 291 for $HgCl_2$+F and m/z=381 for $HgBr_2$+F). Mercury (II) bromide, mercury (II) chloride and mercury(II) bromochloride were detected as fluoride complexes at m/z 287 – 295, 331 – 341, and 388 – 396, respectively. The mercury(II) bromochloride species is likely an artifact of ion source reactions [142]. The corona current, capillary voltage and vaporizer (APCI inlet) temperature were set to 30 μA, 750 V, and 200 °C, respectively. N_2 drying gas flow rate was maintained at 5 L/min and heated to 200 °C. The fragmentor voltage was set to 90 V. These source parameters were optimized across a range of steps and are described by Deeds et al. [142].

Table 4.1. Mercury mass spectrometry (Hg-MS) calibration

	$HgCl_2$ Detection Limit (pg)	**$HgBr_2$ Detection Limit (pg)**	**Sensitivity – $HgCl_2$ (cnts/pg)**	**Sensitivity – $HgBr_2$ (cnts/pg)**	**R^2 – $HgCl_2$**	**R^2 – $HgBr_2$**
Trap 1	16	13	240	480	0.82	0.88
Trap 2	69	61	275	565	0.91	0.90
Trap 3	43	13	280	475	0.95	0.83
Trap 4	39	21	600	805	0.93	0.82
Trap 5	23	16	645	655	0.83	0.91
Trap 6	34	26	390	675	0.90	0.94
Trap 7	16	49	360	765	0.91	0.95
Trap 8	9	7	320	650	0.96	0.89
Trap 9	18	22	515	635	0.88	0.85
Trap 10	13	13	375	810	0.83	0.80
Trap 11	60	56	395	455	0.89	0.91
Trap 12	15	27	470	875	0.92	0.78

*[Originally submitted to Scientific Reports as Supplementary Table 2]

4.2.4. Cold Vapour Atomic Fluorescence Spectroscopy

Gaseous Elemental Mercury was measured using a Tekran Series 2600 Analysis System (Toronto, ON) with dual stage gold preconcentration with samples acquired every 5 minutes except two hours daily as GOM was being measured using a manual denuder and subsequently blanked. Gaseous oxidized was measured manually using KCl-coated annular quartz denuder. The denuder was held at 50 ºC during sampling and heated to 525 °C for

thermal decomposition to gaseous elemental mercury [93]. The system was calibrated daily using a saturated source of mercury under N_2.

4.2.5. Urban Air Campaign

For urban air samples, samples were gathered daily between January 21st, 2016 and February 9th, 2016 with two alternating sets of six PFA-traps drawing 1 LPM for roughly 24 hour intervals except for two 48 hour trials between February 1st and 3rd and February 3rd and 5th. Traps were calibrated over a four-point calibration with detection limits and sensitivities shown in Table 4.1 (n=12). Mercury(II) bromide and mercury(II) chloride were measured as fluoride complexes formed from the decomposition of SF_6 carrier used to desorb these compounds into the APCI ion source.

Given the potential for interferents to mask detection, chemical detection of mercury(II) bromide or mercury(II) chloride required either 3 qualifier-to-quantifier ratios within 20 % of the theoretical value or 2 qualifier-to-quantifier ratios within 10% of the theoretical value. Concurrent GOM samples were drawn for the same sampling periods in addition the GEM measurements using the CVAFS. Additional chemical contaminants (NO_x = NO + NO_2, SO_2, O_3, PM2.5) and meteorological measurements (temperature, relative humidity, snow on ground) were collected from the City of Montreal's Station 61 – Maisonneuve located 400 m from the mercury(II) halide sampling site. To remove particulates, 0.45 um PTFE filters from Corning Incorporated (Corning, NY) were attached to the inlet of the PFA-traps and heated to reduce absorption of gaseous oxidized mercury.

Nano-sized particulate mercury was collected using a M-100 micro-orifice uniform deposit impactor (MOUDI) from MSP Corporation (Shoreview, MN) with 4-submicron stages with aerodynamic diameter cutpoints of 1.0 µm, 0.55 µm, 0.21 µm and 0.18 µm. The MOUDI was situated atop a university research building within 30 meters of building exhaust output. Samples were collected on 0.45 µm quartz filters for 24 hours with an inlet flow rate of 30 L/min and digested overnight with 0.5% (v/v) BrCl before reduction by 60 µL of 20% (w/v) $SnCl_2$. The resulting GEM was purged, pre-concentration using dual stage gold trap amalgamation and analysis by a Tekran Series 2600 Analysis System (Toronto, ON).

4.2.6. HR-STEM Analysis of Ambient Air Nanoparticles

200 mesh Formvar/carbon coated copper TEM grids and 400 mesh Formvar coated copper TEM grids were obtained from Electron Microscope Sciences (Hatfield, PA) and SPI Supplies (West Chester, PA), and placed on the stages of the MOUDI impactor for 24 hours to collect particulate matter for analysis with high-resolution transmission electron microscopy. Samples were analyzed using FEI Tecnai G^2 F20 kV Cryo-STEM with EDAX Octane T Ultra W/Apollo XLT_2 SDD and TEAM EDS Analysis System (Hillsboro, OR).

4.3. Results and Discussion

4.3.1. Characterization of synthetic mercury aerosols

Mercury halide aerosols were formed in the laboratory through two methods: vapour flow condensation [209,210] and by nebulization of aqueous mercury(II) halides. [187,209] Particulate formation was confirmed using SMPS for sources constructed with mercury(II) chloride and mercury(II) bromide with a mixture of compositions (Table 4.2) [142]. The majority of particles formed across sources, range in size from 50 and 175 nm for vapour flow condensation method, and under 65 nm for nebulization (Figure 4.2). The emission rates (in the hundreds of ng/min) from these vapour flow sources were comparable to others used in laboratory studies to simulate industrial stack GOM concentrations [211], but orders of magnitude higher than would be observed in nature [212].

Table 4.2. Total oxidized mercury from halogenated mercury sources

Source	Total Oxidized Mercury Species (ng/min)[a] [n=3]	SMPS Mass Particle Size – Corrected[b] (ng/min)	OPS Mass Particle Size (ng/min)	Correction for Deposition[c] (ng/min)	$\frac{\text{Total Mercury Aerosol}}{\text{Total Oxidized Mercury}}$ (%)
Mixed Source – 25 °C	120 ± 44%	0.42 – 8.49	4.77	10.3 – 26.5	9 – 22 %
$HgBr_2$ Source – 25 °C	164 ± 16%	0.84 – 16.75	4.17	10.0 – 41.8	6 – 25 %
$HgCl_2$ Source – 25 °C	128 ± 43%	0.31 – 6.19	6.05	12.7 – 24.5	10 – 19%

[a] The KCl Denuder – CVAFS measured the mass of Hg which for $HgBr_2$ and $HgCl_2$ were corrected to include the mass of the Br and Cl atoms, respectively. The correction for the mixed source was based on the relative ratio between the vapour pressures of mercury (II) bromide and mercury (II) chloride at 25 °C.
[b] The SMPS unipolar charger typically ionizes between 1% and 20% of particles. As sizing is based on electron mobilities, a charge is required for counting. Ranges for corrected values are given based on this ionization efficiency.
[c] At the highest concentrations and highest temperatures, deposition on tubing downstream from the source was observed. A conservative estimate for deposition (1:1) was chosen based on comparable particle counts for deposits and aerosols in NTA analysis.

*[Originally submitted to Scientific Reports as part of Main Text Figure 4]

The size and morphologies observed from both methods are comparable to oxidized mercury particles formed from vapour phase GEM reactions with BrO and iodine species [183,213] and aqueous divalent mercury (Hg^{2+}) with thioglycolic acid [193]. The highest number densities were associated with particles 500 nm in size and smaller; particles larger than 1 μm were barely observed using the OPS.

Micron-sized particulate bound mercury (>3 μm) will not condense from supersaturated oxidized mercury vapour nor be the product of GEM photo-oxidation processes instead arising from vapour phase Hg absorption on existing fine and coarse aerosols [154]. When accounting for instrument capabilities and deposition, mercury aerosols formed from vapour flow condensation sources comprise 8 – 25% of GOM produced from the sources at 20 °C (Table 4.2), suggesting that these mercury particles can be emitted from stack conditions, in addition to forming from atmospheric photo-oxidation reactions and other transformation pathways.

As the emissions from stacks will contain many organic and inorganic gaseous and particulate contaminants, any mercury-containing particulates released will be a composite of different forms of mercury on the surface of or incorporated into the bulk of multicomponent particles.

4.3.2. Capture of mercury aerosols by KCl denuder (Refer also to 3.2.7)

Mercury(II) bromide and mercury(II) chloride nanoparticles, formed through vapour flow condensation and nebulization of mercury halide aqueous solutions, were exposed to a manual KCl denuder, the conventional method for capturing GOM. [209] With advancements in chemical speciation techniques, a number of chemical species have been identified in GOM such as $HgCl_2$ [13,65,142], $HgBr_2$ [13,65,142], organomercury [65,76,84], $HgSO_4$ [143], HgO [65,143], and nitrogen-containing mercury compounds [65,143]. Each chemical compound that comprises GOM would have varying degrees in capture, retention and decomposition efficiencies. Denuders are hampered by humidity and O_3 interferences that cause GOM loss [10,65], and the KCl coating may also serve as a site of heterogeneous reactions.

4.3.3. Contamination of GOM measurements by mercury nanoparticles

In terms of particulates, particles larger than 2.5 µm are removed using an impactor while others travel unrestricted due to laminar flow conditions [10]. In comparing flow through the denuder against a similar length of conductive tubing designed for particulate transmission, the KCl denuder readily captured nano-sized mercury aerosols at flow rates of 3 litres per minute (LPM). In particular, between 70% and 95% of the smallest nanoparticles (>50 nm) were trapped undergoing diffusion related losses (Figure 4.2) [214], with particle transmission efficiency increasing with size.

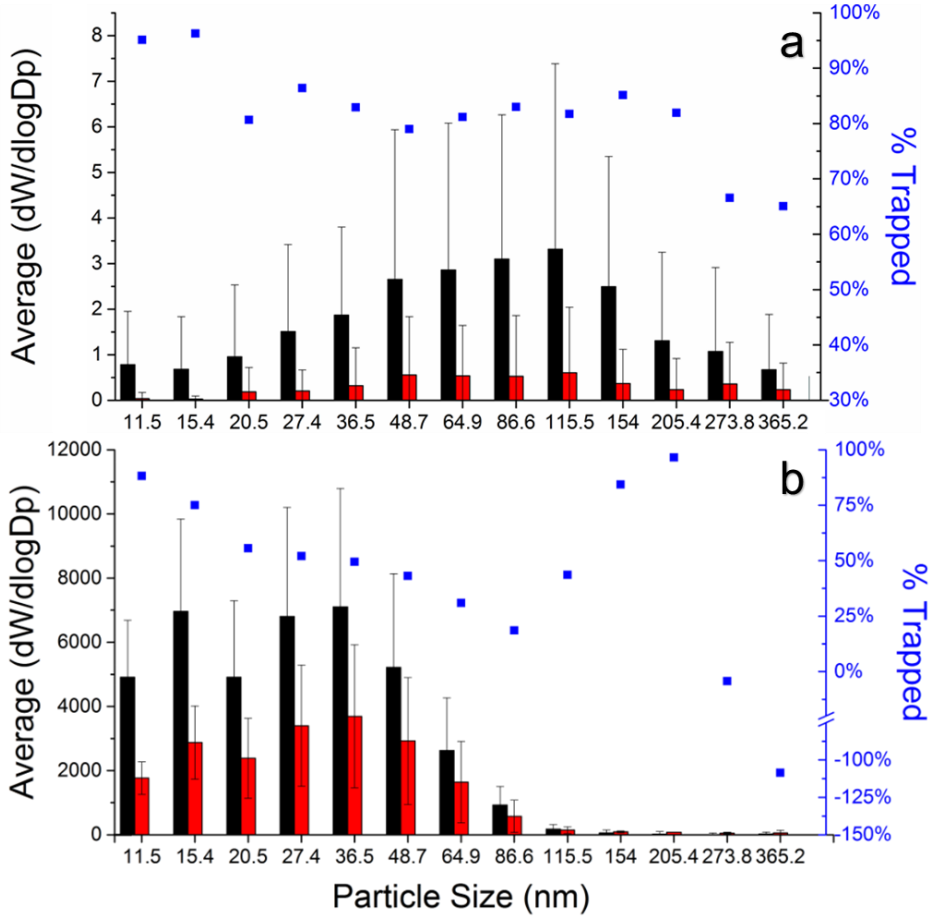

Figure 4.2 Denuder capture of a) synthetic nano-sized mercury(II) bromide particles and b) mercury(II) chloride particles

Particle size distributions for nano-sized mercury(II) bromide particles produced by vapour flow condensation (shown in black) and those produced by vapour flow condensation and subsequently passed through a KCl denuder (shown in red). Flow streams passed through conductive tubing of equivalent length before entering the SMPS inlet at a flow rate of 3LPM. (n=70) Particle size distributions for nano-sized mercury(II) chloride particles produced by aqueous solution nebulization (shown in black) and those produced by vapour flow condensation and subsequently passed through a KCl denuder (shown in red). Flow streams passed through conductive tubing of an equivalent length before entering the SMPS inlet at a flow rate of 3 LPM. (n=70) *[Originally submitted to Scientific Reports as part of Main Text Figure 4]

Significant evaporation of particles, as a cause for the decrease particulate concentrations, cannot entirely be ruled out though had evaporation been occurring, we may expect that the distribution of particles would shift towards smaller particles. For larger nano-sized particles, the denuder trapping efficiency was negative suggesting coagulation of smaller particles or the dislodging of particles from the KCl coating. (Figure 4.2b) While the diffusion of nanosized particles is assumed to play a role in denuder capture, the aerosol diffusion coefficient is still orders of magnitude smaller than the gaseous diffusion coefficient of GOM are greater than 0.1 cm^2/s [189].

4.3.4. Recognizing the contribution of mercury nanoparticles to GOM

With improvements in cut-points for cascade impactors, nanoparticulate mercury, with diameters as small as 30 nm, has been measured [2]. While atmospheric relevant nanoparticulate bound mercury is expected to be heterogeneous, the smallest nanoparticles may contaminate denuder measurements of GOM as would the evaporation of volatile mercury species from these nanoparticles. The contribution of nanoparticles to denuder GOM measurements is an issue given the role that field GOM measurements play in modelling the fate of atmospheric mercury.

4.3.5. Mercury halide aerosols in urban air and influence of urban air co-pollutants

Mercury halides were measured using PFA traps to quantify mercury(II) chloride and mercury(II) bromide in urban air in Montreal [142]. By using filters upstream from the trap, an estimation of the particulate portion of GOM was assessed given the near complete retention of particles by PTFE filters [209]. The entire filter manifold was heated to 50 °C to reduce the adsorption of gaseous oxidized mercury or condensation of water on the filter [10]. Concentrations of mercury(II) chloride ranged from undetected to upwards of 300 pg/m^3, while mercury(II) bromide peaked at 175 pg/m^3 (Figure 4.3). These concentrations are an order of magnitude higher than are typically found in urban environments using KCl-denuder CVAFS measurements but were similar magnitude as manual denuder measurements at the site [215]. However, in comparison to membrane monitors, the denuder system has been shown to underestimate GOM measurements by at least 1.6 fold [141].

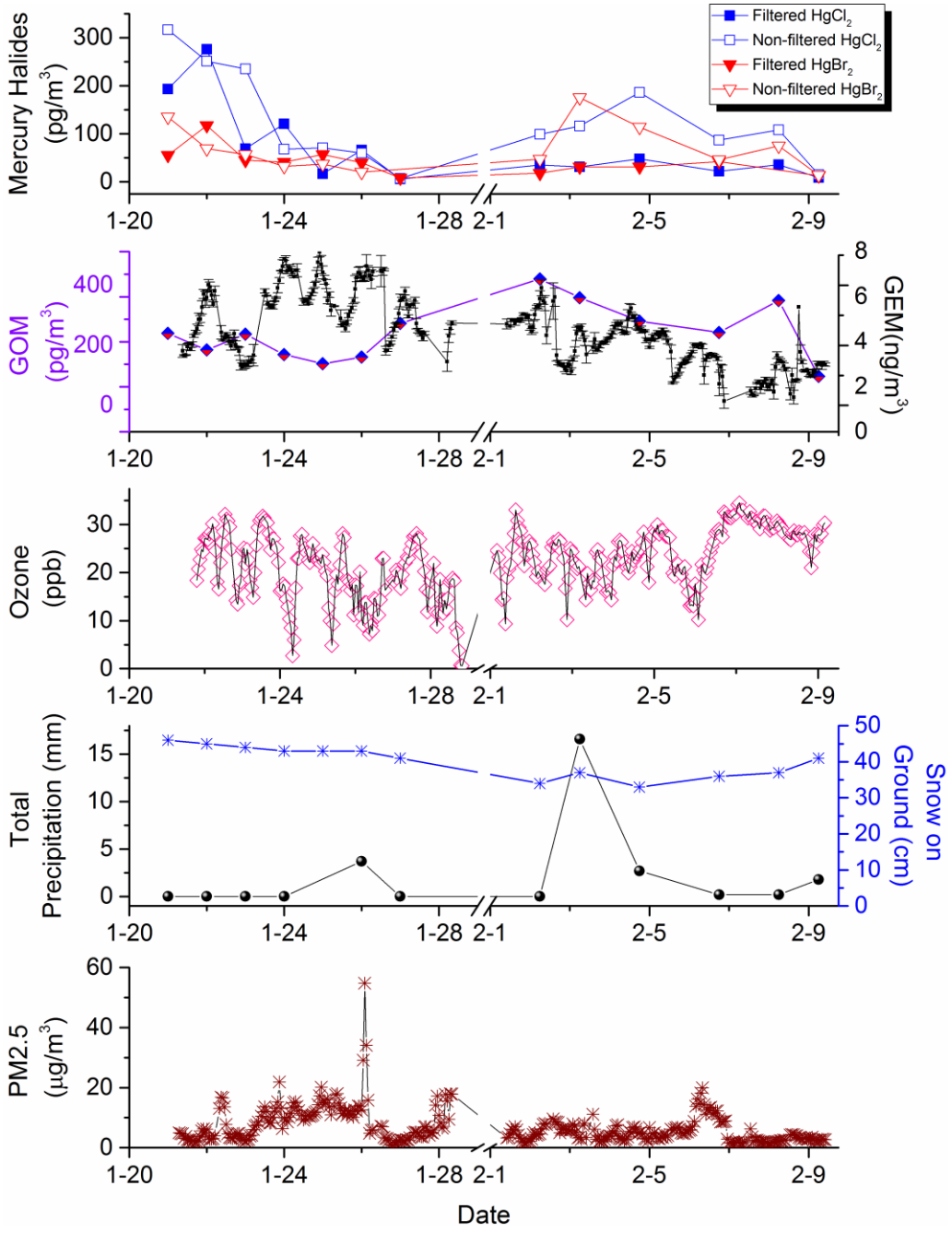

Figure 4.3: Non-filtered and filtered mercury(II) halides concentrations by PFA-preconcentration mercury mass spectrometry in Montreal urban air.

GOM measurements by KCl denuder and GEM measurements by CVAFS. O_3, total precipitation, snow on ground and PM2.5 measurements from 400 m away. GEM is strongly negatively correlated with O_3 ($\rho = -0.67$, $p = 0.01$) and moderately correlated with PM2.5 ($\rho = -0.57$, $p = 0.04$) *[Originally submitted to Scientific Reports as Main Text Figure 3]

At most GOM consisted of 10% of the total atmospheric mercury, and GEM values were between two and four times the average found in North American urban centers. As

mentioned, this is a research facility, where mercury is readily used, and the GEM inlet and denuder were approximately 30 metres from an exhaust stack. The concentrations of mercury(II) chloride and bromide may be high due to both mercury and halogenated solvents used at the site. The concentrations were of similar magnitude (within a factor of 2x) as those observed by Deeds et al. in 2015 [142].

Chemical speciation of particulate mercury has thus far been approached through leaching of mercury during wet digestion procedures where bulk operational species are defined by their propensity to be extracted under certain digest solution conditions [39,88,114,151]. More recently, thermo-desorption is being used, in conjunction with the thermal desorption profiles of inorganic mercury standards, to screen for adsorbed, absorbed and mineral matrix incorporated particulate mercury species [71]. While mass spectrometry has the benefit of providing exact chemical speciation, without adequate separation, there is the potential for artifacts from either ion-source or desorption stage reactions with interferents.

4.3.6. Impact of Filtration on Mercury Halide Trapping

When differences between non-filtered and filtered measures of mercury halides were statistically significant based on ANOVA ($p<0.05$), the estimation mercury aerosols contributions to GOM typically ranged between 60% and 80%. In addition to lower concentrations of oxidants and less available sunlight, colder temperatures will favour greater partitioning to the condensed phase [109]. While the use of filters is a conventional aerosol sampling technique, both positive and negative biases will arise from the heterogeneous reactions of gaseous mercury(II) species with any aerosols trapped on the filter, the trapping of gaseous species in the filter media, or the volatilization of gaseous mercury(II) from aerosols, and the trapping of gaseous species [200].

Non-filtered gaseous and particulate $HgBr_2$ shows a moderate correlation [216] ($0.60 < \rho < 0.75$) with GOM measurements. ($\rho = 0.72$, $p = 0.008$) and we observe a decrease in GOM measurements following two precipitation events. There was also a strong correlation ($0.75< \rho< 0.85$) between filtered and non-filtered $HgCl_2$ ($\rho = 0.68$, $p = 0.01$) and a moderate correlation between the filtered $HgBr_2$ and both non-filtered ($\rho = 0.62$, $p = 0.03$) and filtered $HgCl_2$ ($\rho = 0.60$, $p = 0.04$). As diurnal variations in atmospheric pollutants will influence

aerosol concentrations [109], these measurements have been included for comparison to the mercury(II) halide measurements including NOx, SO_2 and humidity.

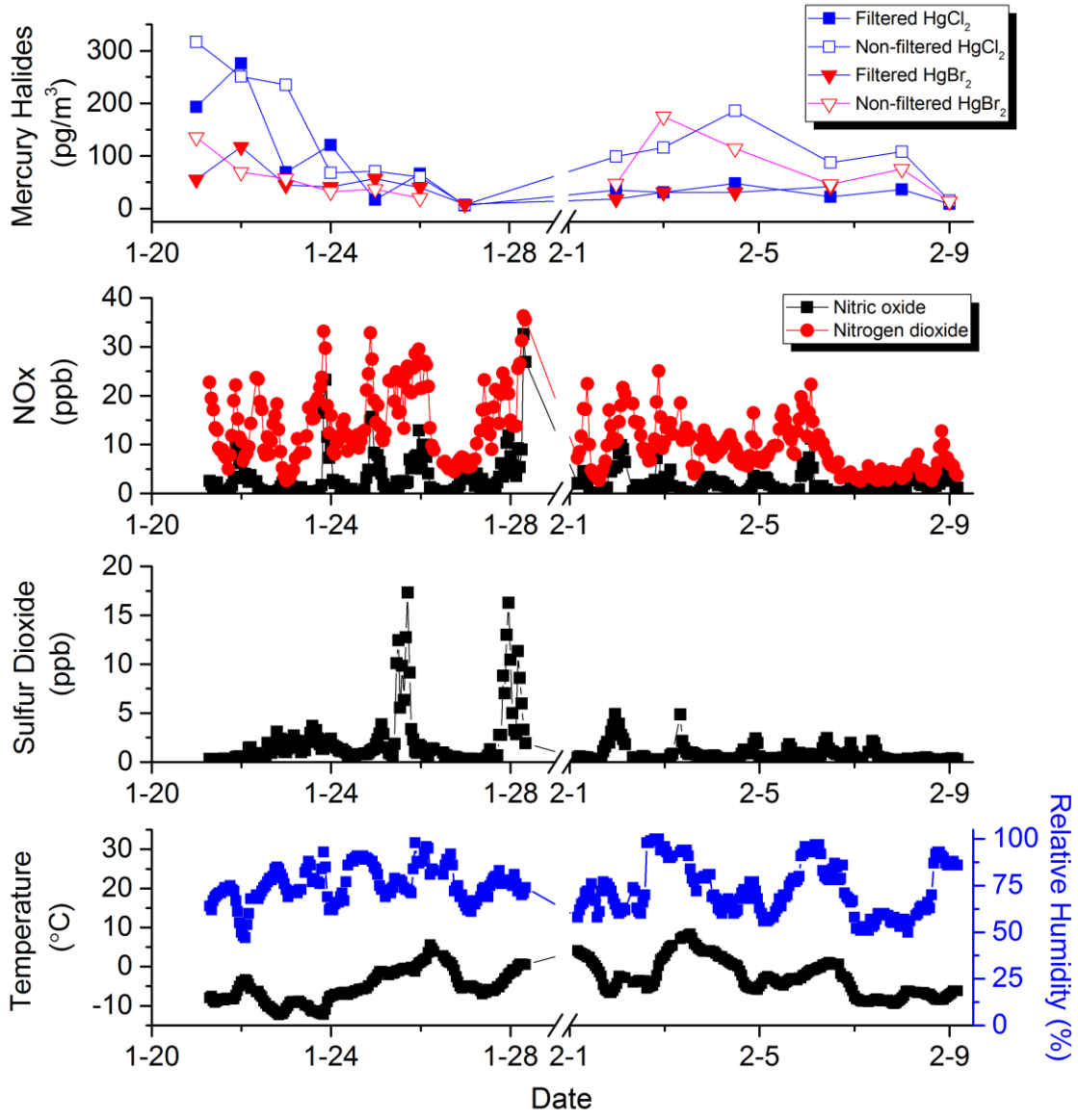

Figure 4.4. Mercury Halides, NO_x, SO_2, humidity and temperature in Montreal.

Teflon preconcentration mercury mass spectrometry in Montreal urban air. NOx, sulphur dioxide, relative humidity and temperature measurements were taken 400 m away. *[Originally submitted to Scientific Reports as Supplementary Figure 2]

4.3.7. Complementary measurements of Mercury Nanoparticles by MOUDI and HR-STEM-EDS

To support the elevated GEM, GOM and mass-spectrometry data, nanosized particulate mercury was captured using a micro-orifice uniform deposit impactor (MOUDI) with four

sub-micron stages. Interestingly, the sub-micron particulate mercury concentrations were on the order of 50 – 100 pg/m^3 with the highest concentrations at the lowest cutoff of 180 nm which is unusual as the accumulation mode for particulate bound mercury occurs around 450 nm. These concentrations are a magnitude higher than typical total mercury particulate levels observed in urban centers [201]. With the development of nano-MOUDI instruments, further study for nanoparticulate mercury is warranted. Analyzing TEM grids adhered to the MOUDI stages, we find mercury and silver by EDS in an HR-STEM sample of a 5-10 nm mercury nanoparticle sampled in ambient air at the site as shown in Figure 4.5.

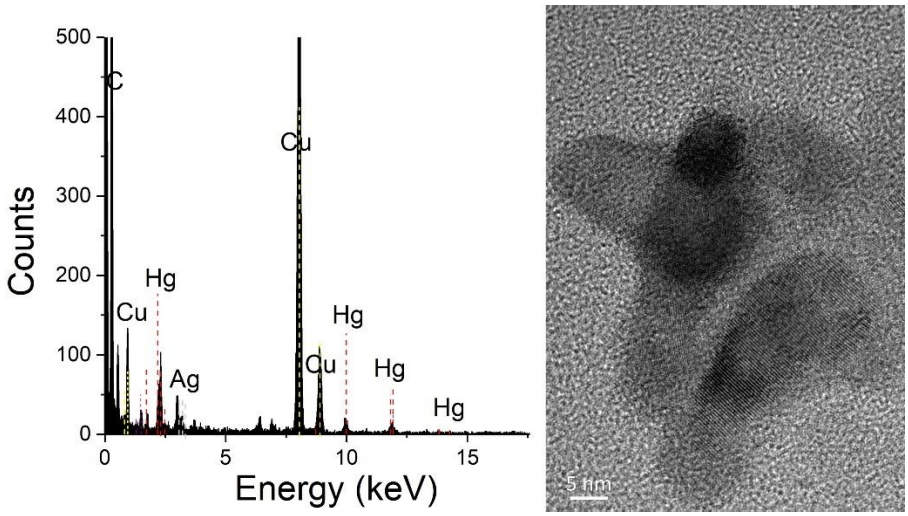

Figure 4.5. Transmission electron microscopy image of mercury nanoparticle collected in Montreal urban air with EDS indicating the presence of mercury and silver.

*[Originally submitted to Scientific Reports as Main Text Figure 2]

4.4. Conclusions: Implications to mercury biogeochemistry and health

We have shown the presence of nanoparticulate mercury compounds in air which current methods of measuring GOM may be unable to distinguish with gaseous oxidized mercury. serve as a universal proxy for GOM in atmospheric field measurements and models, can exist as particles. While laboratory conditions under which these particles are formed are not representative of atmospheric conditions, the existence of heterogeneous mercury-containing nanoparticles is supported by differences we observe in filtered vs non-filtered Hg-MS data, nano-sized particulate mercury collection by MOUDI and TEM images of mercury nanoparticles in ambient air. As a result, the operational field and modelling definitions of particulate and reactive gaseous mercury will need to reflect the emerging

contribution of mercury nano-sized particles. Nanoparticulate mercury will affect physical processes such as wet and dry deposition, atmospheric transport, and chemical processes including plume chemistry, heterogeneous oxidation and reduction processes, surface uptake and catalytic reactions. Furthermore, incorporation in the biogeochemical cycling of mercury and the impact of nanoparticulate mercury in aqueous environments on bio-uptake, bioaccumulation and bio-magnification will be crucial to more accurate modelling of the fate, assessment and regulation of the ecological and human health risks associated with atmospheric mercury.

4.5. Author Acknowledgements.

The authors acknowledge the financial support provided by the Canadian Foundation for Innovation (CFI), the Natural Sciences and Engineering Research Council of Canada (NSERC), Le Fonds Quebecois de la recherché sur la nature et les technologies (FQNRT), Environment and Climate Change Canada, the Walter C. Sumner Foundation and McGill University. Additionally, the authors thank David Liu and Dr. Hojatollah Vali of the Facility for Electron Microscopy Research for their expertise in HR-TEM, and Devendra Pal, Maxwell Morissette, Janani Ramamurthy for their assistance with the KCl denuder experiments, nanoparticulate MOUDI measurements, and proof-reading of the manuscript. Finally, many thanks to Dr. Sonja Melançon and Mme. Diane Boulet of the Réseau de surveillance de la qualité de l'air for the Division de la planification et du suivi environnemental at the City of Montreal for air quality and meteorological measurements.

Chapter 5. Exposure to Nanoscale and Microscale Particulate Air Pollution prior to Mining Development near a Northern Indigenous Community in Québec, Canada

As published in Environmental Science and Pollution Research 2018, 25, 8976-8988

In this paper we use analytical techniques for measuring nanoparticles and micron-sized particles in addition to the elemental analysis of metals in nanoparticles for a practical application and for societal benefit. The work was designed in close conjunction with the wishes and desires of the Cree Nation of Waswanipi to ensure there are baseline measurements of nanoparticles and elemental metal concentrations prior to the beginning of operations of a new rare-earth mining development project.

Contribution by author: For this paper, I assisted with sampling and instrumental operations for all sampling sites, analysis of data, production of tables and figures, and made contributions to the writing and revision of the manuscript.

Abstract

This study serves as a baseline characterization of indoor and outdoor air quality in a remote northern Indigenous community prior to the start of a new major nearby mining operation, including measurements of nanoparticles, which has never been performed in this context before. We performed aerosol sample collection and real time aerosol measurements at 6 different locations at the Montviel campsite, located 45 km west of the Cree First Nation of Waswanipi in the south of the Nord-du-Québec region. High concentrations of airborne nanoparticles (up to $3.98\times10^4 \pm 8.9\times10^3$ cm^{-3} at 64.9 nm midpoint particle diameter) and fine particles (up to $1.99\times10^3 \pm 1.6\times10^2$ cm^{-3} at 0.3 µm midpoint particle diameter) were measured inside a residential home, where we did not find any ventilation and/or air filtration systems. The most abundant particle sizes by mass were between 0.19 and 0.55 µm. The maximum concentration of analyzed heavy metals were detected at the d_{50} cut-off particle size of 0.31 µm; and the most abundant heavy metals in the aerosol samples were Al, Ba, Zn, Cu, Hg and Pb. We concluded that the sources of the relatively high indoor particle concentrations were likely washing machines and cooking emissions in the absence of a sufficient ventilation system. However, the chemical composition of particles resulting from mining activities is expected to be different from that of the aerosol particles from indoor sources. Installation and proper maintenance of sufficient ventilation and air filtration systems may reduce the total burden of disease from outdoor and indoor air pollution and remediate infiltrated indoor particulate pollution from the mining sources as well.

5.1. Introduction

Chronic and acute exposures to air pollution kill between 5.5 and 8.2 million people annually [217-219]. Air pollution has recently been listed as one of the main environmental factors contributing to the incidence of many types of cancer [220] and is a major driver of cardiovascular and pulmonary disease [221,222]. Exposure to air pollution also increases the frequency of respiratory infections in communities [223-226], including young Canadian Inuit children [227,228]. Mining is one of the major sources of anthropogenic air pollutants [229], along with power production [230], industrial operations [231], and engine exhaust [232-234].

Among the different types of gaseous and particulate air pollutants, nano-sized particles (also known as ultrafine particles) are defined as having a diameter between 1 and 100 nm, and their contribution to adverse health effects and disease have been a recent focus of toxicological and health studies [235]. Epidemiological studies showed that exposure to nanoparticles in air particularly harms children [236], elevating blood pressure in schoolchildren [237], and contributing to premature infant mortality [219,238]. The elderly are also adversely impacted by exposure to nanoparticulate air pollution [239]. Nanoparticles have been found to increase the risk of developing myocardial ischemia [240,241], which has a potential to cause negative cardiac outcomes [242]. Several studies showed that even short-term exposure to nanoparticles in air increases the incidence of acute respiratory symptoms and impairment of the lung function [243].

Indigenous and rural communities can be very vulnerable to the environmental factors due to barriers in access to monitored sources of water and food, and lack of real-time accurate information about the status of their living environment as it is being anthropogenically altered [244-254]. Access to clean water and healthy uncontaminated food in these communities has been a concern for a long time. However, little attention has been dedicated to the outdoor and indoor quality of the air people living in Indigenous and remote communities breathe [255]. In remote Indigenous communities in the North people spend more time indoors relative to the time spent outdoors than in the past [256]. A larger body of research has focused on indoor pollution in Africa and Asia, notably in India where cooking on open fire indoors is linked to millions of premature deaths annually [257]. However, little such research has been done with northern and Arctic Indigenous communities [227,228,255].

Multiple environmental factors contribute to the total burden of disease and premature mortality [258-262]. The negative effects of a given factor, including air pollution, are often exacerbated by other factors acting synergistically [263-265]. Numerous studies showed that air pollution from mining activities typically leads to exposure of people, who live near the mines, to harmful chemicals and airborne particulate matter at concentrations that are higher than background levels [266-269]. A subset of such studies demonstrated the acuteness of this problem in areas where mining took place near remote Indigenous communities [270-275]. These studies of air pollution near mines raised awareness of the

problem with the mining companies and the public, including Indigenous communities. The question arose: How can we ensure the sustainable and responsible mining development with the minimal risk to human and environmental health, wellbeing and the traditional ways of life? The answer is to collaboratively develop and implement sufficient evidence-based preventive and remediation measures that will minimize the impact of mining on local communities. This study is the first step in building such evidence to address the problem of air pollution associated with mining activities. Here we describe a background level assessment of air pollution exposure in an Indigenous community located near the site of a future mining operation. We provide the results of both an indoor and outdoor air pollution monitoring campaign carried out prior to a major mining operation development in the area near the Cree First Nation of Waswanipi in Québec, Canada.

This study presents the results of a short-term parallel monitoring of outdoor and indoor air pollution particles in the six homes and communal venues of the Cree First Nation of Waswanipi in Québec, Canada. The monitoring was conducted with the help and in close collaboration with Community members. A rare earth and niobium mining site in the Baie-James region (49°41′57″N, 75°57′27″W) is to be developed in the vicinity in a few years. Therefore, the results presented here provide a baseline on aerosol (airborne particulate matter) concentration and distribution prior to these major mining activities, for both outdoor and indoor air. Sampling of both outdoor and indoor air is important because indoor air quality is linked to outdoor air quality due to infiltration of outdoor air into buildings. Indoor air quality is also heavily dependent on indoor pollutant sources. Indigenous community members spend more time indoors than before [256] – it is a similar trend to the non-indigenous population in several other parts of Canada [276] and the US [277]. The assessment of air quality and pollutant composition both indoors and outdoors is therefore key to obtaining a complete picture of a person's exposure to air pollution. The results provide a benchmark and will facilitate evaluation of the future air-pollution-related effects of mining activities, so their impact on the community members and the environment can be adequately analyzed.

In the course of this study, we found elevated indoor nanoparticulate concentrations in homes and venues in this First Nation community. In response, we also offer here a set of

recommendations to implement simple cost-effective measures to remediate the high indoor air pollution and reduce associated health risks.

5.2. Materials and Methods

5.2.1. Monitoring Locations and Sampling Timetable

The field campaign was carried out on the mining sites of our industrial partner, GéoMégA, and in the Cree First Nation of Waswanipi from June 12, 2016 to June 15, 2016. The aerosol samples were taken from Montviel campsite (49°49′15″N, 76°38′59″W) between June 13, 2016 and June 15, 2016. The site is located approximately 100 km north of Lebel-sur-Quévillon and 45 km west of the Cree First Nation of Waswanipi (49°41′51″N, 75°57′38″W) in the south of the Nord-du-Québec region. The sampling locations (Table 5.1) were chosen to include the maximum number of distinct indoor settings in the Community to cover during the sampling campaign. Measurements and sampling were also carried out outdoors at the same locations.

5.2.2. Aerosol Size Distribution Analysis

Real-time aerosol measurements at the 6 above-mentioned sites were performed using a NanoScan™ scanning mobility particle sizer (SMPS), Model 3910 (TSI, Inc.), and an optical particle sizer (OPS), Model 3330 (TSI, Inc.). The principle of operation of the NanoScan™ SMPS is based on deflecting aerosol particles by an electric field based on their electrical mobility, which is dependent on particle size. It has a measurement size range of 10 nm to 420 nm and measurement time of 60 seconds for size distribution measurements. Its inlet sampling flow rate is 0.75 L/min.

The OPS is a single-particle optical counter of aerosol particles with a measurement size range of 0.3 – 10 μm in 16 aerosol particle size channels. The inlet sampling flow rate of the OPS is 1 L/min. The aerosol measurement instruments register the number of aerosol particles in predefined particle size channels. When we calculated the mass concentrations of aerosol particles, we assumed particle density to be 1.0 g/cm^3. We grouped particle concentrations in multiple channels together according to wider particle size ranges during data analysis, as discussed below.

Table 5.1. Sampling locations at Montviel, QC and at sites in Waswanipi

Site	Location	Date(s) of Measurements	Description of Location
Arena	Inside	6-12 6-13 6-14	Corner in the main foyer of the arena. There was only little pedestrian traffic or movement going in or out of the arena or the interior ice surface.
Camp	Kitchen	6-12	In a living room area immediately after breakfast was made and served in the kitchen and dining area. There was much frying, including bacon.
	Outdoor (Day)	6-13	On the exterior stairs leading up to a cabin site.
	Outdoor (Night)	6-13	
	Outdoor	6-14	
	Woods	6-14	Approximately 30 meters from the campsite on a slightly elevated area surrounded by bush.
	Residence (additional sampling)	6-14	In the interior of a cabin by the bunks where our research team stayed.
Council	Outside	6-12	Picnic tables a few metres away from the main entrance to the Council Center. The main entrance is on the same wall facing a parking lot as the side entrance.
		6-13 6-14	By the side entrance to the Council Center. The side entrance is on the same wall facing a parking lot as the main entrance.
Daycare	Inside	6-13 6-14	Daycare dining room next to a wall with a mural. Some heating vents were within 4 meters of the sampling location and within 1 meter of one another.
	Outside	6-13 6-14	In the parking lot with a gravel surface, about 10 meters from the entrance to the daycare.
Home	Inside	6-12 6-13	Basement table near a television sitting area and within 6 meters of laundry machines and two basement rooms. Laundry machines were operating at the time of sampling with no ventilation system in use. We hypothesized they would be exposed to high concentrations of nanoparticles at this location.
Police Station	Inside	6-12 6-13	Foyer/hallway of the Police Station near a break room.
		6-14	Offices about 3 meters from a bathroom.
	Outside	6-12 6-13 6-14	Near a side door of the Police Station on a paved surface.
Residence	Inside	6-13 6-14	In the interior of a cabin by the bunks where our research team stayed.

*[Originally published in Environmental Science and Pollution Research as Main Text Table 1.]

5.2.3. MOUDI

A Micro-Orifice Uniform Deposit Impactors (MOUDI) unit, model 100-R (MSP Corp., Shoreview, MN, USA) was used to collect size-fractionated aerosol particle samples for subsequent chemical analysis. The unit has 8 impaction stages with the inlet and the stages calibrated to the following d_{50} cut-off points: 18, 9.9, 6.2, 3.1, 1.8, 1.0, 0.55, 0.31, and 0.19 μm equivalent aerodynamic diameter. The MOUDI unit was protected from the weather by a wood box shelter that had a 30 mm wide gap around the perimeter to maximize the sampling efficiency of the large particles. Millipore Quartz Fiber Filters (47 mm) were used in the MOUDI to extract the samples. The MOUDI was operated at an air flow rate of 30 L/min for 24 hour sampling periods. This duration of sampling was determined to provide samples of sufficient mass for subsequent analyses.

5.2.4. ICP-MS

For analysis of the MOUDI samples by inductively coupled plasma – mass spectrometry (ICP-MS), the quartz filters were removed from the MOUDI and brought back to Montreal for processing. First, the filters were digested using 4 % HNO_3 solution at 69 °C for 3 hrs, with sonication. The solutions were filtered through 0.45 μm pore size syringe filters. The resulting processed samples were then subjected to ICP-MS analysis.

5.3. Results and Discussion

Table 5.2 and Table 5.3 provide number-based and mass-based concentrations of aerosol particles divided into particle size ranges. The ranges of aerosol particle sizes reported in Table 5.2 and Table 5.3 are limited by the smallest particles our instrument could measure, which is 10 nm. The boundaries of the size ranges sometimes deviate from the intended boundaries as the measurement particle size channels are fixed. The closest inclusive instrument channel boundaries are used. The range from 10 to 100 nm follows the widely accepted definition of nanoparticles, which is found in regulations worldwide [278,279]. The range from 10 to 237.1 nm corresponds to the measured particle size range where most aerosol particles by number were found in our study. The data expressed in mass concentration metric are provided as PM_1, $PM_{2.5}$ and PM_{10} according to the generally accepted conventions for the mass concentrations of all particles smaller than 1 μm, smaller

than 2.5 μm and smaller than 10 μm, respectively. The $PM_{2.5}$ and PM_{10} as defined above are a close approximation of the existing standard [280] for the definitions of these particle size fractions. $PM_{2.5}$ and PM_{10} are defined in this standard as mass of all airborne (aerosol) particles in a unit volume of air, which pass through a size-selective inlet with a 50 % efficiency cut-off at 2.5 and 10 μm aerodynamic diameter, respectively. We note that due to the slight differences of the upper limits of the measurement size channels of the OPS instrument, PM_1 we report includes particles up to 1.1 μm in diameter and $PM_{2.5}$ up to 2.7 μm. Number-weighted and mass-weighted concentrations in additional sub-ranges of aerosol particle size are provide in the Supporting Information in Table 0.5 and Table 0.6.

Table 5.2. Number-weighted concentrations (cm^{-3}) of nanoparticles and PM_{10} particles measured at Montviel, QC and at sites in Waswanipi.

Site	Description	Date	10 – 100 nm	10 – 237.1 nm	10 nm – 10 μm
Arena	Inside	6-12	$(4.70 \pm 0.49) \times 10^2$	$(6.11 \pm 0.49) \times 10^2$	$(6.14 \pm 0.52) \times 10^2$
	Inside	6-13	$(5.88 \pm 0.63) \times 10^2$	$(6.35 \pm 0.65) \times 10^2$	$(6.37 \pm 0.66) \times 10^2$
	Inside	6-14	$(1.080 \pm 0.036) \times 10^3$	$(1.250 \pm 0.37) \times 10^3$	$(1.252 \pm 0.044) \times 10^3$
Camp	**Kitchen**	6-12	$(6.6 \pm 4.1) \times 10^5$	$(8.2 \pm 5.0) \times 10^5$	No data - OPS failed
	Outdoor (D)	6-13	$(0.60 \pm 1.1) \times 10^3$	$(0.69 \pm 1.2) \times 10^3$	$(0.70 \pm 1.12) \times 10^3$
	Outdoor (N)	6-13	$(1.2 \pm 2.4) \times 10^3$	$(1.7 \pm 3.0) \times 10^3$	$(1.7 \pm 2.6) \times 10^3$
	Outdoor	6-14	$(8.4 \pm 1.1) \times 10^2$	$(9.0 \pm 1.2) \times 10^2$	$(9.1 \pm 1.2) \times 10^2$
	Woods	6-14	$(4.70 \pm 0.27) \times 10^2$	$(9.03 \pm 0.49) \times 10^2$	$(9.05 \pm 0.41) \times 10^2$
	Residence	6-14	$(4.31 \pm 0.21) \times 10^3$	$(8.66 \pm 0.31) \times 10^3$	$(8.71 \pm 0.32) \times 10^2$
Council	Outside	6-12	$(2.3 \pm 5.7) \times 10^2$	$(3.8 \pm 7.4) \times 10^2$	$(3.9 \pm 6.0) \times 10^2$
	Outside	6-13	$(1.2 \pm 1.4) \times 10^2$	$(2.0 \pm 1.4) \times 10^2$	$(2.0 \pm 1.4) \times 10^2$
	Outside	6-14	$(8.28 \pm 0.54) \times 10^2$	$(1.247 \pm 0.055) \times 10^3$	$(1.248 \pm 0.062) \times 10^3$
Daycare	Inside	6-13	$(8.9 \pm 1.7) \times 10^2$	$(9.2 \pm 1.6) \times 10^2$	$(9.2 \pm 1.7) \times 10^2$
	Outside	6-13	$(1.19 \pm 0.80) \times 10^2$	$(1.93 \pm 0.88) \times 10^2$	$(1.95 \pm 0.82) \times 10^2$
	Inside	6-14	$(3.4 \pm 2.0) \times 10^3$	$(3.7 \pm 2.0) \times 10^3$	$(3.7 \pm 2.0) \times 10^3$
	Outside	6-14	$(6.46 \pm 0.76) \times 10^2$	$(1.170 \pm 0.082) \times 10^3$	$(1.174 \pm 0.083) \times 10^3$
Home	**Inside**	6-12	$(1.68 \pm 0.28) \times 10^4$	$(2.28 \pm 0.41) \times 10^4$	$(2.31 \pm 0.31) \times 10^4$
	Inside	6-13	$(1.43 \pm 0.21) \times 10^4$	$(1.62 \pm 0.19) \times 10^4$	$(1.62 \pm 0.22) \times 10^4$
Police Station	**Inside**	6-12	$(7.2 \pm 1.2) \times 10^3$	$(1.10 \pm 0.13) \times 10^4$	$(1.11 \pm 0.12) \times 10^4$
	Outside	6-12	$(2.20 \pm 0.27) \times 10^2$	$(4.53 \pm 0.27) \times 10^2$	$(4.57 \pm 0.34) \times 10^2$
	Outside	6-13	$(1.97 \pm 0.93) \times 10^3$	$(2.5\pm 1.0) \times 10^3$	$(2.47 \pm 0.95) \times 10^2$
	Inside	6-14	$(4.92 \pm 0.28) \times 10^3$	$(6.01 \pm 0.29) \times 10^3$	$(6.04 \pm 0.29) \times 10^3$
	Outside	6-14	$(1.7 \pm 2.4) \times 10^3$	$(1.9 \pm 2.6) \times 10^3$	$(1.9 \pm 2.4) \times 10^3$
Resi-dence	Inside	6-13	$(2.63 \pm 1.8) \times 10^2$	$(2.94 \pm 0.22) \times 10^2$	$(2.97 \pm 0.20) \times 10^2$
	Inside	6-14	$(1.20 \pm 1.1) \times 10^3$	$(1.45 \pm 0.10) \times 10^3$	$(1.45 \pm 0.11) \times 10^3$

The bolded locations had concentrations that exceeded 1×10^4 cm^{-3} (10 – 100 nm or 10 – 237.1 nm) *[Originally published in Environmental Science and Pollution Research as Main Text Table 2.]

The World Health Organization deems 3 – 5 μg/m^3 as the level of either short-term or long-term exposure to $PM_{2.5}$ air pollution, at which no significant adverse health effects are expected to occur [281]. The WHO guidelines for regulators around the world suggest limits of at most 10 μg/m^3 annual mean and 25 μg/m^3 24-hour mean for $PM_{2.5}$ and 20 μg/m^3 annual mean and 50 μg/m^3 24-hour mean for PM_{10}. The Canadian air quality standards are for $PM_{2.5}$: 10 μg/m^3 annual and 28 μg/m^3 24-hour (2015) and will decrease to 8.8 μg/m^3 annual and 27 μg/m^3 24-hour in 2020 [282]. For PM_{10}, there is no Canada-wide air quality standard, and only scarce regional ones. As an example, Ontario's is 50 μg/m^3 24-hour [283]. Montviel and Waswanipi are in the Canadian province of Québec. Québec's standards differ from the Canada-wide standards that Québec did not sign on to. They are 30 μg/m^3 24-hour for $PM_{2.5}$ and 120 μg/m^3 24-hour and for Total PM as of 2011 [284]. No standards based on number-based concentrations exist, but there is a debate to introduce a number-based metric for ambient nanoparticles as a maximum acceptable number concentration of particles smaller than 100 nm in the future.

For the number-based concentrations of particles we measured, we found that the concentrations indoors were generally higher than concentrations outside. We think indoor sources are implicated in these elevated indoor particle concentrations. At several measurement locations, the concentrations exceeded 1×10^4 cm^{-3} (10 – 100 nm or 100 – 237.1 nm). We marked those locations in bold in Table 5.2. They were at the "Kitchen" in the Camp, inside the "Home" on both days we measured there, and inside the "Police Station".
The mass-based levels for $PM_{2.5}$ we measured could be compared to the existing outdoor air quality standards, discussed above. There is no direct regulatory applicability of the outdoor standards to indoor air quality. However, because these standards are based on epidemiological evidence of adverse health effects, the outdoor standards can serve as benchmarks to discuss the potential level of harm from the mass-based indoor concentrations we measured in this study. Only levels higher than the annual, and not 24-hour $PM_{2.5}$ standard were detected at some locations. They were: 1) inside "Home" on one of the two days we measured there, and 2) inside the "Police Station." Unfortunately, the OPS instrument failed during the measurements at the Kitchen, so the potentially high $PM_{2.5}$ concentrations there have not been registered.

The original high-resolution number-based aerosol size distributions that formed a basis to calculate the number-weighted and mass-weighted summary results in Table 5.2 and Table 5.3 are presented below and in the Supporting Information. The figures in the main article include locations where the highest concentrations were measured. The rest are in the Supporting Information.

Table 5.3. Mass-weighted concentrations (μg/m³) of sub-micron particles PM_1, $PM_{2.5}$ particles and PM_{10} particles measured at Montviel, QC and at sites in Waswanipi.

Site	Description	Date	PM_1	$PM_{2.5}$	PM_{10}
Arena	Inside	6-12	$(4.28 \pm 0.37) \times 10^{-2}$	$(3.75 \pm 0.42) \times 10^{-1}$	$(2.7 \pm 2.0) \times 10^{0}$
	Inside	6-13	$(2.74 \pm 0.40) \times 10^{-1}$	$(8.0 \pm 3.8) \times 10^{-1}$	$(2.2 \pm 1.0) \times 10^{0}$
	Inside	6-14	$(1.357 \pm 0.059) \times 10^{-1}$	$(3.07 \pm 0.41) \times 10^{-1}$	$(1.17 \pm 0.061) \times 10^{0}$
Camp	Kitchen	6-12	No data - OPS failed	No data - OPS failed	No data - OPS failed
	Outdoor (D)	6-13	$(7.03 \pm 0.15) \times 10^{-2}$	$(4.1 \pm 6.1) \times 10^{-1}$	$(1.5 \pm 1.1) \times 10^{0}$
	Outdoor (N)	6-13	$(1.6 \pm 3.9) \times 10^{0}$	$(1.0 \pm 1.6) \times 10^{1}$	$(1.2 \pm 1.7) \times 10^{1}$
	Outdoor	6-14	$(4.1 \pm 1.2) \times 10^{-2}$	$(4.1 \pm 1.7) \times 10^{-1}$	$(5.6 \pm 2.0) \times 10^{-1}$
	Woods	6-14	$(1.55 \pm 0.97) \times 10^{-2}$	$(2.44 \pm 0.43) \times 10^{-1}$	$(6.2 \pm 3.5) \times 10^{-1}$
	Residence	6-14	$(1.221 \pm 0.061) \times 10^{-1}$	$(9.33 \pm 0.57) \times 10^{-1}$	$(3.9 \pm 1.8) \times 10^{0}$
Council	Outside	6-12	$(5.13 \pm 0.14) \times 10^{-2}$	$(4.9 \pm 2.1) \times 10^{-1}$	$(1.28 \pm 0.80) \times 10^{0}$
	Outside	6-13	$(1.36 \pm 0.45) \times 10^{-2}$	$(2.29 \pm 0.43) \times 10^{-1}$	$(3.7 \pm 9.3) \times 10^{0}$
	Outside	6-14	$(1.920 \pm 0.087) \times 10^{-1}$	$(6.66 \pm 0.75) \times 10^{-1}$	$(1.01 \pm 0.18) \times 10^{0}$
Daycare	Inside	6-13	$(6.56 \pm 0.88) \times 10^{-2}$	$(1.12 \pm 0.50) \times 10^{-1}$	$(2.9 \pm 1.3) \times 10^{0}$
	Outside	6-13	$(1.55 \pm 0.97) \times 10^{-2}$	$(2.36 \pm 0.44) \times 10^{-1}$	$(2.7 \pm 1.5) \times 10^{0}$
	Inside	6-14	$(2.23 \pm 0.85) \times 10^{-1}$	$(7.4 \pm 1.9) \times 10^{-1}$	$(4.1 \pm 1.4) \times 10^{0}$
	Outside	6-14	$(1.73 \pm 0.88) \times 10^{-1}$	$(1.054 \pm 0.077) \times 10^{0}$	$(7.7 \pm 9.7) \times 10^{0}$
Home	**Inside**	6-12	$(3.30 \pm 0.76) \times 10^{0}$	$(2.38 \pm 0.29) \times 10^{1}$	$(4.60 \pm 0.67) \times 10^{1}$
	Inside	6-13	$(1.79 \pm 0.27) \times 10^{0}$	$(3.62 \pm 0.87) \times 10^{0}$	$(6.22 \pm 0.96) \times 10^{0}$
Police Station	**Inside**	6-12	$(1.37 \pm 0.21) \times 10^{0}$	$(1.117 \pm 0.069) \times 10^{1}$	$(1.62 \pm 0.14) \times 10^{1}$
	Outside	6-12	$(5.82 \pm 0.43) \times 10^{-2}$	$(5.71 \pm 0.66) \times 10^{-1}$	$(4.5 \pm 4.0) \times 10^{0}$
	Outside	6-13	$(1.57 \pm 0.53) \times 10^{-2}$	$(1.22 \pm 0.42) \times 10^{-1}$	$(2.3 \pm 1.3) \times 10^{-1}$
	Inside	6-14	$(7.71 \pm 0.37) \times 10^{-1}$	$(2.47 \pm 0.17) \times 10^{0}$	$(6.55 \pm 0.94) \times 10^{0}$
	Outside	6-14	$(1.88 \pm 0.15) \times 10^{-1}$	$(3.7 \pm 4.1) \times 10^{-1}$	$(1.03 \pm 0.71) \times 10^{0}$
Resi-dence	Inside	6-13	$(2.51 \pm 0.22) \times 10^{-2}$	$(1.64 \pm 0.69) \times 10^{-1}$	$(1.27 \pm 0.92) \times 10^{0}$
	Inside	6-14	$(1.869 \pm 0.075) \times 10^{-1}$	$(3.66 \pm 0.49) \times 10^{-1}$	$(9.5 \pm 2.2) \times 10^{-1}$

The bolded locations had concentrations that exceeded 1×10^{0} μg/m³ (PM_1) or 1×10^{1} μg/m³ ($PM_{2.5}$ or PM_{10}) *[Originally published in Environmental Science and Pollution Research as Main Text Table 3.]

Compared to our other measurement locations, we found very high concentrations of airborne nanoparticles in the air inside the private home on both days of measurements (Figure 5.1) with the most abundant particle sizes around 50 – 80 nm. We also measured

(Figure 5.1) a very high concentration of larger particles (1×10^3 cm^{-3} at 0.3 μm midpoint particle diameter), especially on June 12, 2016, compared to other measurement locations. The concentration of nanoparticles was 10 – 150 times higher than typical outdoor concentrations and the concentration of larger particles was 2 – 3 orders of magnitude higher than typically measured outside. We attribute these comparatively high concentrations of particulate air pollution to the fact that the space housed washing machines, which were operating during the measurements without ventilation or air filtration system working at the time. Two nearby bedrooms suggest the residents were exposed to these comparatively high aerosol particle concentrations.

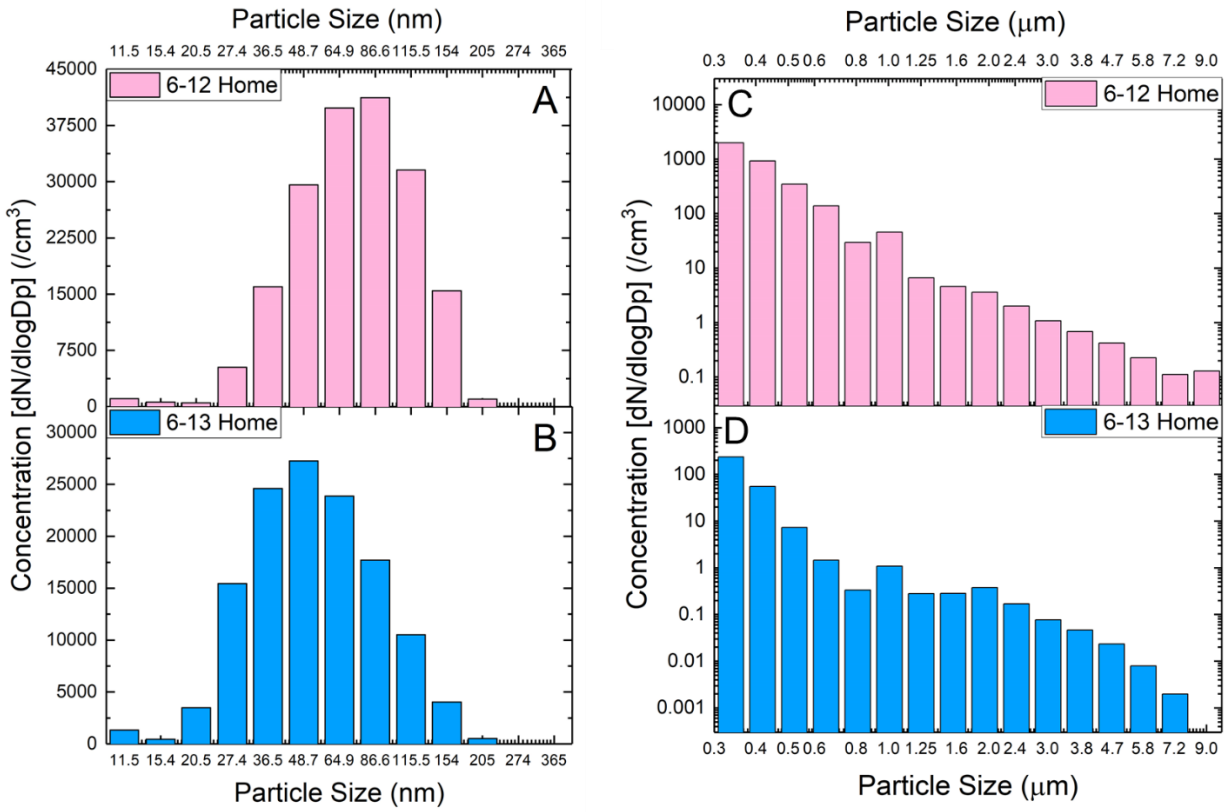

Figure 5.1. Aerosol particle size distributions inside the Private Home (SMPS, OPS).

(A,C) June 12, 2016, time 13:00 to 14:00, temperature 18 °C, 19 °C, 49°41'49"N, 75°57'44"W; (B,D) June 13, 2016, time 17:00 to 17:30, temperature 19 °C, 49°41'49"N, 75°57'44"W. *[Originally published in Environmental Science and Pollution Research as Main Text Figures 1 and 2.]

The nanoparticle size distributions measured inside and outside the Police Station on June 12, 2016 were similar in shape, except that the smaller nanoparticles (< 48.7 nm) were relatively more abundant indoors (Figure 5.2). However, in terms of the absolute

concentration, the nanoparticulate air pollution was about 20 times higher than outside. Likewise, for the larger particles (Figure 5.2), we measured 1 to 2 orders of magnitude higher indoor concentrations of nanoparticles compared to the outside. This observation points to existence of an intense source(s) of airborne particles indoors in the absence of sufficient ventilation and/or air filtration.

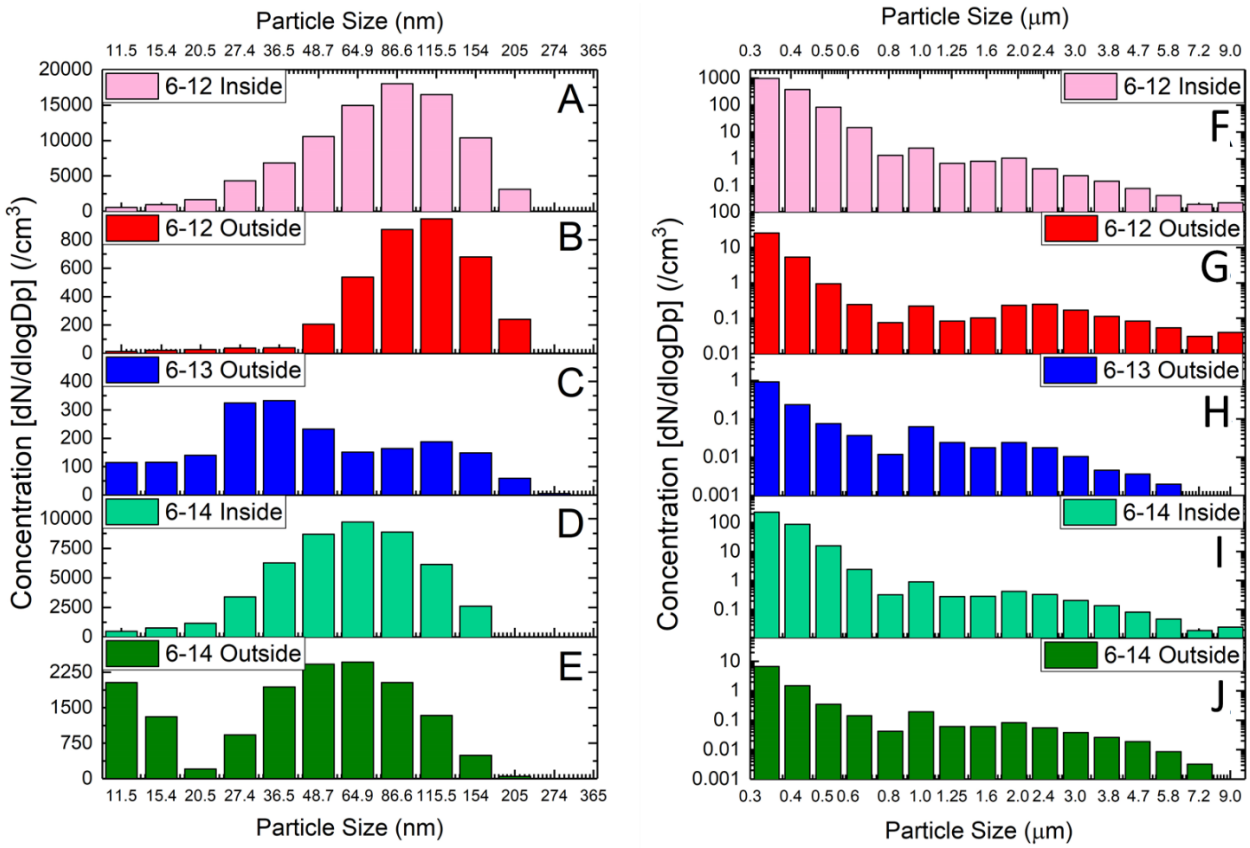

Figure 5.2. Aerosol particle size distributions inside/outside the Police Station (SMPS,OPS).

(A,F) June 12, 2016, time 11:10 to 12:00 inside the Police Station, temperature 23 °C, 49°41'31"N, 75°58'11"W; (B,G) June 12, 2016, time 16:20 to 16:50 outside the Police Station, temperature 12 °C, relative humidity 78 %, wind NNW 19 km/hr, 49°41'31"N, 75°58'11"W; (C,H) June 13, 2016, time 11:50 to 12:20 outside the Police Station, temperature 9 °C, relative humidity 61 %, wind NNW 14 km/hr, 49°41'31"N, 75°58'11"W; (D,I) June 14, 2016, time 10:00 to 10:30 inside the Police Station, temperature 23 °C, 49°41'31"N, 75°58'11"W; (E,J) June 14, 2016, time 22:45 to 23:15 outside the Police Station, temperature 16 °C, relative humidity 59 %, wind NNW 11 km/hr, 49°41'31"N, 75°58'11"W. *[Originally published in Environmental Science and Pollution Research as Main Text Figures 3 and 4.]

The concentration of nanoparticles measured (Figure 5.3) in the Kitchen ($2.2 \pm 1.3 \times 10^5$ cm^{-3} at 64.9 nm mode) was 3 orders of magnitude higher than concentrations measured outside at other locations on the same day (June 12, 2016). In fact, it is at this indoor sampling location that we detected the absolute highest concentration of nanoparticles measured during our sampling campaign. It is now widely known that cooking emissions, particularly

from frying, contain high concentrations of toxic and carcinogenic chemicals, such as CO_2, CO, benzene, toluene, methylene chloride and chloroform, as well as aerosols, potentially contributing to incidence of cancer [285,286]. Fuel combustion indoors results in a substantial burden of disease leading to 4 million annual premature deaths worldwide [257,287,288]. The Government of Canada instructs that indoor $PM_{2.5}$ levels should be kept as low as possible because it deems any reduction to result in health benefits [289]. The Health Canada guidance [289] suggests installation of stove-top fans and installation and operation of adequate ventilation and filtration systems. The low-noise stove fume hoods, modern ventilation systems with heat recovery ventilators and high-efficiency particulate air (HEPA) filtration systems that can be ventilation-system-integrated (in-duct) as well as standalone (less costly but less efficient) have varying costs of installation and maintenance but are readily available.

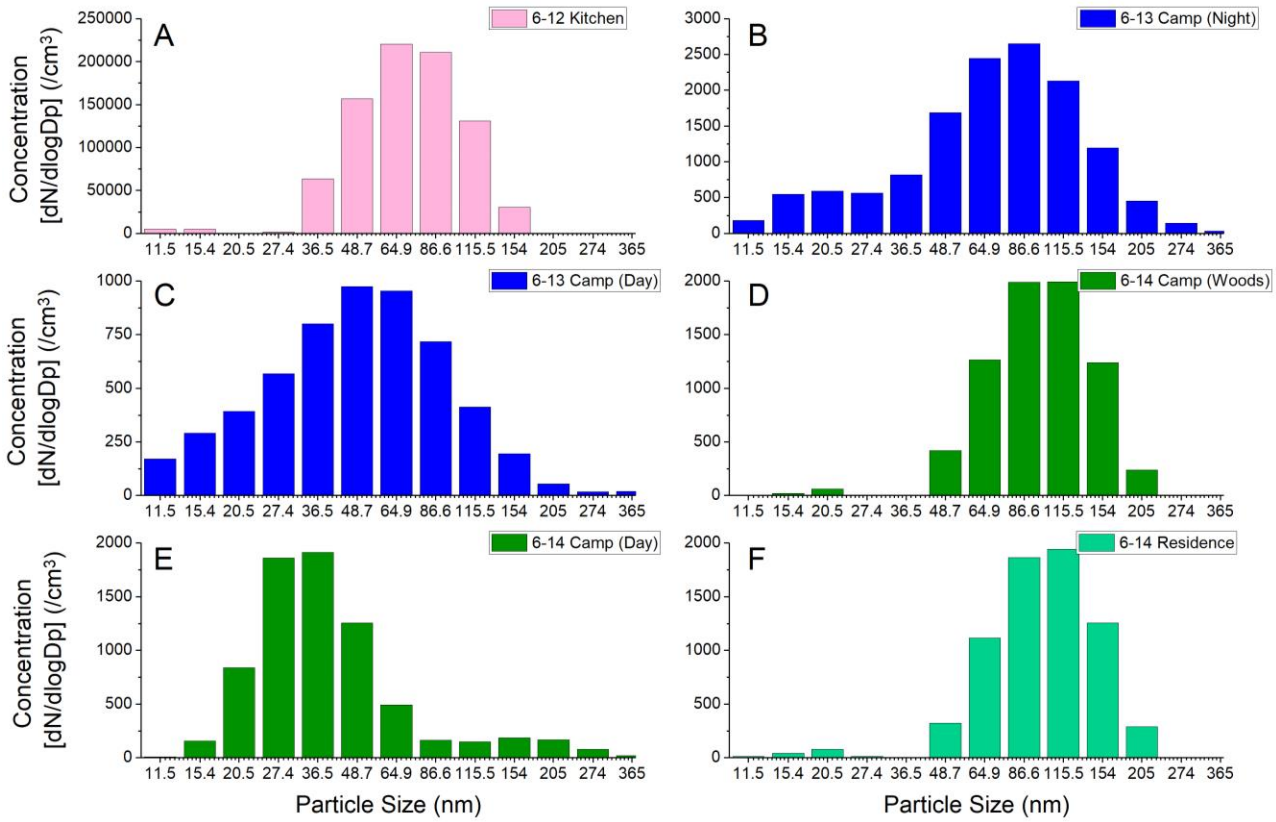

Figure 5.3. Aerosol particle size distributions inside/outside the Campsite (SMPS).

(A) June 12, 2016, time 8:30 to 9:00 inside the Kitchen, temperature 10 °C, 49°49'15"N, 76°32'58"W; (B) June 13, 2016, time 8:10 to 8:40 outside the Campsite, temperature 4 °C, relative humidity 77 %, wind NNW 14 km/hr, 49°49'15"N, 76°32'58"W; (C) June 13, 2016, time 20:30 to 21:00 outside the Campsite, temperature 11 °C, relative humidity 58 %, wind NNW 16 km/hr, 49°49'15"N, 76°32'58"W; (D) June 14, 2016, time 17:30 to 18:30 outside up the hill at the Camp,

temperature 21 °C, relative humidity 44 %, wind NNW 14 km/hr, 49°49'15"N, 76°32'58"W; (E) June 14, 2016, time 18:45 to 19:15 outside the Campsite, Temperature: 21 °C, relative humidity 44 %, wind NNW 14 km/hr, 49°49'15"N, 76°32'58"W; (F) June 14, 2016, time 19:30 to 20:30 inside the Camp Hallway (Residence), temperature 21 °C, relative humidity 44 %, wind NNW 14 km/hr, 49°49'15"N, 76°32'58"W. *[Originally published in Environmental Science and Pollution Research as Main Text Figure 5.]

We detected a comparatively high concentration of nanoparticles outside the Campsite on June 13, 2016 at night (Figure 5.3C). It is possible that this pollution resulted from the generator that was being used in the vicinity. We also found elevated indoor larger particle (> 0.3 μm) concentrations in the Camp Residence on June 14, 2016 (Figure 5.4E). They were about an order of magnitude higher than those measured outside the Campsite later that night (Figure 5.2J).

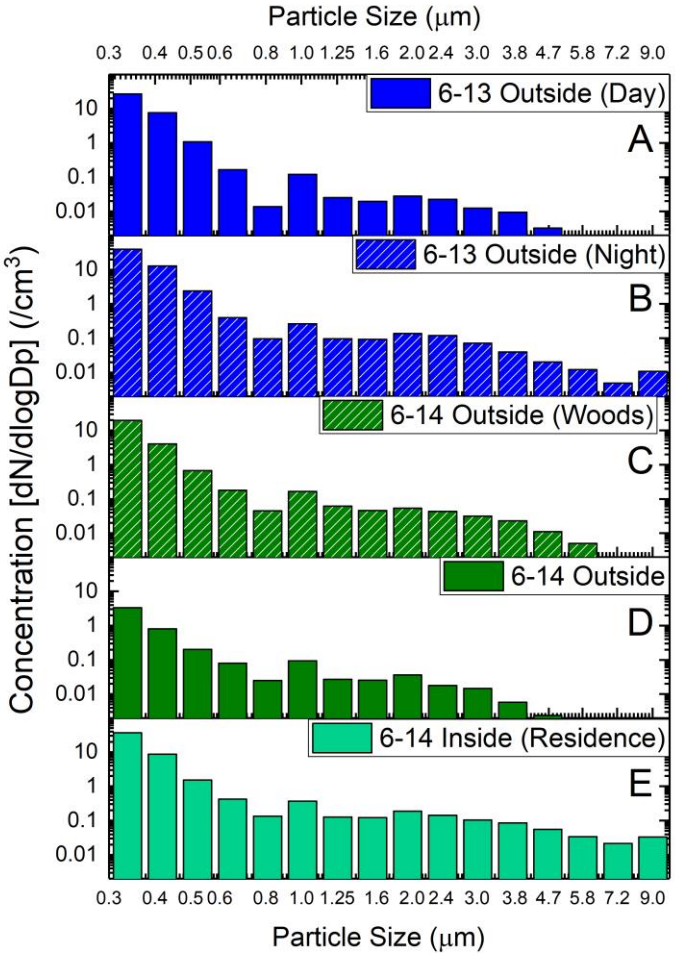

Figure 5.4. Aerosol particle size distribution inside/outside the Campsite (OPS).

(A) June 13, 2016, time 8:10 to 8:40 outside the Campsite, temperature 4 °C, relative humidity 77 %, wind NNW 14 km/hr, 49°49'15"N, 76°32'58"W; (B) June 13, 2016, time 20:30 to 21:00 outside the Campsite, temperature 11 °C, relative humidity 58 %, wind NNW 16 km/hr, 49°49'15"N, 76°32'58"W; (C) June 14, 2016, time 17:30 to 18:30 outside up the hill at the Camp, temperature 21 °C, relative humidity 44 %, wind NNW 14 km/hr, 49°49'15"N, 76°32'58"W; (D) June 14, 2016, time 18:45 to 19:15 outside the Campsite, temperature 21 °C, relative humidity 44 %, wind NNW 14 km/hr, 49°49'15"N, 76°32'58"W; (E) June 14, 2016, time 19:30 to 20:30 inside the Camp Hallway (Residence), temperature 21 °C, relative humidity 44 %,

wind NNW 14 km/hr, 49°49’15”N, 76°32’58”W. *[Originally published in Environmental Science and Pollution Research as Main Text Figure 6.]

As can be seen in Figure 5.5, inside the Daycare, the concentrations were much higher than outside on both June 13 and June 14, 2016. On June 13, 2016, dominant particle size was 115.5 nm both inside and outside. Very few particles smaller than 50 nm were measured inside, but outside, we observed a secondary mode at 27.4 nm. On June 14, 2016, the dominant particle size was different inside and outside. Inside, we measured a very high concentration of nanoparticles with a mode dimeter 27.4 nm. The mode diameter of the aerosol size distribution outside was 86.6 nm and virtually no particles smaller than 50 nm were detected. These results indicate that there must have been an intense source of nanoparticles indoors on June 14, 2016, which was not active on June 13, 2016 in the absence of sufficient ventilation and/or filtration of air. The emissions could have come from heating, combustion, cooking or operation of certain appliances.

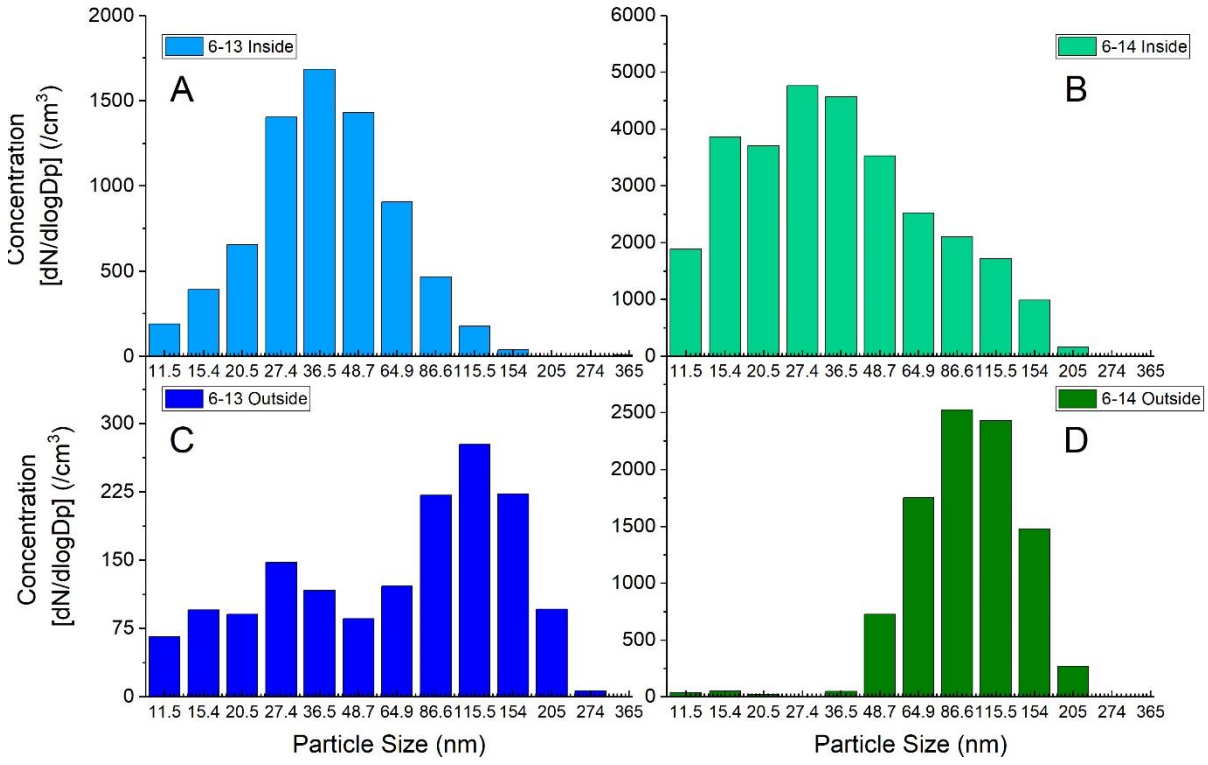

Figure 5.5. Aerosol particle size distributions inside and outside the Daycare (SMPS).

(A) June 13, 2016, time 14:20 to 14:50 inside the Daycare, temperature 10 °C, relative humidity 58 %, wind NNW 13 km/hr, 49°41’57”N, 75°57’27”W; (B) June 14, 2016, time 14:20 to 14:50 inside the Daycare, temperature 21 °C, 49°41’50”N, 75°57’46”W; (C) June 13, 2016, time 15:10 to 15:40 outside the Daycare, temperature 11 °C, relative humidity 56 %, 49°41’50”N, 75°57’46”W; D) June 14, 2016, time 15:00 to 15:30 outside the Daycare, temperature 21 °C, relative humidity 42 %, wind NNW 16 km/hr, 49°41’50”N, 75°57’46”W *[Originally published in Environmental Science and Pollution Research as Supplementary Figure 1]

As can be seen in Figure 5.6, for the Daycare, on both days, the concentrations of larger particles (0.3 μm) were relatively similar, and the shapes of the size distributions were similar too. However, inside, there were fewer smaller particles (< 0.5 μm). It is evidence that the larger indoor particles are mostly due to infiltration of outdoor air.

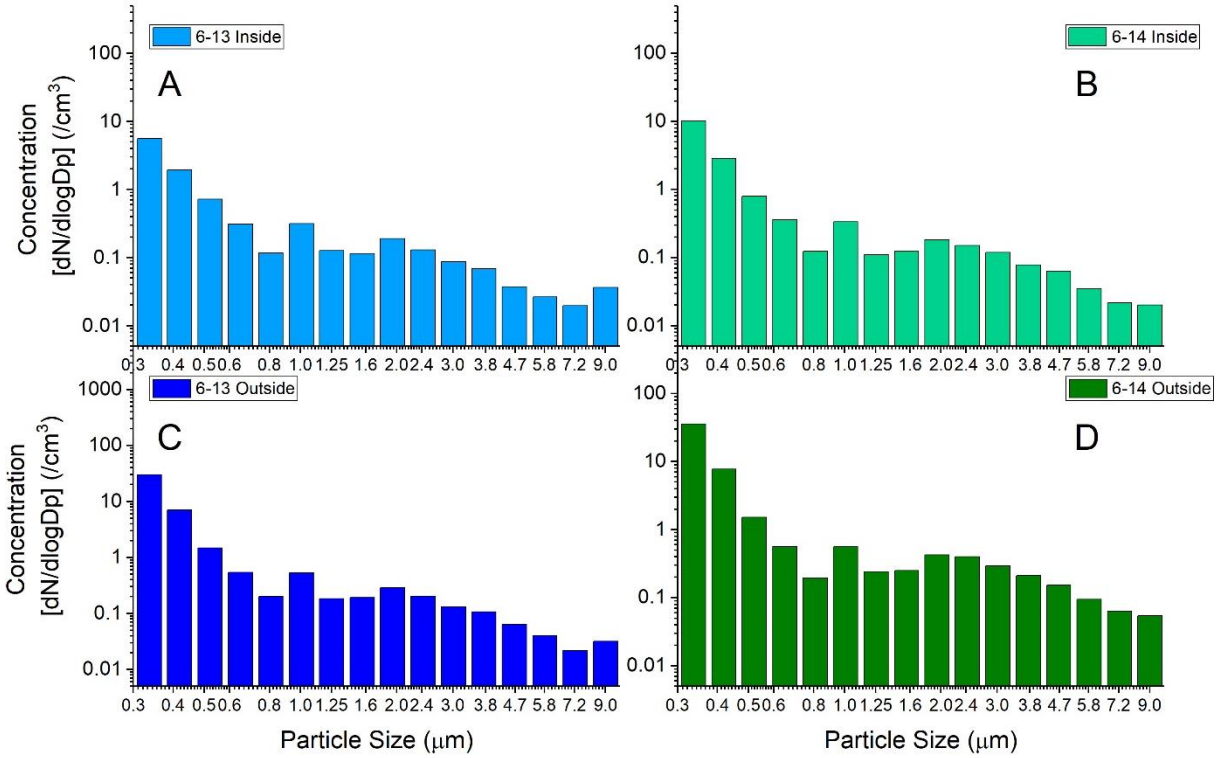

Figure 5.6. Aerosol particle size distributions inside and outside the daycare (OPS).

(A) June 13, 2016, time 14:20 to 14:50 inside the Daycare, temperature 22 °C, 49°41'57"N, 75°57'27"W; (B) June 14, 2016, time 14:20 to 14:50 inside the Daycare, temperature 21 °C, 49°41'50"N, 75°57'46"W; (C) June 13, 2016, Time 15:10 to 15:40 outside the Daycare, temperature 11 °C, relative humidity 56 %, 49°41'50"N, 75°57'46"W; D) June 14, 2016, time 15:00 to 15:30 outside the Daycare, temperature 21 °C, relative humidity 42 %, wind NNW 16 km/hr, 49°41'50"N, 75°57'46"W. *[Originally published in Environment Science and Pollution Research as Supplementary Figure 2.]

The nanoparticle aerosol size distributions inside the Arena (Figure 5.7) on the three measurement days (June 12 – June 14, 2016) were quite different despite the similar meteorological conditions. We observed a broad bimodal size distribution with modes at 27.4 and 115.5 nm on June 12, a unimodal (36.5 nm) size distribution on June 13 and a unimodal (64.9 nm) size distribution on June 14, 2016. The concentrations of the most abundant particle sizes were somewhat higher on June 14 than on June 13 and on June 12, 2016. The aerosol particle size distributions inside the Arena on the three measurement days were also very similar. The difference in abundance of particles was again for the sizes

smaller than 0.5 µm. These particles were several times more abundant on June 13 compared to June 12 and 14, 2016.

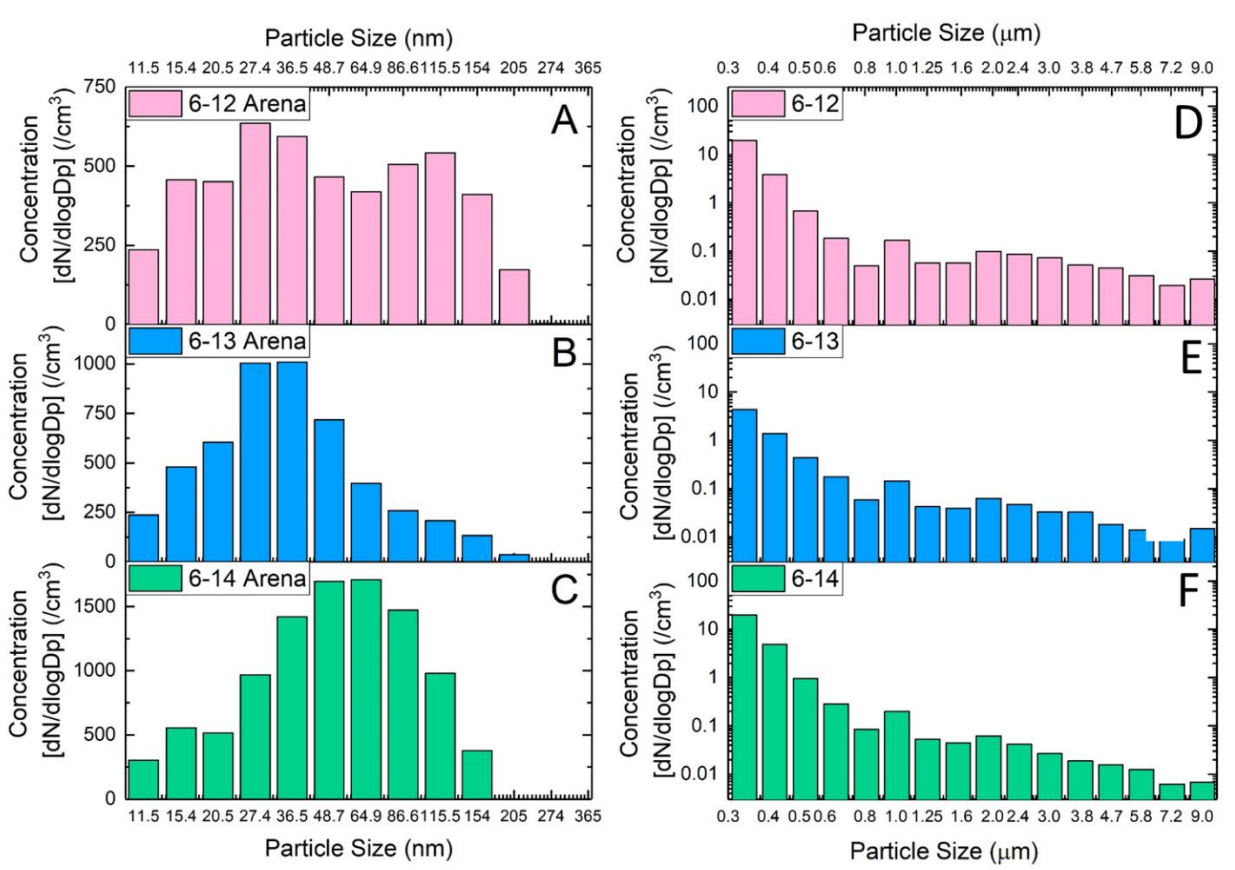

Figure 5.7. Aerosol particle size distributions inside the Arena (SMPS, OPS).

(A,D) June 12, 2016, time 15:30 to 16:00 inside the Arena, temperature 23 °C, 49°41'57"N, 75°57'27"W; (B,E) June 13, 2016, time 13:20 to 13:50 inside the Arena, temperature 23 °C, 49°41'57"N, 75°57'27"W; (C,F) June 14, 2016, time 12:30 to 13:00 inside the Arena, temperature 23 °C, relative humidity 56 %, 49°41'57"N, 75°57'27"W *[Originally published in Environment Science and Pollution Research as Supplementary Figures S3 and S4.]

The nanoparticle size distributions outside the City Council (Figure 5.8) were similar in shape on June 12 and June 14, with the mode diameter at 86.6 nm, however, the concertation of particles was 4 times higher on June 14 than on June 12. On June 13, 2016, we observed a relatively very low concertation of particles, broadly distributed across the size spectrum, with two modes at 15.4 and 115.5 nm. For the larger particles measured outside the City Council (Figure 5.8) in parallel with the nanoparticles, the concentration of the smaller particles (< 0.5 µm) was several times higher on June 12 than on June 13 and 14, 2016. The abundance of the larger particles (> 0.5 µm) was relatively similar. The difference in abundance of the smaller < 0.5 µm particles and similarity in abundance of the larger

particles (> 0.5 μm) is a similar trend as observed at other locations. These results indicate a large variability of the concentrations of nanoparticles at the background of the lower variability of the concentrations of larger particles. This means that the current monitoring strategies, which are mass-based and limited by $PM_{2.5}$ being the smallest monitored particles, are expected to miss high nanoparticle concentrations. This has implications for our ability to identify nanoparticulate air pollution and remediate it.

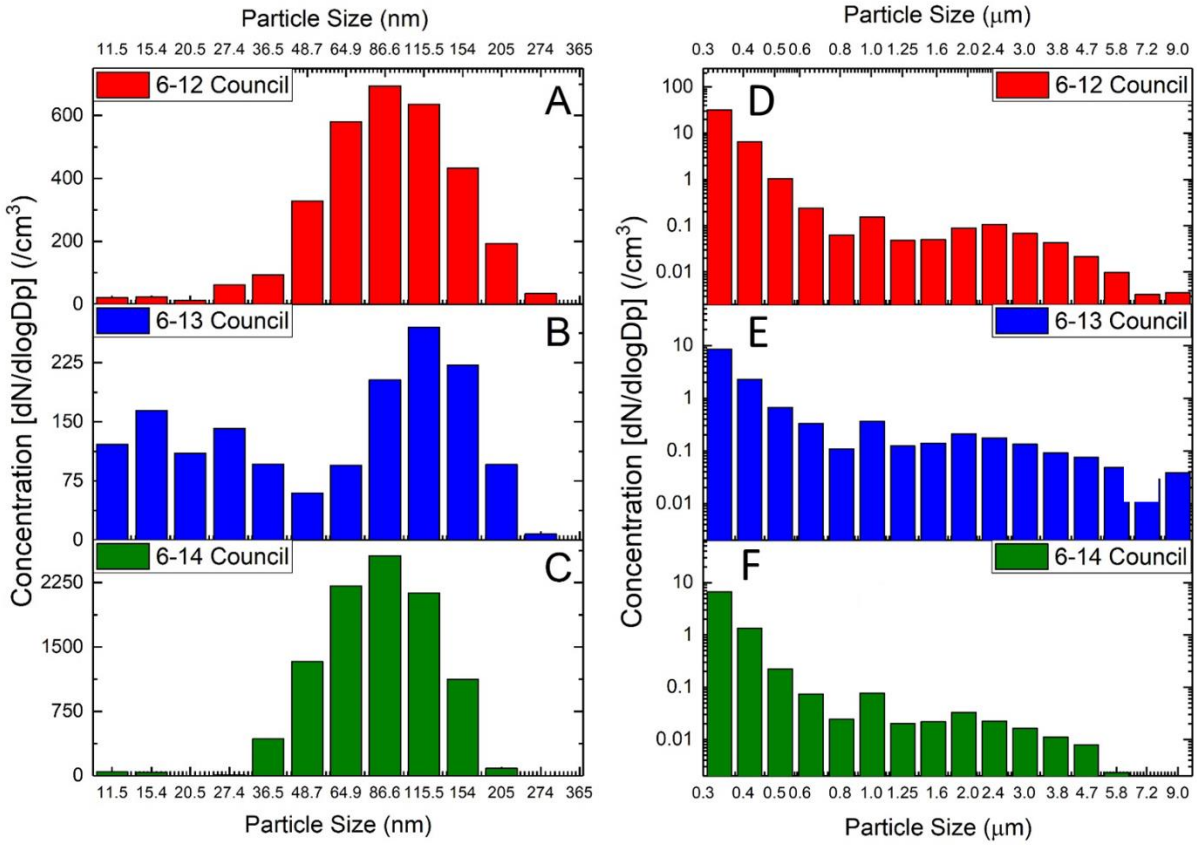

Figure 5.8. Aerosol particle size distributions outside the City Council (OPS).

(A,D) June 12, 2016, time 14:30 to 15:00 outside the Council, temperature 9 °C, relative humidity 84 %, wind NNW 18 km/hr, 49°42'9"N, 75°57'32"W; (B,E) June 13, 2016, time 16:00 to 16:30 outside the Council, temperature 11 °C, relative humidity 55 %, wind NNW 16 km/hr, 49°42'9"N, 75°57'32W; (C,F) June 14, 2016, time 13:20 to 13:50 outside the Council, temperature 19 °C, relative humidity 55 %, wind NNW 13 km/hr, 49°42'9"N, 75°57'32"W. *[Originally published in Environmental Science and Pollution Research as Supplementary Figure S5 and S6.]

In the aerosol samples collected by the MOUDI, the most abundant particle sizes by mass were between 0.55 and 0.19 μm cut-off point diameter. The chemical analysis of the airborne particles by ICP-MS showed that the maximum concentrations of the analyzed heavy metals occur at the d_{50} cut-off point aerosol particle diameter of 0.31 μm. Compared with the responses for the blank solution and filter blank, the most abundant heavy metals

in the aerosol samples were Al, Ba, Zn, Cu, Hg and Pb (Table S1 in the Supporting Information). Also, some ultra-trace rare earth metals like Neodymium (Nd), Samarium (Sm) and Europium (Eu) were detected in the samples collected by the MOUDI. The results of the quantification of these heavy metals in the aerosol particle fraction smaller than d_{50} = 0.31 μm based on the sampling flow rate of 30 L/min and the duration of sampling of 24 hrs are presented in Table 5.4.

Table 5.4. Concentrations of the heavy metals measured by ICP-MS in the aerosol particles smaller than d_{50} 0.31 μm in the sampled air

Element Identified	Aluminum (Al)	Barium (Ba)	Zinc (Zn)	Copper (Cu)	Mercury (Hg)	Lead (Pb)
Concentration, $\mu g/m^3$	0.63	8.8×10^{-2}	2.3×10^{-2}	5.9×10^{-2}	4.5×10^{-2} ng/m^3	3.2×10^{-3}

*[Originally published in Environmental Science and Pollution Research as Main Text Table 4.]

It is only possible to effectively target responses to the challenge of health-damaging poor air quality when we measure all of the harmful constituents, including nanoparticles, and know and can predict the sources of air pollutants and modifying factors. This targeting of responses to tackle the causes of poor air quality also requires adequate understanding of the air pollutants' chemical and physical interactions in the atmosphere. These interactions involve formation and dynamics of aerosols and their further interactions with clouds, aerosols being a major player in climate change, extreme weather and air pollution [290].

There are a large number of important chemical and physical transformations involving atmospheric entities in the Arctic regions. These include the reactions with halogens [291], transformation of organic compounds [292], processes involving trace metals such as mercury [192,293] and complex chemical reactions with O_3 [294], gas phase OH• [293], as well as further heterogeneous reactions in/on snow and ice [295,296] and microbiological transformations [297,298]. Several of these processes are sensitive to temperature, and they are catalyzed or influenced on snow/ice surfaces [299-301]. The measurements of ambient nanoparticles in the Arctic are just emerging [302]. It is expected that the chemical composition, number density and size distribution of aerosols, including nanoparticles will be altered as a function of climate change, atmospheric oxidation

potential, low ambient temperature, light and availability of effective surfaces, particularly those of snow and ice.

The data presented here represent a current snapshot of the outdoor and indoor particulate air pollution profiles in the environment where the Cree First Nation community of Waswanipi live in Québec, Canada near the proposed mining location. We advise that more mining companies engage in similar pre-emptive work with Indigenous communities to ensure a collaborative approach to air quality management over the long term. Such efforts involving all stakeholders have a potential to result in implementation of specific preventive and remediation practices to achieve lower impact of mining operations on the quality of air near the Indigenous communities.

We recommend consideration of the following specific efforts as essential to the sustainability and responsibility of the future development of mining near Indigenous communities. First, the stakeholders must arrange for the systematic field study of airborne pollutants during the development of mining facilities and after the exploration stage. Second, focused laboratory studies to evaluate the fate of secondary products of aerosols formed upon transport from the mining sources should be set up. And third, remediation techniques must be developed and implemented to decrease direct emission from mining activities, which will minimize health risks, and reduce the environmental footprint, required to achieve the future "green" mining standards.

5.4. Conclusions

This short-term monitoring study was undertaken prior to a major mining exploration. This is the first outdoor and indoor air quality monitoring study, in which airborne nanoparticles have been measured. The results showed that the measured airborne nanoparticle concentrations can be substantially higher compared to other measurements even if microscale particle concentrations change to a lesser extent. Monitoring of nanoparticle concentrations is therefore essential to detect the health threat they pose and remediate the problem where it exists.

The microscale outdoor particulate air pollution at Waswanipi was generally well below the existing ambient air quality standards. However, high levels of indoor air particulate pollutants were observed inside some homes and venues. Notably, the levels of

nano-sized particles in some indoor locations were particularly elevated compared to other measurements in this campaign, and exposure to nano-sized particles is known to increase the risk of certain diseases and adverse health effects. This study revealed specific deficiencies in indoor air quality management that we conclude are the cause of the comparatively high indoor particulate matter concentrations. These deficiencies were found to result from insufficient ventilation and specific practices such as laundering and cooking in spaces lacking proper ventilation and air filtration systems. The technology to remediate this indoor air pollution is relatively easy to install and sufficiently common in homes throughout Canada. The relatively moderate costs of these systems can be expected to be offset by the improved health and, over the long term, lower incidences of diseases known to result from air pollution, notably cardiovascular, respiratory disease and cancer. We recommend: 1) switching to less polluting heating sources, 2) installation and upgrades of the indoor air ventilation systems, and 3) additional air filtration and purification using household air purifiers equipped with HEPA-filters, especially during the cold-season to reduce exposure to particulate matter.

We recommend creation of a government funding program aimed at improving indoor air quality in First Nations communities. This program should fund and facilitate installation of proper ventilation systems, ideally equipped with heat recovery ventilators, and possibly HEPA filtration systems in homes and communal venues, and subsidies for standalone HEPA filtration units. These also have potential to dramatically reduce indoor exposure to infiltrated particulate air pollution from sources such as mining. We expect the health benefits from such a program to outweigh the expenses due to the resulting lower burden of disease of First Nations community members.

Further air pollution studies on mining and Indigenous sites over a medium and long term are recommended to capture the expected temporal and spatial variation of pollutant concentrations. Both indoor and outdoor monitoring of pollutants must be carried out in parallel.

5.5. Acknowledgments

We are thankful to the Waswanipi community members and leaders who graciously opened their homes, schools and communal venues to us. We are also grateful to GéoMégA for

providing logistical assistance and accommodations to our team during the field campaign. The study is jointly funded by Natural Science and Engineering Research Council of Canada (NSERC), the NSERC Engage Program, the NSERC CREATE *Mine of Knowledge* and by Fonds de recherche du Québec - Nature et technologies. McGill University is situated on land which has long served as a site of meeting and exchange amongst Indigenous peoples, including the Haudenosaunee and Anishinabeg nations. We honour and respect the diverse Indigenous peoples connected to this territory. The views expressed in the manuscript are solely of the authors and do not necessarily reflect those of the funding agencies.

Chapter 6. Concluding Remarks

6.1. Summary

In this work, the chemical speciation of gaseous oxidized mercury was explored through the development of a soft ionization mass spectrometry technique for the detection of mercury(II) bromide and mercury(II) chloride, and the phase distribution of what is currently known as gaseous oxidized mercury was assessed. The original contribution of this work is the first quantitative detection of mercury(II) chloride and mercury(II) bromide, the development of reproducible mercury(II) halide nanoparticulate sources and characterization of those particles, the determination of particulates containing mercury(II) halides in urban air and the measurement of nanoparticles in indoor and outdoor air in a remote Indigenous community.

6.2. Main Findings and Contribution to Knowledge

[1] Atmospheric mercury has long since been measured in terms of operational bulk species: gaseous elemental mercury, gaseous oxidized mercury and particulate-bound mercury. Our research shows the potential for using mass spectrometric methods for determining the actual chemical speciation of gaseous oxidized mercury. Using nano- and micro-particle sorbent traps, we are able to selectively trap gaseous oxidized mercury species and thermally desorb these species intact to be quantified via mass spectrometry. Detection limits in the low pg/m^3 are achieved through preconcentration and soft chemical ionization using sulfur hexafluoride, and the first detection of mercury(II) chloride and mercury(II) bromide was made in urban and indoor air in Montreal.

[2] Aside from the permeation of gaseous elemental mercury which is well characterized, there are no standard sources for gaseous oxidized mercury or particulate bound mercury sources. In this work, we provide two methods of producing reproducible sources of oxidized mercury nanoparticles in particulate mercury(II) chloride and mercury(II) bromide. These nanoparticles were characterized through a variety of techniques including scanning mobility particle sizing, optical particle sizing, nanotracking analysis, high resolution scanning transmission electron microscopy and mercury mass spectrometry. Using these particulate-bound nanoparticles, we were able to assess the

degree of capture through KCl denuder, the conventional technique for measuring gaseous oxidized mercury; a significant amount of nanoparticles are captured by the denuder contaminating GOM results. We assessed the degree of penetration of mercury nanoparticles through membrane and syringe filters as well as micro- and nano-particulate traps used in mercury mass spectrometry.

[3] Using the results of capture efficiencies by filters and sorbent traps, we assessed the existence of nanoparticulate mercury(II) halides in urban air in Montreal versus gaseous mercury(II) halides in urban air in Montreal. In the winter time, we concluded that as much as 50% of mercury(II) halides are present as particulates. This has significant implications on the biogeochemistry of mercury, its fate, transformations and eventual risk to human and ecological health. We also provided evidence of mercury nanoparticles through the first image of a mercury nanoparticle trapped from ambient air.

[4] Working with the Cree nation of Waswanipi, we use scanning mobility particle sizing techniques and optical sizing techniques and metal particulate techniques to measure nanoparticles and micron-sized particles in indoor and outdoor to serve as a baseline prior to the beginning of mining operations 50 km from the community. The scope of the work was largely defined by the community and to our knowledge these are among the first measurements of nanoparticles in an Indigenous community in Canada.

6.3. Future Work

[1] ***Development of new sorbent traps for the efficient capture and desorption of gaseous oxidized mercury species*** – The challenge with direct measurements of gaseous oxidized mercury species is the ultra-trace concentrations at which these contaminants are present in the atmosphere. While we have shown success with PFA Teflon and polysulfide sorbent traps, more work must be done to identify sorbent materials that quantitatively and selectively capture GOM species without changing their speciation and allow for the complete desorption for eventual analysis. Sulfide-coated metal cores offer potential in providing greater surface area sites for adsorption and preferential binding to mercury.

[2] ***Extending the technique to gaseous mercuric oxide, nitrogen-based and sulfur-based gaseous mercury compounds*** – As shown by Professor Gustin's group, there are a number of possible gaseous oxidized mercury compounds that have been detected via

cation exchange membranes and thermal desorption curves. [65] The soft ionization APCI-MS technique that we have developed should be explored with other GOM proxies especially those which have already been detected. The uptake of mercury(II) oxide on micro- and nano-particle sorbent traps has already been assessed by our group; an optimization of the parameters for the APCI-MS mercury mass spectrometry method with the mercury(II) oxide trapped could yield promising results.

[3] ***Long term studies of mercury(II) halides using mercury mass spectrometry and cation exchange membrane techniques*** – The difficulty with APCI-MS mercury mass spectrometry is the amount of trap cleaning time required to reduce blanks to baseline levels. However, with a cycling of traps and personnel, a longer-term study of mercury(II) halides in urban air will yield important information about the sources, transformations, and seasonal variation of species. This in conjunction with GEM, GOM and PBM data via double-gold amalgamation, KCl denuder and quartz filter data will provide convincing evidence and support for the technique. Determining the mercury concentrations trapped on filters preceding the mercury(II) halide PFA-sorbent traps will also provide more conclusive evidence for the contribution of mercury(II) halides on particulates.

[4] ***Understanding the impact of dissolved organic matter on particulate mercury nanoparticles in aqueous environments –*** Using Nanotracking analysis, not only can we study the oxidized mercury nanoparticles that we can generate from aqueous nebulization or vapour-phase condensation, by adding organic matter to suspended nanoparticles in the aqueous phase, we can elucidate the impact that humic acids and other dissolved organics can have on the size and distributions of nanoparticle populations. Changing other characteristics of the aqueous medium in which nanoparticles are suspended, such as the pH, salinity, chlorinity, and others, allow us to examine the fate of mercury nanoparticles directly, phase transformations and ultimately, the bioavailability of these compounds to microorganisms.

References

1. Li YX, Wang Y, Li Y, Li T, Mao HT, Talbot R, Nie XL, Wu C, Zhao YF, Hou CX, Wang GR, Zhou J, Qie GH (2017) xCharacteristics and potential sources of atmospheric particulate mercury in Jinan, China. Sci Total Environ 574, 1424-1431. doi:10.1016/j.scitotenv.2016.08.069

2. Pyta H, Rogula-Kozlowska W (2016) Determination of mercury in size-segregated ambient particulate matter using CVAAS. Microchem J 124, 76-81. doi:10.1016/j.microc.2015.08.001

3. Guo JM, Kang SC, Huang J, Zhang QG, Rupakheti M, Sun SW, Tripathee L, Rupakheti D, Panday AK, Sillanpaa M, Paudyal R (2017) Characterizations of atmospheric particulate-bound mercury in the Kathmandu Valley of Nepal, South Asia. Sci Total Environ 579, 1240-1248. doi:10.1016/j.scitotenv.2016.11.110

4. Wangberg I, Mastromonaco MGN, Munthe J, Gardfeldt K (2016) Airborne mercury species at the Rao background monitoring site in Sweden: distribution of mercury as an effect of long-range transport. Atmos Chem Phys 16, (21), 13379-13387. doi:10.5194/acp-16-13379-2016

5. Hylander LD, Meili M (2003) 500 years of mercury production: global annual inventory by region until 2000 and associated emissions. Sci Total Environ 304, (1), 13-27. doi:https://doi.org/10.1016/S0048-9697(02)00553-3

6. Tejero J, Higueras PL, Garrido I, Esbri JM, Oyarzun R, Espanol S (2015) An estimation of mercury concentrations in the local atmosphere of Almaden (Ciudad Real Province, South Central Spain) during the twentieth century. Environmental Science and Pollution Research 22, (7), 4833-4841. doi:10.1007/s11356-014-2860-5

7. Huber ML, Laesecke A, Friend DG (2006) Correlation for the Vapor Pressure of Mercury. Ind Eng Chem Res 45, (21), 7351-7361. doi:10.1021/ie060560s

8. Johansson K, Bergbäck B, Tyler G (2001) Impact of Atmospheric Long Range Transport of Lead, Mercury and Cadmium on the Swedish Forest Environment. Water, Air and Soil Pollution: Focus 1, (3), 279-297. doi:10.1023/a:1017528826641

9. Kumari A, Kulshrestha U (2018) Trace ambient levels of particulate mercury and its sources at a rural site near Delhi. J Atmos Chem. doi:10.1007/s10874-018-9377-0

10. Lyman SN, Jaffe DA, Gustin MS (2010) Release of mercury halides from KCl denuders in the presence of ozone. Atmos Chem Phys 10, (17), 8197-8204. doi:10.5194/acp-10-8197-2010

11. Lindberg S, Bullock R, Ebinghaus R, Engstrom D, Feng X, Fitzgerald W, Pirrone N, Prestbo E, Seigneur C (2007) A Synthesis of Progress and Uncertainties in Attributing the Sources of Mercury in Deposition. AMBIO: A Journal of the Human Environment 36, (1), 19-33. doi:10.1579/0044-7447(2007)36[19:ASOPAU]2.0.CO;2

12. Fitzgerald WF, Engstrom DR, Mason RP, Nater EA (1998) The case for atmospheric mercury contamination in remote areas. Environ Sci Technol 32, (1), 1-7. doi:DOI 10.1021/es970284w

13. Jones CP, Lyman SN, Jaffe DA, Allen T, O'Neil TL (2016) Detection and quantification of gas-phase oxidized mercury compounds by GC/MS. Atmos Meas Tech 9, (5), 2195-2205. doi:10.5194/amt-9-2195-2016

14. Sheu G-R, Mason RP (2001) An Examination of Methods for the Measurements of Reactive Gaseous Mercury in the Atmosphere. Environ Sci Technol 35, (6), 1209-1216. doi:10.1021/es001183s

15. Schroeder WH, Munthe J (1998) Atmospheric mercury - An overview. Atmospheric Environment 32, (5), 809-822. doi:Doi 10.1016/S1352-2310(97)00293-8

16. Schroeder WH, Jackson RA (1985) An Instrumental Analytical Technique for Speciation of Atmospheric Mercury. Int J Environ an Ch 22, (1-2), 1-18. doi:Doi 10.1080/03067318508076405

17. Song XJ, Cheng I, Lu J (2009) Annual atmospheric mercury species in Downtown Toronto, Canada. J Environ Monitor 11, (3), 660-669. doi:10.1039/b815435j

18. Driscoll CT, Han Y-J, Chen CY, Evers DC, Lambert KF, Holsen TM, Kamman NC, Munson RK (2007) Mercury Contamination in Forest and Freshwater Ecosystems in the Northeastern United States. BioScience 57, (1), 17-28. doi:10.1641/B570106

19. Choi H-D, Holsen TM, Hopke PK (2008) Atmospheric Mercury (Hg) in the Adirondacks: Concentrations and Sources. Environ Sci Technol 42, (15), 5644-5653. doi:10.1021/es7028137

20. Hernández A, Jébrak M, Higueras P, Oyarzun R, Morata D, Munhá J (1999) The Almadén mercury mining district, Spain. Mineralium Deposita 34, (5), 539-548. doi:10.1007/s001260050219

21. Wängberg I, Munthe J, Amouroux D, Andersson ME, Fajon V, Ferrara R, Gårdfeldt K, Horvat M, Mamane Y, Melamed E, Monperrus M, Ogrinc N, Yossef O, Pirrone N, Sommar J, Sprovieri F (2008) Atmospheric mercury at mediterranean coastal stations. Environ Fluid Mech 8, (2), 101-116. doi:10.1007/s10652-007-9047-2

22. Sznopek JL, Goonan TG (2000) The materials flow of mercury in the economies of the United States and the world. US Department of the Interior, US Geological Survey,

23. Chan TYK (2011) Inorganic mercury poisoning associated with skin-lightening cosmetic products. Clinical Toxicology 49, (10), 886-891. doi:10.3109/15563650.2011.626425

24. Blumenthal I (1992) Should we ban the mercury thermometer? Discussion paper. Journal of the Royal Society of Medicine 85, (9), 553-555

25. Dumarey R, Dams R (1985) Selective gathering of mercury-batteries: A possible way to lower mercury emissions from a municipal waste incineration plant. Environ Technol Lett 6, (1-11), 149-152. doi:10.1080/09593338509384331

26. Jen YH, Chen WH, Yuan CS, Ie IR, Hung CH (2014) Seasonal variation and spatial distribution of atmospheric mercury and its gas-particulate partition in the vicinity of a semiconductor manufacturing complex. Environmental Science and Pollution Research 21, (8), 5474-5483. doi:10.1007/s11356-013-2441-z

27. Ram RN, Sathyanesan A (1987) Histopathological and biochemical changes in the liver of a teleost fish, Channa punctatus (Bloch) induced by a mercurial fungicide. Environ Pollut 47, (2), 135-145

28. Lalit BY, Ramachandran TV (1977) Concentration of mercury in wheat samples stored with mercury tablets as preservative. Journal of Radioanalytical Chemistry 36, (2), 369-374. doi:10.1007/BF02517005

29. Rumble JR, Lide DR, Bruno TJ (2018) CRC handbook of chemistry and physics : a ready-reference book of chemical and physical data

30. Council NR (2000) CHEMISTRY, EXPOSURE, TOXICOKINETICS, AND TOXICODYNAMICS. In: Toxicological Effects of Methylmercury. National Academies Press (US),

31. Goggin P, Woodward L (1966) Vibrational spectra of methyl mercuric chloride, bromide, iodide and cyanide. Transactions of the Faraday Society 62, 1423-1430

32. Perry DL (2016) Handbook of inorganic compounds. CRC press,

33. Long L, Cattanach J (1961) Antoine vapour-pressure equations and heats of vaporization for the dimethyls of zinc, cadmium and mercury. J Inorg Nucl Chem 20, (3-4), 340-342

34. Clever HL, Johnson SA, Derrick ME (1985) The Solubility of Mercury and Some Sparingly Soluble Mercury Salts in Water and Aqueous Electrolyte Solutions. J Phys Chem Ref Data 14, (3), 631-680. doi:10.1063/1.555732

35. Tong X, Barat RB, Poulos AT (1999) Detection of Mercuric Bromide in a Gas Phase Flow Cell by Laser Photofragment Fluorescence Spectroscopy. Environ Sci Technol 33, (18), 3260-3263. doi:10.1021/es9813461

36. Lee EPF, Wright TG (2003) Thermochemistry of HgCH3 and HgCH3+ and the ionization energy of HgCH3. Chem Phys Lett 376, (3), 418-423. doi:https://doi.org/10.1016/S0009-2614(03)01022-4

37. Kochi J (2012) Organometallic mechanisms and catalysis: the role of reactive intermediates in organic processes. Elsevier,

38. Carson PA (2002) Hazardous chemicals handbook. Elsevier,

39. Zverina O, Coufalik P, Komarek J, Gadas P, Sysalova J (2014) Mercury associated with size-fractionated urban particulate matter: three years of sampling in Prague, Czech Republic. Chem Pap 68, (2), 197-202. doi:10.2478/s11696-013-0436-3

40. Rutter AP, Snyder DC, Stone EA, Schauer JJ, Gonzalez-Abraham R, Molina LT, Márquez C, Cárdenas B, de Foy B (2009) In situ measurements of speciated atmospheric mercury and the identification of source regions in the Mexico City Metropolitan Area. Atmos Chem Phys 9, (1), 207-220. doi:10.5194/acp-9-207-2009

41. Liu B, Keeler GJ, Timothy Dvonch J, Barres JA, Lynam MM, Marsik FJ, Morgan JT (2010) Urban–rural differences in atmospheric mercury speciation. Atmospheric Environment 44, (16), 2013-2023. doi:https://doi.org/10.1016/j.atmosenv.2010.02.012

42. Johnson DL, Braman RS (1974) Distribution of atmospheric mercury species near ground. Environ Sci Technol 8, (12), 1003-1009

43. Duan L, Wang XH, Wang DF, Duan YS, Cheng N, Xiu GL (2017) Atmospheric mercury speciation in Shanghai, China. Sci Total Environ 578, 460-468. doi:10.1016/j.scitotenv.2016.10.209

44. Pirrone N, Cinnirella S, Feng X, Finkelman RB, Friedli HR, Leaner J, Mason R, Mukherjee AB, Stracher GB, Streets DG (2010) Global mercury emissions to the atmosphere from anthropogenic and natural sources. Atmos Chem Phys 10, (13), 5951-5964

45. Zhang L, Wang S, Wang L, Wu Y, Duan L, Wu Q, Wang F, Yang M, Yang H, Hao J, Liu X (2015) Updated emission inventories for speciated atmospheric mercury from anthropogenic sources in China. Environ Sci Technol 49, (5), 3185-3194. doi:10.1021/es504840m

46. Pacyna EG, Pacyna JM, Sundseth K, Munthe J, Kindbom K, Wilson S, Steenhuisen F, Maxson P (2010) Global emission of mercury to the atmosphere from anthropogenic sources in 2005 and projections to 2020. Atmospheric Environment 44, (20), 2487-2499. doi:10.1016/j.atmosenv.2009.06.009

47. Mason RP, Lawson NM, Sheu GR (2001) Mercury in the Atlantic Ocean: factors controlling air-sea exchange of mercury and its distribution in the upper waters. Deep-Sea Res Pt Ii 48, (13), 2829-2853. doi:Doi 10.1016/S0967-0645(01)00020-0

48. Finley BD, Swartzendruber PC, Jaffe DA (2009) Particulate mercury emissions in regional wildfire plumes observed at the Mount Bachelor Observatory. Atmospheric Environment 43, (38), 6074-6083. doi:10.1016/j.atmosenv.2009.08.046

49. Siudek P, Frankowski M, Siepak J (2016) Atmospheric particulate mercury at the urban and forest sites in central Poland. Environmental Science and Pollution Research 23, (3), 2341-2352. doi:10.1007/s11356-015-5476-5

50. Pacyna JM, Pacyna EG, Steenhuisen F, Wilson S (2003) Mapping 1995 global anthropogenic emissions of mercury. Atmospheric Environment 37, S109-S117. doi:10.1016/S1352-2310(03)00239-4

51. Fostier AH, Michelazzo PAM (2006) Gaseous and particulate atmospheric mercury concentrations in the Campinas Metropolitan Region (Sao Paulo State, Brazil). J Brazil Chem Soc 17, (5), 886-894. doi:Doi 10.1590/S0103-50532006000500011

52. Soerensen AL, Skov H, Jacob DJ, Soerensen BT, Johnson MS (2010) Global Concentrations of Gaseous Elemental Mercury and Reactive Gaseous Mercury in the Marine Boundary Layer. Environ Sci Technol 44, (19), 7425-7430. doi:10.1021/es903839n

53. Cheng I, Zhang LM, Mao HT (2015) Relative contributions of gaseous oxidized mercury and fine and coarse particle-bound mercury to mercury wet deposition at nine monitoring sites in North America. J Geophys Res-Atmos 120, (16), 8549-8562. doi:10.1002/2015jd023769

54. Freitas MC, Farinha MM, Ventura MG, Almeida SM, Reis MA, Pacheco AMG (2005) Gravimetric and Chemical Features of Airborne PM10 AND PM2.5 in Mainland Portugal. Environ Monit Assess 109, (1), 81-95. doi:10.1007/s10661-005-5841-9

55. Schleicher NJ, Schafer J, Blanc G, Chen Y, Chai F, Cen K, Norra S (2015) Atmospheric particulate mercury in the megacity Beijing: Spatiotemporal variations and source apportionment. Atmospheric Environment 109, 251-261. doi:10.1016/j.atmosenv.2015.03.018

56. Assessment UGM (2013) Sources, emissions, releases and environmental transport. UNEP Chemicals Branch, Geneva, Switzerland 42,

57. Wang Q, Shen WG, Ma ZW (2000) Estimation of mercury emission from coal combustion in China. Environ Sci Technol 34, (13), 2711-2713. doi:DOI 10.1021/es990774j

58. Wang Z, Zhang X, Chen Z, Zhang Y (2006) Mercury concentrations in size-fractionated airborne particles at urban and suburban sites in Beijing, China. Atmospheric Environment 40, (12), 2194-2201. doi:https://doi.org/10.1016/j.atmosenv.2005.12.003

59. Neville G (1967) Toxicity of mercury vapour. Can Chem Educa 3, (1), 4-7

60. Ren XR, Luke WT, Kelley P, Cohen M, Ngan F, Artz R, Walker J, Brooks S, Moore C, Swartzendruber P, Bauer D, Remeika J, Hynes A, Dibb J, Rolison J, Krishnamurthy N, Landing WM, Hecobian A, Shook J, Huey LG (2014) Mercury Speciation at a Coastal Site in the Northern Gulf of Mexico: Results from the Grand Bay Intensive Studies in Summer 2010 and Spring 2011. Atmosphere-Basel 5, (2), 230-251. doi:10.3390/atmos5020230

61. Fu XW, Feng XB, Qiu GL, Shang LH, Zhang H (2011) Speciated atmospheric mercury and its potential source in Guiyang, China. Atmospheric Environment 45, (25), 4205-4212. doi:10.1016/j.atmosenv.2011.05.012

62. Fang GC, Tsai KH, Huang CY, Yang KPO, Xiao YF, Huang WC, Zhuang YJ (2018) Seasonal variations of ambient air mercury species nearby an airport. Atmos Res 202, 96-104. doi:10.1016/j.atmosres.2017.11.008

63. Ramanathan R (2005) An analysis of energy consumption and carbon dioxide emissions in countries of the Middle East and North Africa. Energy 30, (15), 2831-2842. doi:10.1016/j.energy.2005.01.010

64. Pacyna EG, Pacyna JM, Steenhuisen F, Wilson S (2006) Global anthropogenic mercury emission inventory for 2000. Atmospheric environment 40, (22), 4048-4063

65. Huang JY, Miller MB, Edgerton E, Gustin MS (2017) Deciphering potential chemical compounds of gaseous oxidized mercury in Florida, USA. Atmos Chem Phys 17, (3), 1689-1698. doi:10.5194/acp-17-1689-2017

66. Chemicals U (2002) Global mercury assessment. UNEP Chemicals, Geneva, 1-270

67. Mason RP, Fitzgerald WF, Morel FMM (1994) The Biogeochemical Cycling of Elemental Mercury - Anthropogenic Influences. Geochim Cosmochim Ac 58, (15), 3191-3198. doi:Doi 10.1016/0016-7037(94)90046-9

68. Harada M (1995) Minamata Disease - Methylmercury Poisoning in Japan Caused by Environmental-Pollution. Crit Rev Toxicol 25, (1), 1-24. doi:Doi 10.3109/10408449509089885

69. Choi AL, Budtz-Jørgensen E, Jørgensen PJ, Steuerwald U, Debes F, Weihe P, Grandjean P (2008) Selenium as a potential protective factor against mercury developmental neurotoxicity. Environ Res 107, (1), 45-52. doi:https://doi.org/10.1016/j.envres.2007.07.006

70. Malcolm EG, Ford AC, Redding TA, Richardson MC, Strain BM, Tetzner SW (2010) Experimental investigation of the scavenging of gaseous mercury by sea salt aerosol. J Atmos Chem 63, (3), 221-234. doi:10.1007/s10874-010-9165-y

71. Bełdowska M, Saniewska D, Gębka K, Kwasigroch U, Korejwo E, Kobos J (2018) Simple screening technique for determination of adsorbed and absorbed mercury in particulate matter in atmospheric and aquatic environment. Talanta 182, 340-347

72. Zahir F, Rizwi SJ, Haq SK, Khan RH (2005) Low dose mercury toxicity and human health. Environ Toxicol Pharmacol 20, (2), 351-360. doi:10.1016/j.etap.2005.03.007

73. Munthe J, Wängberg I, Pirrone N, Iverfeldt Å, Ferrara R, Ebinghaus R, Feng X, Gårdfeldt K, Keeler G, Lanzillotta E, Lindberg SE, Lu J, Mamane Y, Prestbo E, Schmolke S, Schroeder WH, Sommar J, Sprovieri F, Stevens RK, Stratton W, Tuncel G, Urba A (2001) Intercomparison of methods for sampling and analysis of atmospheric mercury species. Atmospheric Environment 35, (17), 3007-3017. doi:https://doi.org/10.1016/S1352-2310(01)00104-2

74. EPA U (2012) Final Mercury and Air Toxics Standards (MATS) for power plants. Final rule.

75. Ludden J, Brady J (2018) Trump EPA Says Mercury Limits On Coal Plants Too Costly, Not 'Necessary' NPR. https://www.npr.org/2018/12/28/679129613/trump-epa-says-mercury-limits-on-coal-plants-too-costly-not-necessary.

76. Schroeder WH, Jackson RA (1987) Environmental measurements with an atmospheric mercury monitor having speciation capabilities. Chemosphere 16, (1), 183-199. doi:https://doi.org/10.1016/0045-6535(87)90123-8

77. Dommergue A, Ferrari CP, Planchon FAM, Boutron CF (2002) Influence of anthropogenic sources on total gaseous mercury variability in grenoble suburban air (France). Sci Total Environ 297, (1), 203-213. doi:https://doi.org/10.1016/S0048-9697(02)00133-X

78. Pirrone N, Cinnirella S, Feng XB, Finkelman RB, Friedli HR, Leaner J, Mason R, Mukherjee AB, Stracher G, Streets DG, Telmer K (2009) Global Mercury Emissions to the Atmosphere from Natural and Anthropogenic Sources. Mercury Fate and Transport in the Global Atmosphere, 3-49. doi:10.1007/978-0-387-93958-2_1

79. Xu LL, Chen JS, Yang LM, Niu ZC, Tong L, Yin LQ, Chen YT (2015) Characteristics and sources of atmospheric mercury speciation in a coastal city, Xiamen, China. Chemosphere 119, 530-539. doi:10.1016/j.chemosphere.2014.07.024

80. Slemr F, Brunke EG, Ebinghaus R, Temme C, Munthe J, Wangberg I, Schroeder W, Steffen A, Berg T (2003) Worldwide trend of atmospheric mercury since 1977. Geophys Res Lett 30, (10). doi:Artn 1516

10.1029/2003gl016954

81. Braman RS, Johnson DL (1974) Selective absorption tubes and emission technique for determination of ambient forms of mercury in air. Environ Sci Technol 8, (12), 996-1003

82. Dumarey R, Heindryckx R, Dams R, Hoste J (1979) Determination of volatile mercury compounds in air with the coleman mercury analyzer system. Anal Chim Acta 107, 159-167. doi:https://doi.org/10.1016/S0003-2670(01)93206-4

83. Dumarey R, Heindryckx R, Dams R (1980) Determination of Total Particulate Mercury in Air with the Coleman Mercury Analyzer System. Anal Chim Acta 116, (1), 111-117. doi:Doi 10.1016/S0003-2670(01)84320-8

84. Brosset C, Lord E (1995) Methylmercury in ambient air. Method of determination and some measurement results. Water, Air, Soil Pollut 82, (3), 739-750. doi:10.1007/bf00479423

85. Slemr F, Schuster G, Seiler W (1985) Distribution, Speciation, and Budget of Atmospheric Mercury. J Atmos Chem 3, (4), 407-434. doi:Doi 10.1007/Bf00053870

86. Lindqvist O, Rodhe H (1985) Atmospheric Mercury - a Review. Tellus Series B-Chemical and Physical Meteorology 37, (3), 136-159. doi:DOI 10.1111/j.1600-0889.1985.tb00062.x

87. Steffen A, Bottenheim J, Cole A, Ebinghaus R, Lawson G, Leaitch WR (2014) Atmospheric mercury speciation and mercury in snow over time at Alert, Canada. Atmos Chem Phys 14, (5), 2219-2231. doi:10.5194/acp-14-2219-2014

88. Xiu GL, Cai J, Zhang WY, Zhang DN, Bueler A, Lee SC, Shen Y, Xu LH, Huang XJ, Zhang P (2009) Speciated mercury in size-fractionated particles in Shanghai ambient air. Atmospheric Environment 43, (19), 3145-3154. doi:10.1016/j.atmosenv.2008.07.044

89. Iverfeldt Å, Persson I (1985) The solvation thermodynamics of methylmercury(II) species derived from measurements of the heat of solution and the Henry's law constant. Inorg Chim Acta 103, (2), 113-119. doi:https://doi.org/10.1016/S0020-1693(00)87476-9

90. Sander R (2015) Compilation of Henry's law constants (version 4.0) for water as solvent. Atmospheric Chemistry & Physics 15, (8),

91. Laurier FJG, Mason RP, Whalin L, Kato S (2003) Reactive gaseous mercury formation in the North Pacific Ocean's marine boundary layer: A potential role of halogen chemistry. J Geophys Res-Atmos 108, (D17). doi:Artn 4529

10.1029/2003jd003625

92. Ullrich SM, Tanton TW, Abdrashitova SA (2001) Mercury in the aquatic environment: A review of factors affecting methylation. Crit Rev Env Sci Tec 31, (3), 241-293. doi:Doi 10.1080/20016491089226

93. Landis MS, Stevens RK, Schaedlich F, Prestbo EM (2002) Development and Characterization of an Annular Denuder Methodology for the Measurement of Divalent Inorganic Reactive Gaseous Mercury in Ambient Air. Environ Sci Technol 36, (13), 3000-3009. doi:10.1021/es015887t

94. Stratton WJ, Lindberg SE, Perry CJ (2001) Atmospheric Mercury Speciation: Laboratory and Field Evaluation of a Mist Chamber Method for Measuring Reactive Gaseous Mercury. Environ Sci Technol 35, (1), 170-177. doi:10.1021/es001260j

95. Lindberg SE, Stratton WJ (1998) Atmospheric mercury speciation: Concentrations and behavior of reactive gaseous mercury in ambient air. Environ Sci Technol 32, (1), 49-57. doi:DOI 10.1021/es970546u

96. Galbreath KC, Zygarlicke CJ (2000) Mercury transformations in coal combustion flue gas. Fuel Process Technol 65, 289-310. doi:Doi 10.1016/S0378-3820(99)00102-2

97. Wilcox J, Blowers P (2004) Decomposition of Mercuric Chloride and Application to Combustion Flue Gases. Environ Chem 1, (3), 166-171. doi:https://doi.org/10.1071/EN04036

98. Holmes CD, Jacob DJ, Yang X (2006) Global lifetime of elemental mercury against oxidation by atomic bromine in the free troposphere. Geophys Res Lett 33, (20),

99. Lin CJ, Pongprueksa P, Lindberg SE, Pehkonen SO, Byun D, Jang C (2006) Scientific uncertainties in atmospheric mercury models I: Model science evaluation. Atmospheric Environment 40, (16), 2911-2928. doi:10.1016/j.atmosenv.2006.01.009

100. Gustin MS, Kolker A, Gardfeldt K (2008) Transport and fate of mercury in the environment. Appl Geochem 23, (3), 343-344. doi:10.1016/j.ipgeocheni.2007.12.005

101. Li J, Sommar J, Wängberg I, Lindqvist O, Wei S-q (2008) Short-time variation of mercury speciation in the urban of Göteborg during GÖTE-2005. Atmospheric Environment 42, (36), 8382-8388. doi:https://doi.org/10.1016/j.atmosenv.2008.08.007

102. Lamborg CH, Fitzgerald WF, Vandal GM, Rolfhus KR (1995) Atmospheric Mercury in Northern Wisconsin - Sources and Species. Water Air Soil Poll 80, (1-4), 189-198. doi:Doi 10.1007/Bf01189667

103. Poissant L, Pilote M, Beauvais C, Constant P, Zhang HH (2005) A year of continuous measurements of three atmospheric mercury species (GEM, RGM and Hgp) in southern Québec, Canada. Atmospheric Environment 39, (7), 1275-1287. doi:http://dx.doi.org/10.1016/j.atmosenv.2004.11.007

104. Choi HD, Huang JY, Mondal S, Holsen TM (2013) Variation in concentrations of three mercury (Hg) forms at a rural and a suburban site in New York State. Sci Total Environ 448, 96-106. doi:10.1016/j.scitotenv.2012.08.052

105. Brosset C (1987) The behavior of mercury in the physical environment. Water, Air, Soil Pollut 34, (2), 145-166

106. Brosset C, Iverfeldt Å (1989) Interaction of solid gold with mercury in ambient air. Water, Air, Soil Pollut 43, (1-2), 147-168

107. Obrist D, Tas E, Peleg M, Matveev V, Fain X, Asaf D, Luria M (2011) Bromine-induced oxidation of mercury in the mid-latitude atmosphere. Nat Geosci 4, (1), 22-26. doi:10.1038/Ngeo1018

108. Swartzendruber PC, Jaffe DA, Prestbo EM, Weiss-Penzias P, Selin NE, Park R, Jacob DJ, Strode S, Jaegle L (2006) Observations of reactive gaseous mercury in the free troposphere at the Mount Bachelor Observatory. J Geophys Res-Atmos 111, (D24). doi:Artn D24302

10.1029/2006jd007415

109. Lynam MM, Keeler GJ (2005) Artifacts associated with the measurement of particulate mercury in an urban environment: The influence of elevated ozone concentrations. Atmospheric Environment 39, (17), 3081-3088. doi:10.1016/j.atmosenv.2005.01.036

110. Peterson C, Gustin M, Lyman S (2009) Atmospheric mercury concentrations and speciation measured from 2004 to 2007 in Reno, Nevada, USA. Atmospheric Environment 43, (30), 4646-4654. doi:10.1016/j.atmosenv.2009.04.053

111. Marumoto K, Hayashi M, Takami A (2015) Atmospheric mercury concentrations at two sites in the Kyushu Islands, Japan, and evidence of long-range transport from East Asia. Atmospheric Environment 117, 147-155. doi:https://doi.org/10.1016/j.atmosenv.2015.07.019

112. Williston SH (1968) Mercury in the atmosphere. Journal of Geophysical Research 73, (22), 7051-7055

113. Sakata M, Marumoto K (2002) Formation of atmospheric particulate mercury in the Tokyo metropolitan area. Atmospheric Environment 36, (2), 239-246. doi:https://doi.org/10.1016/S1352-2310(01)00432-0

114. Xiu GL, Jin Q, Zhang D, Shi S, Huang X, Zhang W, Bao L, Gao P, Chen B (2005) Characterization of size-fractionated particulate mercury in Shanghai ambient air. Atmospheric Environment 39, (3), 419-427. doi:https://doi.org/10.1016/j.atmosenv.2004.09.046

115. Subir M, Ariya PA, Dastoor AP (2012) A review of the sources of uncertainties in atmospheric mercury modeling II. Mercury surface and heterogeneous chemistry - A missing link. Atmospheric Environment 46, 1-10. doi:10.1016/j.atmosenv.2011.07.047

116. Subir M, Ariya PA, Dastoor AP (2011) A review of uncertainties in atmospheric modeling of mercury chemistry I. Uncertainties in existing kinetic parameters – Fundamental limitations and the importance of heterogeneous chemistry. Atmospheric Environment 45, (32), 5664-5676. doi:https://doi.org/10.1016/j.atmosenv.2011.04.046

117. Hedgecock IM, Pirrone N (2004) Chasing Quicksilver: Modeling the Atmospheric Lifetime of Hg0(g) in the Marine Boundary Layer at Various Latitudes. Environ Sci Technol 38, (1), 69-76. doi:10.1021/es034623z

118. Hall B (1995) The Gas Phase Oxidation of Elemental Mercury by Ozone. In: Porcella DB, Huckabee JW, Wheatley B (eds) Mercury as a Global Pollutant: Proceedings of the Third International Conference held in Whistler, British Columbia, July 10–14, 1994. Springer Netherlands, Dordrecht, pp 301-315. doi:10.1007/978-94-011-0153-0_34

119. Ariya PA, Khalizov A, Gidas A (2002) Reactions of Gaseous Mercury with Atomic and Molecular Halogens: Kinetics, Product Studies, and Atmospheric Implications. The Journal of Physical Chemistry A 106, (32), 7310-7320. doi:10.1021/jp020719o

120. Schroeder WH, Yarwood G, Niki H (1991) Transformation processes involving mercury species in the atmosphere—results from a literature survey. Water Air & Soil Pollution 56, (1), 653-666

121. Lynam MM, Keeler GJ (2006) Source-receptor relationships for atmospheric mercury in urban Detroit, Michigan. Atmospheric Environment 40, (17), 3144-3155. doi:10.1016/j.atmosenv.2006.01.026

122. Pal B, Ariya PA (2004) Gas-Phase HO•-Initiated Reactions of Elemental Mercury: Kinetics, Product Studies, and Atmospheric Implications. Environmental Science & Technology 38, (21), 5555-5566. doi:10.1021/es0494353

123. Sommar J, Hallquist M, Ljungstrom E, Lindqvist O (1997) On the gas phase reactions between volatile biogenic mercury species and the nitrate radical. J Atmos Chem 27, (3), 233-247. doi:Doi 10.1023/A:1005873712847

124. Calvert JG, Lindberg SE (2005) Mechanisms of mercury removal by O-3 and OH in the atmosphere. Atmospheric Environment 39, (18), 3355-3367. doi:10.1016/j.atmosenv.2005.01.055

125. Tossell JA (2006) Calculation of the energetics for the oligomerization of gas phase HgO and HgS and for the solvolysis of crystalline HgO and HgS. J Phys Chem A 110, (7), 2571-2578. doi:10.1021/jp056280s

126. Seigneur C, Abeck H, Chia G, Reinhard M, Bloom NS, Prestbo E, Saxena P (1998) Mercury adsorption to elemental carbon (soot) particles and atmospheric particulate matter. Atmospheric Environment 32, (14-15), 2649-2657. doi:Doi 10.1016/S1352-2310(97)00415-9

127. Lyman SN, Gustin MS, Prestbo EM (2010) A passive sampler for ambient gaseous oxidized mercury concentrations. Atmospheric Environment 44, (2), 246-252. doi:10.1016/j.atmosenv.2009.10.008

128. Lyman SN, Jaffe DA (2012) Formation and fate of oxidized mercury in the upper troposphere and lower stratosphere. Nat Geosci 5, (2), 114-117. doi:10.1038/Ngeo1353

129. Zhang H, Lindberg SE (2001) Sunlight and iron(III)-induced photochemical production of dissolved gaseous mercury in freshwater. Environ Sci Technol 35, (5), 928-935. doi:DOI 10.1021/es001521p

130. Spangler WJ, Spigarelli JL, Rose JM, Miller HM (1973) Methylmercury - Bacterial Degradation in Lake Sediments. Science 180, (4082), 192-193. doi:DOI 10.1126/science.180.4082.192

131. Niki H, Maker P, Savage C, Breitenbach L (1983) A long-path Fourier transform infrared study of the kinetics and mechanism for the hydroxyl radical-initiated oxidation of dimethylmercury. The Journal of Physical Chemistry 87, (24), 4978-4981

132. St. Louis VL, Sharp MJ, Steffen A, May A, Barker J, Kirk JL, Kelly DJ, Arnott SE, Keatley B, Smol JP (2005) Some sources and sinks of monomethyl and inorganic mercury on Ellesmere Island in the Canadian High Arctic. Environ Sci Technol 39, (8), 2686-2701

133. Rutter AP, Hanford KL, Zwers JT, Perillo-Nicholas AL, Schauer JJ, Olson ML (2008) Evaluation of an offline method for the analysis of atmospheric reactive gaseous mercury and particulate mercury. J Air Waste Manage 58, (3), 377-383. doi:10.3155/1047-3289.58.3.377

134. Poissant L, Pilote M, Xu XH, Zhang H, Beauvais C (2004) Atmospheric mercury speciation and deposition in the Bay St. Francois wetlands. J Geophys Res-Atmos 109, (D11). doi:Artn D11301

10.1029/2003jd004364

135. Durnford D, Dastoor A (2011) The behavior of mercury in the cryosphere: A review of what we know from observations. J Geophys Res-Atmos 116. doi:Artn D06305

10.1029/2010jd014809

136. Grigal DF (2003) Mercury sequestration in forests and peatlands: A review. J Environ Qual 32, (2), 393-405

137. Prestbo EM, Gay DA (2009) Wet deposition of mercury in the US and Canada, 1996-2005: Results and analysis of the NADP mercury deposition network (MDN). Atmospheric Environment 43, (27), 4223-4233. doi:10.1016/j.atmosenv.2009.05.028

138. Nair US, Wu Y, Holmes CD, Ter Schure A, Kallos G, Walters JT (2013) Cloud-resolving simulations of mercury scavenging and deposition in thunderstorms. Atmos Chem Phys 13, (19), 10143-10157. doi:10.5194/acp-13-10143-2013

139. Weigelt A, Temme C, Bieber E, Schwerin A, Schuetze M, Ebinghaus R, Kock HH (2013) Measurements of atmospheric mercury species at a German rural background site from 2009 to 2011-methods and results. Environ Chem 10, (2), 102-110. doi:10.1071/En12107

140. Feng XB, Lu JY, Gregoire DC, Hao YJ, Banic CM, Schroeder WH (2004) Analysis of inorganic mercury species associated with airborne particulate matter/aerosols: method development. Anal Bioanal Chem 380, (4), 683-689. doi:10.1007/s00216-004-2803-y

141. Huang JY, Miller MB, Weiss-Penzias P, Gustin MS (2013) Comparison of Gaseous Oxidized Hg Measured by KCl-Coated Denuders, and Nylon and Cation Exchange Membranes. Environ Sci Technol 47, (13), 7307-7316. doi:10.1021/es4012349

142. Deeds DA, Ghoshdastidar A, Raofie F, Guerette EA, Tessier A, Ariya PA (2015) Development of a Particle-Trap Preconcentration-Soft Ionization Mass Spectrometric Technique for the Quantification of Mercury Halides in Air. Anal Chem 87, (10), 5109-5116. doi:10.1021/ac504545w

143. Gustin MS, Pierce AM, Huang JY, Miller MB, Holmes HA, Loria-Salazar SM (2016) Evidence for Different Reactive Hg Sources and Chemical Compounds at Adjacent Valley and

High Elevation Locations. Environ Sci Technol 50, (22), 12225-12231. doi:10.1021/acs.est.6b03339

144. Lynam MM, Keeler GJ (2002) Comparison of methods for particulate phase mercury analysis: sampling and analysis. Anal Bioanal Chem 374, (6), 1009-1014. doi:10.1007/s00216-002-1584-4

145. Kim KH, Ebinghaus R, Schroeder WH, Blanchard P, Kock HH, Steffen A, Froude FA, Kim MY, Hong SM, Kim JH (2005) Atmospheric mercury concentrations from several observatory sites in the northern hemisphere. J Atmos Chem 50, (1), 1-24. doi:10.1007/s10874-005-9222-0

146. Slemr F, Brunke EG, Ebinghaus R, Kuss J (2011) Worldwide trend of atmospheric mercury since 1995. Atmos Chem Phys 11, (10), 4779-4787. doi:10.5194/acp-11-4779-2011

147. Sprovieri F, Pirrone N, Bencardino M, D'Amore F, Carbone F, Cinnirella S, Mannarino V, Landis M, Ebinghaus R, Weigelt A, Brunke EG, Labuschagne C, Martin L, Munthe J, Wangberg I, Artaxo P, Morais F, Barbosa HDJ, Brito J, Cairns W, Barbante C, Dieguez MD, Garcia PE, Dommergue A, Angot H, Magand O, Skov H, Horvat M, Kotnik J, Read KA, Neves LM, Gawlik BM, Sena F, Mashyanov N, Obolkin V, Wip D, Bin Feng X, Zhang H, Fu XW, Ramachandran R, Cossa D, Knoery J, Marusczak N, Nerentorp M, Norstrom C (2016) Atmospheric mercury concentrations observed at ground-based monitoring sites globally distributed in the framework of the GMOS network. Atmos Chem Phys 16, (18), 11915-11935. doi:10.5194/acp-16-11915-2016

148. Hynes AJ, Everhart S, Bauer D, Remeika J, Ernest CT (2017) In situ and denuder-based measurements of elemental and reactive gaseous mercury with analysis by laser-induced fluorescence results from the Reno Atmospheric Mercury Intercomparison Experiment. Atmos Chem Phys 17, (1), 465-483. doi:10.5194/acp-17-465-2017

149. Arruti A, Fernández-Olmo I, Irabien Á (2010) Evaluation of the contribution of local sources to trace metals levels in urban PM2.5 and PM10 in the Cantabria region (Northern Spain). J Environ Monitor 12, (7), 1451-1458. doi:10.1039/B926740A

150. Gustin MS, Huang JY, Miller MB, Peterson C, Jaffe DA, Ambrose J, Finley BD, Lyman SN, Call K, Talbot R, Feddersen D, Mao HT, Lindberg SE (2013) Do We Understand What the Mercury Speciation Instruments Are Actually Measuring? Results of RAMIX. Environ Sci Technol 47, (13), 7295-7306. doi:10.1021/es3039104

151. Cheng N, Duan L, Xiu G, Zhao M, Qian G (2017) Comparison of atmospheric PM2.5-bounded mercury species and their correlation with bromine and iodine at coastal urban and island sites in the eastern China. Atmos Res 183, 17-25. doi:https://doi.org/10.1016/j.atmosres.2016.08.009

152. Shannon JD, Voldner EC (1995) Modeling Atmospheric Concentrations of Mercury and Deposition to the Great-Lakes. Atmospheric Environment 29, (14), 1649-1661. doi:Doi 10.1016/1352-2310(95)00075-A

153. Peters K, Eiden R (1992) Modeling the Dry Deposition Velocity of Aerosol-Particles to a Spruce Forest. Atmos Environ a-Gen 26, (14), 2555-2564. doi:Doi 10.1016/0960-1686(92)90108-W

154. Keeler G, Glinsorn G, Pirrone N (1995) Particulate Mercury in the Atmosphere - Its Significance, Transport, Transformation and Sources. Water Air Soil Poll 80, (1-4), 159-168. doi:Doi 10.1007/Bf01189664

155. Holmes CD (2012) ATMOSPHERIC CHEMISTRY Quick cycling of quicksilver. Nat Geosci 5, (2), 95-96. doi:10.1038/ngeo1389

156. Lyman SN, Gustin MS, Prestbo EM, Marsik FJ (2007) Estimation of Dry Deposition of Atmospheric Mercury in Nevada by Direct and Indirect Methods. Environ Sci Technol 41, (6), 1970-1976. doi:10.1021/es062323m

157. Rutter AP, Schauer JJ (2007) The impact of aerosol composition on the particle to gas partitioning of reactive mercury. Environ Sci Technol 41, (11), 3934-3939. doi:10.1021/es062439i

158. Fleming EJ, Mack EE, Green PG, Nelson DC (2006) Mercury methylation from unexpected sources: Molybdate-inhibited freshwater sediments and an iron-reducing bacterium. Appl Environ Microb 72, (1), 457-464. doi:10.1128/Aem.72.1.457-464.2006

159. Fang FM, Wang QC, Li JF (2001) Atmospheric particulate mercury concentration and its dry deposition flux in Changchun City, China. Sci Total Environ 281, (1-3), 229-236. doi:Doi 10.1016/S0048-9697(01)00849-X

160. Andronache C (2003) Estimated variability of below-cloud aerosol removal by rainfall for observed aerosol size distributions. Atmos Chem Phys 3, 131-143. doi:DOI 10.5194/acp-3-131-2003

161. Lu J, Schroeder W (1999) Sampling and determination of particulate mercury in ambient air: a review. Water, Air, Soil Pollut 112, (3-4), 279-295

162. Coufalik P, Cervenka R, Komarek J (2011) Mercury speciation in soil in vicinity of coal beds using sequential extraction. Environ Earth Sci 62, (2), 421-427. doi:10.1007/s12665-010-0537-z

163. Shepler BC, Peterson KA (2003) Mercury monoxide: A systematic investigation of its ground electronic state. J Phys Chem A 107, (11), 1783-1787. doi:10.1021/jp027512f

164. Morel FMM, Kraepiel AML, Amyot M (1998) THE CHEMICAL CYCLE AND BIOACCUMULATION OF MERCURY. Annual Review of Ecology and Systematics 29, (1), 543-566. doi:10.1146/annurev.ecolsys.29.1.543

165. Amos HM, Jacob DJ, Streets DG, Sunderland EM (2013) Legacy impacts of all-time anthropogenic emissions on the global mercury cycle. Global Biogeochem Cy 27, (2), 410-421. doi:doi:10.1002/gbc.20040

166. Streets DG, Devane MK, Lu Z, Bond TC, Sunderland EM, Jacob DJ (2011) All-Time Releases of Mercury to the Atmosphere from Human Activities. Environ Sci Technol 45, (24), 10485-10491. doi:10.1021/es202765m

167. Lin CJ, Pehkonen SO (1999) The chemistry of atmospheric mercury: a review. Atmospheric Environment 33, (13), 2067-2079. doi:Doi 10.1016/S1352-2310(98)00387-2

168. Steffen A, Douglas T, Amyot M, Ariya P, Aspmo K, Berg T, Bottenheim J, Brooks S, Cobbett F, Dastoor A, Dommergue A, Ebinghaus R, Ferrari C, Gardfeldt K, Goodsite ME, Lean D, Poulain AJ, Scherz C, Skov H, Sommar J, Temme C (2008) A synthesis of atmospheric mercury depletion event chemistry in the atmosphere and snow. Atmos Chem Phys 8, (6), 1445-1482. doi:DOI 10.5194/acp-8-1445-2008

169. Olson ES, Sharma RK, Pavlish JH (2002) On the analysis of mercuric nitrate in flue gas by GC-MS. Anal Bioanal Chem 374, (6), 1045-1049. doi:10.1007/s00216-002-1602-6

170. McClure CD, Jaffe DA, Edgerton ES (2014) Evaluation of the KCl Denuder Method for Gaseous Oxidized Mercury using HgBr2 at an In-Service AMNet Site. Environ Sci Technol 48, (19), 11437-11444. doi:10.1021/es502545k

171. Engle MA, Tate MT, Krabbenhoft DP, Schauer JJ, Kolker A, Shanley JB, Bothner MH (2010) Comparison of atmospheric mercury speciation and deposition at nine sites across central and eastern North America. Journal of Geophysical Research: Atmospheres 115, (D18). doi:doi:10.1029/2010JD014064

172. Risch MR, Gay DA, Fowler KK, Keeler GJ, Backus SM, Blanchard P, Barres JA, Dvonch JT (2012) Spatial patterns and temporal trends in mercury concentrations, precipitation depths, and mercury wet deposition in the North American Great Lakes region, 2002–2008. Environ Pollut 161, 261-271. doi:https://doi.org/10.1016/j.envpol.2011.05.030

173. Hynes AJ, Donohoue DL, Goodsite ME, Hedgecock IM (2009) Our current understanding of major chemical and physical processes affecting mercury dynamics in the atmosphere and at the air-water/terrestrial interfaces. In: Mason R, Pirrone N (eds) Mercury Fate and Transport in the Global Atmosphere: Emissions, Measurements and Models. Springer US, Boston, MA, pp 427-457. doi:10.1007/978-0-387-93958-2_14

174. Ariya PA, Peterson K, Snider G, Amyot M (2009) Mercury chemical transformations in the gas, aqueous and heterogeneous phases: state-of-the-art science and uncertainties. In: Mason R, Pirrone N (eds) Mercury Fate and Transport in the Global Atmosphere: Emissions,

Measurements and Models. Springer US, Boston, MA, pp 459-501. doi:10.1007/978-0-387-93958-2_15

175. Harland PW, Thynne JCJ (1971) Autodetachment lifetimes, attachment cross sections, and negative ions formed by sulfur hexafluoride and sulfur tetrafluoride. The Journal of Physical Chemistry 75, (23), 3517-3523. doi:10.1021/j100692a005

176. Meyer DE, Sikdar SK, Hutson ND, Bhattacharyya D (2007) Examination of Sulfur-Functionalized, Copper-Doped Iron Nanoparticles for Vapor-Phase Mercury Capture in Entrained-Flow and Fixed-Bed Systems. Energ Fuel 21, (5), 2688-2697. doi:10.1021/ef070120t

177. Bombach G, Bombach K, Klemm W (1994) Speciation of mercury in soils and sediments by thermal evaporation and cold vapor atomic absorption. Fresenius' journal of analytical chemistry 350, (1-2), 18-20

178. Denis MS, Song X, Lu JY, Feng X (2006) Atmospheric gaseous elemental mercury in downtown Toronto. Atmospheric Environment 40, (21), 4016-4024. doi:http://dx.doi.org/10.1016/j.atmosenv.2005.07.078

179. Cairns E, Tharumakulasingam K, Athar M, Yousaf M, Cheng I, Huang Y, Lu JL, Yap D (2011) Source, concentration, and distribution of elemental mercury in the atmosphere in Toronto, Canada. Environ Pollut 159, (8-9), 2003-2008. doi:10.1016/j.envpol.2010.12.006

180. Gustin M, Jaffe D (2010) Reducing the Uncertainty in Measurement and Understanding of Mercury in the Atmosphere. Environ Sci Technol 44, (7), 2222-2227. doi:10.1021/es902736k

181. Yang H (2002) Effects of fly ash on the oxidation of mercury during post-combustion conditions.

182. Kos G, Ryzhkov A, Dastoor A, Narayan J, Steffen A, Ariya PA, Zhang L (2013) Evaluation of discrepancy between measured and modelled oxidized mercury species. Atmos Chem Phys 13, (9), 4839-4863. doi:10.5194/acp-13-4839-2013

183. Raofie F, Ariya PA (2004) Product study of the gas-phase BrO-initiated oxidation of Hg0: evidence for stable Hg1+ compounds. Environ Sci Technol 38, (16), 4319-4326

184. Murphy DM, Thomson DS, Mahoney MJ (1998) In Situ Measurements of Organics, Meteoritic Material, Mercury, and Other Elements in Aerosols at 5 to 19 Kilometers. Science 282, (5394), 1664-1669. doi:10.1126/science.282.5394.1664

185. Malcolm EG, Keeler GJ (2007) Evidence for a sampling artifact for particulate-phase mercury in the marine atmosphere. Atmospheric Environment 41, (16), 3352-3359. doi:10.1016/j.atmosenv.2006.12.024

186. Marusczak N, Sonke JE, Fu X, Jiskra M (2016) Tropospheric GOM at the Pic du Midi Observatory-Correcting Bias in Denuder Based Observations. Environ Sci Technol. doi:10.1021/acs.est.6b04999

187. Nazarenko Y, Rangel-Alvarado RB, Kos G, Kurien U, Ariya PA (2016) Novel aerosol analysis approach for characterization of nanoparticulate matter in snow. Environmental Science and Pollution Research, 1-14. doi:10.1007/s11356-016-8199-3

188. Liu J, Pui DYH, Wang J (2011) Removal of airborne nanoparticles by membrane coated filters. Sci Total Environ 409, (22), 4868-4874. doi:http://dx.doi.org/10.1016/j.scitotenv.2011.08.011

189. Seinfeld JH, Pandis SN (2012) Atmospheric chemistry and physics: from air pollution to climate change. John Wiley & Sons,

190. Grassian VH (2008) When Size Really Matters: Size-Dependent Properties and Surface Chemistry of Metal and Metal Oxide Nanoparticles in Gas and Liquid Phase Environments†. The Journal of Physical Chemistry C 112, (47), 18303-18313. doi:10.1021/jp806073t

191. Murphy DM, Hudson PK, Thomson DS, Sheridan PJ, Wilson JC (2006) Observations of Mercury-Containing Aerosols. Environ Sci Technol 40, (10), 3163-3167. doi:10.1021/es052385x

192. Ariya PA, Amyot M, Dastoor A, Deeds D, Feinberg A, Kos G, Poulain A, Ryjkov A, Semeniuk K, Subir M, Toyota K (2015) Mercury Physicochemical and Biogeochemical Transformation in the Atmosphere and at Atmospheric Interfaces: A Review and Future Directions. Chemical Reviews 115, (10), 3760-3802. doi:10.1021/cr500667e

193. Si L, Ariya PA (2015) Photochemical reactions of divalent mercury with thioglycolic acid: Formation of mercuric sulfide particles. Chemosphere 119, 467-472. doi:https://doi.org/10.1016/j.chemosphere.2014.07.022

194. Pham AL-T, Morris A, Zhang T, Ticknor J, Levard C, Hsu-Kim H (2014) Precipitation of nanoscale mercuric sulfides in the presence of natural organic matter: Structural properties, aggregation, and biotransformation. Geochim Cosmochim Ac 133, (0), 204-215. doi:http://dx.doi.org/10.1016/j.gca.2014.02.027

195. Mwilu SK, El Badawy AM, Bradham K, Nelson C, Thomas D, Scheckel KG, Tolaymat T, Ma L, Rogers KR (2013) Changes in silver nanoparticles exposed to human synthetic stomach fluid: Effects of particle size and surface chemistry. Sci Total Environ 447, (0), 90-98. doi:http://dx.doi.org/10.1016/j.scitotenv.2012.12.036

196. Tchounwou PB, Ayensu WK, Ninashvili N, Sutton D (2003) Review: Environmental exposure to mercury and its toxicopathologic implications for public health. Environ Toxicol 18, (3), 149-175

197. Aschner M, Aschner JL (1990) Mercury neurotoxicity: mechanisms of blood-brain barrier transport. Neuroscience & Biobehavioral Reviews 14, (2), 169-176

198. Atwell L, Hobson KA, Welch HE (1998) Biomagnification and bioaccumulation of mercury in an arctic marine food web: insights from stable nitrogen isotope analysis. Canadian Journal of Fisheries and Aquatic Sciences 55, (5), 1114-1121

199. Sommar J, Feng X, Gardfeldt K, Lindqvist O (1999) Measurements of fractionated gaseous mercury concentrations over northwestern and central Europe, 1995-99. J Environ Monitor 1, (5), 435-439. doi:10.1039/A902729G

200. Lu JY, Schroeder WH, Berg T, Munthe J, Schneeberger D, Schaedlich F (1998) A device for sampling and determination of total particulate mercury in ambient air. Anal Chem 70, (11), 2403-2408

201. Kim P-R, Han Y-J, Holsen TM, Yi S-M (2012) Atmospheric particulate mercury: Concentrations and size distributions. Atmospheric Environment 61, 94-102. doi:https://doi.org/10.1016/j.atmosenv.2012.07.014

202. Zhang L, Gong S, Padro J, Barrie L (2001) A size-segregated particle dry deposition scheme for an atmospheric aerosol module. Atmos Environ 35, (3), 549-560. doi:http://dx.doi.org/10.1016/S1352-2310(00)00326-5

203. Malcolm E, Ford A, Redding T, Richardson M, Strain B, Tetzner S (2010) Experimental investigation of the scavenging of gaseous mercury by sea salt aerosol. J Atmos Chem 63, (3), 221-234. doi:10.1007/s10874-010-9165-y

204. Rutter AP, Schauer JJ (2007) The effect of temperature on the gas–particle partitioning of reactive mercury in atmospheric aerosols. Atmos Environ 41, (38), 8647-8657. doi:http://dx.doi.org/10.1016/j.atmosenv.2007.07.024

205. Int Panis L, de Geus B, Vandenbulcke G, Willems H, Degraeuwe B, Bleux N, Mishra V, Thomas I, Meeusen R (2010) Exposure to particulate matter in traffic: A comparison of cyclists and car passengers. Atmos Environ 44, (19), 2263-2270. doi:http://dx.doi.org/10.1016/j.atmosenv.2010.04.028

206. Wick P, Malek A, Manser P, Meili D, Maeder-Althaus X, Diener L, Diener P-A, Zisch A, Krug HF, von Mandach U (2010) Barrier Capacity of Human Placenta for Nanosized Materials. Environ Health Persp 118, (3), 432-436. doi:10.1289/ehp.0901200

207. Jun Lee S, Seo Y-C, Jurng J, Hong J-H, Park J-W, Hyun JE, Gyu Lee T (2004) Mercury emissions from selected stationary combustion sources in Korea. Sci Total Environ 325, (1–3), 155-161. doi:http://dx.doi.org/10.1016/j.scitotenv.2003.12.002

208. Kotnik J, Horvat M, Mandic V, Logar M (2000) Influence of the Šoštanj coal-fired thermal power plant on mercury and methyl mercury concentrations in Lake Velenje, Slovenia. Sci Total Environ 259, (1–3), 85-95. doi:http://dx.doi.org/10.1016/S0048-9697(00)00576-3

209. Ghoshdastidar AJ, Ramamurthy J, Morrisette M, Ariya PA (2019) Development of Methodology to Generate, Measure and Characterize the Chemical Composition of Oxidized Mercury Nanoparticles. Anal Bioanal Chem Submitted,

210. Swihart MT (2003) Vapor-phase synthesis of nanoparticles. Current Opinion in Colloid & Interface Science 8, (1), 127-133. doi:http://dx.doi.org/10.1016/S1359-0294(03)00007-4

211. Wängberg I, Edner H, Ferrara R, Lanzillotta E, Munthe J, Sommar J, Sjöholm M, Svanberg S, Weibring P (2003) Atmospheric mercury near a chlor-alkali plant in Sweden. Sci Total Environ 304, (1–3), 29-41. doi:http://dx.doi.org/10.1016/S0048-9697(02)00554-5

212. Ghoshdastidar AJ, Ariya PA (2019) Mercury on the Move: The Chemical Speciation and Phase Distribution of Atmospheric Oxidized Mercury. Environmental Science: Processes and Impacts Submitted,

213. Raofie F, Snider G, Ariya PA (2008) Reaction of gaseous mercury with molecular iodine, atomic iodine, and iodine oxide radicals - Kinetics, product studies, and atmospheric implications. Canadian Journal of Chemistry-Revue Canadienne De Chimie 86, (8), 811-820. doi:Doi 10.1139/V08-088

214. Ye Y, Tsai C-J, Pui DYH, Lewis CW (1991) Particle Transmission Characteristics of an Annular Denuder Ambient Sampling System. Aerosol Sci Tech 14, (1), 102-111. doi:10.1080/02786829108959475

215. Sprovieri F, Pirrone N, Ebinghaus R, Kock H, Dommergue A (2010) A review of worldwide atmospheric mercury measurements. Atmos Chem Phys 10, (17), 8245-8265

216. Kozak M (2009) What is strong correlation? Teaching Statistics 31, (3), 85-86

217. Prüss-Ustün A, Wolf J, Corvalán C, Bos R, Neira M (2016) Preventing disease through healthy environments: a global assessment of the burden of disease from environmental risks. A global assessment of the burden of disease from environmental risks. World Health Organication, Geneva, Switzerland

218. Brauer M (2016) The Global Burden of Disease from Air Pollution. Paper presented at the AAAS 2016 Annual Meeting, Washington, DC,

219. World Health Organization (WHO) (2014) 7 million premature deaths annually linked to air pollution. World Health Organization. http://www.who.int/mediacentre/news/releases/2014/air-pollution/en/. Accessed 2015/09/28 2014

220. IARC (International Agency for Research on Cancer) (2013) Air Pollution and Cancer. IARC Scientific Publication No. 161. International Agency for Research on Cancer, Lyon, France

221. Hetland R, Cassee F, Refsnes M, Schwarze P, Låg M, Boere A, Dybing E (2004) Release of inflammatory cytokines, cell toxicity and apoptosis in epithelial lung cells after exposure to ambient air particles of different size fractions. Tox In Vitro 18, (2), 203-212. doi:10.1016/S0887-2333(03)00142-5

222. Brook RD, Franklin B, Cascio W, Hong Y, Howard G, Lipsett M, Luepker R, Mittleman M, Samet J, Smith SC (2004) Air pollution and cardiovascular disease. Circulation 109, (21), 2655-2671

223. Lin H-H, Ezzati M, Murray M (2007) Tobacco smoke, indoor air pollution and tuberculosis: a systematic review and meta-analysis. PLoS Med 4, (1), e20

224. Brauer M, Hoek G, Van Vliet P, Meliefste K, Fischer PH, Wijga A, Koopman LP, Neijens HJ, Gerritsen J, Kerkhof M (2002) Air pollution from traffic and the development of respiratory infections and asthmatic and allergic symptoms in children. Am J Respir Crit Care Med 166, (8), 1092-1098

225. Ezzati M, Kammen DM (2001) Indoor air pollution from biomass combustion and acute respiratory infections in Kenya: an exposure-response study. The Lancet 358, (9282), 619-624

226. Douglas J, Waller R (1966) Air pollution and respiratory infection in children. Br J Prev Soc Med 20, (1), 1

227. Kovesi T, Creery D, Gilbert NL, Dales R, Fugler D, Thompson B, Randhawa N, Miller JD (2006) Indoor air quality risk factors for severe lower respiratory tract infections in Inuit infants in Baffin Region, Nunavut: a pilot study. Indoor Air 16, (4), 266-275. doi:10.1111/j.1600-0668.2006.00423.x

228. Kovesi T, Gilbert NL, Stocco C, Fugler D, Dales RE, Guay M, Miller JD (2007) Indoor air quality and the risk of lower respiratory tract infections in young Canadian Inuit children. Can Med Assoc J 177, (2), 155-160

229. Williamson BJ, Udachin V, Purvis OW, Spiro B, Cressey G, Jones GC (2004) Characterisation of Airborne Particulate Pollution in The Cu Smelter and Former Mining Town of Karabash, South Ural Mountains of Russia. Environmental Monitoring and Assessment 98, (1), 235-259. doi:10.1023/b:emas.0000038189.45002.78

230. Barrie LA (1980) The fate of particulate emissions from an isolated power plant in the oil sands area of western Canada. Ann N Y Acad Sci 338, (1), 434-452. doi:10.1111/j.1749-6632.1980.tb17138.x

231. Stern AC (2014) Fundamentals of air pollution. Elsevier,

232. Myung CL, Park S (2012) Exhaust nanoparticle emissions from internal combustion engines: A review. International Journal of Automotive Technology 13, (1), 9-22. doi:10.1007/s12239-012-0002-y

233. U.S. Environmental Protection Agency (2006) The Master List of Compounds Emitted by Mobile Sources. National Service Center for Environmental Publications (NSCEP), Research Triangle Park, NC

234. U.S.EPA (2014) Air Toxic Emissions from On-road Vehicles in MOVES2014. Assessment and Standards Division, Office of Transportation and Air Quality, U.S. Environmental Protection Agency,

235. Chen R, Hu B, Liu Y, Xu J, Yang G, Xu D, Chen C (2016) Beyond PM2.5: The role of ultrafine particles on adverse health effects of air pollution. Biochimica et Biophysica Acta (BBA) - General Subjects 1860, (12), 2844-2855. doi:http://dx.doi.org/10.1016/j.bbagen.2016.03.019

236. Heinzerling A, Hsu J, Yip F (2015) Respiratory Health Effects of Ultrafine Particles in Children: a Literature Review. Water Air Soil Pollut 227, (1), 32. doi:10.1007/s11270-015-2726-6

237. Pieters N, Koppen G, Van Poppel M, De Prins S, Cox B, Dons E, Nelen V, Panis LI, Plusquin M, Schoeters G, Nawrot TS (2015) Blood Pressure and Same-Day Exposure to Air Pollution at School: Associations with Nano-Sized to Coarse PM in Children. Environ Health Perspect 123, (7), 737-742. doi:10.1289/ehp.1408121

238. World Health Organization (WHO) (2013) Outdoor air pollution a leading environmental cause of cancer deaths. http://www.euro.who.int/en/health-topics/environment-and-health/urban-health/news/news/2013/10/outdoor-air-pollution-a-leading-environmental-cause-of-cancer-deaths. Accessed 2015/09/28 2014

239. Díaz-Robles LA, Fu JS, Vergara-Fernández A, Etcharren P, Schiappacasse LN, Reed GD, Silva MP (2014) Health risks caused by short term exposure to ultrafine particles generated by residential wood combustion: A case study of Temuco, Chile. Environment International 66, 174-181. doi:http://dx.doi.org/10.1016/j.envint.2014.01.017

240. Pekkanen J, Peters A, Hoek G, Tiittanen P, Brunekreef B, de Hartog J, Heinrich J, Ibald-Mulli A, Kreyling WG, Lanki T, Timonen KL, Vanninen E (2002) Particulate Air Pollution and Risk of ST-Segment Depression During Repeated Submaximal Exercise Tests Among Subjects With Coronary Heart Disease. The Exposure and Risk Assessment for Fine and Ultrafine Particles in Ambient Air (ULTRA) Study 106, (8), 933-938. doi:10.1161/01.cir.0000027561.41736.3c

241. Ostro B, Hu J, Goldberg D, Reynolds P, Hertz A, Bernstein L, Kleeman MJ (2015) Associations of mortality with long-term exposures to fine and ultrafine particles, species and sources: results from the California Teachers Study Cohort. Environ Health Perspect 123, (6), 549

242. Terzano C, Di Stefano F, Conti V, Graziani E, Petroianni A (2010) Air pollution ultrafine particles: toxicity beyond the lung. Eur Rev Med Pharmacol Sci 14, (10), 809-821

243. Slezakova K, Morais S, do Carmo Pereira M (2013) Atmospheric Nanoparticles and Their Impacts on Public Health. In: Rodriguez-Morales AJ (ed) Current Topics in Public Health. InTech, Rijeka, Croatia, p 742. doi:http://dx.doi.org/10.5772/54775

244. Cosgrove WJ, Rijsberman FR (2014) World water vision: making water everybody's business. Routledge,

245. Stamoulis KG, Zezza A (2003) A conceptual framework for national agricultural, rural development, and food security strategies and policies. Food and Agriculture Organization of the United Nations. Agricultural and Development Economics Division,

246. Arlappa N, Kokku S (2015) Drought, Food security and Micronutrient malnutrition. In: Handbook of public health in natural disasters: Nutrition, food, remediation and preparation. Wageningen Academic Publishers, pp 1899-1909

247. Maru YT, Smith MS, Sparrow A, Pinho PF, Dube OP (2014) A linked vulnerability and resilience framework for adaptation pathways in remote disadvantaged communities. Global Environmental Change 28, 337-350

248. Afifi T, Jäger J (2010) Environment, forced migration and social vulnerability. Springer, Heidelberg

249. Chapin III FS, Peterson G, Berkes F, Callaghan T, Angelstam P, Apps M, Beier C, Bergeron Y, Crépin A-S, Danell K (2004) Resilience and vulnerability of northern regions to social and environmental change. AMBIO: A Journal of the Human Environment 33, (6), 344-349

250. Durkalec A, Furgal C, Skinner MW, Sheldon T (2015) Climate change influences on environment as a determinant of Indigenous health: relationships to place, sea ice, and health in an Inuit community. Soc Sci Med 136, 17-26

251. Eakin H, Luers AL (2006) Assessing the vulnerability of social-environmental systems. Annu Rev Environ Resour 31, 365-394

252. Ford JD, Smit B (2004) A framework for assessing the vulnerability of communities in the Canadian Arctic to risks associated with climate change. Arctic, 389-400

253. McDowell G, Ford J, Jones J (2016) Community-level climate change vulnerability research: trends, progress, and future directions. Environmental Research Letters 11, (3), 033001

254. Mercer J, Dominey-Howes D, Kelman I, Lloyd K (2007) The potential for combining indigenous and western knowledge in reducing vulnerability to environmental hazards in small island developing states. Environmental Hazards 7, (4), 245-256

255. Weichenthal S, Mallach G, Kulka R, Black A, Wheeler A, You H, St-Jean M, Kwiatkowski R, Sharp D (2013) A randomized double-blind crossover study of indoor air filtration and

acute changes in cardiorespiratory health in a First Nations community. Indoor Air 23, (3), 175-184. doi:10.1111/ina.12019

256. Chapin III SF, Berman M, Callaghan TV, Convey P, Crepin A-S, Danell K, Ducklow H, Forbes B, Kofinas G, McGuire AD, Nuttall M, Virginia R, Young O, Zimov SA, Christensen T, Godduhn A, Murphy EJ, Wall D, Zockler C, Fitzharris B (2005) Polar Systems. In: Rashid M. Hassan RS, Neville Ash (ed) Ecosystems and Human Well-Being: Current State and Trends: Findings of the Condition and Trends Working Group, vol 1. Island Press, Washington, DC, p 917

257. Ezzati M, Kammen DM (2002) The health impacts of exposure to indoor air pollution from solid fuels in developing countries: knowledge, gaps, and data needs. Environ Health Perspect 110, (11), 1057

258. Tzoulaki I, Elliott P, Kontis V, Ezzati M (2016) Worldwide Exposures to Cardiovascular Risk Factors and Associated Health Effects. Circulation 133, (23), 2314-2333

259. Nelson L, Valle J, King G, Mills PK, Richardson MJ, Roberts EM, Smith D, English P (2017) Estimating the Proportion of Childhood Cancer Cases and Costs Attributable to the Environment in California. Am J Public Health, (0), e1-e7

260. World Health Organization (2009) Global health risks: mortality and burden of disease attributable to selected major risks. World Health Organization,

261. Smith KR, Corvalán CF, Kjellstrom T (1999) How much global ill health is attributable to environmental factors? Epidemiology-Baltimore 10, (5), 573-584

262. Ezzati M, Lopez AD, Rodgers A, Vander Hoorn S, Murray CJ, Group CRAC (2002) Selected major risk factors and global and regional burden of disease. The Lancet 360, (9343), 1347-1360

263. Clougherty JE, Levy JI, Kubzansky LD, Ryan PB, Suglia SF, Canner MJ, Wright RJ (2007) Synergistic effects of traffic-related air pollution and exposure to violence on urban asthma etiology. Environ Health Perspect, 1140-1146

264. Davies HW, Vlaanderen J, Henderson S, Brauer M (2009) Correlation between co-exposures to noise and air pollution from traffic sources. Occup Environ Med 66, (5), 347-350

265. Clougherty JE, Kubzansky LD (2009) A framework for examining social stress and susceptibility to air pollution in respiratory health. Environ Health Perspect 117, (9), 1351

266. Zhang X, Yang L, Li Y, Li H, Wang W, Ye B (2012) Impacts of lead/zinc mining and smelting on the environment and human health in China. Environmental monitoring and assessment 184, (4), 2261-2273

267. Banza CLN, Nawrot TS, Haufroid V, Decrée S, De Putter T, Smolders E, Kabyla BI, Luboya ON, Ilunga AN, Mutombo AM (2009) High human exposure to cobalt and other metals in Katanga, a mining area of the Democratic Republic of Congo. Environ Res 109, (6), 745-752

268. Qu C-S, Ma Z-W, Yang J, Liu Y, Bi J, Huang L (2012) Human exposure pathways of heavy metals in a lead-zinc mining area, Jiangsu Province, China. PloS one 7, (11), e46793

269. Cordy P, Veiga MM, Salih I, Al-Saadi S, Console S, Garcia O, Mesa LA, Velásquez-López PC, Roeser M (2011) Mercury contamination from artisanal gold mining in Antioquia, Colombia: The world's highest per capita mercury pollution. Sci Total Environ 410, 154-160

270. Brugge D, Cajero M, Downs M, Durant JL, George CM, Henio-Adeky S, Nez T, Manning T, Rock T, Seschillie B (2009) Development of risk maps to minimize uranium exposures in the Navajo Churchrock mining district. Environmental Health 8, (1), 29

271. Oyarzún J, Oyarzún R (2011) Sustainable development threats, inter-sector conflicts and environmental policy requirements in the arid, mining rich, northern Chile territory. Sustainable Development 19, (4), 263-274

272. Quigley D, Sanchez V, Handy D, Goble R, George P (2000) Participatory research strategies in nuclear risk management for native communities. Journal of health communication 5, (4), 305-331

273. Lewis DR (1995) Native Americans and the environment: a survey of twentieth-century issues. American Indian Quarterly 19, (3), 423-450

274. LaDuke W (2017) All our relations: Native struggles for land and life. Haymarket Books,

275. Sandloss J, Keeling A (2012) Claiming the New North: Development and Colonialism at the Pine Point Mine, Northwest Territories, Canada. Environment and History 18, (1), 5-34

276. Leech JA, Wilby K, McMullen E, Laporte K (1996) The Canadian Human Activity Pattern Survey: report of methods and population surveyed. Chronic Dis Can 17, (3-4), 118-123

277. Klepeis NE, Nelson WC, Ott WR, Robinson JP, Tsang AM, Switzer P, Behar JV, Hern SC, Engelmann WH (2001) The National Human Activity Pattern Survey (NHAPS): a resource for assessing exposure to environmental pollutants. J Expo Anal Environ Epidemiol 11, (3), 231-252

278. Auffan M, et al. (2009) Towards a definition of inorganic nanoparticles from an environmental, health and safety perspective. Nature nanotechnology 4, (10), 634-641

279. Balogh LP (2010) Why do we have so many definitions for nanoscience and nanotechnology? Nanomedicine: Nanotechnology, Biology and Medicine 6, (3), 397-398

280. International Organization for Standardization (1995) ISO 7708:1995 Air quality - Particle size fraction definitions for health-related sampling.

281. World Health Organization (WHO) (2006) WHO Air quality guidelines for particulate matter, ozone, nitrogen dioxide and sulfur dioxide. Summary of risk assessment. Geneva, Switzerland

282. Environment and Climate Change Canada (ECCC) (2013) Canadian Ambient Air Quality Standards. http://www.ec.gc.ca/default.asp?lang=En&n=56D4043B-1&news=A4B2C28A-2DFB-4BF4-8777-ADF29B4360BD. Accessed 2017-05-26

283. Ontario Ministry of the Environment (OME) (2012) Ontario's Ambient Air Quality Criteria.

284. Ministère du Développement durable dlEedlLclccM (2016) Normes et critères de qualité de l'atmosphère.

285. Zhong L, Goldberg MS, Gao Y-T, Jin F (1999) Lung cancer and indoor air pollution arising from Chinese-style cooking among nonsmoking women living in Shanghai, China. Epidemiology, 488-494

286. Lee SC, Li W-M, Yin Chan L (2001) Indoor air quality at restaurants with different styles of cooking in metropolitan Hong Kong. Sci Total Environ 279, (1), 181-193. doi:https://doi.org/10.1016/S0048-9697(01)00765-3

287. Chafe ZA, Brauer M, Klimont Z, Van Dingenen R, Mehta S, Rao S, Riahi K, Dentener F, Smith KR (2014) Household cooking with solid fuels contributes to ambient PM2. 5 air pollution and the burden of disease. Environ Health Perspect 122, (12), 1314

288. World Health Organization (WHO) (2016) Household air pollution and health. World Health Organization (WHO). http://www.who.int/mediacentre/factsheets/fs292/en/. Accessed October 9, 2017 2017

289. Health Canada (2012) Guidance for fine particulate matter (PM2.5) in residential indoor air. https://www.canada.ca/en/health-canada/services/publications/healthy-living/guidance-fine-particulate-matter-pm2-5-residential-indoor-air.html. Accessed 2017-05-26

290. Stocker T (2014) Climate change 2013: the physical science basis: Working Group I contribution to the Fifth assessment report of the Intergovernmental Panel on Climate Change. Cambridge University Press,

291. Coquet S, Ariya PA (2000) Kinetics of the gas-phase reactions of Cl atom with selected C2–C5 unsaturated hydrocarbons at 283 < T < 323 K. International Journal of Chemical Kinetics 32, (8), 478-484. doi:10.1002/1097-4601(2000)32:8<478::AID-KIN5>3.0.CO;2-S

292. Ryzhkov AB, Ariya PA (2003) A theoretical study of the reactions of carbonyl oxide with water in atmosphere: The role of water dimer. Chemical physics letters 367, (3), 423-429

293. Ariya PA, Niki H, Harris GW, Anlauf KG, Worthy DE (1999) Polar sunrise experiment 1995: hydrocarbon measurements and tropospheric Cl and Br-atoms chemistry. Atmos Environ 33, (6), 931-938

294. Avzianova EV, Ariya PA (2002) Temperature-dependent kinetic study for ozonolysis of selected tropospheric alkenes. International journal of chemical kinetics 34, (12), 678-684

295. Poulain AJ, Garcia E, Amyot M, Campbell PG, Ariya PA (2007) Mercury distribution, partitioning and speciation in coastal vs. inland High Arctic snow. Geochimica et Cosmochimica Acta 71, (14), 3419-3431

296. Grannas AM, Jones AE, Dibb J, Ammann M, Anastasio C, Beine HJ, Bergin M, Bottenheim J, Boxe CS, Carver G, Chen G, Crawford JH, Dominé F, Frey MM, Guzmán MI, Heard DE, Helmig D, Hoffmann MR, Honrath RE, Huey LG, Hutterli M, Jacobi HW, Klán P, Lefer B, McConnell J, Plane J, Sander R, Savarino J, Shepson PB, Simpson WR, Sodeau JR, von Glasow R, Weller R, Wolff EW, Zhu T (2007) An overview of snow photochemistry: evidence, mechanisms and impacts. Atmos Chem Phys 7, (16), 4329-4373. doi:10.5194/acp-7-4329-2007

297. Côté V, Kos G, Mortazavi R, Ariya PA (2008) Microbial and “de novo” transformation of dicarboxylic acids by three airborne fungi. Sci Total Environ 390, (2), 530-537

298. Mortazavi R, Attiya S, Ariya P (2015) Arctic microbial and next-generation sequencing approach for bacteria in snow and frost flowers: selected identification, abundance and freezing nucleation. Atmospheric Chemistry and Physics 15, (11), 6183-6204

299. Ariya PA, Domine F, Kos G, Amyot M, Côté V, Vali H, Lauzier T, Kuhs WF, Techmer K, Heinrichs T, Mortazavi R (2011) Snow – a photobiochemical exchange platform for volatile and semi-volatile organic compounds with the atmosphere. Environmental Chemistry 8, (1), 62-73. doi:10.1071/EN10056

300. Nazarenko Y, Kurien U, Nepotchatykh O, Rangel-Alvarado RB, Ariya P (2016) Role of Snow and Cold Environment in the Fate and Effects of Nanoparticles and Select Organic Pollutants from Gasoline Engine Exhaust. Environmental Science: Processes & Impacts 18, (2), 190-199. doi:10.1039/C5EM00616C

301. Nazarenko Y, Fournier S, Kurien U, Rangel-Alvarado RB, Nepotchatykh O, Seers P, Ariya PA (2017) Role of snow in the fate of gaseous and particulate exhaust pollutants from gasoline-powered vehicles. Environmental Pollution 223, 665-675. doi:http://dx.doi.org/10.1016/j.envpol.2017.01.082

302. Rangel-Alvarado RB, Nazarenko Y, Ariya PA (2015) Snow-borne nanosized particles: Abundance, distribution, composition, and significance in ice nucleation processes. Journal of Geophysical Research: Atmospheres 120, (22), 11,760-711,774. doi:10.1002/2015JD023773

303. Baya A, Van Heyst B (2010) Assessing the trends and effects of environmental parameters on the behaviour of mercury in the lower atmosphere over cropped land over four seasons. Atmospheric Chemistry & Physics 10, (17),

304. Cheng I, Zhang L, Mao H, Blanchard P, Tordon R, Dalziel J (2014) Seasonal and diurnal patterns of speciated atmospheric mercury at a coastal-rural and a coastal-urban site. Atmospheric Environment 82, 193-205. doi:https://doi.org/10.1016/j.atmosenv.2013.10.016

305. Lee G-S, Kim P-R, Han Y-J, Holsen TM, Seo Y-S, Yi S-M (2016) Atmospheric speciated mercury concentrations on an island between China and Korea: sources and transport pathways. Atmos Chem Phys 16, (6), 4119-4133

Appendices

Table 0.1. Analytical Methodologies for Quantifying Atmospheric Gaseous and Particulate Mercury

Reference	Analysis	Sample Collection	Sample Preparation	Separation	Analysis
Braman and Johnson 1974 [81]	Total Mercury	Gold-coated glass beads	Air drawn through speciation stack at 1.5 L/min passes through glass wool filter before a gold-coated glass trap.	Heated to 470 °C, GEM is transferred to the detector with helium carrier gas.	DC Discharge Emission Spectroscopy
	Gaseous Elemental Mercury	Silver coated glass beads	Air drawn through speciation stack at 1.5 L/min passes through 1) glass wool filter, 2) HCl treated Chromosorb W trap, 3) NaOH treated Chromosorb W trap, and a combined silvered glass followed by gold-coated glass bead trap.		
	Gaseous Hg(II) type compounds	HCl treated – Chromosorb-W		Heated to 250 °C for 12 minutes and transferred to a gold trap heated 470 °C with helium carrier gas.	
	Gaseous Methylmercury (II) type compounds	NaOH treated – Chromosorb-W		Heated to 300 °C for 6 minutes and transferred to a gold trap heated 470 °C with helium carrier gas.	
	Gaseous Dimethylmercury	Gold-coated glass beads		Heated to 470 °C and transferred to the detector with helium carrier gas.	
	Particulate Bound Mercury	Quartz Type A Filters		Heated in a blanked pyrex tube at 550 °C and transferred to the detector with helium carrier gas.	
Dumarey et al. 1978, 1979 [82,83]	Total Gaseous Mercury	Gold-coated sand	Air is sampled between 2.5 – 3.5 L/min through a filter on to gold-coated sand absorption tubes.	Desorption at 0.1 L/min at 800 °C.	Mercury Analyzer System – Coleman MAS-50
	Particulate Mercury	Quartz Filter		Filter is heated to 800 °C and mercury-free air sweeps mercury through 800 °C heated silver wool, silica, alumina, room-temperature magnesium perchlorate to remove interferents before amalgamation to a gold-trap.	
Schroeder and Jackson 1985, 1987 [16,76]	Gaseous Elemental Mercury	Gold Wire	Ambient air is drawn through a quartz fibre filter and then through a four sorbent speciation train at 6 L/min for 10 to 60 minutes. Chromosorb-W (HCl) and Carbosieve B sorbent traps were held at 180 °C while the Gold Trap and Tenax GC sorbent trap was at ambient temperatures. Particulate mercury was collected for 24 hours.	Each collector tube is sequentially heated between 250 °C and 450 °C for 5 – 10 minutes and desorbed to a pyrolyzer. Elemental mercury from the decomposition of species is collected on a gold trap, concentrated and desorbed at 500 °C and measured using a spectrophotometer. Particulate mercury was decomposed to GEM and desorbed at 900 °C	AFS - Barringer
	Gaseous Mercuric Chloride	HCl treated – Chromosorb-W			
	Gaseous Methylmercuric Chloride	Tenax GC			
	Gaseous Dimethyl Mercury	Carbosieve B			
	Particulate Bound Mercury	Quartz Filter			

Brosset and Lord 1995 [84]	Methylmercury chloride	MilliQ Water	Ambient air was drawn through a quartz bubble with 200 mL of milliQ at sub L/min flow rates for 6 to 10 days. Methylmercury chloride was extracted using dichloromethane and concentrated in a small volume of milliQ by heating off the organic layer and collected on a Carbotrap column	Analytes were introduced to a cryogenic GC column and separated, pyrolyzed to GEM at 700-800 °C.	CVAFS
Stratton et al. 2001 [94]	Reactive Gaseous Mercury	HCl Absorbing Solution	Sampling at 15 – 20 L/min for 1 – 2 hours using a refluxing mist chamber with a fine mist of 20 mL of HCl/NaCl absorbing solution. A Teflon membrane retains the Hg(II)-enriched absorbing solution.	The absorbing solution and rinse solution for the chamber are withdrawn and reduced with stannous(II) chloride ($SnCl_2$) and measured as GEM.	CVAFS – Brooks Rand
Sheu and Mason 2001 [14]	Gaseous Oxidized Mercury	Cation Exchange Membranes	Sampling at 3 – 5 L/min over 6 and 24 hours through a five-stage filter pack with Teflon and cation exchange membranes.	Reduction by $SnCl_2$.	CVAFS
	Particulate Bound Mercury	Teflon Filters		Filters oxidized in BrCl for 30 minutes followed by pre-reduction using hydroxylamine hydrochloride and reduction by $SnCl_2$.	
Dommergue et al. 2002 [77]	Total Gaseous Mercury	Gold Trap	Sampling at 1 L/min for 15 minutes through 0.5 µm Teflon filter with amalgamation to gold trap.	Double amalgamation and thermal desorption.	CVAFS – Gardis 1A+
Sakata and Marumoto 2001 [113]	Particulate Bound Mercury	Quartz Filters	Sampling at 1200 L/min for 24 hours.	Thermal desorption to AAS.	CVAAS – Nippon Instruments AM-2
	Total Gaseous Mercury	Gold Trap	Sampling at 0.5 LPM for 55 minutes through Teflon filter with amalgamation to gold trap.	Thermal desorption to AAS.	
Landis et al. 2002 [93]	Gaseous Elemental Mercury	Gold Trap	Sampling at 1.5 L/min for 5 minute intervals.	Thermal desorption of amalgamated mercury to detector.	CVAFS – Tekran 2537
	Gaseous Oxidized Mercury	KCl Denuder	Sampling at 10 L/min through a 2.5 µm cut-point impactor maintained at 50 °C followed by a Teflon Filter Pack or quartz thermal filter tube for 1-2 hours.	Pyrolyzer heated to 800 °C to decompose mercury compounds to GEM. Filter heated to 800 °C to measure PBM followed by thermal desorption at 500 °C of the denuder in a clamshell furnace to decompose GOM to GEM.	CVAFS – Tekran 1130
	Particulate Bound Mercury	Quartz Filters			CVAFS – Tekran 1135
Freitas et al. 2005 [54]	Particulate Bound Mercury	Polycarbonate Filters	Sampling at 15 – 17 L/min for 10 min every 2h for 1 week using a Gent-type, stacked-filter unit sampler with PM10 and PM2.5 fractions.	Filters placed in polyethylene or Al foil containers were subjected to thermal neutral irradiation for 7 hours with Hg determined based on gamma emissions 4 weeks later.	Instrumental Neutron Activation Analysis (INAA)
Lynam et al. 2005 [109]	Particulate Bound Mercury	Quartz Filter	Sampling at 10 LPM through a 2.5 µm Teflon-coated cyclone, to denuded and undenuded filters where KCl and/or KI denuders were heated to 50 °C. Sampling times ranged for 10, 14 and 24 hours.	Filters heated to 700 °C and swept by argon carrier gas to an ICP-MS.	ICP-MS
Xiu et al. 2005[114]	Particulate Bound Mercury	Glass Fiber and Quartz Fiber Filter		Filters are digested in $KMnSO_4/H_2SO_4$ solution at 95 °C under reflux and then Hg^{2+} is reduced by $SnCl_2$ to GEM.	CVAAS

	Inert Particulate Phase Mercury		Sampling at 600 L/min for 24 hours through four size fractionator with 18 µm, 8 µm, 3.7 µm and 1.6 µm cut-offs.	The difference between TPM and the sum of VPM and RPM	
	Reactive Particulate Phase Mercury			VPM Filters are sonicated for 30 minutes to release RPM.	
	Volatile Particulate Phase Mercury			Filters extracted with 0.33 M HCl and solution bubbled with 600 L/min of N_2. Vapour collected in $KMnSO_4/H_2SO_4$ and analyzed as above.	
Fostier and Michelazzo 2006 [51]	Total Gaseous Mercury	Gold-coated glass grains	Ambient air is drawn through a humidity-removing soda-lime trap and then pre-concentrated on a gold trap at 300 mL/min for 2 hours.	Mercury is decomposed and desorbed to an analytical column using argon.	AFS – Brooks Rand
	Particulate Bound Mercury	Quartz Filter	Air is sampled at 30 L/min for 24 hours according to USEPA method. Filters are stored in Petri dishes.	Filters are digested, and PBM is oxidized in 10% nitric acid with BrCl, followed by reduction with SnCl2 in 10% HCl. The solution is purged with argon drawing mercury to the gold trap.	
Choi et al. 2008 [19]	Gaseous Elemental Mercury	Gold Trap	Sampling at 10 L/min through a 2.5 µm cyclone for 1 hr for KCl-denuder/quartz filter and 5 minutes for gold cartridges.	Desorption occurs over 1 hour at 800 °C for the particulate filter and subsequently at 500 °C for the KCl denuder.	CVAFS – Tekran 2537
	Reactive Gaseous Mercury	KCl coated Quartz Denuder			CVAFS – Tekran 1130
	Particulate Bound Mercury	Quartz Filter			CVAFS – Tekran 1135
Wängberg et al. 2008 [21]	Total Gaseous Mercury	Gold Trap	Sampling at 200-400 mL/min through a gold surface in a quartz glass tube.	Mercury desorbed at 400-500 °C and carried by argon flow to a second gold surface quartz trap before a second desorption to a CVAFS detector.	CVAFS – Tekran 2500
			Sampling at 0.5 L – 15 through a gold trap for 5 minutes.	Mercury desorbed to CVAFS detected while second Au trap samples.	CVAFS - Tekran 2537A
	Reactive Gaseous Mercury	KCl Denuder	Sampling at 10 L/min for 12 hours through 2.5 µm impactor into a denuder heated to 50 °C.	Denuders brought into the lab, purged with inert N_2 or Argon and heated to 500 °C and decomposed to GEM and measured by CVAFS.	CVAFS – Tekran 2500
		KCl Denuder and Quartz Filter Assembly	Sampling at 10 L/min for 2 hours through a 2.5 µm impactor into a denuder and quartz filter.	Quartz filter is heated 800 °C, and PBM is detected as GEM by CVAFS. The KCl denuder is subsequently heated to 500 °C and detected as GEM by CVAFS.	CVAFS – Tekran 1130/2537A
	Particulate Bound Mercury				CVAFS – Tekran 1135/2537A
		AES Mini-Trap	Sampling at 3-5 L/min for 24 hours. through quartz micro-fibre filter in a quartz glass tube with a 4 m/s wind speed cut-off of 7 µm diameter particles.	Mercury is pyrolyzed at 800 – 900 °C and decomposed to GEM and captured on a gold trap.	CVAFS – Tekran 2500
Rutter et al. 2008 [133]	Reactive Gaseous Mercury	KCl coated Quartz Filters		Heated to 500 °C in sample furnace. Flow through 900 °C pyrolyzer to decompose in-tact GOM.	CVAFS – Tekran 2537A

	Particulate Bound Mercury	Uncoated Quartz Filters	Teflon-coated aluminum particle cyclone removes particles 2.5 microns. 92 L/min through successive quartz and KCl-coated quartz filters.	Heated to 900 °C in sample furnace.	
	Reactive Gaseous Mercury	KCl Denuder		Thermal reduction to GEM at 500 °C before passing through a 900 °C pyrolyzer and soda lime trap and CVAFS.	CVAFS – Tekran 1130
	Particulate Bound Mercury	Particle Filter		Filters heated to 850 °C, pyrolyzed to 850 °C and before CVAFS.	CVAFS – Tekran 1135
Song et al. 2009 [17]	Gaseous Elemental Mercury	Gold Trap	Outflow from Quartz Filter sampled at 1 L/min	Flush KCl denuder and Quartz filters with zero-air for 15 minutes. Heat to 800 C and 600 C for 15 minutes to convert PBM and GOM to GEM.	CVAFS
	Reactive Gaseous Mercury	KCl Denuder	The impactor excluded particles greater than 2.5 um in diameter. Air is drawn at a flow rate of 10 L/min through theKCl denuder and then the Quartz Filter.		
	Particulate Bound Mercury	Quartz Filter			
Xiu et al. 2009 [88]	Particulate Bound Mercury	Glass Fibre Filter	Air was sampled at 600 L/min four 24 hours through a four-stage fractionator: with an 18 µm inlet cutoff, and three stages with 8.0, 3.7, 1.6 µm cutoffs and a final filter.	Filters were digested in 10 mL of 5% $KMnSO_4$ and 5 mL 1:1 H_2SO_4 at 95 °C under reflux. Then Hg^{II} is reduced with $SnCl_2$ with NH_2OH•HCl to GEM.	CVAAS
	Exchangeable PM			Filters are digested in 15 mL 0.1 M $CaCl_2$ with sonication followed by analysis for PBM.	
	HCl-soluble PM			Filters are then digested in 20 mL 1 M HCl and 0.5 mL 1% $CuSO_4$ stabilizer, sonicated and analyzed for PBM.	
	Elemental PM			Filters are then digested in 10 mL 2 M HNO_2, sonicated and analyzed for PBM.	
	Residual PM			Filters are finally digested as per PBM analysis.	
Arruti et al. 2010 [149]	Particulate Bound Mercury	Glass Fibre Filters	High volume sampler operated at 500 L/min for 24 hours.	Microwave digestion using nitric acid – hydrogen peroxide acid mixture slowly heated to 185 °C.	ICP-MS
Baya and Van Heyst 2010 [303]	Gaseous Elemental Mercury	Gold Trap	Air drawn through 0.45 µm Teflon filter from two intake heights, 0.35 m and 1.5 m above ground cover, for 10 minutes.	Amalgamated gold thermally desorbed at 500 °C.	CVAFS – Tekran 2537A
	Gaseous Oxidized Mercury	KCl Denuder	Sampling at 10 L/min for 2 hours. See Landis et al 2002.	Desorbed at 500 °C and converted to GEM.	CVAFS – Tekran 1130
	Particulate Bound Mercury	Quartz Filter		Pyrolyzed at 800 °C and converted to GEM.	CVAFS – Tekran 1135
Liu et al. 2010 [41]	Gaseous Elemental Mercury	Gold Trap	Sampling at 10 L/min through impactor removing particles >2.5 um, KCl denuder, Quartz Filter and finally gold trap.	Amalgamated gold thermally desorbed at 500 °C.	CVAFS – Tekran 2537
	Reactive Gaseous Mercury	KCl Denuder		Heated to 500 °C to convert to Hg^0	CVAFS – Tekran 1130
	Particulate Bound Mercury	Quartz Filter Disk		Heated to 800 °C to convert to Hg^0	CVAFS – Tekran 1135

Soerensen et al. 2010 [52]	Gaseous Elemental Mercury	Gold Trap	Sampling at 1 L/min for 5 minute intervals over 80 minutes.	Gold trap thermally desorbed at 500 °C.	CVAFS – Tekran 2537A
	Gaseous Oxidized Mercury	KCl Denuder	Sampling for 80 minutes.	40 minute thermal desorption period	CVAFS – Tekran 1130
Choi et al. 2013 [104]	Gaseous Elemental Mercury	Gold Trap	Sampling at 10 LPM for 2 hours followed by a 1-hour desorption process according to Mercury Monitoring Network SOPs (currently AMNet). Soda lime traps prevented gold-trap passivation from intereferents.	Thermal desorption of amalgamated mercury.	CVAFS – Tekran 2537
	Gaseous Oxidized Mercury	KCl Denuder		See Landis et al. 2002 and Choi et al. 2008	CVAFS – Tekran 1130
	Particulate Bound Mercury	Quartz Filter Disk		See AMnet guidelines for current standard operating procedures.	CVAFS – Tekran 1135
Huang et al. 2013 [141]	Gaseous Elemental Mercury	Gold Trap	Ambient air, scrubbed of particles, sampled at 1 L/min.	Thermal desorption of amalgamated mercury. See AMnet guidelines for standard operating and cleaning procedures	CVAFS – Tekran 2537
	Gaseous Oxidized Mercury	KCl Denuder	Ambient air, scrubbed of particles, sampled at 4 L/min for manual denuders for either 1 or 2 hours followed by 1 hour desorption time.	Thermal desorption from denuder followed by pyrolysis decomposition to GEM. See AMnet guidelines for standard operating and cleaning procedures	CVAFS – Tekran 1130
		Cation Exchange Membranes	Sampling at 1 L/min for 8 hours through two membranes in series.	Membranes were heated in a tube furnace whose temperature was ramped 2.2 °C/min from 60 °C to 185 °C. Desorbed mercury passed through a pyrolyzer to fully convert species to GEM, before passing through soda lime and Teflon particulate filter on route to the CVAFS. Residual mercury analyzed using EPA Method 1631E.	CVAFS – Tekran 2537
		Nylon Membranes			
Weigelt et al. 2013 [139]	Gaseous Elemental Mercury	Gold Trap	Integrated sampling with GOM collected on 50 °C KCl denuder and PBM on regenerable filter assembly at 10.0 L/min for 3 hours. Air then filtered through a soda lime trap and 0.2 µm PTFE filter for 5 minute GEM sampling	GOM and PBM thermally decomposed to GEM according to specifications in GMOS Hg Speciation SOP.	CVAFS – Tekran 2537
	Gaseous Oxidized Mercury	KCl Denuder			
	Particulate-Bound Mercury	Quartz Filters		Species are sequentially thermally desorbed and measured as GEM	CVAFS – Tekran 1130
	Total Gaseous Mercury	Gold Trap	Ambient air was sampled at 1.0 L/min through a 0.2 µm PTFE filter for 15 minutes to the Tekran analyzer. No soda lime trap was used following DIN EN 15852 standards.	Gold Trap in the analyzer heated to convert mercury species to GEM.	CVAFS – Tekran 2537
Cheng et al. 2014 [304]	Gaseous Elemental Mercury	Gold Trap	Sampling at 10 L/min for 3 hour sampling cycle: 2 hours of cycling and 1 hour of analysis, and 5 minute GEM samples. See AMnet guidelines for standard operating procedures	See Landis et al. 2002	CVAFS – Tekran 2537A
	Gaseous Oxidized Mercury	KCl Denuder			CVAFS – Tekran 1130
	Particulate Bound Mercury	Quartz Filter			CVAFS – Tekran 1135

Zverina et al. 2014 [39]	Morphology and Elemental Analysis	Fibrous Filters	Sample was fixed to glass plate and coated with a layer of 20 nm thick gold.	None	SEM-EDX – JEOL JSM-6490 LV
	Total Mercury		Sample placed in nickel boat.	Combustion of solid sample through dry ashing.	CVAAS – Altec AMA-254
	Water extractable Mercury		Trapped dust samples are dried at ambient temperatures and screened through four-sieve size fractions. 100 mg samples are successively extracted using leaching solutions. See Coufalik et al. 2012.	Samples extracted with deionized water for 18 hours in a end-over-end shaker set to 300 min^{-1}, centrifuged then analyzed. Solid residue is rinsed and extracted in the next step.	
	Acid-released Mercury			Extraction with 0.5 M HCl.	
	Organic-bound Mercury			Extraction with 0.2 M KOH.	
	Elemental and complex bound mercury			Extraction with 50% (m/v) HNO_3. Elemental and complex bound fractions are separated through a 48hour desorption at 105 °C.	
	Residual mercury			Solid residue from previous extraction is dried for 48 hour at 45 °C and analyzed.	
Jen et al. 2014 [26]	Total Gaseous Mercury	Gold-coated Sand	Sampling at 0.3 L/min collected for 24 hours.	Desorbed between 300 – 400 °C.	CVAFS – Brooks Rand Model III
	Particulate Bound Mercury	Glass Fiber Filters	Sampling at 30L/min collected for 24 hours.	The filter is microwave digested with 1.6M trace metal grade nitric acid, BrCl oxidized and subsequently reduced with SnCl2 before being purged with inert Argon and collected on gold-coated sand.	
Steffen et al. 2014 [87]	Gaseous Elemental Mercury	Gold Trap	Sampling at 10.0 L/min through a Teflon-coated, >2.5 µm particle-removing impactor. Flows through KCl-coated denuder, particulate filter before 1 L/min split to measure GEM. GOM and PBM collected for 2 or 3 hours. See Landis et al. 2002.	Pyrolyzer is heated to 800 °C, thermally decomposing PBM to GEM. Denuder is heated to 600 °C to thermally desorb and decompose GOM to GEM which subsequently passes through heated pyrolyzer to the detector.	CVAFS – Tekran 2537
	Gaseous Oxidized Mercury	KCl Denuder			CVAFS – Tekran 1130
	Particulate Bound Mercury	Quartz Filter			CVAFS – Tekran 1135
Deeds et al. 2015 [142]	Mercury(II) Bromide Mercury(II) Chloride	Shredded PFA Teflon	Sampling at 1L/min through traps heated to 50 °C for 12 – 24 hours.	Analytes are heated in a modified APCI-MS inlet at 200 °C for 1.2 minutes before desorbing using 1 L/min SF_6:Isobutane carrier gas drawing analyte into the APCI ion source forming mercury(II) halide-fluoride adducts.	APCI-MS – Agilent 6130
Marumoto et al. 2015 [111]	Gaseous Elemental Mercury	Gold Trap	Sampling at 10 L/min through 2.5 µm impactor. GEM measured every 5 minutes, and GOM and PBM collected every 2 hours with 1 hour of analysis time.	See Tekran 2002 – Tekran 2537 User Manual	CVAFS – Tekran 2537B
	Gaseous Oxidized Mercury	KCl-Denuder		See Tekran - Tekran 1130 Use Manual	CVAFS – Tekran 1130
	Particulate Bound Mercury	Quartz Fibre Filter		See Tekran - Tekran 1135 Use Manual	CVAFS – Tekran 1135

	Total Gaseous Mercury	Gold Trap	Sampling through PTFE filter at 0.5 L/min for 12 minutes.	3 minute thermal desorption and analysis time.	CVAFS – Nippon AM-5
Schleicher et al. 2015 [55]	Particulate Bound Mercury	Quartz Fibre Filters	Sampling at 3.33 L/min for $PM_{2.5}$ samples and 16.67 L/min for TSP.	Oxygen-stream calcination followed by gold trap amalgamation from 5 mm diameter filter punches.	CVAAS – Milestone DMA-80
Gustin et al. 2016 [143]	Gaseous Elemental Mercury	Gold Trap	See AMnet guidelines. Sampling at 7 LPM through 3.0 µm impactor, denuder and particulate filter following a 1 hour sampling and 1 hour desorption cycle.	See Landis et al. 2002.	CVAFS – Tekran 2537
	Gaseous Oxidized Mercury	KCl Denuder			CVAFS – Tekran 1130
	Particulate Bound Mercury	Quartz Filter			CVAFS – Tekran 1135
	Reactive Mercury - UNRRMAS	Cation Exchange Membranes	Six port sampling system with three sets of two cation exchange and three sets of two nylon membranes in series.	See Huang et al. 2013	
		Nylon Membranes			
Jones et al. 2016 [13]	Mercury(II) Bromide Mercury(II) Chloride	Quartz wool Filters	Sampling at 30 L/min for 3 hr.	Filters placed in a deactivated fused silica coated stainless steel chamber with analytes desorbed between 80 – 160 °C with UHP Helium. A cryotrap focuser was set at 0 °C and analytes were desorbed at 240 °C into an 100% dimethyl polysiloxane GC column set to 140 – 220 °C.	GC-EI-MS – Shimadzu GC-2010 Plus & QP2010 Ultra MS
		Nylon membranes	Sampling at 1 L/min for 2 weeks. See Huang et al. 2013.		
Lee et al. 2016 [305]	Total Gaseous Mercury	Gold Cartridges	Sampling at 1.0 L/min for five minutes on alternating gold cartridges.	Mercury is thermally desorbed from the non-sampling cartridge every 5 minutes.	CVAFS – Tekran 2537B
	Gaseous Oxidized Mercury	KCl Denuder	Sampling at 10 L/min through an elutriator, impactor, KCl denuder and quartz filter for 12 hours between beginning at 7 am and 7 pm. Heated to 45 °C.	The KCl denuder is desorbed at 525 °C.	
	Particulate Bound Mercury	Quartz Filter		The quartz filter is desorbed at 900 °C and the denuder at 525 °C, manually, and resulting GEM measured.	
Pyta et al. 2016 [2]	Particulate Bound Mercury	Quartz Filters	Sampling at 21.67 L/min through 13-stage impactor ($PM_{0.03}$ to PM_{40}).	Pyrolysis of PM samples at 700 °C, with interfering nitrogen oxides, sulfur oxides and halides removed through additives and catalytic oxidation at 850 °C. Mercury trapped on gold trap and thermally desorbed.	CVAAS – Nippon MA-2 Analyzer
Siudek et al. 2016 [49]	Particulate Bound Mercury (+ Retained Gaseous Species)	Quartz and Glass-Fiber Filters	Pre-combust fiters at 500 °C for 5 hours. Sampling at 30 L/min for 24 hr at an urban site and 1 week at a rural site. No preceding denuder.	Microwave acid digestion in 60% HNO_3 following EPA 1631E.	CVAFS –P.S. Analytical 10.025
Wängberg et al. 2016 [4]	Gaseous Elemental Mercury	Gold Traps	Sampling at 10 L/min for 3 hours through 2.5 µm impactor through KCl-coated denuder and quartz fibre filter and then before 1 LPM is split to the CVAFS detector for 5-minute GEM sampling.	Analysis cycle of 1 hour with pyrolysis of PBM followed by decomposition of GOM from the KCl denuder to GEM. See Landis et al 2002)	CVAFS – Tekran 2537B
	Gaseous Oxidized Mercury	KCl denuder			CVAFS – Tekran 1130
	Particulate Bound Mercury	Quartz Fibre Filter			CVAFS – Tekran 1135

Cheng et al. 2017 [151]	Particulate Bound Mercury	Quartz Filter	Sampling at 100 L/min for 23 hours. See Xiu et. al 2009.	Microwave digestion using 1.6M HNO_3 at 160 °C and 70 psi for 20 minutes following US EPA IO-5.0. The digest was diluted, mercury was oxidized using BrCl and $NH_2OH{\cdot}HCl$ and subsequently reduced using $SnCl_2$ to GEM following EPA Method 1631E.	CVAFS – AFS-9130
	HCl-soluble Particulate Mercury			See Xiu et. al 2009.	
	Elemental-soluble Particulate Mercury				
	Residual Particulate Mercury				
Duan et al. 2017 [43]	Gaseous Element Mercury	Gold Cartridges	Sampling at 1 L/min for 5 minute time resolution.	Preceded by collection of GOM and PBM.	CVAFS – Tekran 2437B
	Gaseous Oxidized Mercury	KCl coated quartz denuder	Sampling at 10 L/min for 1 hour through a sampling train of the denuder followed by the PBM filter. Sampling is followed by 1 hour desorption.	Heated to 500 °C and thermally decomposed to GEM.	CVAFS – Tekran 1130
	Particulate Bound Mercury	Quartz Filters		Preceded by collection of GOM. Heated to 800 °C and decomposed to GEM.	CVAFS – Tekran 1135
Guo et al. 2017 [3]	Particulate Bound Mercury	Quartz Filters	Pre-treat filters by baking at 550 °C. Sample at 100 L/min for 24 hours.	Calcination in O_2 stream and amalgamation on Gold Trap following US EPA Method 7473.	CVAAS – Teledyne Leeman Hydra-II_C
Huang et al. 2017 [65]	Gaseous Elemental Mercury	Gold Trap	Sampling for 1 hour followed by 1 hour desorption.	See Landis et al. 2002.	CVAFS – Tekran 2537
	Gaseous Oxidized Mercury	KCl Denuder			CVAFS – Tekran 1130
	Particulate Bound Mercury	Quartz Filters			CVAFS – Tekran 1135
	Reactive Mercury	Cation-Exchange Membranes	Two CEM in series deployed for 2 week sampling time. See Pierce and Gustin 2017	Digested following EPA Method 1631 E (Peterson et al. 2012)	CVAFS
	Reactive Mercury	Nylon Membranes		Thermally Desorbed and analyzed using EPA Method 1631 E (Huang et al. 2013)	CVAFS
Bełdowska et al. 2018 [71]	Particulate Bound Mercury	Glass Fibre Filters	Sampling at 23 L/min for 48–96 h until Hg^{Tot} > 2 ng.	Samples were burned in pure oxygen environments based on four, six or twenty-two temperature steps. (See Saniewska and Bełdowska 2017)	UV-AAS (Milestone DMA-80)
Fang et al. 2018 [62]	Gaseous Elemental Mercury	Gold coated Bead Trap	Sampling at 0.3 L/min	Double gold trap amalgamation. Carried by either He or Ar to detector.	CVAFS – Brooks Rand

	Reactive Mercury	KCl denuder	Sampling for 24 hours ± 1 hour at 10 L/min with a 2.5 µm impactor with the denuder temperature set to 50 °C.	Heated according to Landis et al., 2002. Analyte blown into the CVAFS using argon.	
	Total Gaseous Mercury	Gold coated Bead Trap	Sampling for 24 hours at 250 L/min through an in-house built, four stage gold trap sampling device.	Double gold trap amalgamation. Carried by either He or Ar to detector.	
	Particulate Bound Mercury	Projection Film Filter	Sampling for 24 hours at 200 L/min	The sample is dried at 200 °C before decomposed and combusted at 650 °C. Collected on gold amalgamator, subsequently heated and analyzed. (See Fang et al. 2016)	UV-AAS (Milestone DMA-80)
Kumari and Kulshrestha 2018 [9]	Particulate Bound Mercury	Quartz Filters – Whatman QM-A	Pre-treat filters by baking at 450 °C for 1 hour. Weigh filters after equilibrating in a desiccator for 24 hours. Sample at 910 – 1240 L/min for 24 hours.	Extraction from the filter using 5% nitric acid with sonication and passing through 0.22 mm nylon filter.	DPASV – Metrohm 797 VA Computrace

Table 0.2. Measurements of Gaseous Elemental, Oxidized and Particulate Mercury

Reference	Site	Time	GEM (ng/m^3)	GOM (pg/m^3)	PBM (pg/m^3)	Notes
Johnson and Braman 1974 [42]	Tampa, FL (USA)	3 August and 3 November 1973	4.5 [2, 7]	ND	1 [0, 2]	Urban Site
			11.0 ± 15.8 [2.4 – 49]	$HgCl_2$: 35 ± 81 [ND – 220] (× 10^3) MMC: 8 ± 10 [ND – 2.2] (× 10^3) DMM: 100 ± 350 [ND – 1000]	2.8 ± 4.8 [ND – 13] (× 10^3)	Industrial Sites
			2.9 ± 1.4 [ND – 4.4]	$HgCl_2$: 8.1 ± 8.9 [ND – 24] (× 10^3) MMC: 5.6 ± 7.6 [ND – 19] (× 10^3) DMM: ND	1.8 ± 2.5 [ND – 7] (× 10^3)	Suburban Sites
Dumarey et al. 1979 [82]	Ghent, East Flanders (Belgium)	> November 1978	1793 ± 553 [1448 – 2616]		NA	Mercury Laboratories
			103 ± 50 [54 – 158]			University Buildings
			789			Room – Mercury Spill
			7.16 ± 0.30			Outdoor Urban
Dumarey et al. 1980 [83]		> September 1979	1076 ± 849 [205 – 1903]		809,000 ± 626,000	Mercury Laboratories
			112 ± 24 [90 – 145]		25,000 ± 15,0000	University Buildings
			14 ± 14		320 ± 110	Outdoor Urban
Brosset 1987 [105]	Unknown	April – June 1982	1245 ± 1183 [520 – 3010]	1618 ± 580 [800 – 2070] (× 10^6)	NA	Coal Combustion Smoke
	Ekeröd, Skåne (Sweden)	July – November 1983	2.65	190		Rural site
	Onsala, Halland (Sweden)		2.52	140		Rural site
	Vindeln, Västerbotten (Sweden)		2.13	90		Rural site
Schroeder and Jackson 1987 [76]	Toronto, ON (Canada)	October 20 – November 9 1981	7.5 [3 – 24]	$HgCl_2$: ND MMC: 1.3 [ND – 3] (× 10^3) DMM: 200 [ND – 1900]	70 ± 17 [60 – 90]	Rural Site
			8.2 [4 – 13]	$HgCl_2$: 300 [ND – 1900] MMC: 2.2 [ND – 6.2] (× 10^3) DMM: 400 [ND – 1300]	70 ± 26 [40 –100]	Urban Site
			12.4 [8 – 19]	$HgCl_2$: ND MMC: 1.9 [0.2 – 3.5] (× 10^3) DMM: 700 [ND – 1600]	45 ± 21[30 – 60]	Near Incineration and Waste Treatment
			90.9 [62 – 110]	$HgCl_2$: 1.4 [0.5 – 2.4] (× 10^3) MMC: 800 [ND – 2200] DMM: 1.6 [ND – 3.7] (× 10^3)	160	Mercury Battery Manufacturing Site
Brosset and Iverfeldt 1989 [106]	Onsala, Halland (Sweden)	November 1987	3.01 ± 0.62 [2.23 – 4.15]	37.5 ± 22.5 [10 – 70]	85 ± 137 [10 – 420]	
	Onsala, Halland (Sweden)		NA	MMX: 75	NA	March

Reference	Site	Time	GEM (ng/m^3)	GOM (pg/m^3)	PBM (pg/m^3)	Notes
Brosett and Lord, 1995 [84]		March – September 1993		MMX: 19		April
				MMX: 26		May
				MMX: 6		June
				MMX: 2		July
				MMX: 4		August
Munthe et al. 2001 [73]	Tuscany, (Italy)	June 1998	NA	22 [3 – 41]	56 [13 – 314]	
			1.98 [12.8 – 3.38]			
			NA	18 ± 5 [10 – 23]	NA	Tubular Denuder
				20 ± 12 [4 – 35]		Annular Denuder
				17 ± 11 [3 – 32]		Mist Chamber
				39 ± 2 [37 – 41]		Annular Denuder Rinse
Sheu and Mason 2001 [14]	Solomons, MD (USA)	July 1998, October 1999	1.89 ± 0.94	40 ± 50	20 ± 50 [ND – 147]	Filter Pack Method
			1.83 ± 0.43 [1.03 – 2.50]			Filter Pack Method
Stratton et al. 2001 [94]	Oak Ridge, TN (USA)	March 1995	NA	123, 106	NA	Research Watershed
				361, 458	NA	Laboratory Rooftop
	Richmond, IN (USA)	September – October 1995	NA	102 ± 29	NA	0.05 M NaCl, Sept.
				94 ± 16	NA	0.25 HCl, Sept.
				141 ± 44	NA	0.25 NaCl/0.01 M HCl, Sept
				80 ± 14	NA	0.25 NaCl/0.01 M HCl, Oct
Dommergue et al. 2002 [77]	Grenoble, ARA (France)	November 1999, January, April, July 2000	3.4 ± 3.6 [0.1 – 37.1]		NA	Near Chlor-alkali plant
Feng et al. 2004 [140]	Toronto, ON (Canada)	November 2001	2.5 ± 0.5		24.8 ± 1.4 [23.2 – 25.9]	PM10
Freitas et al. 2005 [54]	Carregado, Greater Lisboa (Portugal)	March 1995 - 1996	No Data	No Data	140 ± 120	PM10; Oil Power Plant (PP)
	Faralhão, Greater Setúbal, (Portugal)	January 1995 - 1996			260 ± 280	PM2.5
					300 ± 380	PM10; Near Oil PP
	Monchique (Portugal)	November 1994 – July 1995			70 ± 40	PM2.5
					150 ± 160	PM10; Rural
	Palmela, Greater Setúbal (Portugal)	June 1994 - 1995			170 ± 120	PM2.5
					170 ± 120	PM10; Rural
	Sines (Portugal)	July 1994 – 1995			2300 ± 1200	PM2.5
					2700 ± 2000	PM10; near Coal PP
	Tapada do Outeiro, Greater Porto (Portugal)	August 1994 - 1995			970 ± 1100	PM2.5
					1500 ± 1800	PM10; Rural near Coal PP

Reference	Site	Time	GEM (ng/m^3)	GOM (pg/m^3)	PBM (pg/m^3)	Notes
Lynam and Keeler 2005 [109]	Detroit, MI (USA)	July 2001, 2002	No Data	No Data	[1 – 31], [4 – 20]	KCl denuded filters
					NA , [2 – 13]	KI denuder filters
					[3 – 39], [4 – 28]	KI/KCl denuded filters
					[2 – 18], [4 – 17]	Undenuded filters
Xiu et al. 2005[114]	Shanghai (China)	March 2002 – September 2003	No Data	No Data	370 ± 110 [233 – 529]	Urban Site
Wang et al. 2006 [58]	Beijing (China)	Monthly 2003; Seasonally 2004	No Data	No Data	680 ± 620 [130 – 2400]	Suburban site
					1180 ± 820 [180 – 3510]	Urban site
Fostier and Michelazzo 2006 [51]	Campinas, São Paulo State (Brazil)	December 2002 & May 2003	7.7 ± 7/1 [0.8 – 37.8]		465 ± 252 [104 – 778]	Residential Site
		January & May 2003	6.3 ± 3.9 [0.3 – 15.4]		332 ± 351 [24 – 1231]	Industrial Site
Choi et al. 2008 [19]	Huntington, NY (USA)	June 2006 – May 2007	1.4 ± 0.4 [0.5 – 2.5]	1.8 ± 2.2 [ND – 45.4]	3.2 ± 3.7 [ND – 54.0]	
Li et al. 2008 [101]	Femman, Göteborg, (Sweden)	January – March 2005	1.96 ± 0.38 [1.35 – 6.42]	2.53 ± 4.09 [0.34 – 32.84]	12.50 ± 5.88 [3.89 – 20.26]	Industrial Site
	Rörvik, (Sweden)		1.63 ± 0.19 [1.37 – 19.7]		No Data	Rural Site
Rutter et al 2008 [133]	Milwaukee, WI (USA)	April 2004 and May 2005	No Data	[3 – 55]	[3 – 90]	< 2.5 μm
Wängberg et al. 2008 [21]	Cabo de Creus, Catalonia (Spain)	October 2003, January, April & July 2004	1.80		9.9 [2 – 30]	Coastal Site, Automated TGM, Automated and Manual RGM & AES Trap
			NA	2.4 [0 – 19]		
	Étang de Thau, Occitania (France)		2.42		183 [1 – 1,160]	Coastal Site, Manual TGM, RGM & AES Trap
			NA	62.8		
	Piran (Slovenia)		2.91 4.0 [2.0 – 16.4] – Summer		12.1	Coastal Site, Manual TGM, RGM & AES Trap
			NA	7.5		
	San Lucido, Cosenza (Italy)		1.75		2.7	Coastal Site, Automated TGM/RGM/TPM, Manual RGM & AES Trap
			NA	2.6		
	Neve Yam, Haifa, Israel		NA	13.5	47.3 [1- 730]	Coastal Site, Automated & Manual RGM & AES Trap
Rutter et al. 2009 [40]	Mexico City, USA	March 2006	7.2 ± 4.8	62 ± 64	187 ± 300	< 2.5 μm
	Toronto, ON (Canada)		4.5 ± 3.1 [0.5 – 44.1]	14.2 ± 13.2 [<4 – 284]	21.5 ± 16.4 [<4 – 252]	< 2.5 μm

Reference	Site	Time	GEM (ng/m^3)	GOM (pg/m^3)	PBM (pg/m^3)	Notes
Song et al. 2009 [17]		December 2003 – November 2004			46.9	Total Filterable Mercury
Xiu et al. 2009 [88]	Shanghai, China	July 2004 – April 2006	NA	NA	560 ± 220 [7 – 1450]	Urban Site
					330 ± 90 [200 – 470]	Suburban Site
Arruti et al 2010 [149]	Santander, Cantabria (Spain)	2008	No Data	No Data	1400 ± 3710 [ND – 25400]	PM10
					800 ± 950 [ND – 5100]	PM2.5
Baya and Van Heyst [303]	Elora, ON (Canada)	November 2006 – August 2007	1.2 ± 0.51 [0.08 – 5.97]	15.1 ± 10.0 [0.8 – 124.6]	16.4 ± 9.5 [0.4 – 150.9]	Overall
			1.3 ± 0.53	14.0 ± 8.50	17.3 ± 10.23	Fall; Bare/Snow Cover
			0.9 ± 0.61	12.5 ± 9.51	13.5 ± 9.67	Winter; Snow/Bare Cover
			1.3 ± 0.63	17.9 ± 4.82	19.5 ± 9.22	Spring; Bare/Corn Cover
			1.1 ± 0.44	13.9 ± 10.88	12.2 ± 2.94	Summer; Corn Cover
Liu et al. 2010 [41]	Detroit, MI (USA)	2004	2.47 ± 1.43 [0.36 – 26.50]	15.48 ± 54.94 [1.00 – 2473]	18.05 ± 61.00 [1.00 – 1345.20]	Urban Site
	Dexter, MI (USA)		1.59 ± 0.59 [0.26 – 14.82]	3.80 ± 6.62 [1.00 – 121.73]	6.10 ± 5.51 [1.00 – 90.56]	Rural Site
Soerensen et al. 2010 [52]	Global	August 2006 – April 2007	1.53 ± 0.58	3.1 ± 11	NA	
	North Atlantic	August 2006	1.32 ± 0.16	0.4 ± 3		
	Atlantic Ocean	April 2007	2.26 ± 0.26	0.1 ± 1		
	Sargasso Sea		2.86 ± 0.17	1.2 ± 2		
	South Africa	October 2006	1.36 ± 0.24	3.4 ± 4		
	Indian Ocean		1.11 ± 0.19	4.6 ± 5		
	West Australia	November 2006	1.03 ± 0.16	5.0 ± 6		
	East Australia		1.33 ± 0.24	1.9 ± 3		
	Coral Sea	December 2006	1.21 ± 0.18	0.3 ± 1		
	New Zealand	January 2007	1.19 ± 0.17	0.1 ± 0		
	Antarctic Ocean		1.30 ± 0.16	0.0 ± 0		
	Antarctic Coast		1.55 ± 0.38	43.0 ± 39		
	Coast of Chile	February 2007	1.11 ± 0.11	28.6 ± 30		
Choi et al 2013 [104]	Huntington, NY (USA)	December 2007 – November 2009	1.3 ± 0.4 [0.2 – 3.7]	1.3 ± 3.3 [<DL – 63.9]	4.1 ± 7.8 [<DL – 97.6]	Rural Site
	Rochester, NY (USA)		1.6 ± 0.4 [0.9 – 6.4]	5.6 ± 10.3 [<DL – 177.6]	8.7 ± 12.8 [<DL – 271.2]	Urban Site
Weigelt et al. 2013 [139]	Waldhof, Lower Saxony (GER)	2009 – 2011	1.61 ($\tilde{x}$) [0.86 – 7.68]	1.0 ($\tilde{x}$) [<0.4 – 133]	6.3 ($\tilde{x}$) [<0.4 – 262]	Rural agricultural; <2.5 µm
Cheng et al. 2014 [304]	Dartmouth, NS (Canada)	January 2010 – December 2011	1.67 ± 0.20	2.07 ± 3.35	2.32 ± 3.09	Urban Site
	Kejimkujik, NS (Canada)		1.38 ± 1.01	0.41 ± 0.95	3.51 ± 4.46	Rural Site
Ren et al. 2014 [60]	Moss Point, MI (USA)	July – August 2010	1.42 ± 0.12 [1.06 – 1.70]	5.4 ± 10.2 [0.0 – 70.8]	3.1 ± 1.9 [0.0 – 8.8]	
		April – May 2011	1.53 ± 0.11 [1.07 – 3.12]	5.3 ± 10.2 [0.0 – 68.7]	5.7 ± 6.2 [0.0 – 37.0]	

Reference	Site	Time	GEM (ng/m^3)	GOM (pg/m^3)	PBM (pg/m^3)	Notes
Steffen et al. 2014 [87]	Alert, NV (Canada)	2002 – 2012		22.6 ± 51.99 [0 – 877.85]	41.3 ± 82.3 [0 –748.69]	Overall
				2.36 ± 1.22 [≤ 7.79]	20.4 ± 18.08 [≤ 99.26]	January
				11.35 ± 15.63 [≤ 220.56]	136.67 ± 110.38 [≤ 541.51]	March
				120.11 ± 94.67 [≤ 877.85]	45.46 ± 71.74 [≤ 698.03]	May
				14.78 ± 30.77 [≤ 260.95	7.36 ± 7.10 [≤ 40.98]	July
				4.35 ± 8.75 [≤ 108.82]	6.22 ± 9.55 [≤ 85.76]	August
				1.08 ± 0.99 [≤ 10.71]	15.25 ± 17.46 [≤ 122.30]	November
Zverina et al. 2014 [39]	Prague (Czech Republic)	2009 – 2011	No Data	No Data	0.82 mg kg^{-1} (± 1.8%)	< 25 μm
					0.76 mg kg^{-1} (± 0.4%)	< 63 μm
					0.65 mg kg^{-1} (± 7.2%)	63 – 119 μm
					0.50 mg kg^{-1} (± 3.8%)	119 – 507 μm
Marumoto et al. 2015[111]	Fukuoka, Kyushu Islands (JPN)	June 2012 – May 2013	2.33 ± 0.49 [1.47 – 6.39]	5.7 ± 9.4 [ND – 123]	10 ± 11 [ND – 139]	< 2.5 μm
	Minamata, Kyushu Islands (JPN)		1.90 ± 0.40 [≥ 5.82]		No Data	
Schleicher et al. 2015 [55]	Beijing (China)	2006	No Data	No Data	573 ± 551	TSP
					263 ± 246	PM2.5 (day)
					280 ± 383	PM2.5 (night)
Lee et al. 2016 [305]	Yongheung Island, Korea	January 2013 – August 2014	2.8 ± 1.1	8.3 ± 9.7	10.9 ± 11.2	
Siudek et al. 2016 [49]	Poznań, Wielkolska (Poland)	April 2013 – October 2014	No Data	No Data	7.3 ± 9.1 [<1.7 – 77.1]	< 0.7 μm (urban)
					22.6 ± 45.3 [<1.7 – 604.9]	< 2.2 μm (urban)
	Jeziory, Wielkolska (Poland)				2.4 ± 2.8 [<1.7 – 16.1]	< 0.7 μm (rural)
					20.8 ± 21.6 [<1.7 – 142.5]	< 2.2 μm (rural)
Gustin et al. 2016 [143]	Reno, NV (USA)	Winter 2013 – 2014	2.3 ± 0.5	27 ± 7	24.3 ± 13.2	Tekran
				76 ± 56		CEM (GOM only)
		Spring 2014	2.1 ± 0.4	22 ± 5	36.2 ± 9.6	Tekran
				59 ± 11		CEM (GOM only)
		Summer 2014	1.9 ± 0.3	18 ± 2	13.7 ± 4.8	Tekran
				106 ± 29		CEM (GOM only)
		Spring 2015	1.7 ± 0.2	14 ± 11	11.4 ± 3.9	Tekran
				38 ± 22		CEM (GOM only)
Pyta et al. 2016 [2]	Zabrze (Poland)	January – December 2013	No Data	No Data	2.6 (± 3.3) [0.3 – 12.5]	30 – 60 nm
					1.4 (± 1.0) [0.3 – 4.3]	60 – 108 nm
					2.6 ± 3.3 [0.7 – 10.6]	108 – 170 nm

Reference	Site	Time	GEM (ng/m^3)	GOM (pg/m^3)	PBM (pg/m^3)	Notes
					4.9 ± 5.7 [1.3 – 23.1]	170 – 260 nm
					8.8 ± 11.7 [1.2 – 47.9]	260 – 400 nm
					13.2 ± 14.1 [1.2 – 58.6]	400 – 650 nm
					9.7 ± 7.9 [1.6 – 36.1]	0.65 µm – 1.0 µm
					6.7 ± 4.1 [1.3 – 17.8]	1 µm – 1.6 µm
					4.2 ± 2.4 [0.9 – 9.8]	1.6 µm – 2.5 µm
					4.5 ± 2.6 [1.6 – 10.5]	2.4 µm – 4.4 µm
					2.4 ± 0.9 [1.1 – 4.6]	4.4 µm – 6.8 µm
					2.4 ± 2.2 [0.7 – 8.9]	6.8 µm – 10 µm
					1.9 ± 1.2 [0.6 – 4.2]	10 µm – 40 µm
Wängberg et al. 2016 [4]	Råö, Halland, (Sweden)	May 2012 – July 2013, February 2014 – May 2015	1.42 ± 0.20, x̃: 1.41	0.80 ± 1.6, x̃:0.23	3.6 ± 4.5, x̃: 2.21	PM2.5
Cheng et al. 2017 [151]	Xuhui, Shanghai (China)	September 2014 – August 2015	NA	NA	320 ± 130 [70 – 1880]	Urban
	Shengsi, Zhejiang (China)				220 ± 180 [20 – 1250]	Island
Duan et al. 2017 [43]	Qingpu, Shanghai (China)	June – December 2014	4.19 ± 9.13 [>0.1 – 550]	21 ± 100 [ND – 3876]	197.8 ± 877.2 [ND – 12260]	Suburban
Guo et al. 2017 [3]	Kathmandu Valley (Nepal)	April 2013 – April 2014	No Data	No Data	850.5 ± 962.8 [24.8 – 3079.3]	Suburban
Huang et al. 2017 [65]	Pensacola, FL (USA)	Summer 2012	1.2 ± 0.1	0.6 ± 1.3	2.4 ±2.6	Tekran
		Fall 2012	1.2 ± 0.1	1.1 ± 2.8	3.6 ± 3.8	Tekran
		Winter 2012	1.3 ± 0.1	1.0 ± 2.2	7.3 ± 8.8	Tekran
		Spring 2013	1.2 ± 0.2	2.9 ± 6.8	5.9 ± 6.8	Tekran
				43 ± 110		Cation-exchange
				4 ± 10		Nylon Membranes
		Summer 2013	1.1 ± 0.1	0.5 ± 1.0	2.3 ± 2.0	Tekran
				24 ± 57		Cation-exchange
				0.4 ± 1.3		Nylon Membranes
		Fall 2013	1.0 ± 0.1	1.1 ± 2.1	2.9 ± 2.3	Tekran
				14 ± 18		Cation-exchange
				1.2 ± 1.1		Nylon Membranes
		Winter 2013	1.2 ± 0.3	1.3 ± 2.5	4.9 ± 5.3	Tekran
				17 ± 23		Cation-exchange
				0.6 ± 0.6		Nylon Membranes
		March 2014	1.2 ± 0.1	2.0 ± 3.6	4.0 ±3.4	Tekran
				24 ± 15		Cation-exchange

Reference	Site	Time	GEM (ng/m^3)	GOM (pg/m^3)	PBM (pg/m^3)	Notes
				0.6 ± 0.5		Nylon Membranes
Li et al, 2017 [1]	Jinan, SD (China)	July 2014 – December 2015	No Data	No Data	508.5 (402.74) [0 – 2500]	Suburban $PM_{2.5}$
Bełdowska et al. 2018 [71]	Gdynia, Pomeranian Voivodeship, (Poland)	January 2016 – 2017	No Data	No Data	26.4 ± 16.0 [12.2 – 43.7]	Total PBM
					26.2 ± 16.1[10.7 – 42.8]	Sum of Speciated PBM
Fang et al. 2018 [62]	Taichung, Taiwan	April 2016 – March 2017	4.70 ± 2.63	29.58 ± 80.54	350 ± 80	Total Suspended Solids
			5.04 ± 2.43		90 ± 30	PM2.5
Kumari and Kulshrestha 2018 [9]	Mahasar, Haryana (India)	Winter 2014-15, Summer 2015	No Data	No Data	1010 ± 300 [590 – 1530]	Winter PM_{10}
					320 ± 200 [40 – 830]	Summer PM_{10}

Table 0.3. A multi-point calibration of preconcentration + APCI analysis of HgX_2

HgX_2	APCI gas	n	Mass Range (ng)	Sensitivity (cts pg^{-1})	R^2	Method Detection Limit (pg)
$HgCl_2$	10% IB in N_2	12	0.05 – 1.6	6×10^1	0.95	14
$HgBr_2$		13	0.09 – 3.6	12	0.96	4×10^1
$HgCl_2$	0.5% SF_6 in IB	11	0.3 – 1.0	1.4×10^2	0.78	6
$HgBr_2$		14	0.6 – 18	5×10^1	0.99	17

Table 0.4. Urban/indoor air measurements in Montreal, Canada 2013-2014

Year	Start Date	Stop Date	Trap	$HgCl_2$	$HgBr_2$
				pg m^{-3}	
Burnside Hall, McGill University Campus, Montreal Canada (urban, ~50 m above ground level)					
2013	224.67	225.67	PS	5×10^1	<11
			Tef A	1×10^2	$<6 \times 10^1$ *
			GB	7×10^1	19
	228.67	231.67	Tef A	8×10^1	9×10^1
			TL	<17*	12
			Tef B + PS	<29*	<24*
	242.67	245.67	TL	<12*	<11
			Tef B + PS	<6*	<11
	273.67	274.67	Tef A	4×10^1	3×10^1
			TL	$<4 \times 10^1$ *	<24 *
			T	29	9×10^1
2014	14.67	15.67	PS	<4	<11
			Tef A	7	<11
			Tef B	<6 *	<11
Memorial Pool, McGill University Campus, Montreal Canada (indoor)					
2014	27.92	28.42	PS	$<6 \times 10^1$ *	<19 *
			Tef A	8×10^1	$<6 \times 10^1$ *
			CoCl	$<2 \times 10^2$ *	<11
	34.92	35.42	PS	27	<26 *
			Tef A	5×10^1	29
	64.92	65.42	PS	16	5×10^1
			Tef A	8×10^1	$<1.4 \times 10^2$ *
	65.92	66.42	PS	<4	<11
			Tef A	4×10^1	$<1.2 \times 10^2$ *

PS – Polysulfide-coated copper/iron nanoparticles, GB – glass beads, Tef – shredded Teflon, TL – shredded Teflon in GC liner, T – shredded Teflon in Teflon tubing (all Teflon), CoCl – cobalt chloride crystals, Tef + PS – Teflon trap with PS precolumn.
* - Contaminants present based on qualifier-target ion ratios. Concentration is an upper limit to possible HgX_2 concentration.

Table 0.5 Number-weighted concentrations (cm^{-3}) of submicron and microscale particles measured at Montviel, QC and at sites in Waswanipi

Site	Description	Date	100 nm – 1.1 µm	1.1 – 10 µm
Arena	Inside	6-12	$(1.43 \pm 0.19) \times 10^{2}$	$(5.2 \pm 3.7) \times 10^{-2}$
	Inside	6-13	$(4.8 \pm 1.9) \times 10^{1}$	$(3.0 \pm 1.3) \times 10^{-2}$
	Inside	6-14	$(1.72 \pm 0.26) \times 10^{2}$	$(2.7 \pm 1.3) \times 10^{-2}$
Camp	Kitchen	6-12	No data - OPS failed	No data - OPS failed
	Outdoor (D)	6-13	$(0.92 \pm 1.0) \times 10^{2}$	$(5.8 \pm 1.4) \times 10^{-2}$
	Outdoor (N)	6-13	$(5.0 \pm 7.9) \times 10^{2}$	$(1.16 \pm 0.61) \times 10^{-2}$
	Outdoor	6-14	$(7.5 \pm 1.9) \times 10^{1}$	$(1.25 \pm 0.35) \times 10^{-2}$
	Woods	6-14	$(4.36 \pm 0.30) \times 10^{2}$	$(2.65 \pm 0.81) \times 10^{-2}$
	Residence	6-14	$(4.40 \pm 0.24) \times 10^{2}$	$(8.7 \pm 2.8) \times 10^{-2}$
Council	Outside	6-12	$(1.7 \pm 1.7) \times 10^{2}$	$(4.2 \pm 1.0) \times 10^{-2}$
	Outside	6-13	$(7.55 \pm 0.97) \times 10^{1}$	$(1.0 \pm 1.8) \times 10^{-1}$
	Outside	6-14	$(4.19 \pm 0.30) \times 10^{2}$	$(1.28 \pm 0.89) \times 10^{-2}$
Daycare	Inside	6-13	$(2.9 \pm 1.4) \times 10^{1}$	$(8.0 \pm 2.1) \times 10^{-2}$
	Outside	6-13	$(7.7 \pm 1.8) \times 10^{1}$	$(8.6 \pm 3.7) \times 10^{-2}$
	Inside	6-14	$(3.64 \pm 0.69) \times 10^{2}$	$(1.20 \pm 0.26) \times 10^{-1}$
	Outside	6-14	$(5.28 \pm 0.32) \times 10^{2}$	$(2.1 \pm 2.4) \times 10^{-2}$
Home	Inside	6-12	$(6.3 \pm 1.4) \times 10^{3}$	$(1.85 \pm 0.45) \times 10^{0}$
	Inside	6-13	$(1.92 \pm 0.31) \times 10^{3}$	$(1.20 \pm 0.14) \times 10^{-1}$
Police Station	Inside	6-12	$(3.88 \pm 0.26) \times 10^{3}$	$(3.29 \pm 0.32) \times 10^{-1}$
	Outside	6-12	$(2.37 \pm 0.21) \times 10^{2}$	$(1.07 \pm 0.63) \times 10^{-2}$
	Outside	6-13	$(5.0 \pm 1.6) \times 10^{1}$	$(9.9 \pm 8.6) \times 10^{-3}$
	Inside	6-14	(1.125 ± 0.099)	$(1.76 \pm 0.19) \times 10^{-1}$
	Outside	6-14	$(2.4 \pm 1.9) \times 10^{2}$	$(3.4 \pm 3.6) \times 10^{-2}$
Residence	Inside	6-13	$(3.49 \pm 0.90) \times 10^{1}$	$(4.7 \pm 1.3) \times 10^{-2}$
	Inside	6-14	$(2.46 \pm 0.32) \times 10^{2}$	$(4.6 \pm 1.6) \times 10^{-2}$

Table 0.6. Mass-weighted concentrations (μg/m³) of nanoparticles, submicron particles, and microscale particles measured at Montviel, QC and at sites in Waswanipi

Site	Description	Date	10 – 100 nm	100 nm – 1.1 μm	1 – 10 μm
Arena	Inside	6-12	$(4.28 \pm 0.37) \times 10^{-2}$	$(3.75 \pm 0.42) \times 10^{-1}$	$(2.3 \pm 2.0) \times 10^{0}$
	Inside	6-13	$(2.74 \pm 0.40) \times 10^{-1}$	$(8.0 \pm 3.8) \times 10^{-1}$	$(1.16 \pm 0.93) \times 10^{0}$
	Inside	6-14	$(1.357 \pm 0.059) \times 10^{-1}$	$(3.07 \pm 0.41) \times 10^{-1}$	$(7.3 \pm 6.1) \times 10^{-1}$
Camp	Kitchen	6-12	$(1.7 \pm 1.0) \times 10^{1}$	No data - OPS failed	No data - OPS failed
	Outdoor (D)	6-13	$(7.03 \pm 0.15) \times 10^{-2}$	$(4.1 \pm 6.1) \times 10^{-1}$	$(1.08 \pm 0.85) \times 10^{0}$
	Outdoor (N)	6-13	$(1.6 \pm 3.9) \times 10^{0}$	$(1.0 \pm 1.6) \times 10^{1}$	$(1.02 \pm 0.75) \times 10^{-1}$
	Outdoor	6-14	$(4.1 \pm 1.2) \times 10^{-2}$	$(4.1 \pm 1.7) \times 10^{-1}$	$(1.09 \pm 0.96) \times 10^{-1}$
	Woods	6-14	$(1.55 \pm 0.97) \times 10^{-2}$	$(2.44 \pm 0.43) \times 10^{-1}$	$(3.6 \pm 3.5) \times 10^{-1}$
	Residence	6-14	$(1.221 \pm 0.061) \times 10^{-1}$	$(9.33 \pm 0.57) \times 10^{-1}$	$(2.8 \pm 1.8) \times 10^{0}$
Council	Outside	6-12	$(4.28 \pm 0.37) \times 10^{-2}$	$(3.75 \pm 0.42) \times 10^{-1}$	$(2.3 \pm 2.0) \times 10^{0}$
	Outside	6-13	$(2.74 \pm 0.40) \times 10^{-1}$	$(8.0 \pm 3.8) \times 10^{-1}$	$(1.16 \pm 0.93) \times 10^{0}$
	Outside	6-14	$(1.357 \pm 0.059) \times 10^{-1}$	$(3.07 \pm 0.41) \times 10^{-1}$	$(7.3 \pm 6.1) \times 10^{-1}$
Daycare	Inside	6-13	$(1.7 \pm 1.0) \times 10^{1}$	$(2.5 \pm 1.4) \times 10^{1}$	NA
	Outside	6-13	$(7.03 \pm 0.15) \times 10^{-2}$	$(4.1 \pm 6.1) \times 10^{-1}$	$(1.08 \pm 0.85) \times 10^{0}$
	Inside	6-14	$(1.6 \pm 3.9) \times 10^{0}$	$(1.0 \pm 1.6) \times 10^{1}$	$(1.02 \pm 0.75) \times 10^{-1}$
	Outside	6-14	$(4.1 \pm 1.2) \times 10^{-2}$	$(4.1 \pm 1.7) \times 10^{-1}$	$(1.09 \pm 0.96) \times 10^{-1}$
Home	Inside	6-12	$(1.55 \pm 0.97) \times 10^{-2}$	$(2.44 \pm 0.43) \times 10^{-1}$	$(3.6 \pm 3.5) \times 10^{-1}$
	Inside	6-13	$(1.221 \pm 0.061) \times 10^{-1}$	$(9.33 \pm 0.57) \times 10^{-1}$	$(2.8 \pm 1.8) \times 10^{0}$
Police Station	Inside	6-12	$(4.28 \pm 0.37) \times 10^{-2}$	$(3.75 \pm 0.42) \times 10^{-1}$	$(2.3 \pm 2.0) \times 10^{0}$
	Outside	6-12	$(2.74 \pm 0.40) \times 10^{-1}$	$(8.0 \pm 3.8) \times 10^{-1}$	$(1.16 \pm 0.93) \times 10^{0}$
	Outside	6-13	$(1.357 \pm 0.059) \times 10^{-1}$	$(3.07 \pm 0.41) \times 10^{-1}$	$(7.3 \pm 6.1) \times 10^{-1}$
	Inside	6-14	$(1.7 \pm 1.0) \times 10^{1}$	$(2.5 \pm 1.4) \times 10^{1}$	NA
	Outside	6-14	$(7.03 \pm 0.15) \times 10^{-2}$	$(4.1 \pm 6.1) \times 10^{-1}$	$(1.08 \pm 0.85) \times 10^{0}$
Residence	Inside	6-13	$(1.6 \pm 3.9) \times 10^{0}$	$(1.0 \pm 1.6) \times 10^{1}$	$(1.02 \pm 0.75) \times 10^{-1}$
	Inside	6-14	$(4.1 \pm 1.2) \times 10^{-2}$	$(4.1 \pm 1.7) \times 10^{-1}$	$(1.09 \pm 0.96) \times 10^{-1}$